AN EVALUATION OF LONG-TERM AIR QUALITY TRENDS IN NORTH TEXAS USING STATISTICAL AND MACHINE LEARNING TECHNIQUES

Guo Quan Lim

Dissertation Prepared for the Degree of

DOCTOR OF PHILOSOPHY

UNIVERSITY OF NORTH TEXAS

May 2020

APPROVED:

Kuruvilla John, Major Professor and Chair of the Department of Mechanical and Energy Engineering
Hamid Sadat-Hosseini, Committee Member
Sheldon Shi, Committee Member
Chetan Tiwari, Committee Member
Richard Zhang, Committee Member
Hanchen Huang, Dean of the College of Engineering
Victor Prybutok, Dean of the Toulouse Graduate School

Lim, Guo Quan. *An Evaluation of Long-Term Air Quality Trends in North Texas Using Statistical and Machine Learning Techniques*. Doctor of Philosophy (Mechanical and Energy Engineering), May 2020, 167 pp., 14 tables, 48 figures, 2 appendices, 184 numbered references.

While ozone design values have decreased since 2000, the values measured in Denton Airport South (DEN), an exurban region in the northwest tip of the Dallas-Fort Worth (DFW) metroplex, remains above those measured in Dallas Hinton (DAL) and Fort Worth Northwest (FWNW), two extremely urbanized regions; in addition, all three sites remained in nonattainment of National Ambient Air Quality Standards (NAAQS) ozone despite reductions in measured NO_x and CO concentrations. The region's inability to achieve ozone attainment is tied to its concentration of total non-methane organic compounds (TNMOC). The mean concentration of TNMOC measured at DAL, FWNW, and DEN between 2000 and 2018 were 67.4 ± 1.51 ppb-C, 89.31 ± 2.12 ppb-C, and 220.69 ± 10.36 ppb-C, respectively. Despite being the least urbanized site of the three, the TNMOC concentration measured at DEN was over twice as large as those measured at the other two sites. A factor-based source apportionment analysis using positive matrix factorization technique showed that natural gas was a major contributing source factor to the measured TNMOC concentrations at all three sites and the dominant source factor at DEN. Natural gas accounted for 32%, 40%, and 69% of the measured TNMOC concentration at DAL, FWNW, and DEN, respectively. The Barnett Shale region, an active shale gas region adjacent to DFW, is a massive source of unconventional TNMOC emissions in the region. Also, the ozone formation potential (OFP) of the TNMOC pool in DEN were overwhelmingly dominated by slow-reacting alkanes emitted from natural gas sources. While the air pollutant trends and characteristics of an urban airshed can be determined using long-term ambient air quality measurements, this is difficult in regions with sparse air quality monitoring. To solve the lack in spatial and temporal datasets in non-urban regions,

various machine learning (ML) algorithms were used to train a computer cluster to predict air pollutant concentrations. Models built using certain ML algorithms performed significantly better than others in predicting air pollutants. The model built using the random forest (RF) algorithm had the lowest error. The performance of the prediction models was satisfactory when the local emission characteristics at the tested site were like the training site. However, the performance dropped considerably when tested against sites with significantly different emission characteristics or with extremely aggregated data points.

ACKNOWLEDGMENTS

Firstly, I want to express my most sincere gratitude to my mentor and academic advisor, Dr. Kuruvilla John, for the continuous support he has provided throughout my master's and doctoral degrees. Dr. John's guidance had helped me tremendously in my research, my writing, and has helped shaped my attitude towards research and academia. I would also like to thank Dr. John for always looking out for me outside of my studies and had taught me the importance of networking with other researchers. I could not have had imagined having a better mentor for my Ph.D. study.

Besides my advisor, I would like to thank the rest of my thesis committee: Dr. Hamid Sadat, Dr. Sheldon Shi, Dr. Chetan Tiwari, and Dr. Richard Zhang. I would also like to express my gratitude to Dr. Saritha Karnae for being a fantastic collaborator in many projects. I also want to acknowledge the help I had received from Dr. Mahdi Ahmadi, Mr. Constant Marks, and Ms. Maleeha Matin. They were critical in helping me reach many milestones throughout my research.

Last but certainly not least, I would like to thank my fiancé, my parents, my sister, and my family. They were there to show me the love and support I needed for me to get through my Ph.D. study. They were there to keep me motivated when I couldn't see the light at the end of the tunnel. They were there for me to talk to when I was depressed and needed someone the most. Without them, I would never have made it to the end of this journey.

TABLE OF CONTENTS

Page

LIST OF TABLES

Page

LIST OF FIGURES

Page

CHAPTER 1

INTRODUCTION

The Dallas – Fort Worth (DFW) metroplex region is one of the largest metropolitan regions in the United States [1] and had seen a massive increase in oil and gas production activities in the past two decades from the Barnett Shale region [2]. The expansion in shale gas production had drastically increased emissions from non-conventional shale gas sources, and this threatens the environment and the people living in the metroplex. Shale gas production is a significant source of volatile organic compounds (VOC), a precursor for ground-level ozone formation. Ozone is a criteria pollutant that can cause severe health issues, especially in the sensitive group of young children, older adults, and those with existing lung conditions. Overexposure to ozone leads to several health problems such as chronic obstructive pulmonary disease (COPD), shortness of breath, and other respiratory ailments [3]. While the ozone levels in DFW had shown improvements since 2000, ten of the twelve DFW counties still consistently fail to comply with the design value designated by the United States Environmental Protection Agency (EPA) through the Clean Air Act's National Ambient Air Quality Standard (NAAQS) [4]. Denton, Johnson, Tarrant, and Wise are the leading shale gas producing counties in the Barnett Shale, and all four counties consistently fail to meet ozone attainment under the NAAQS.

The objective of this work is to study the long-term impact on DFW air quality due to elevated shale gas production over the past two decades. While the air quality impacts of shale gas are well-documented, relatively few studies truly focus on the Barnett Shale and its impact on the DFW metroplex region. The available literature on the subject does not provide a consensus on whether the increased shale gas production in the neighboring Barnett Shale had any significant impact on DFW's air quality [5, 6, 7]. To the best of the author's knowledge, this dissertation is the most comprehensive work on long-term VOC, oxides of nitrogen (NO_x),

carbon monoxide (CO), and ozone concentrations measured in DFW. Data mining and data analysis techniques were also implemented to correlate unconventional shale gas production and local VOC concentrations. However, the lack of consistent air quality data from non-urban regions within the Barnett Shale severely hinders the progress of understanding the full extent of the shale gas production's impacts. While traditional photochemical models can simulate air pollutant concentration and deposition at these non-urban/rural regions, the scale of these simulation predictions are very coarse and simulated by using specific air pollution episodes [8]. This dissertation describes an attempt to incorporate machine learning (ML) algorithms in air pollutant concentration prediction models. A model can be trained using regression-based ML algorithms to predict the non-linear ozone concentration in remote regions using the robust data collected from the DFW metroplex used as the training set.

This dissertation covers the following issues:

(i) Perform data mining and analysis to characterize the air quality trends observed in the DFW metroplex between 2000 and 2019.

(ii) Identify the potential impacts of unconventional shale gas development in the Barnett Shale on local and regional air quality.

(iii) Perform source apportionment analysis to identify major emission sources contributing to air pollutant concentrations.

(iv) Compare the performance of various ML algorithms on their ability to predict non-linear ozone concentrations and whether the ML models are comparable to more traditional air quality simulation models.

Chapter 1 of this report introduces this study and states the objectives and outlines the work performed. Chapter 2 highlights the background and provides a detailed literature review relevant to this study. Chapter 3 details the descriptions of the study area covering the DFW metroplex, the air quality monitoring stations, and the data used in this study. Chapter 4 summarizes the methods and techniques used in this dissertation. The results and discussions of each part of this study are available from Chapters 5 through 9. Chapter 5 describes the study of short-term VOC concentrations collected from five monitoring stations in DFW. Chapter 6

describes a long-term analysis of various air pollutants from three DFW monitoring stations. In Chapter 7, the impacts of unconventional gas development on the VOC concentrations in Denton, Texas, was studied. Chapter 8 details a source apportionment analysis using positive matrix factorization (PMF) method on long-term VOC concentration data collected in DFW. Chapter 9 describes a comparative study of various ozone prediction models trained using ML algorithms, their performance against traditional photochemical models, and their adaptability using non-local data. The conclusion of this study and recommendations for future work are provided in Chapter 10.

The contents of Chapter 5 and Chapter 7 have been published in peer reviewed journals such as Science of the Total Environment [9] and Atmospheric Pollution Research [10], respectively. As of the writing of this dissertation report, a portion of the contents discussed in Chapter 6 was submitted for publication in Atmospheric Pollution Research. Additional manuscripts from Chapters 8 and 9 are currently being developed for journal article submission.

CHAPTER 2

BACKGROUND

Energy production is predicted to rise in the upcoming decades to supply the growing demands from rapid urbanization and industrialization of many regions across the world. An increasing number of countries, including China and certain parts of Europe, sees natural gas as a cleaner alternative to coal due to significantly lower oxides of nitrogen (NO_x), carbon dioxide (CO_2), and sulfur dioxide (SO_2) emissions [11, 12, 13, 14, 15]. The Energy Information Administration (EIA) has estimated a rapid growth in natural gas production by 7% per year (+7%/year) between 2018 and 2020, followed by a +1%/year increase through 2050. The EIA estimated the natural gas production by 2029 to be at 22.4 MMBtu/day from 13.5 MMBtu/day in 2018, and further development in shale gas resources is required to support this growth [16].

Shale gas is natural gas trapped under shale formation and is an increasingly valuable energy resource in the United States. Through advancements in hydraulic fracturing and horizontal drilling technologies [17], significantly harvesting shale gas is now possible, and the access to shale gas has increased the world's available natural gas resources [18]. Shale gas production in the United States accounted for only 5% of total dry gas production in 2004; in 2015, shale gas production was 56% of total dry gas production in the United States [15]. In 2017, the United States Energy Information Administration (EIA) estimated about 62% of the total dry natural gas produced in the United States was from shale resources, which totals approximately 16.9 trillion cubic feet of dry natural gas. [19]. The International Energy Agency (IEA) has predicted the natural gas demand to increase by 42% by 2040 [18].

Environmental health controversies often surround shale gas extraction and production. Countless factors, from gas well preparation to gas processing, play a crucial role in increasing pollutant concentrations. The increased shale gas production activities around the U.S. are negatively affecting many local neighborhoods and communities. Contamination of water

resources, ambient air pollution, light and noise pollution, and seismic activities are among the most prominent environmental issues caused by shale gas production [20, 21]. Also, the extraction processes cause a significant drain on water resources as 12 to 20 million liters of water on average are required to produce a single horizontal well [22, 23]. Commonly used hydraulic fracturing liquids also contain toxic and carcinogenic chemicals that can affect human health [24]. Ground-water pollution from faulty seals in gas wells are not uncommon, and hydraulic fracturing liquid often contains toxic and carcinogenic elements [24, 25]. Regions with a large amount of shale gas production often have heightened the risk of seismic events, as fracking operations may lead to low magnitude earthquakes and gas well blowouts [26]. Shale gas operations tend to generate a lot of noise and light pollution [27]. The massive deforestation during shale gas operations also endangers the natural habitats of wildlife [28].

Rapid development in the Marcellus Shale, a shale formation that underlies parts of Ohio, West Virginia, Pennsylvania, and New York, caused an estimated $7.2 million to $32 million in air quality damages. The population living close to active gas well regions is often at elevated health risks [29]. Shale gas productions in the United States tend to stay away from densely populated areas as much as possible. However, this was possible because the population density in the United States is considerably lower than in parts of Europe and China. Increased shale gas development in more densely populated regions may lead to endangerment of the population, especially in regions lacking a proper legal framework to protect both people and the environment [23].

Shale gas operations emit a lot of air pollutants and greenhouse gases (GHG) into the atmosphere, which contributes to global warming and threatens human health [30, 31, 32]. Composition of natural gas emissions varies, and they usually contain 88% methane, 5% ethane, 2% propane, 1.4% carbon dioxide, 1.2% nitrogen, and 0.6% n-butane [33]. Methane is a potent GHG emitted during shale gas operations. Methane's hundred-year global warming

potential is 28 times that of CO_2 [34]. An estimated 3.6% to 7.9% of shale gas produced escapes into the atmosphere as fugitive methane. Fugitive methane emissions escape through leaks from equipment during gas well completion, transportation, storage, and distribution [11]. In a typical shale gas operation, between 1.3% and 1.9% of the natural gas produced are lost to the atmosphere as fugitive methane [32]. 49 of the 50 sampling events in a study of ambient hydrocarbon analysis in North Texas's Barnett Shale observed methane concentrations above the laboratory detection limit, and the concentrations in the region were higher than the reported urban background concentration of 1.8 to 2 ppm [7]. Direct exposure to the hydrocarbons released from petrochemical operations is known to be damaging to human health [29].

The U.S. EPA has listed: (i) completions with fracking, (ii) pneumatic vents, (iii) injection pumps, (iv) leakage from equipment, (v) workovers without fracking, (vi) liquid unloading, (vii) condensate tanks, (viii) gas engines, (ix) dehydrator vents, (x) reciprocating compressors, (xi)drilling of wells, (xii) well blowouts, and (xiii) coal beds as dominant active sources of methane emissions in most common shale gas production locations [30, 31]. During the development phase, major VOC sources include completion vents and condensate tanks, whereas drill rigs, fracturing pumps, and traffic emissions from trucks are minor VOC sources. Compressor stations are major VOC sources, while wellhead compressors, heaters, blowdown vents, and pneumatics are minor VOC sources during the production phase [35].

Litovitz et al. [36] found Pennsylvania's Marcellus Shale had gas well emissions that were ten times larger than associated diesel and road dust emissions. They identified shale gas production to be an incredibly damaging factor to regional air quality. Volatile organic compounds (VOC) are a group of carbon-based chemicals emitted from either anthropogenic or biogenic sources. The U.S. EPA defines VOCs as carbon compounds that react photochemically in the atmosphere, which also includes compounds with low photochemical reactivity, such as methane and ethane, but excludes carbon monoxide (CO), CO_2, carbonic

acid, and carbonates [37]. Many VOC species are considered air toxins, and overexposure to VOC can lead to irritations, nausea, headaches, and damages to the nervous system, kidney, or liver [38]. Annual emissions of VOC in 2011 were in the range of 2,500 to 11,000 metric tons. There was a lasting long-term effect on air quality from enhanced shale gas operation as the VOC emission levels maintained despite a decrease in the number of active natural gas wells since 2011 [36].

According to Schade and Roest [39], unregulated flaring operations at the Eagle Ford Shale gas region (SGR) in South Texas has resulted in a significant increase in the ethane mixing ratios in San Antonio and Floresville, Texas along the direction where the air mass interacted significantly with shale gas emissions. They suggested that these unconventional pollutant sources may undermine any ozone pollution reduction progress by the EPA. Monitoring stations closer to the SGR had considerably higher concentrations of oil and gas production-related alkanes species compared to monitoring stations further away [40]. Areas downwind of the Eagle Ford Shale formation in South Texas saw an increase in ethane, propane, n-butane, and isobutane concentrations, which are alkane VOC species closely associated with oil and gas production [39].

The National Ambient Air Quality Standards (NAAQS) ozone design value is the annual fourth-highest daily maximum 8-hour average ozone concentration averaged over three years. 1997, 2008, and 2015 ozone design values are 80 parts-per-billion (ppb), 75 ppb, and 70 ppb, respectively. Ten of the twelve DFW counties consistently fail to achieve ozone attainment under the NAAQS [4]. Ahmadi and John [6] studied the effects of Barnett Shale operations on regional ozone. They broke the study period into pre-2007 and post-2007 to reflect the increasing oil and gas well activities in the region since 2007. Before 2007, the average number of new gas wells build every year was 700, and this increased to an average of 1700 new shale gas wells post-2007. There were higher numbers of days exceeding the

ozone standard in the SGR than in the non-SGR. The DFW counties have never failed to achieve nitrogen dioxide (NO_2) attainment status [41]. Oxides of nitrogen (NO_x), which includes NO_2, is one of the precursors to ozone generation [42]. The consistent NO_2 achievement would suggest that NO_x was not the cause of ozone attainment in the three counties. Traffic, power plants, and other combustion sources are the primary NO_x source in urban regions [43, 44]. Thus, DFW's failure to achieve ozone compliance under the NAAQS was unlikely the product of conventional urban emission sources and the emission of NO_x.

In a typical urban region, anthropogenic sources are the primary sources of VOC, which include gasoline vehicle exhaust, solvent use, fugitive emissions, industrial emissions, and oxidation [45, 46]. However, the elevated Barnett Shale natural gas production served as an unconventional source that adds to the VOC emissions from conventional urban emission sources in the DFW metroplex; natural gas production releases large concentrations of ethane, propane, n-butane, isobutane, isopentane, and n-pentane [47]. Alkanes were the most abundant total non-methane organic carbon (TNMOC) group measured in DFW, and there was a higher concentration of TNMOC in less urbanized regions with high natural gas production volume than in highly urbanized regions [9]. The dominant portion by weight percentage related to oil and natural gas extraction wells was found to be n-alkanes, including ethane, propane, isobutane, and n-butane. Vehicle traffic is the primary source of alkenes and alkynes emissions. While benzene and toluene are generally associated with traffic emissions, oil and gas activities also emit these hydrocarbon species [48, 49, 50, 51, 52, 53, 54]. Rutter et al. [46] identified natural gas emissions (25%) to be the most significant contributor to measured TNMOC at a monitoring station downwind of the city of Fort Worth. Natural gas emissions were followed by fugitive emissions (15%), internal combustion engine (15%), biogenic sources (7%), industrials emissions or oxidation 1 (8%), and oxidation 2 (18%).

In the realm of air pollution concentration studies, deterministic methods, statistical methods, and machine learning (ML) are the three most commonly utilized approaches [55]. In a deterministic method, a simulation model of atmospheric chemistry dispersion and transport can be built for air quality predictions. Deterministic method models can achieve detailed modeling of the diffusion mechanisms in ambient pollutants. However, the accuracy of deterministic method model predictions is considerably lower than other approaches because of the extensive use of default parameters and lack in the incorporation of real measurements [55, 56, 57]. On the other hand, the statistical method incorporates a large number of real-world measurements. However, the downfall of the statistical method came in the form that it assumes a linear relationship between the variables, which is unrealistic in a real-world setting [55]. The third most-commonly-used technique, the ML method, allowed researchers to built non-linear models that incorporate large amounts of real-world measurements. As a result, an increasing number of researchers are incorporating various forms of ML into air pollution studies [58, 59, 60, 61, 62, 63].

CHAPTER 3

STUDY REGION AND DATA

The DFW metroplex region is currently ranked as the fourth largest metropolitan area in the USA and is among the top urban areas reporting strong population growth since 2010 [1]. DFW is a massive commercial and economic hub in the southern United States with specialization in (i) mining, quarrying, oil and gas extraction, (ii) company and enterprise management, and (iii) insurance and finances. As of June 2018, the metroplex region had over 3.7 million in employment, with the most prominent group within the transportation, trade, and utility sector, followed by the professional and business service sector. Between 2015 and 2016, DFW saw a 1.84% growth in population, a 3.52% growth in median household income, 2.88% growth in employment, and 9.6% growth in median property value [64].

The Barnett Shale formation, located within the Bend Arch-Fort Worth basin and underlines 5,000 square-miles, lies just west of the DFW metroplex region. The edge of the formation lies beneath the City of Fort Worth, and the most productive counties fall within the DFW metroplex region. Due to the Barnett Shale activities, the mining, quarrying, oil, and gas extraction industries in DFW is twice as large as expected based on the region's population and size [64]. The mining, logging, and construction sector saw the most significant change in percentage, by 5.5%, of all work sectors between 2017 and 2018 [65]. Significant growth in gas production occurred in the formation in the 2000s, when the gas well count increased from around 700 wells in 2000 to more than 18,000 wells in 2013 [66]. Natural gas production peaked in 2012, producing up to 5,743 million cubic feet (ft^3) or 163 million cubic meters (m^3) per day [67].

The Texas Commissions on Environmental Quality (TCEQ) operates a network of air pollution monitoring stations across the DFW metroplex. The air pollutant concentration data is available at the Texas Air Monitoring Information System (TAMIS) online portal

(https://www17.tceq.texas.gov/tamis/index.cfm?fuseaction=home.welcome). Ozone, CO, and NO_x concentrations were available in hourly updated values, whereas TNMOC concentration data were available either as canister data, daily average values collected over three days, or Automated Gas Chromatography (Auto-GC) data, hourly updated values. Canister TNMOC concentrations are collected using steel SUMMA canisters and analyzed using gas chromatograph-mass spectrometers by TCEQ scientists [33]. The Auto-GC sampler collects air samples with a Sorbent Trap, which are used to capture the compounds of interest and could be performed even with the presence of other compounds. Target compounds are separated chromatographically, and the separated compounds are detected by one or more detection methods, which could be Photoionization Detector (PID) or Flame Ionization Detector (FID). Finally, the onboard system identifies and quantifies the compounds [68].

3.1 Monitoring Sites Equipped with Canister TNMOC Monitors

Dallas Hinton (DAL), Fort Worth Northwest (FWNW), and Denton Airport South (DEN) are three monitoring stations equipped with SUMMA canister systems. Figure 3.1 shows the locations of the monitoring stations and the active oil and gas wells within the Barnett Shale region. Dallas Hinton (DAL) is a monitoring station located in a highly urbanized region with no oil and gas operations (32.82006N; -96.860117W) in Dallas County. Landmarks around the site include the Dallas Love Field Airport and Interstate 35-East highway. DAL is in the city of Dallas, one of the largest cities in the state of Texas. Based on the 2017 U.S. Census vintage, an estimated 1.7 million people live in the city of Dallas. The city of Dallas saw a 12% growth in population between April 1, 2010, and July 1, 2017 [69]. In 2017, the daily vehicle miles traveled (DVMT) in the city of Dallas was 122.8-million miles per day [70]. Fort Worth Northwest (FWNW), in Tarrant County, is a moderately urbanized region with oil and gas operations (32.805818N; -97.356568W). FWNW is located just south of Fort Worth Meacham International Airport and is about 8-km north of downtown Fort Worth, one of the

fastest-growing large cities within the U.S. There are two major highways within proximity to the monitoring station, the Interstate 35-West and the Interstate 820. There are an estimated 874,000 people that live in the city of Fort Worth, and the population grew by 17.3% from 2010 through 2017 [69]. In 2017, the DVMT in the city of Fort Worth was approximately 62.7-million miles per day [70], which was roughly half of the city of Dallas'. Denton Airport South (DEN) is in an exurban region located in Denton County with a large amount of oil and gas operations (33.219069N; -97.1962836W). DEN is located 1-km north of the Denton Enterprise Airport and is just outside of the Denton city limit. The city of Denton has an estimated 136,000 inhabitants, and the city saw a 17.1% growth in population since 2010 [69]. The city had a DVMT of 16.2-million miles per day in 2017 [70], which was the lowest among the three sites.

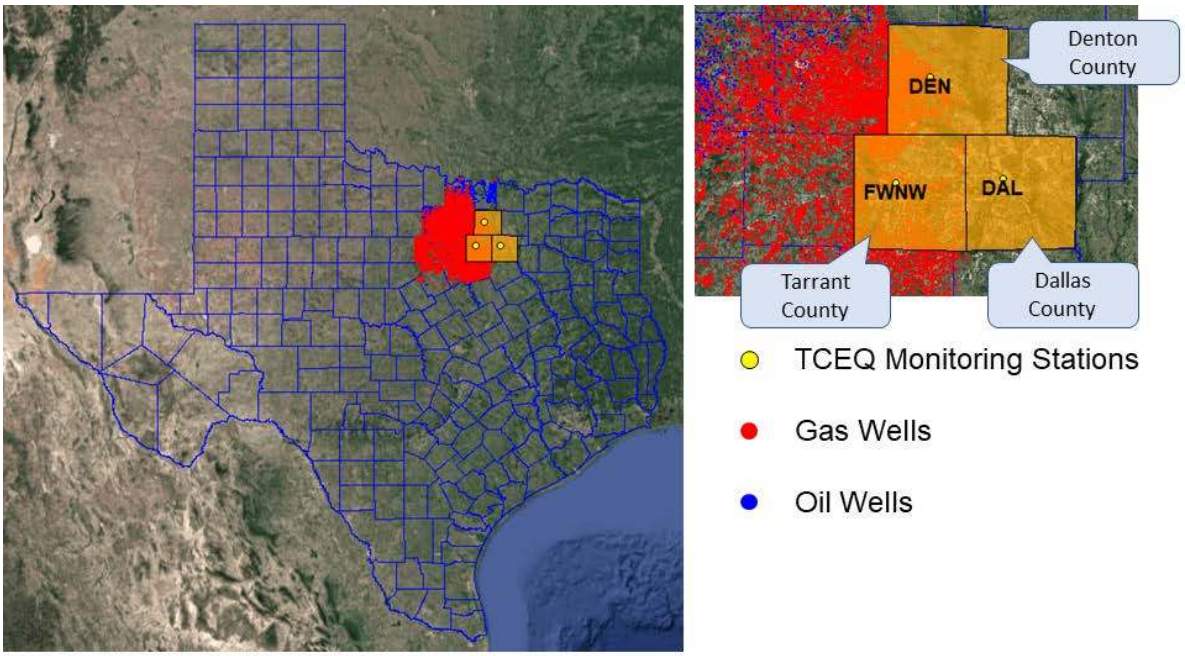

Figure 3.1: Map of SUMMA canister sites along with active oil and gas wells.

3.2 Monitoring Sites Equipped with Auto-GC TNMOC Monitors

As the canister TNMOC samples were collected once every sixth-day, air pollution conditions between each cycle and diurnal characteristics of measured TNMOC concentrations could not be analyzed. The TNMOC dataset collected by the Auto-GC monitors will provide 144 data points for each canister TNMOC data point and allowed for continuous monitoring

data. There was a total of fifteen Auto-GC monitoring stations set up within the DFW metroplex region; however, only five met the criteria of (i) located within the Barnett Shale region and (ii) activated before 2011. As shown in Figure 3.2, all five monitoring sites are in shale gas producing counties of the Barnett Shale; two of the five sites were in urban regions while the other three were in non-urban regions.

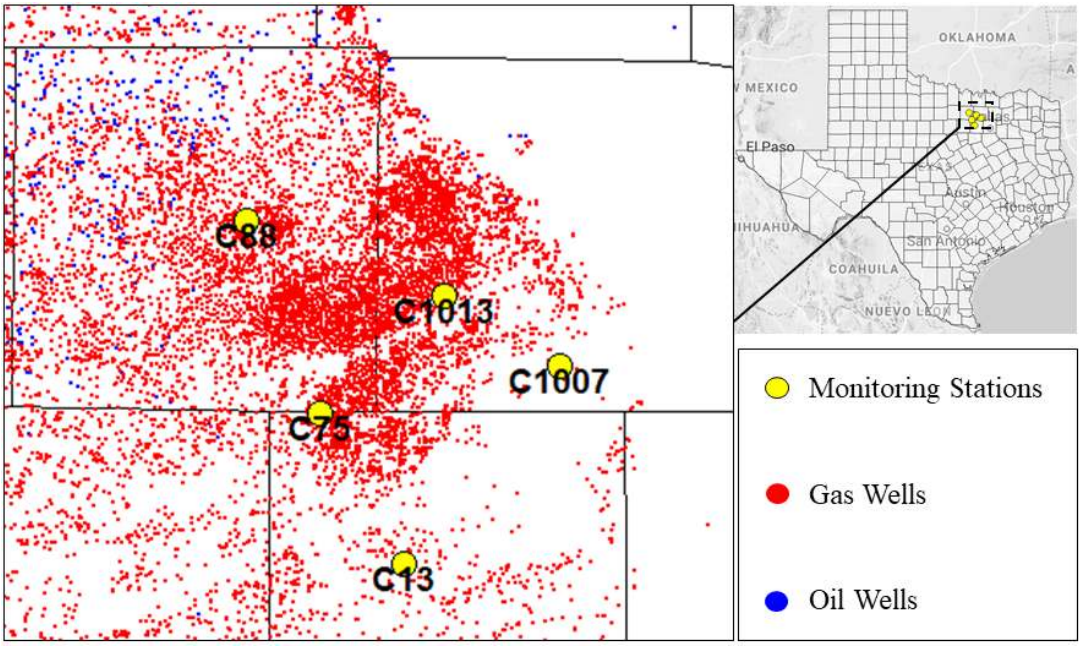

Figure 3.2: Map of Auto-GC monitoring station along with active oil and gas wells.

The Flower Mound Shiloh (C1007) monitoring station in Denton County's town of Flower Mound (+33.045862N; -97.130002W). The monitoring station is located in a suburban residential area, close to a small urban forest, and is 5-km north of the Grapevine Lake. The 2010 census data shows that C13 had a population of 22,545 on the zip code level [71]. By the end of 2015, there were 64 active gas wells within a 5-km radius from the monitoring station, 200 active gas wells within 10-km, and 596 active gas wells within 15-km. The Fort Worth Northwest (C13) monitoring station, in Tarrant County, had a population of 35,389 on zip code level [71], which was the largest among the five Auto-GC sites. While Tarrant County had the highest natural gas production volume in the Barnett Shale, C13 had a significantly lower number of active gas wells compared to the non-urban sites. The number of active gas wells

within 5-, 10-, and 15-km from C13 during 2015 were 175, 483, and 1155, respectively. The Eagle Mountain Lake (C75) monitoring station, in northwest Tarrant County (+32.987891N; -97.477175W), is located at the Eagle Mountain Lake reservoir and is 1.5-km from the Kenneth Copeland Airport. C75 is in a rural region, and the closest town to it, Newark, had an estimated population of only 1,005 [71]. There were 431, 1385, and 2893 active natural gas wells within 5-, 10-, and 15-km from the monitoring station in 2015. The DISH Airfield (C1013) monitoring station in Denton County is on the small privately-owned Clark Airfield (+33.130930N; -97.297650W). On the zip code level, C1013 had a population of 13,098 [71]. Also, a large natural gas facility owned by Atmos Energy is just south of the monitoring station. Among the five Auto-GC sites, C1013 had the highest number of active gas wells. There were 420 active gas wells within a 5-km radius, 1473 active gas wells within 10-km, and 3047 active gas wells within 15-km. Wise County's Decatur Thompson (C88) monitoring station is in an exurban region (+33.221721N; -97.584445W). The monitoring station is located near Highway 81 and had a population of 15,587 at the zip code level, according to 2010's census data [71]. During 2015, there were 257, 837, and 1886 active gas wells within 5-, 10-, and 15-km from the monitoring station, respectively. C88 had the fewest gas wells among the non-urban sites, and it is also the only one of five sites located on the west side of the gas clusters (Figure 3.2).

CHAPTER 4

METHODOLOGY

4.1 R Programming Language

The R programming language is an open-source statistical computing language and widely used in statistical applications, data analysis, and data visualization. R is an incredibly powerful open-source programming language specifically for statistical computing. Codes written using R can be easily modified or improved using extensions, which could be downloaded, unpacked, and added to the library within the console itself. The R is exceptionally effective at data handling and storage facility. There are numerous arrays of calculation operators for statistical applications, mainly matrices. The R also comes with a large-coherent-and-integrated collection of intermediate data analysis tools [72]. Also, many tools and packages are readily available online via GitHub [73]. The version of R used in this study was R-3.6.1 on the R-studio platform.

The spatial-temporal analysis and PMF source apportionment analysis were enhanced through the “openair” package in R [74, 75]. The bivariate polar plot aids spatial analysis by visualizing the effect of wind speed and direction on the measured concentration of an air pollutant species. The bivariate polar plots were generated using the "polarPlot" command in "openair." The input data required are the source concentration profile (which can be either raw pollutant concentration or a PMF output), wind speed, and wind direction. The bivariate polar plots are accepted as equivalent to more traditionally used techniques, such as conditional probability function (CPF), and are powerful visualization tools for air pollution studies. The CPF plots are also generated using “openair” by setting the “polarPlot” statistics to “cpf” and the percentile to 90^{th}. GIS tools can be included to quantify potential sources, such as power plants, traffic sources, and population size within the region [74, 75]. One of the hallmarks of

using the GIS tool is a regression analysis of variables. The “sp” package was used for analyzing spatial data and is comparable to a GIS tool [76].

R was also implemented to perform statistical analysis using the Mann-Kendall’s (MK) test, the Kruskal-Wallis (KW) test, and the Dunn’s test. The MK test determines if the trend experienced by the group was significant [77]. The KW test was performed to identify if there were at least one significant difference in mean value within the group [78]. Finally, Dunn's test was used to determine whether a specific mean value was significant from the rest [79]. The alpha is 0.05, and the null hypothesis is rejected if the P-value was under 0.05.

4.2 Machine Learning Algorithms

Machine learning (ML) teaches a computer to learn from patterns and inference alone through an array of algorithms and statistical models [80]. The regression models of the artificial neural network (ANN), classification and regression tree (CaRT), k-nearest neighbor (knn), random forest (RF), and support vector machine (SVM) algorithms were implemented in this dissertation. Like any predictive simulation model, the accuracy of the model is a critical factor in determining its performance. In most ML-based studies, the performance of an ML model is evaluated through root-mean-square-error (RMSE), mean-absolute-error (MAE), and coefficient of determination (R^2). The RMSE is the square root of the second sample moment of the differences between the predicted values of a model and the measured values, the MAE is the average of the absolute errors between the predicted and measured values, and the R^2-value measures the model’s ability to explain the total variance in data, scaled from 0-to-1 [80]. The equation for RMSE and MAE is given in Eq. (4.1) and Eq. (4.2), respectively. While there is no governing rule on what constitutes an acceptable RMSE and MAE, in general, a higher value depicts a less accurate system. The MAE assigns the same weight to all errors, whereas the RMSE assigns more weight to the errors with larger absolute values than the errors with smaller absolute values. Chai and Draxler [81] state that the RMSE is a more desirable measure

than the MAE when a larger error needs to be penalized more, where an error by 10 is more than twice as bad as an error by 5.

$$RMSE = \sqrt{\frac{\sum_{i=1}^{N}(Predicted_i - Observed_i)^2}{N}} \quad \textit{(Eq. 4.1)}$$

$$MAE = \frac{1}{n}\sum_{i=1}^{n}|Predicted_i - Observed_i| \quad \textit{(Eq. 4.2)}$$

In addition to the RMSE, MAE, and R^2-value, the performance of a predictive model can also be determined through fractional bias (FB), fractional error (FE), mean normalized bias (MNB), and mean normalized error (MNE) [82]. Bias is a measure of a model's tendency to under- or over-estimate predicted values. Error is a measure of the difference between predicted and observed values in terms of magnitude. The formulas for calculating these statistical metrics are given in Eq. (4.3) through Eq. (4.6). FB ranges from -200% to +200%, while NMB and NME range from -100% to positive-infinity [8].

$$FB = 100\% \times \frac{2}{N}\sum\frac{(Predicted_i - Observed_i)}{(Predicted_i + Observed_i)} \quad \text{(Eq. 4.3)}$$

$$FE = 100\% \times \frac{2}{N}\sum\frac{|Predicted_i - Observed_i|}{(Predicted_i + Observed_i)} \quad \text{(Eq. 4.4)}$$

$$NMB = 100\% \times \frac{1}{N}\sum\left(\frac{Predicted_i - Observed_i}{Observed_i}\right) \quad \text{(Eq. 4.5)}$$

$$NME = 100\% \times \frac{1}{N}\sum\left|\frac{Predicted_i - Observed_i}{Observed_i}\right| \quad \text{(Eq. 4.6)}$$

4.2.1 Artificial Neural Network

The artificial neural network (ANN) is the most widely known ML algorithm and is based on the biological neural network. The ANN is a network that consists of weighted interconnecting neutrons that form an input layer, an output layer, and an in-between hidden layer [83, 84, 85, 86]. Figure 4.1 shows a multilayer ANN framework based on work performed by Mitchell [80]. A multilayer ANN consists of multiple interconnected nodes, input X, output Y, and weighted vectors A_{ij} and B_{ij}. Initially, the algorithm a random weigh to all the linkages.

The algorithm then finds the activation rate of the hidden nodes using the input nodes and the linkages between the input and hidden nodes. Similarly, the activation rate of the output nodes is found using the activation rate of the hidden nodes and their linkages to the output nodes. The error rate at the output node is then used to recalibrate the linkages of the hidden and output nodes. The calculated weight and output errors then cascade down to the hidden nodes and are used to recalibrate the weights between hidden and input nodes. This process repeats until meeting a defined convergence criterion. The final linkage weights are then used to score the activation rate of the output nodes [87].

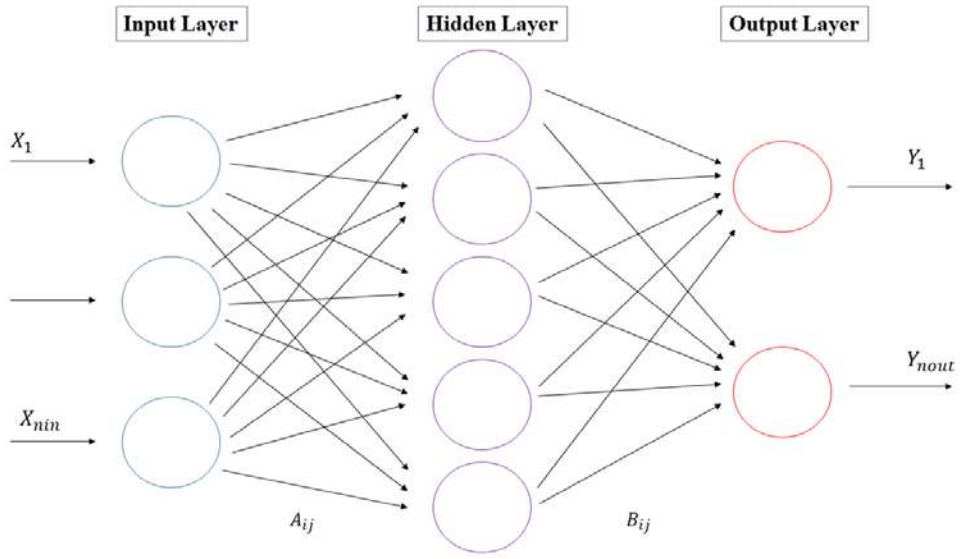

Figure 4.1: Framework of an artificial neural network (ANN) [80].

ANN requires a large amount of training data; thus, it is prone to over-fitting and generalization [87]. An ANN fitted too close to the training set causes over-fitting, and that made it difficult for the mode to generalize and make predictions. Generalization is the ability of a model to handle unseen data, mostly determined through the complexity and training of the ANN [88]. Due to the extensive training data, training the ANN can be very time consuming and computationally expensive [80].

The "caret" package on R was used to train the ANN algorithm in this study using the "nnet" method under the function "train" [89]. The training dataset must first be scaled from 0

to 1 because the ANN only outputs values from 0 to 1. The predicted values would have to be scaled back to the original scale.

4.2.2 Classification and Regression Tree

A decision tree, or classification and regression tree (CaRT), is a recursive data mining algorithm. The CaRT is a recursive algorithm that explores the structures of the dataset and develops a decision rule for predicting either a categorical (classification) and a continuous (regression) variable [90, 91]. The CaRT algorithm partitions and splits the data space repeatedly based on the governing formula of $X_j \leq s$, where an optimal split is available for all variables *j* and all possible split points *s*. In a regression tree, the splitting rule tries to minimize the expected sum variances for two resulting nodes, as shown in Eq. (4.7). $Var(Y_i)$ and $Var(Y_r)$ are the response variables for the corresponding child nodes of a parent-node *Y*, x_j is the variable *j*, x_j^R is the best splitting value of variable x_j, and *M* is the number of variables x_j [91]. The algorithm repeats this process until the stopping rule in Eq. (4.8) is met. Where $\{R_m\}$ is the terminal nodes, and c_m is the constant for the *m*-th region. These partitions can be visualized as a decision tree [92].

$$argmin\,[P_i\,Var(Y_i) + P_r\,Var(Y_r)];\; x_j \leq x_j^R; j = 1, \cdots, M \qquad \text{(Eq. 4.7)}$$

$$f(x) = \sum_M c_m I(x \in R_m) \qquad \text{(Eq. 4.8)}$$

The CaRT can handle missing data and outliers easier than most algorithms because its algorithm deals with splitting data space into two based on predefined criteria and does not depend on the magnitude of the difference [91]. However, due to the binary split, any minor changes that occur at the trunk would propagate down the branches of the tree and affect all subsequent split decisions. Minor changes in the variables can often lead to drastically different terminal nodes on the tree [92].

The "rprart" package in R was used to build the regression tree using the "ANOVA" function [93]. Pruning of the tree was performed using the "prune" function in "rpart." The

complexity parameter (cp) is a vital variable in pruning a decision tree. A variable will not be added to the tree if adding the variable will cost more than the designated cp value [93]. The pruning of a tree depends on the balance between the RMSE, the number of terminal nodes, and the cp.

4.2.3 K-Nearest Neighbors

The k-nearest neighbor (kNN) is a lazy learner algorithm, and it does not learn anything from the training data. The kNN algorithm uses the training data to populate the data space alongside the data used for prediction. First, the algorithm calculates the distance metric between samples from the target dataset against samples from the training dataset. The distance metric can be calculated using either Euclidean, Hamming, Manhattan, and Minkowski distance. The algorithm then adds the calculated distance and the index of the target to an ordered data frame where the distances and indices are sorted in ascending order by the distances. The kNN then picks the first k-entries from the sorted data frame and returns the mean value of the target output [94, 95, 96].

The kNN is very slow at making predictions because it performs its entire algorithm during the predicting phase and none during the training phase [94, 95, 96]. When the k-value is too small for the dataset, the density estimation of the algorithm is unreliable, whereas the density estimate may be too coarse when the k-value is too large [97]. The performance of the kNN is susceptible to the scale of data. The curse of dimensionality is a phenomenon that occurs when processing data with large dimensions. It refers to when the dimensionality and volume increase at a rate where available data could not keep up. Due to the curse of dimensionality, the kNN algorithm's performance is weaker when dealing with a larger dataset compared to a smaller one [98].

The "knnreg" functions in the "class" package [99] in R were used to perform regression kNN models. The Euclidean distance metric is the most commonly used distance

metric in a kNN application. Eq. (4.9) shows the equation for Euclidean distance. Where, $d(x, y)$ is Euclidean distance between samples *x* and *y*, and n is the number of dimensions in feature space.

$$d(x, y) = (\sum_{i=1}^{n}(x_i - y_i)^2)^{1/2} \quad \text{(Eq. 4.9)}$$

4.2.4 Random Forest

The random forest (RF) algorithm was first proposed by Breiman to introduce an additional random layer to the bagging process [100]. The RF constructs multiple decision trees during training time, and it outputs the class that was most frequently observed for classification models and outputs the mean prediction for regression models [100]. The user first defines the number of trees in the forest, n_{tree}. The regression RF algorithm draws n_{tree} number of bootstrap samples from the training dataset and grows a regression tree for each bootstrap sample drawn. The splitting criterion of each tree is identical to the previously discussed CaRT algorithm. The predictions made by the trees are aggregated as output [101].

Since the RF overcomes overfitting through averaging and combining the results of n_{tree}-number of decision trees. Thus, RF is also less prone to variance than a single decision tree and can work with a broader range of dataset than a single decision tree [100]. However, compared to building a single decision tree, the RF requires significantly more computational resources and time to construct.

The RF model was constructed using the "randomForest" package on R [102]. The number of trees, n_{tree}, was set to 350. The importance of each variable was also computed using the "randomForest" function with "importance = TRUE."

4.2.5 Support Vector Machines

The support vector machine (SVM) is an algorithm to find the hyperplane between the data of two classes. The SVM algorithm finds the support vectors, which are points closest to

the hyperplane from both classes. The algorithm then calculates the margin, which is the distance between the hyperplane and the support vectors. The hyperplane with the maximized margin is considered the optimal hyperplane. the SVM algorithm uses a kernel trick to maximize the margin [103]. The kernel transforms input data into the required form and can be either linear, polynomial, or Gaussian-exponential [104].

The SVM implements the Structure Risk Minimization (SRM), which allows it to avoid overfitting training and local minima by balancing the complexity of the model against its success at fitting the training dataset [105, 106]. The goal of the SRM is to minimize $E_{train} + \beta H(w)$, where E_{train} is the training error, $H(w)$ is a user defined regulation function, and β is a constant [103]. While allowing the user to choose Kernels brings tremendous flexibility, choosing a wrong kernel for the application can lead to a catastrophic drop in model accuracy.

The SVM model was constructed using the "SVM" function on the "e1071" package on R using the command line "type = eps-regression" [107]. A detailed description of the SVM tuning process can be found online [108].

4.3 Positive Matrix Factorization (PMF)

The positive matrix factorization (PMF) is a multivariate table-driven source apportionment model first developed by Paatero [109]. The model is used to determine the number of source factors affecting an air pollutant concentration. It also calculates the factor contribution and factor profile of each source. The goal of the PMF is to minimize the Q-value, as shown in Eq. (4.10), where *X* is the data matrix consisting of concentration of *n* chemical species in *m* samples, *p* is the number of factors, *f* is the chemical profile of each factor, and *g* is the factor's contribution to sample [110]. Also, it has been reported that the $Q_{(robust)}/Q_{(True)}$ value must be under 1.5 to be for the run to be considered [111]. The PMF model used in this was the EPA PMF 5.0 version; its user guide is available online [110].

$$Q = \sum_{i=1}^{n}\sum_{j=1}^{m}\left[\frac{X_{ij}-\sum_{k=1}^{p} g_{ik}f_{kj}}{u_{ij}}\right]^2 \quad \text{(Eq. 4.10)}$$

The EPA PMF 5.0 requires two inputs: a concentration file and an uncertainty file. Air pollutant data is organized into columns in the concentration file. The PMF 5.0 does not take zeroes or non-available (NA) data. The user must classify all instances of zeroes and NA as "-999", which signals the model to either replace them with species median or remove the entire column. The model detection limit (MDL) of the air pollutant monitor is required to generate uncertainty values in the uncertainty input file. The uncertainty is calculated using Eq. (4.11), if the measured concentration was lower than or equal to species MDL of species. If species MDL was lower than the measured concentration, uncertainty is calculated using Eq. (4.12) instead [110]. The MDL is air pollutant species-specific and can be retrieved from the TAMIS.

$$Uncertainty = \frac{5}{6} \times MDL \quad \text{(Eq. 4.11)}$$

$$Uncertainty = \sqrt{(Error\ fraction \times concentration)^2 + (0.5 \times MDL)^2} \quad \text{(Eq. 4.12)}$$

The quality of data is generally more critical than the volume of data. To improve model accuracy, only data that passes a specific signal-to-noise (S/N) ratio should be considered. The PMF 5.0 calculates the S/N ratio of each input species based on the concentration and uncertainty inputs. A “bad” species is removed from the dataset, and a “weak” species is kept, but the uncertainty assigned to it is tripled. The user guide recommends assigning any species with S/N ratio <0.5 as “bad”, 0.5≤ S/N ≤1 as “weak”, and >1 as “strong” species [110]; Paatero and Hopke’s [112] report shows that assigning species with S/N ratio <0.2 as “bad”, 0.2≤S/N≤2 as “weak”, and >2 as “strong” yields a better model accuracy.

CHAPTER 5

SPATIAL AND TEMPORAL CHARACTERISTICS OF AMBIENT ATMOSPHERIC HYDROCARBONS IN AN ACTIVE SHALE GAS REGION IN NORTH TEXAS*

A trend analysis study was performed using the Auto-GC TNMOC concentration data collected between 2011 and 2015 at five monitoring stations within the Barnett Shale. A 40-minute air sample is collected by the Auto-GC monitors every hour and process through on-board chromatography systems. However, most of the Auto-GC sites in the DFW metroplex were built in the 2010s and did not have data points that showcased the shale gas boom and the recession period air quality.

All five monitoring stations are within active shale gas producing counties of the Barnett Shale; however, there were significantly lesser shale gas production activities surrounding Flower Mound Shiloh (C1007) and Fort Worth Northwest (C13) as compared to Eagle Mountain Lake (C75), DISH Airfield (C1013), and Decatur Thompson (C88), as shown in Figure A9. The total natural gas production volume (MMBtu) from all producing gas wells within each 1.2 km × 1.2 km square box between 2011 and 2015 were summed up and were color scaled from blue (0) to red (3×10^7 MMBtu). The highest density of wells near C1007 northwest of the monitoring station and were mostly outside of the 5-km radius. At C13, there were significantly more wells at the northwest and southeast sides, and the highest producing wells in the area were within 5-km from the monitoring station. C75 and C1013 have significantly higher number active wells compared to the two urban sites in all directions, and some of the highest producing wells near the respective sites were within 5-km. Active gas wells also surrounded C88 in all directions like the other two non-urban sites; however, the high producing wells in the region were outside the 10-km radius.

---

* This chapter is reproduced from G. Q. Lim, M. Matin and K. John, "Spatial and temporal characteristics of ambient atmospheric hydrocarbons in an active shale gas region in North Texas," Science of the Total Environment, vol. 656, pp. 347-363, 2019, with permission from Elsevier.

Slower wind speed often leads to an increase in localized air pollution events and results in higher ambient concentrations of air pollution near source-rich regions. On the contrary, the effects of dispersion and rapid dilution become stronger with increasing wind speeds, which results in decreased concentration of air pollutants [113]. In Figure 5.1, the wind rose diagrams were plotted using wind data collected from 2011 to 2015. The predominant winds at all five monitoring stations were from the south-southeast. C1007 had the slowest recorded wind speeds with a mean value of 8.1 kph or 2.25 m/s, whereas C75 had the fastest winds at 9.6 kph or 2.67 m/s. The wind rose diagrams showed no significant difference between wind speed measured at all five sites; however, C75 had a higher frequency of high-speed winds blowing from the northwestern side of the monitoring station.

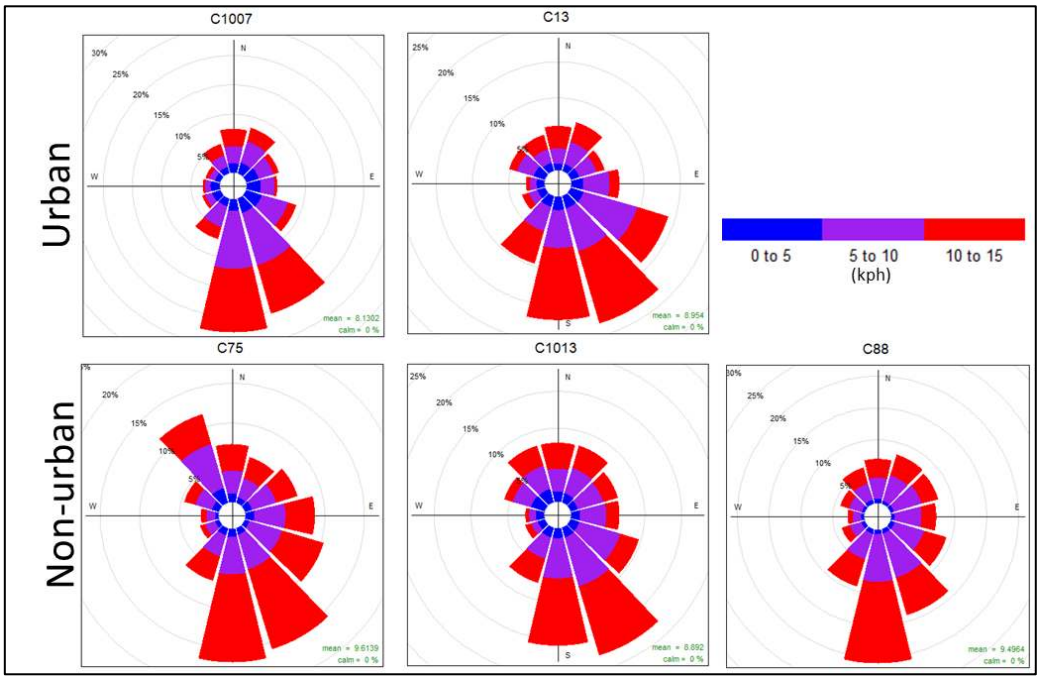

Figure 5.1: Wind rose diagrams for C1007, C13, C75, C88, and C1013: 2011-2015.

5.1 Spatial Variation in TNMOC Concentration Distribution

The TNMOC concentrations measured at the five sites between 2011 and 2015 are in Figure 5.2. C1007 had the lowest TNMOC concentrations, whereas C88 had the highest. Table 5.1 highlights the summary statistics of TNMOC and the hydrocarbon groups of alkanes,

alkenes, alkynes, aromatics, and biogenic. C88's mean TNMOC concentration was 2 ppb-C lower than C1013's, but its median concentration was 34% larger than C1013's, at 93.7 ppb-C and 69.89 ppb-C, respectively. The mean TNMOC concentration at C1013 was higher than its 75th-percentile and was the only monitoring site of the five to show this characteristic. Outliers significantly influenced the mean TNMOC concentration at C1013, where its 95th-percentile value was 152.58 ppb-C higher than the next highest site's.

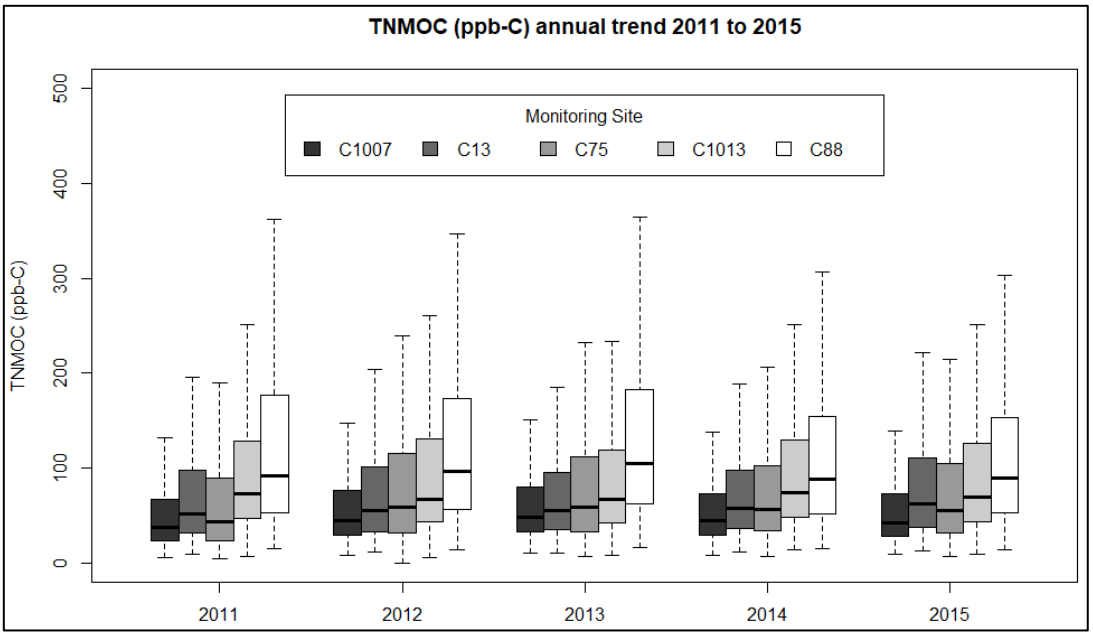

Figure 5.2: Annual trend of TNMOC (ppb-C) concentrations measured at C1007, C13, C75, C1013, and C88 from 2011 to 2015.

Alkanes were the group with the highest measured concentrations at all five sites, making up 84% of the measured TNMOC concentrations at the urban sites and 93% of the TNMOC concentrations measured at the non-urban sites. C1013 had the highest mean concentration of alkane, at 131.85 ppb-C, whereas C1007 had the smallest mean alkane concentration, at 57.86 ppb-C. The aromatics group was the second-largest group, making up roughly 7% of the TNMOC at the urban sites and 4% of the TNMOC at the non-urban sites. C13 had the highest mean concentration of aromatics, at 4.04 ppb-C, whereas C75had the lowest, at 1.87 ppb-C. C13 also had the largest mean concentration of alkene, at 4.11 ppb-C, and C75 had the lowest mean concentration, at 1.77 ppb-C.

Table 5.1: Summary of TNMOC and hydrocarbon groups (ppb-C).

		TNMOC	Alkane	Alkene	Alkyne	Aromatic	Isoprene
C1007	Mean	65.68	57.89	2.07	0.62	3.37	2.71
	Min	5.97	4.30	0.01	0.03	0.06	0.00
	Median	43.45	36.31	1.61	0.51	2.45	0.55
	95th	187.39	175.51	5.03	1.39	8.53	10.09
	Max	3427.85	3218.73	206.70	196.53	983.97	96.37
	IQR	28.3 - 73.35	21.87 - 64.87	1.06 – 2.46	0.31 – 0.78	1.56 – 4.04	0.11 – 3.2
	StDev	76.61	73.11	2.65	1.16	6.79	4.83
	Num.	36996	36996	36969	36531	36926	23899
C13	Mean	88.46	77.36	3.55	0.96	6.21	0.36
	Min	8.82	7.04	0.18	0.02	0.25	0.01
	Median	56.00	47.57	2.19	0.67	3.83	0.19
	95th	271.99	242.57	11.19	2.71	19.39	1.21
	Max	1791.59	1715.34	155.71	20.81	228.00	6.44
	IQR	34.67 - 99.99	28.38 - 88.31	1.46 – 3.71	0.44 – 1.04	2.55 – 6.58	0.08 – 0.49
	StDev	98.55	90.03	4.57	1.05	7.71	0.43
	Num.	36614	36614	36614	33696	36614	27056
C75	Mean	96.55	91.44	1.71	0.56	2.66	0.59
	Min	4.47	2.64	0.01	0.03	0.01	0.00
	Median	54.39	50.01	1.27	0.42	1.93	0.26
	95th	307.10	297.03	4.52	1.36	7.45	2.17
	Max	3631.70	3499.52	29.38	12.36	118.88	20.15
	IQR	30.22 - 105.17	26.98 - 99.13	0.85 – 2.01	0.25 – 0.68	1.16 – 3.29	0.09 – 0.74
	StDev	140.37	137.48	1.50	0.55	2.51	0.88
	Num.	36145	36145	35703	30240	35498	20727
C1013	Mean	138.22	131.92	1.84	0.54	3.67	0.46
	Min	5.53	4.01	0.04	0.02	0.06	0.00
	Median	69.89	64.72	1.37	0.45	2.47	0.24
	95th	517.17	504.17	4.97	1.21	10.35	1.69
	Max	3688.11	3649.67	42.62	14.63	195.32	9.22
	IQR	44.48 - 126.74	40.58 - 118.93	0.86 – 2.21	0.28 – 0.68	1.5 – 4.25	0.09 – 0.58
	StDev	223.31	219.81	1.73	0.42	4.54	0.63
	Num.	36335	36335	36311	35790	36321	20313
C88	Mean	136.04	129.21	2.19	0.59	3.56	0.91
	Min	14.03	10.12	0.05	0.04	0.32	0.00
	Median	93.70	87.78	1.84	0.51	2.82	0.47
	95th	364.59	352.37	4.56	1.26	8.10	2.36
	Max	53320.20	51811.34	817.59	30.28	660.89	24.46
	IQR	54.7 - 165.65	49.94 - 158	1.3 – 2.61	0.3 – 0.79	1.88 – 4.26	0.11 – 1.38
	StDev	319.57	311.30	4.48	0.46	4.93	1.14
	Num.	37090	37090	37088	36963	37087	20016

C13 and C75 had the highest and the lowest mean alkyne concentrations, respectively, where the corresponding mean concentrations were 0.88 ppb-C and 0.47 ppb-C. The aromatic, alkene, and alkyne TNMOC species were more prevalent in urban areas than in the non-urban areas. The mean concentration of isoprene measured in C1007 was significantly higher than all the other sites, at 2.71 ppb-C. The mean concentrations of isoprene at the other sites were significantly lower than C1007's, ranging from 0.36 ppb-C in C13 to 0.91 ppb-C in C88. The mean isoprene concentration at C1007 was more comparable to ground-level isoprene concentrations measured in the other major Texas cities, which ranges from 3.15 ppb-C in Houston, Texas [114] to 6 ppb-C in Austin, Texas [115]. Isoprene is a biogenic TNMOC species, and the most likely source was a small urban forest close to C1007.

5.2 TNMOC Components and Characteristics

Ethane, propane, and n-butane had the highest concentrations among measured TNMOC species at all five sites, and the non-urban sites had higher concentrations of these n-alkane species than the urban sites. These n-alkanes are common emission species from oil and gas production activities [116, 117]. Inversely, the alkene, alkyne, and aromatic species had a higher composition percentage at the urban sites compared to non-urban sites, and C13 had the highest measured mean concentration of these three groups.

The ratio between each group and TNMOC was calculated to determine further the impacts each group had on the measured TNMOC concentrations. There was a distinct variation between the urban and non-urban sites, as shown in Figure 5.3. The urban sites' alkane/TNMOC ratios were lower than the non-urban sites, and urban sites' median values were lower than the non-urban sites' 25^{th} percentile values. The interquartile range (IQR) for the urban sites' alkane/TNMOC ratio was also significantly larger than the non-urban sites'. While the alkane/TNMOC ratios were at least 0.8 across all five sites, the alkane/TNMOC ratios had a significant separation between the urban and the non-urban sites. C13 had a lower

mean concentration, lower median value, and a larger IQR, whereas C75 had a higher mean, a higher median, and a smaller IQR.

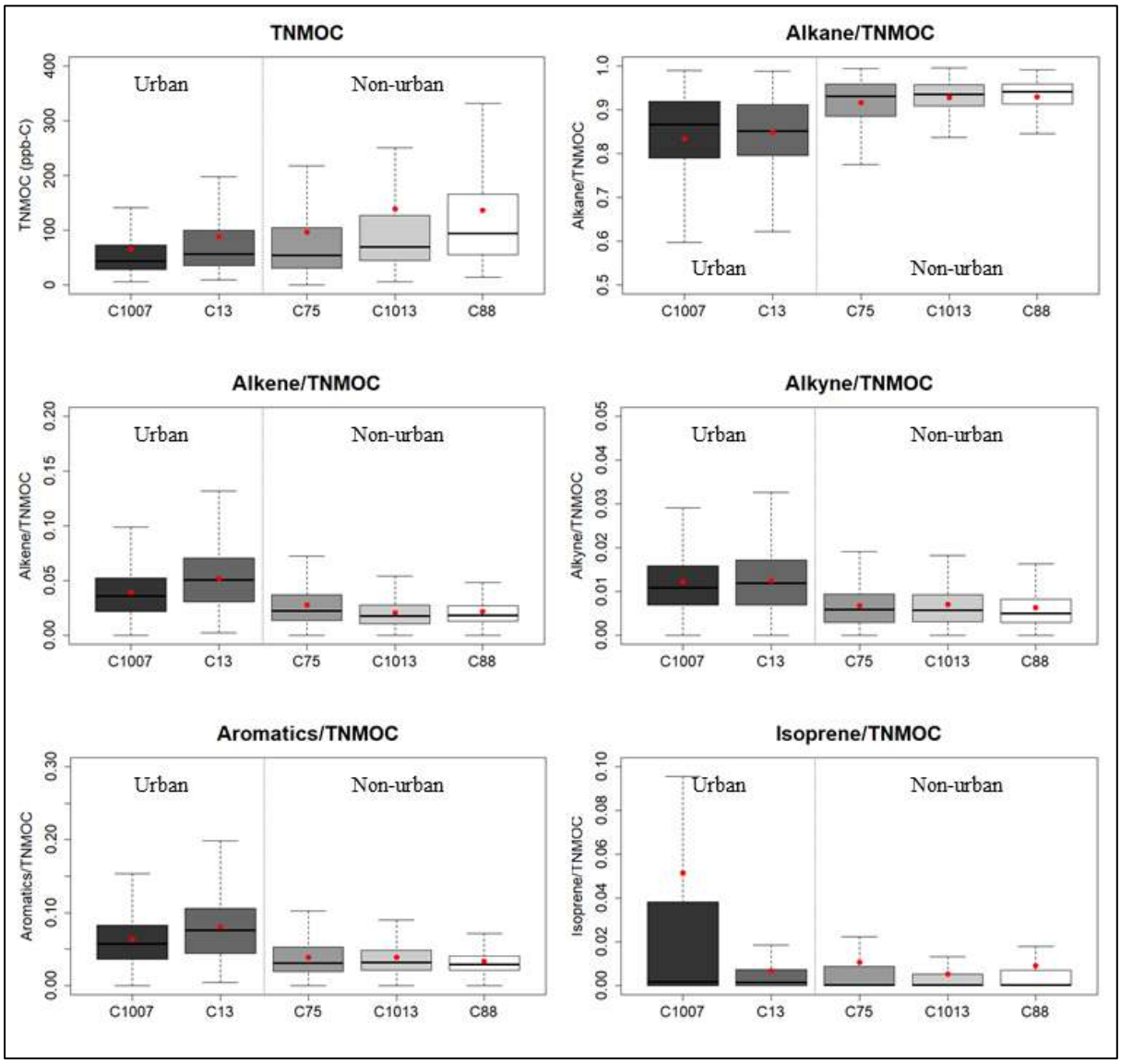

Figure 5.3: Comparison between urban and non-urban site TNMOC concentration, alkane/TNMOC, alkene/TNMOC, alkyne/TNMOC, aromatic/TNMOC, and isoprene/TNMOC concentration ratio.

5.3 Seasonal Trend Analysis

The combination of a lower photochemical reactivity in the atmosphere coupled with conducive meteorological conditions, such as lower mixing depths during winter months, typically contributes to a higher measured TNMOC concentration [118, 119]. In the northern hemisphere, the winter months are December through February, the spring months are March

through May, the summer months are June through August, and the fall months are September through November. The measured TNMOC concentrations were higher during winter months compared to summer months at all five monitoring sites, as shown in Figure 5.4. The mean concentration of TNMOC during winter months at C1007, C13, C75, C1013, and C88 were 104.58 ppb-C, 136.76 ppb-C, 156.54 ppb-C, 210.05 ppb-C, and 181.35 ppb-C, respectively; the mean concentration of TNMOC during summer months were 40.39 ppb-C, 51.19 ppb-C, 54.21 ppb-C, 89.86 ppb-C, and 112.78 ppb-C, respectively. The mean TNMOC concentration decreased by -61.59% at C1007, -62.56% at C13, -65.37% at C75, -57.22% at C1013, and -37.8% at C88 from winter to summer months. The change between summer and winter months mean TNMOC concentration at C88 was significantly different from the other monitoring sites where the KW-test P-value was 0.012 (<0.05).

Each hydrocarbon group should have different impacts on the TNMOC concentration during different seasons. As shown in Figure 5.4(a), the alkane/TNMOC ratios measured at all five monitoring sites had similar characteristics to their corresponding total TNMOC concentration, where winter months had the highest values and summer months had the lowest values. The mean concentrations of the alkane group for C1007, C13, C75, C1013, and C88 during winter months were 96.86 ppb-C, 123.11 ppb-C, 150.15 ppb-C, 202.53 ppb-C, and 173.92 ppb-C, respectively; while the corresponding mean concentrations during summer months were 30.61 ppb-C, 42.44 ppb-C, 49.79 ppb-C, 84.46 ppb-C, and 105.47 ppb-C, respectively. C1007 had the largest decrease in mean alkane concentrations from winter to summer, at -68.4%, whereas C88 had the smallest increase, at -39.4%. Again, the percentage change from summer to winter months at C88 was significantly different from the other sites where the KW-test P-value was 0.013. It is important to note that the median summer alkane/TNMOC value at the urban sites was closer to 0.8, while the median values at the non-urban sites were closer to 0.9. The alkane concentrations measured at the urban sites were less

consistent than the non-urban sites where a larger alkane/TNMOC IQR was measured at the urban sites. The more abundant and more consistent alkane sources at the non-urban sites indicated a stronger influence from oil and gas production activities.

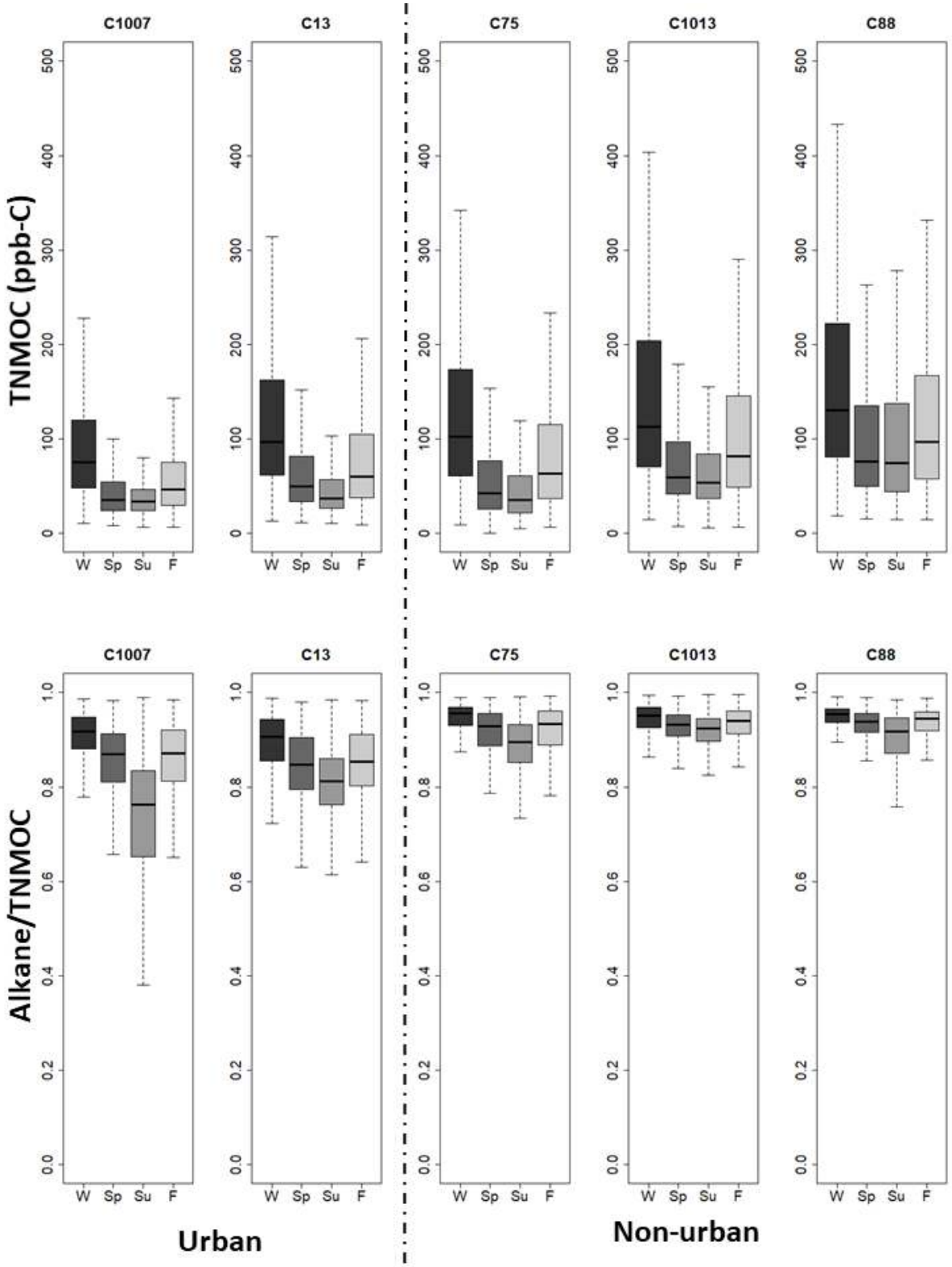

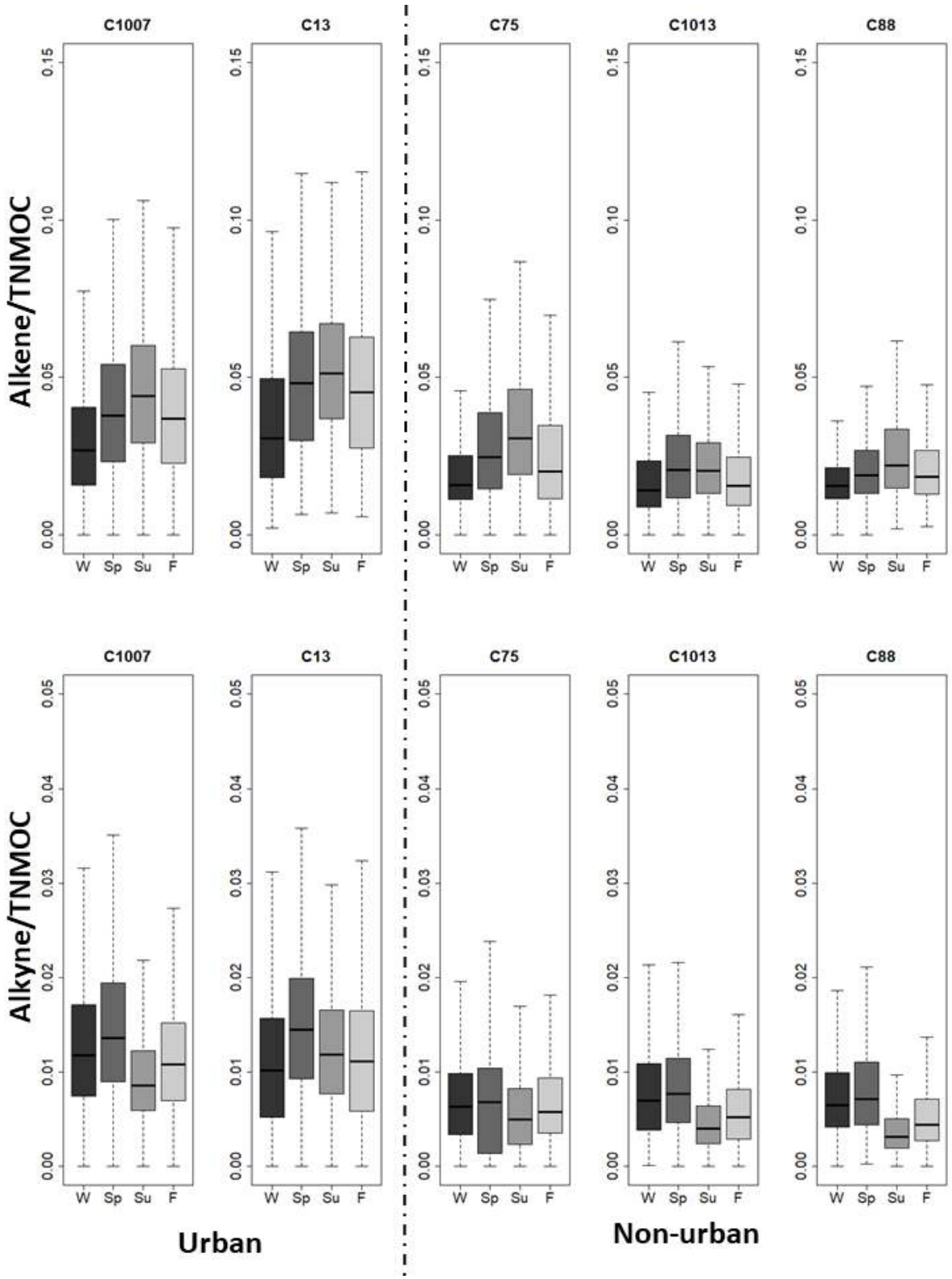
C1007
C13
C75
C1013
C88
Alkene/TNMOC
Alkyne/TNMOC
W Sp Su F
Urban
Non-urban

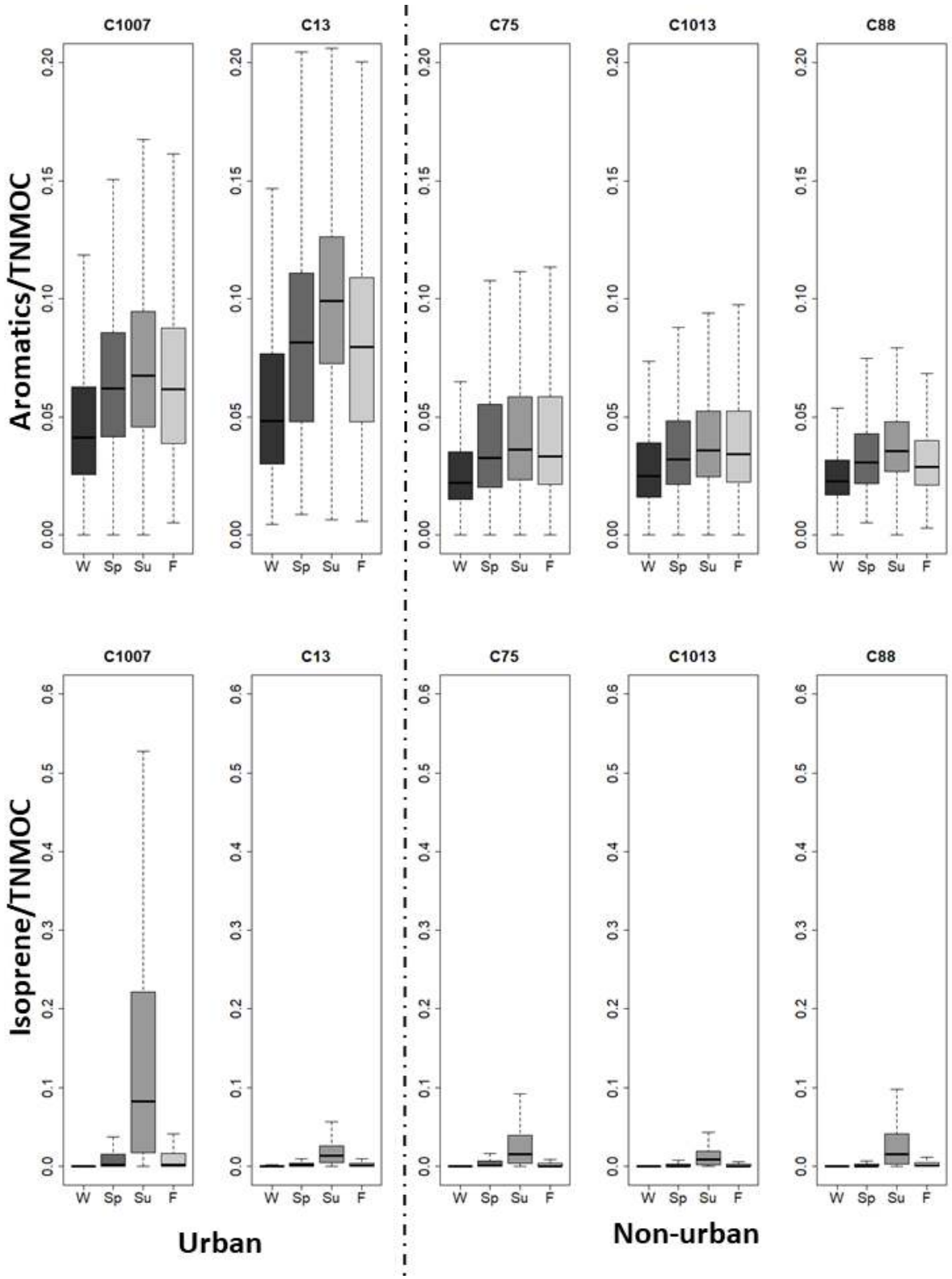

Figure 5.4: Seasonal variation of (a) TNMOC (ppb-C) and alkane/TNMOC concentration ratio, (b) alkene/TNMOC and alkyne/TNMOC concentration ratio, and (c) aromatics/TNMOC and isoprene/TNMOC concentration ratio.

Four of the five monitoring sites, minus C1013, showed alkene/TNMOC ratio characteristics that were inverse to their respective alkane/TNMOC ratios, as shown in Figure

5.4(b), where the summer months had the highest ratios, followed by spring and fall, and the winter months had the lowest ratios. At C1013, the ratios measured in spring was slightly higher than in summer. The mean alkene concentrations measured in C1007, C13, C75, C88 and C1013 during winter months were 2.69 ppb-C, 4.69 ppb-C, 2.34 ppb-C, 2.47 ppb-C, and 2.66 ppb-C, respectively; while the mean concentrations measured during summer were 1.69 ppb-C, 2.43 ppb-C, 1.3 ppb-C, 1.42 ppb-C, and 2.03 ppb-C, respectively. The decrease in alkene concentrations from winter to summer months ranged between -23.8% (C88) to -47% (C13). The percentile change in-between seasons at C88 was again statistically significantly different from the other sites with a KW-test P-value of 0.015. Despite higher alkene concentrations during winter, the alkene/TNMOC ratios were lower during winter months compared to the summer months. The higher summer month alkene/TNMOC ratios were the results of lower TNMOC concentrations during summer months and a lower denominator. There was a significantly larger decrease in the denominator (TNMOC) value from winter to summer months compared to the numerator (alkene) value where the TNMOC concentrations dropped by 88.17 ppb-C on average compared to the 1.19 ppb-C drop in alkene concentrations.

Common anthropogenic sources of alkynes include vehicular exhaust emissions and industrial combustion sources. The highest alkyne/TNMOC ratios were measured during spring at all five monitoring sites, as shown in Figure 5.4(b). At C1007, C75, C1013, and C88, summer months had the lowest alkyne/TNMOC median values; however, at C13, the summer month median values were higher than the fall and winter months, where winter had the lowest median values. The mean concentration of alkyne measured during the winter months at C1007, C13, C75, C88, and C1013 were 0.98 ppb-C, 1.23 ppb-C, 0.77 ppb-C, 0.85 ppb-C, and 0.92 ppb-C, respectively; in the summer months, the corresponding mean concentrations were 0.34 ppb-C, 0.57 ppb-C, 0.25 ppb-C, 0.28 ppb-C, and 0.3 ppb-C, respectively. C1007 had the largest decrease in mean alkyne concentration from the winter to summer months, at 68.1%,

and C13 had the smallest decrease, at 53.9%. The percent-change at C13 was significantly different from the rest of the five sites where the KW-test P-value was 0.011. The larger alkyne/TNMOC ratios at urban sites were the result of lower TNMOC concentrations. The most urbanized C13 had the highest measured concentration of alkyne during the summer months and the smallest decrease in alkyne/TNMOC ratio from winter to spring, which indicated more abundant and more consistent alkyne sources from the urban combustion sources.

As shown in Figure 5.4(c), the median values of the aromatics/TNMOC ratios measured at the urban sites were higher than the non-urban sites. Summer months have the highest aromatics/TNMOC ratios, whereas the lowest ratios were during winter months, despite aromatics concentration being the highest during winter and lowest during summer. The mean concentration of aromatics measured during winter at C1007, C13, C75, C88, and C1013 were 4.03 ppb-C, 7.41 ppb-C, 3.26 ppb-C, 4.19 ppb-C, and 3.84 ppb-C, respectively; while their corresponding summer mean concentrations were 2.79 ppb-C, 4.98 ppb-C, 1.98 ppb-C, 3.03 ppb-C, and 3.61 ppb-C, respectively. C75 had the highest decrease in mean aromatics concentration between winter and summer at -39.3%, whereas C88 had the smallest drop, at only 5.9%. The KW-test showed the difference in percentile change at C88 to be statistically significant from all the other sites with a P-value of 0.013.

The isoprene concentrations measured at C1007 were significantly larger than the other sites. As shown in Figure 5.4(c), the isoprene/TNMOC ratio at C1007 was considerably higher than the other sites. The isoprene concentrations measured at all five sites were highest during summer months and lowest during winter months. Isoprene is a biogenic emission species and is commonly the most abundant during summer months [120]. The mean concentrations for isoprene measured during summer months were 4.96 ppb-C for C1007, 0.63 ppb-C for C13, 0.88 ppb-C for C75, 0.67 ppb-C for C1013, and 1.38 ppb-C for C88, while their corresponding

mean concentrations during winter months were 0.025 ppb-C, 0.082 ppb-C, 0.013 ppb-C, 0.009 ppb-C, and 0.01 ppb-C, respectively. Summer isoprene concentrations at C1007 were 201 times larger than winter between winter concentrations; comparatively, the non-urban sites' isoprene concentrations increased by an average of 92 times while C13 only increased by 6.7 times. The percentile increase observed at C1007 and C13 were statistically significantly different from all other sites according to the KW-test, the P-values were 0.024 and 0.036, respectively.

The variations in alkane concentrations were predominately responsible for the seasonal variations in TNMOC concentrations. The change in the mean concentration of TNMOC, alkane, alkene, and aromatics from winter to summer at C88 was statistically significantly different from the other site. Meteorological conditions at C88 were not significantly different from the other sites; thus, they were unlikely to have been the catalyst behind the significant difference in the seasonal change in TNMOC, alkane, alkene, and aromatics concentrations.

5.4 Spatio-Temporal Distribution of TNMOC

The conditional bivariate probability function (CBPF) plots for the 50^{th}-75^{th} percentile, 75^{th}-95^{th} percentile, and >95^{th} percentile TNMOC measured at the urban and non-urban sites are shown in Figure 5.5 and Figure 5.6, respectively. The 50^{th}-75^{th} percentile plot represents average concentrations, the 75^{th}-95^{th} percentile plot represents high concentrations, and the >95^{th} percentile plot represents extreme conditions.

The 75^{th}-95^{th} percentile CBPF plot for C1007 and C13 had high concentration regions that match the gas well surrounding the sites. The majority of the gas wells surrounding C1007 are on the west-northwest-north sides of the monitoring station, which coincides with the 75^{th}-95^{th} TNMOC CBPF. The 50^{th}-75^{th} CBPF at C13 showed similarities to the gas wells producing less than 1×10^7 MMBtu (blue squares) on Figure A9, whereas the 75^{th}-95^{th} CBPF plot

resembles the pattern formed by the gas wells producing between 1×10^7 and 2×10^7 MMBtu (green squares). C75's 50th-75th TNMOC CBPF also resembles the gas wells surrounding the monitoring station. The other two CBPF plots from C75 showed the highest probability at the northwest side of the monitoring station, which did not visually match the gas-producing wells at the site. Gas wells at C88 had the highest productivity at the southeast and the northwest end of the map, while the 75th-95th CBPF at C1013 had some similarities to its gas production map, as seen in the highest density of wells in the west-northwest-north side of the monitoring station.

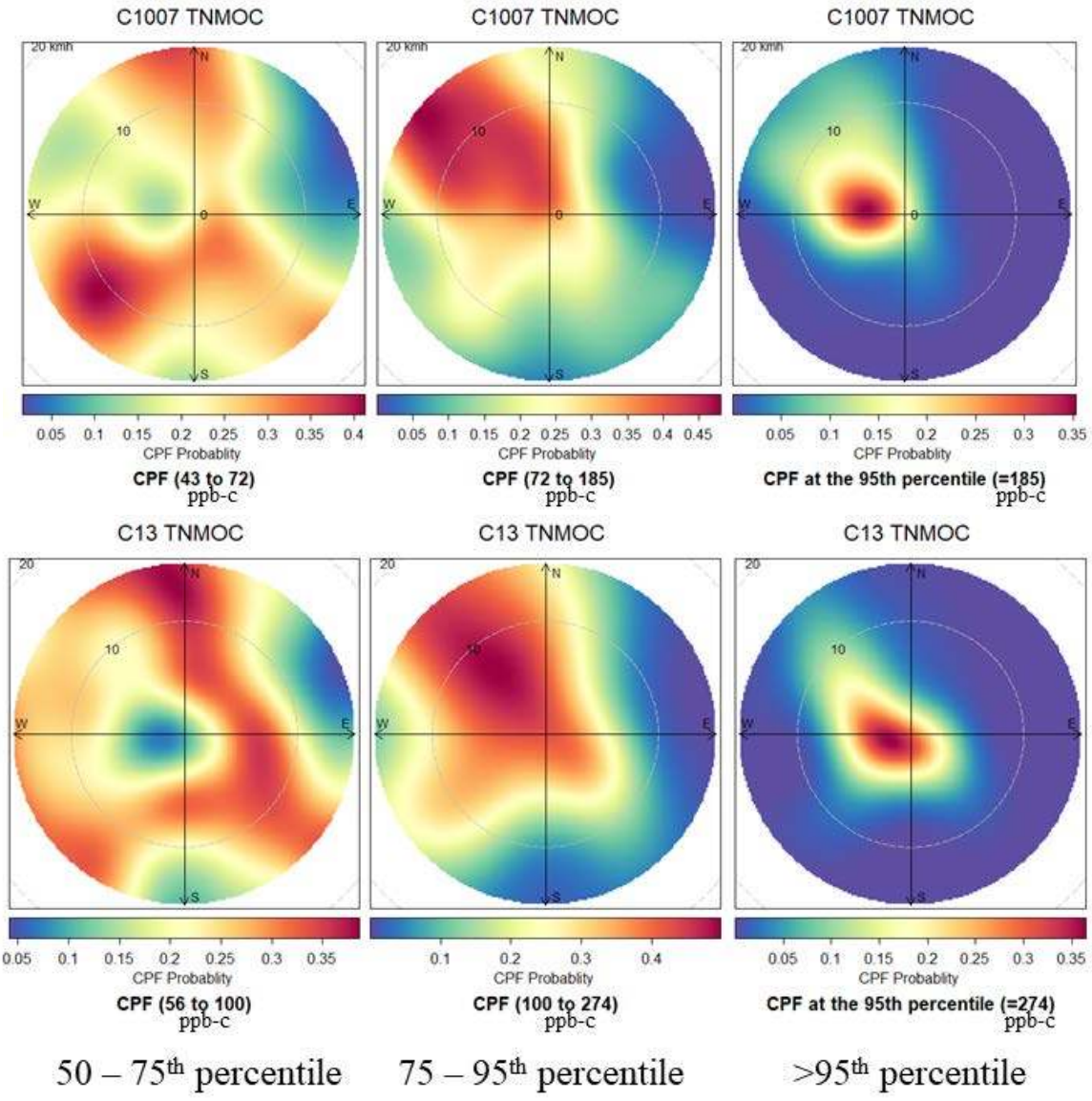

Figure 5.5: Conditional Bivariate Probability Function plot for 50th to 75th percentile, 75th to 95th percentile, and >95th percentile at C1007 and C13.

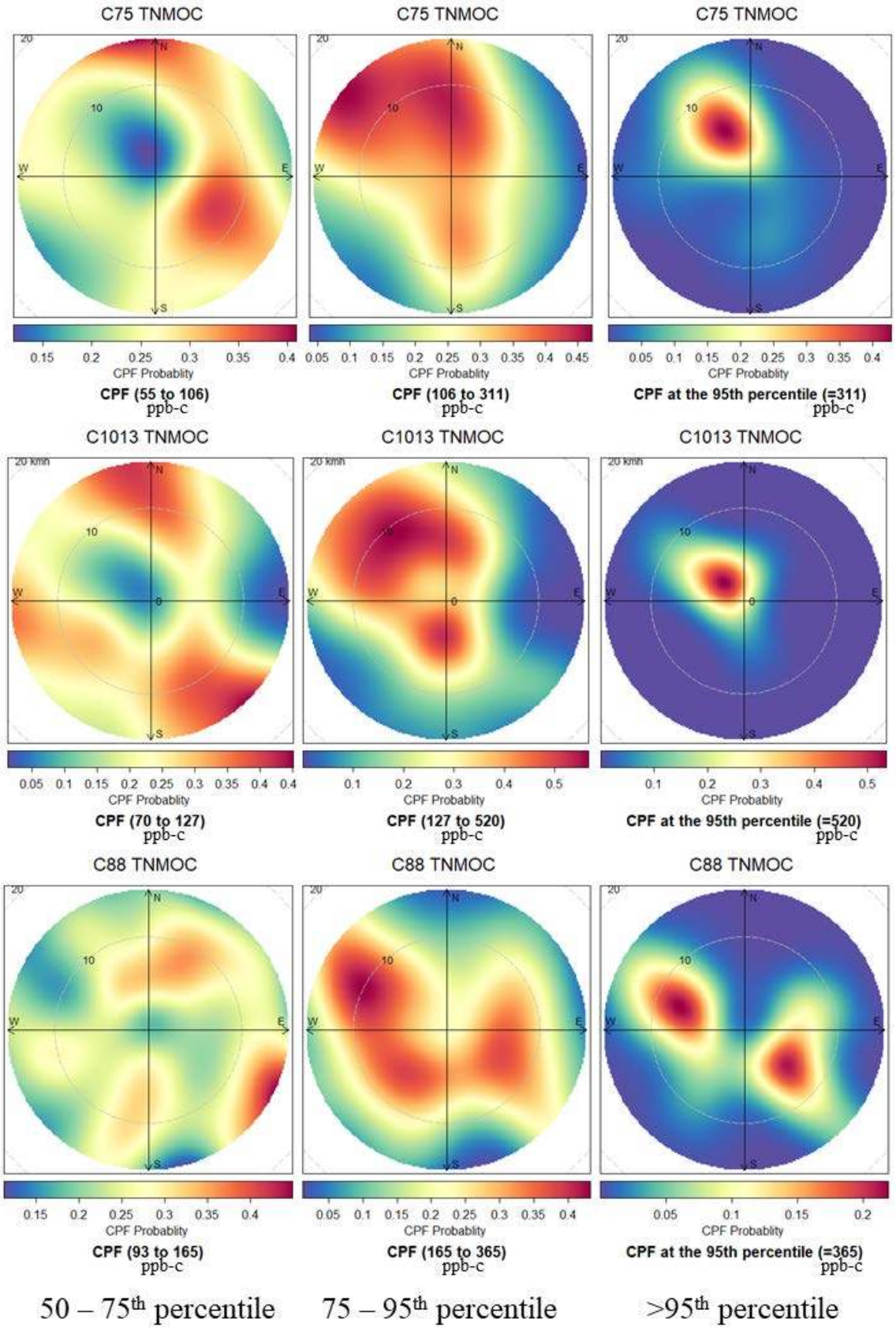

Figure 5.6: Conditional Bivariate Probability Function plot for 50th to 75th percentile, 75th to 95th percentile, and >95th percentile at C75, C1013, and C88.

The CBPF plot shows two higher probability regions, one in the gas well-dense region northwest of the C1013 site and one just south of it. The 50^{th}-75^{th} CBPF also showed a high concentration region at the southeast end of the plot. The Atmos Energy facility is located just south of the monitoring station and was likely the source of this emission. The 75^{th}-95^{th} and the over-95^{th} CBPF plots showed similarities to the gas wells where the highest probability regions were either dense with gas wells (75^{th}-95^{th} plot) or having high production volume (95^{th} plot). The 50^{th}-75^{th} CPBF at C88 had the highest probability at the southeast end of the plot, which was likely emissions from the densely packed gas wells at the southeast end. High probability regions on the >95^{th} CBPFs were on the west side of C1007 and C13, northwest side of C75 and C1013, and both northwest and southeast sides of C88.

5.5 Summary Findings

The emissions from unconventional oil and gas production activities within the Barnett Shale region has had a significant impact on the measured TNMOC concentrations at five ambient air quality monitoring stations in North Texas during 2011-2015. TNMOC concentrations observed at the non-urban sites were, on average, 1.61 times larger than those at urban sites. Alkanes, predominately ethane, were among the most significant contributors to the overall measured TNMOC concentrations. Approximately 88% of the measured TNMOC concentrations at urban sites and 95% of the TNMOC at non-urban sites were n-alkanes. Despite the higher measured concentrations of n-alkanes, the urban sites also were influenced by anthropogenic sources of VOC from motor vehicles and industries, as highlighted by higher alkene, alkyne, and aromatics/TNMOC ratios. The IQR in alkane/TNMOC ratios at the urban sites were also larger than at non-urban sites. While all sites were close to nearby oil and gas activities, there was an evident spatio-temporal variation in the measured TNMOC concentration between the urban and non-urban sites. The measured TNMOC concentrations experienced winter highs and summer lows. However, one of the non-urban sites (C88) was

impacted by VOC year-round from nearby oil and gas production activities. Also, there were significantly elevated isoprene concentrations from biogenic emissions at C1007. The impact of elevated concentrations of TNMOC from oil and gas sources will be an essential factor in understanding the nature of local and regional air quality in North Texas.

CHAPTER 6

A LONG-TERM TREND ANALYSIS OF AIR QUALITY IN THE DALLAS-FORT WORTH AREA: DISCERNING THE IMPACT OF OIL AND GAS EMISSIONS FROM THE BARNETT SHALE

With the increase in exploration for and extraction of unconventional energy sources on a global scale, the impact of unconventional shale gas emissions on air quality has become an increasingly important factor. In this chapter, a long-term study on ground-level ozone and its precursors was conduction using concentration data collected from 2000 to 2018. Air pollutant concentration data from monitoring stations at locations with the following characteristics were retrieved: (i) highly urbanized region with no oil and gas operations (Dallas Hinton, DAL), (ii) moderately urbanized region with significant oil and gas operations (Fort Worth Northwest, FWNW), and (iii) exurban region with a large amount of oil and gas operations (Denton Airport South, DEN). The air pollutant concentration data is on the TAMIS. Ozone, NO_x, CO, and TNMOC concentrations collected between January 1, 2000, and December 31, 2018, were used. Ozone and NO_x concentrations were available in hourly updated values at all three sites. Hourly CO concentration was only available at DAL and FWNW; however, FWNW discontinued its CO monitoring in 2014. While hourly updated TNMOC samples were available in DAL and FWNN, DEN only had access to daily averaged values. These daily averaged TNMOC values were updated every sixth-day. They are collected using steel SUMMA canisters and are analyzed using gas chromatograph-mass spectrometers by TCEQ scientists [33]. Also, FWNW had only started collecting TNMOC samples in November 2003. Since the sixth-day cannister TNMOC data were available for all three sites, we had decided to use this dataset in the study.

Table 6.1 shows the 2008, 2011 and 2014 National Emissions Inventory (NEI) for Criteria and Hazardous Air Pollutants by 60 Emissions Inventory System (EIS) emission

sectors of CO, NO_x, and volatile organic compound (VOC) for Dallas, Tarrant, and Denton county [121]. VOC is synonymous with TNMOC, except for the inclusion of methane concentrations. The U.S. EPA maintains and updates the NEI database every three years. However, the EIS data before 2008 was not publicly available, and the 2017 data was not ready at the time of writing this paper. Dallas county had the highest emissions for all three pollutant types, followed by Tarrant and Denton counties. Also, the emission trends of all three pollutant types were in the decrease between 2008 and 2014.

Table 6.1: National Emissions Inventory (NEI) for Criteria and Hazardous Air Pollutants by 60 Emissions Inventory System (EIS) emission sectors of VOC, CO, and NO_x (tons) [121].

		2008	2011	2014	Change (%/Year)
Dallas	NO_x	62,707.54	51,422.35	45,223.37	-4.65%
	CO	309,104.00	287,281.23	249,323.80	-3.22%
	VOC	68,678.98	56,808.05	50,763.77	-4.35%
Tarrant	NO_x	65,053.60	45,081.84	34,374.22	-7.86%
	CO	203,221.49	200,727.20	151,909.60	-4.21%
	VOC	55,176.21	50,651.33	45,873.04	-2.81%
Denton	NO_x	20,877.80	13,784.60	12,331.40	-6.82%
	CO	62,935.37	60,568.24	50,934.00	-3.18%
	VOC	29,722.38	27,267.55	25,050.71	-2.62%

Temperature, relative humidity, and wind speed play essential roles in ozone production and destruction [122, 123]. Between 2000 and 2018, the regional outdoor temperature increased while relative humidity decreased. The fastest winds (Figure A1) occurred during spring, and the mean wind speed at DAL, FWNW, and DEN were 8.87 km/hour, 11.92 km/hour, and 11.51 km/hour, respectively. Aside from slightly slower wind speeds at DAL, all three sites had very similar meteorological conditions. Thus, the variation in air pollutant concentrations was unlikely to be caused by meteorological conditions. Figure A1 shows the seasonal wind rose diagram of each monitoring station. Throughout the year, the winds are

predominantly southeasterly. Since the monitoring stations were on the eastern end of the Barnett Shale, fugitive emissions from the Barnett Shale had to be carried in by westerly winds, which are uncommon in the region. Hence, any traces of oil and gas emissions found at the monitoring stations are mainly from local sources.

The study period was divided into four distinct periods: 2000-2006, 2007-2009, 2010-2012, and 2013-2018. Between December 2007 and June 2009, the U.S. economy went through a period of turmoil. It ultimately resulted in an economic recession, and this also influenced energy demand and production, which also had a downturn [124]. The observations made between 2000 and 2006 represented the pre-recession period, where the Barnett Shale region saw a massive expansion in shale gas operations. The 2010-2012 period saw the rebound of the U.S. economy and energy production demand. Finally, the 2013-2018 period saw a drop in natural gas productions across the Barnett Shale post-2013 due to low natural gas prices [2].

6.1 Oxides of Nitrogen (NO_x)

Conventional urban anthropogenic sources of NO_x, a precursor to the ozone formation, include gasoline vehicle exhaust, commercial and industrial solvent uses, and power plant emissions [43, 44]. Heavy-duty off-road trucks are used to bring materials to and from the gas wells, and these trucks emit NO_x [125]. There are not many stationary NO_x emission sources, outside of diesel-powered trucks, on shale gas production sites. Thus, NO_x is a good indicator of conventional urban sources.

Between 2000 and 2018, the mean NO_x concentration measured at DAL, FWNW, and DEN were 20.853 ± 0.0814 ppb, 15.852 ± 0.0579 ppb, and 9.094 ± 0.028 ppb, respectively. Between 2000 and 2018, the NO_x concentration decreased by -0.878 ± 0.612 ppb/year (-3.87%/year) at DAL, -0.461 ± 0.374 ppb/year (-2.69%/year) at FWNW, and -0.231 ± 0.353 ppb/year (-1.21%/year) at DEN. The decline in measured NO_x concentration shown at all three sites was likely the result of improvement as a result of better emission control technologies

and the effective implementation of emissions regulation policies [126, 127]. While the mean and 90th-percentile NO_x concentrations at DAL and FWNW had decreased consistently since 2000, DEN's concentration saw an increase from 2002 to 2005, and then followed by a decline post-2006, as shown in Figure 6.1. We suspect the increase in measured NO_x concentrations at DEN from 2002 to 2005 was likely caused by high truck traffic during the development phase as the NO_x emissions from diesel-powered vehicles are significantly higher than gasoline-powered vehicles [128].

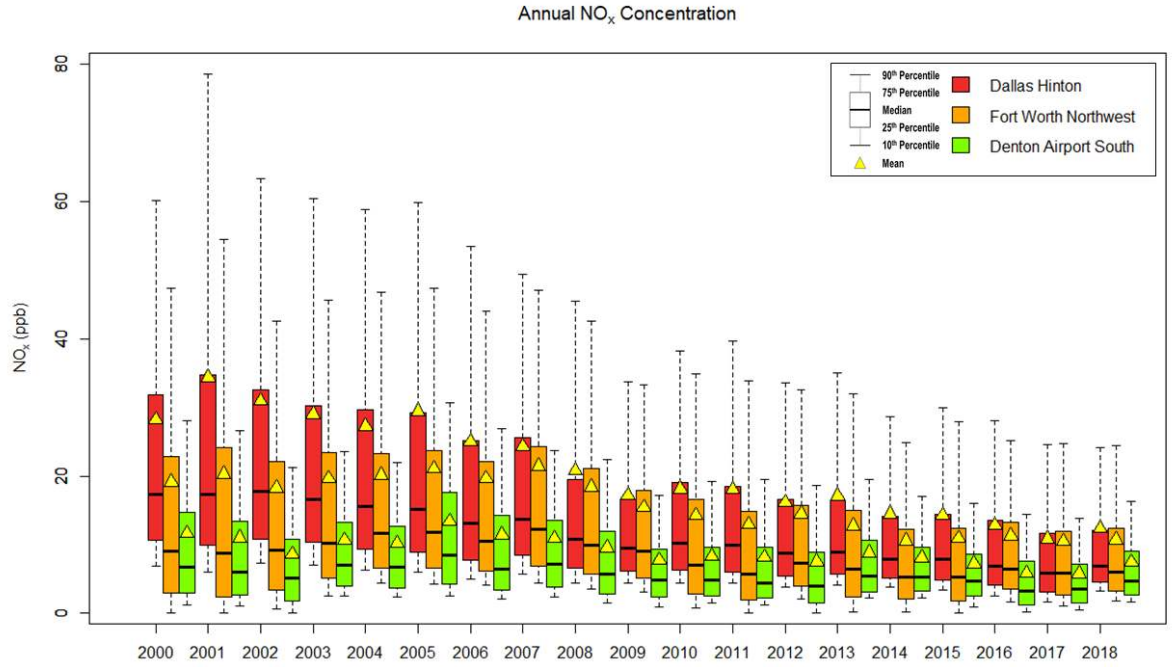

Figure 6.1: Trends of NO_x concentration (ppb) at Dallas Hinton, Fort Worth Northwest, and Denton Airport South.

The mean concentration of NO_x measured at DAL during 2000-2006, 2007-2009, 2010-2012, and 2013-2018 were 29.2 ± 0.177 ppb, 20.7 ± 0.201 ppb, 17.5 ± 0.151 ppb, and 13.7 ± 0.09 ppb, respectively. The mean concentration of NO_x at DAL had decreased by -0.53 ± 1.64 ppb/year (-1.23%/year) during 2000-2006, -3.55 ± 0.05 ppb/year (-15.86%/year) during 2007-2009, -0.95 ± 0.95 ppb/year (-5.25%/year) during 2010-2012, and -0.94 ± 0.72 ppb/year (-5.63%/year) during 2013-2018. The mean NO_x concentration measured at FWNW during 2000-2006, 2007-2009, 2010-2012, and 2013-2018 were 19.8 ± 0.114 ppb, 18.4 ± 0.151 ppb,

13.9 ± 0.132 ppb, and 11.1 ± 0.073 ppb, respectively. Despite an overall downward trend, the annual mean NO_x concentration saw a slight increase from 2000 to 2006 and from 2010 to 2012, at the rate of +0.083 ± 0.592 ppb/year (+0.66%/year) and +0.1 ± 1.4 ppb/year (+1.22%/year), respectively. The mean concentration of NO_x saw a decline by -3.05 ± 0.05 ppb/year (-15.36%/year) during 2007-2009 during the recession and -0.4 ± 0.5 ppb/year (-2.98%/year) during 2013-2018. The mean concentration of NO_x measured at DEN was 11 ± 0.053 ppb during 2000-2006, 9.44 ± 0.069 ppb during 2007-2009, 8.01 ± 0.067 ppb during 2010-2012, and 7.24 ± 0.038 ppb during 2013-2018. The mean NO_x concentration increased by +0.03 ± 0.91 ppb/year (+1.51%/year) during 200-2006, followed by decreased concentrations during the next three periods. The mean NO_x concentration decreased at the rate of -1.625 ± 0.215 ppb/year (-16%/year), -0.425 ± 0.275 ppb/year (-5.17%/year), and -0.286 ± 0.529 ppb/year (-2.2%/year) during 2007-2009, 2010-2012, and 2013-2018, respectively.

The NEI for NO_x (Table 6.1) had decreased by -4.65%/year at DAL, -7.86%/year at FWNW, and -6.82%/year at DEN between 2008 and 2014. During the same period, the mean concentration of NO_x measured at DAL, FWNW, and DEN had decreased by -5.05%/year, -7.12%/year, and -2.5%/year, respectively. The decreased in the measured concentrations at DAL and FWNW were very within a ±1% different from the decrease in the NEI for their respective counties. Both the measured concentrations at DEN and the NEI for Denton county experienced a decline between 2008 and 2014. However, the percent change in NEI was more significant than the percent change in the measured concentration of NO_x at DEN. Thus, it appears that the percent reduction in NEI for NO_x in Denton county may not accurately reflect the local NO_x emissions from sources surrounding DEN.

6.2 Carbon Monoxide (CO)

Carbon monoxide (CO) is a combustion by-product closely associated with traffic and power plant emissions. Conventional urban anthropogenic emission sources can also be

quantified using measured CO concentrations. A high CO concentration is an indicator of fossil-based fuel combustion sources, including gasoline vehicle exhaust and power plant emissions. CO can react with hydroxyl radicals (OH) to form hydroperoxyl radical (HO_2) and carbon dioxide (CO_2), which can lead to ground-level ozone formation [129].

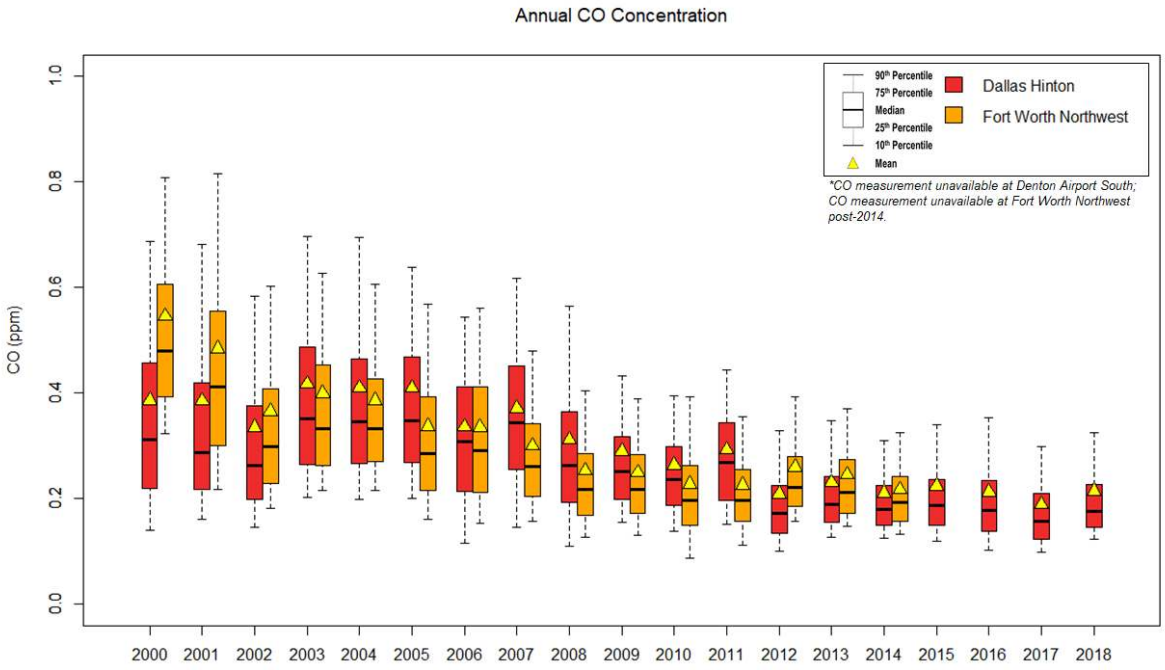

Figure 6.2: Trends of CO concentration (ppm) at Dallas Hinton and Fort Worth Northwest.

The mean concentration of CO measured at DAL between 2000 and 2018 was 0.299 ± 0.0006 ppm, whereas the mean concentration of CO measured at FWNW from 2000 to 2014 was 0.322 ± 0.0006 ppm. DAL and FWNW both saw a decrease in the mean and 90th-percentile CO concentrations, as shown in Figure 6.2. At the beginning of the monitoring period in 2000, the mean and 90th-percentile CO concentrations at FWNW was larger than DAL. While both sites saw an increase in CO concentration between 2002 and 2003, the increase at DAL was more significant than FWNW from 2003 through 2011 as a result of a higher mean and 90th-percentile CO concentrations at DAL. In 2012, the CO concentration at FWNW was higher than DAL. It remained above that recorded in DAL until the monitoring stopped in 2015. Between 2000 and 2018, the mean concentration of CO at DAL decreased by -0.009 ± 0.009

ppm/year (-2.38%/year), whereas FWNW saw a decrease at the rate of -0.023 ± 0.01 ppm/year (-5.85%/year) between 2000 and 2014.

The mean concentration of CO at DAL had experienced a decrease across all four periods. The mean concentrations of CO measured during 2000-2006, 2007-2009, 2010-2012, and 13-08 were 0.384 ± 0.0012 ppm, 0.328 ± 0.0015 ppm, 0.255 ± 0.0009 ppm, and 0.214 ± 0.0006 ppm, respectively. The mean concentration of CO decreased by -0.0085 ± 0.022 ppm/year (-1.46%/year), -0.0405 ± 0.0185 ppm/year (-11.48%/year), -0.0275 ± 0.0565 ppm/year (-8.84%/year), and -0.0034 ± 0.0096 ppm/year (-1.09%/year) during 2000-2006, 2007-2009, 2010-2012, and 13-08, respectively.

At FWNW, the mean concentration of CO was 0.405 ± 0.0011 ppm during 2000-2006, 0.266 ± 0.001 ppm during 2007-2009, and 0.238 ± 0.0009 ppm during 2010-2012. During 2000-2006 and 2007-2009, the mean concentration of CO had decreased by -0.035 ± 0.022 ppm/year (-7.17%/year) and -0.0255 ± 0.0215 ppm/year (-8.62%/year), respectively. Despite a lower mean concentration during 2010-2012 than the previous period, the mean concentration of CO during 2010-2012 increased by +0.016 ± 0.019 ppm/year (+7.12%/year). The increased in CO concentrations observed during 2010-2012 was also observed in the NO_x concentrations measured during the 2010-2012 period.

Between 2008 and 2014, the CO emissions in Dallas and Tarrant counties (Table 6.1) had decreased by -3.22%/year and -4.21%/year, respectively. During the same timeframe, the mean concentration of measured CO from DAL and FWNW had experienced a decrease at the rate of -5.4%/year and -2.31%/year, respectively. While the NEI and measured concentrations both showed decreases, the percent change in the measured concentrations of CO at DAL was significantly higher than the NEI for Dallas county whereas the percent change in the measured concentrations at FWNW was lower than the decreased in Tarrant county NEI for CO. The NEI for CO were countywide estimations whereas the measured concentrations are the result

of local emission sources and the percent change in CO emissions are not necessarily uniform across the county.

Incomplete combustion of gasoline is the primary source of CO in an urban region. The decreased in measured CO concentration at DAL and FWNW was likely achieved through the improvements in vehicle engine efficiency and exhaust control technologies [126, 127].

6.3 Total Non-Methane Organic Carbon (TNMOC)

TNMOC are carbon compounds that react photochemically in the atmosphere. TNMOC includes compounds with low photochemical reactivity, such as methane and ethane, but excludes carbon monoxide (CO), CO2, carbonic acid, and carbonates. In a typical urban region, TNMOC sources include vehicular exhaust emissions, fossil fuel combustion, power plant emissions, industrial and domestic solvent use, oil and gas production facilities, and fugitive emission leaking from pipelines and storage tanks of fuels.

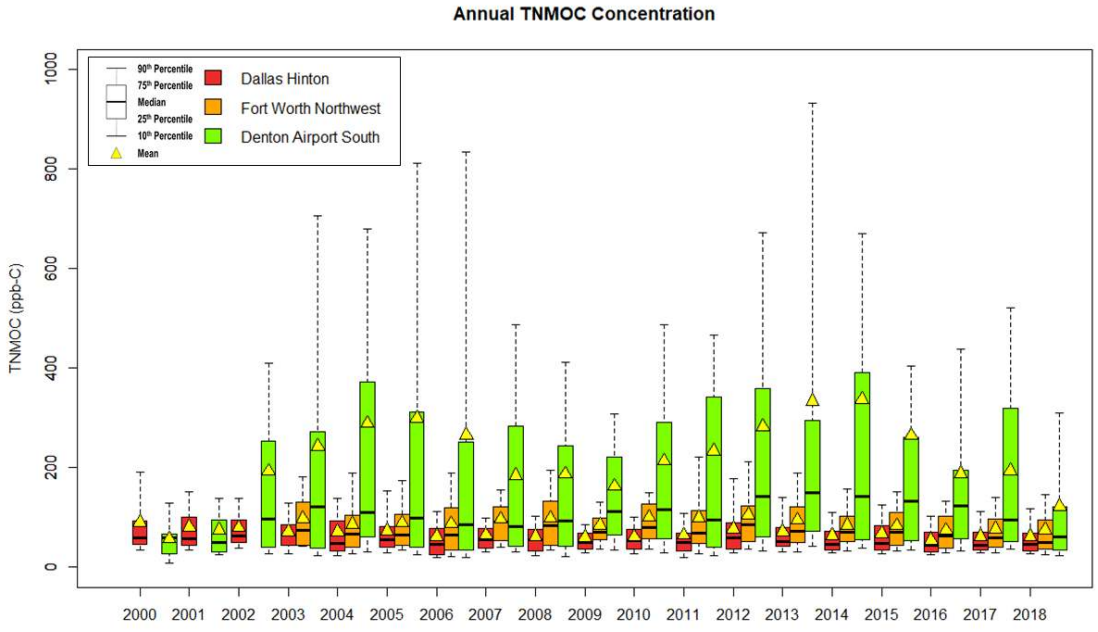

Figure 6.3: Trends of TNMOC concentration (ppb-C) at Dallas Hinton, Fort Worth Northwest, and Denton Airport South.

A detailed summary of the 84 TNMOC species measured at DAL, FWNW, and DEN is available in Table B1. Compared to DAL and FWNW, the mean concentration of TNMOC

measured at DEN was significantly larger. The mean concentration of TNMOC measured at DAL, FWNW, and DEN were 67.4 ± 1.51 ppb-C, 89.31 ± 2.12 ppb-C, and 220.69 ± 10.36 ppb-C, respectively. The TNMOC concentration measured in DEN was 3.3 times larger than DAL and 2.5 times larger than FWNW. DEN was also the only one of the three sites to had shown an increase in measured TNMOC concentration between 2000 and 2018, as shown in Figure 6.3. The enhanced shale gas production activities from surrounding natural gas wells were likely responsible for the extremely high TNMOC concentrations measured at DEN. While not as significant as DEN, the TNMOC concentrations measured FWNW was 32.5% larger than DAL, despite only having approximately half the population size and traffic volume. Thus, unconventional shale gas sources had likely enhanced the TNMOC concentrations measured at FWNW. DAL is not within the Barnett Shale region; conventional urban sources, such as vehicular exhaust and powerplants, were the primary sources of TNMOC at DAL. Like NO_x and CO, the downward trend in the TNMOC concentrations measured at DAL was the result of the successful implementation of clean air act regulations and improvement in emissions control technology.

Between 2000 and 2018, the mean TNMOC concentration measured at DAL had decreased by -1.57 ppb-C/year (-1.62 %/year). The mean concentration of TNMOC measured during 2000-2006 was 73.8 ± 2.84 ppb-C and had experienced a decreased at the rate of -4.63 ppb-C/year (-5.74%/year). During the economic recession in 2008, the mean concentration of TNMOC had dropped to 62.21 ± 2.83 ppb-C and decreased by -2.45 ppb-C/year (-3.87%/year). The mean concentration of TNMOC rebounded to 67.2 ± 3.94 ppb-C during 2010-2012 as the economy came out from the recession; this period saw growth by +8.3 ppb-C/year (+13.06%/year). Finally, the mean concentration of TNMOC dropped to 63.4 ± 2.51 ppb-C and had decreased at the rate of -1.9 ppb-C/year (-2.13%/year) during 2013-2018.

From 2004 to 2018, the mean concentration of TNMOC measured at FWNW saw a slight decrease of -0.81 ppb-C/year (-0.63%/year). The mean concentration of TNMOC during 2000-2006 was 88.2 ± 5.11 ppb-C, and it increased slightly by +0.75 ppb-C/year (+0.91%/year). While the mean concentration of 93.4 ± 4.24 ppb-C was higher when compared to the preceding period, TNMOC concentrations had experienced a decreased by -6.1 ppb-C/year (-6.19%/year) during 2007-2009. The mean concentration of TNMOC measured during 2007-2009 was 101.5 ± 5.6 ppb-C and saw an increase of +2.5 ppb-C/year (+2.51%/year). Lastly, the mean concentrations dropped to 81.4 ± 2.96 ppb-C had decreased by -4ppb-C/year (-4.43%/year) during 2013-2018.

DEN was also the only site to had shown an increase in the mean concentrations of TNMOC between 2000 and 2018 at the rate of +3.59 ppb-C/year (+9.97%/year). The mean concentrations of TNMOC measured at DEN during 2000-2006 was 211 ± 17.6 ppb-C, and there was a +34.61 ppb-C/year (+37.53%/year) increase in the mean concentrations measured during this period. During the recession period of 2007-2009, the mean concentrations dropped to 178.3 ± 16.3 ppb-C, which corresponds to a decreased by -11 ppb-C/year (-5.88%/year). During 2010-2012, the mean concentration of TNMOC was 243.7 ± 23.3 ppb-C and saw an increased by +34.5 ppb-C/year (+15.14%/year). The mean concentration of TNMOC dropped to 241 ± 25 ppb-C and saw a decline by -42.4ppb-C/year (-16.69%/year) during 2013-2018.

Between 2008 and 2014, the NEI for VOC (Table 6.1) decreased by -4.35%/year in Dallas county, -2.81%/year in Tarrant county, and -2.62%/year in Denton county. During 2008-2014, the measured TNMOC concentrations at FWNW had a similar percent change as the NEI for Tarrant county, at the rate of -2.42%/year. However, DAL and DEN both saw an increase in the mean concentration of the TNMOC measured in the same period, at the rate of +0.48%/year and +13.37%/year, respectively. At DAL, the mean concentrations of TNMOC saw an increase during the 2010-2012 period as the economy was recovering from the 2008

recession. The NEI shows that the VOC emissions in Dallas county were decreasing during 2008-2014. However, the decline may not be reflected in the emissions surrounding downtown Dallas, which is one of the largest economic hubs in the state of Texas. Despite a decreased in the NEI for VOC in Denton county, the measured TNMOC concentrations at DEN had increased significantly during 2008-2014. Extremely localized emission sources may impact the TNMOC concentrations measured at DEN. Also, the percent change in the NEI for VOC may not have accurately reflected the percent change in slow reactive hydrocarbon species. These slow reactive species more commonly found in unconventional emission sources, which include shale gas production.

6.3.1 Benzene, Toluene, Ethylbenzene, and Xylene (BTEX)

Benzene, toluene, ethylbenzene, and xylene (BTEX) falls under the U.S. EPA's hazardous air pollutants (HAPs) list, which contains 189 pollutants [130]. Exposure to elevated concentrations of BTEX can lead to eye, nose, and throat irritation, asthma, and increased risk of cancer [131].

DAL had the highest mean concentration of BTEX (sum of mean concentrations of each species) at 7.529 ± 0.825 ppb-C, followed by FWNW at 6.303 ± 0.83 ppb-C, and finally DEN at 5.384 ± 1.099 ppb-C. There was a significant outlier in the measured concentrations at DEN. The mean concentration of toluene measured in 2004 at DEN (8.83 ppb-C) was significantly higher than the rest of the monitoring period (mean of 2.45 ppb-C). Removing the outlier, the mean concentration of BTEX was shown to be in decline at all three sites between 2000 to 2018 at the rate of -0.263 ppb-C/year (-2.08%/year) in DAL, -0.183 ppb-C/year (-2.19%/year) in FWNW, and -0.141 ppb-C/year (-1.99%/year) in DEN. Figure 6.4 shows the annual median concentration of each BTEX species at the three sites. The median concentrations in 2018 were significantly lower than the beginning of the monitoring period at all three sites.

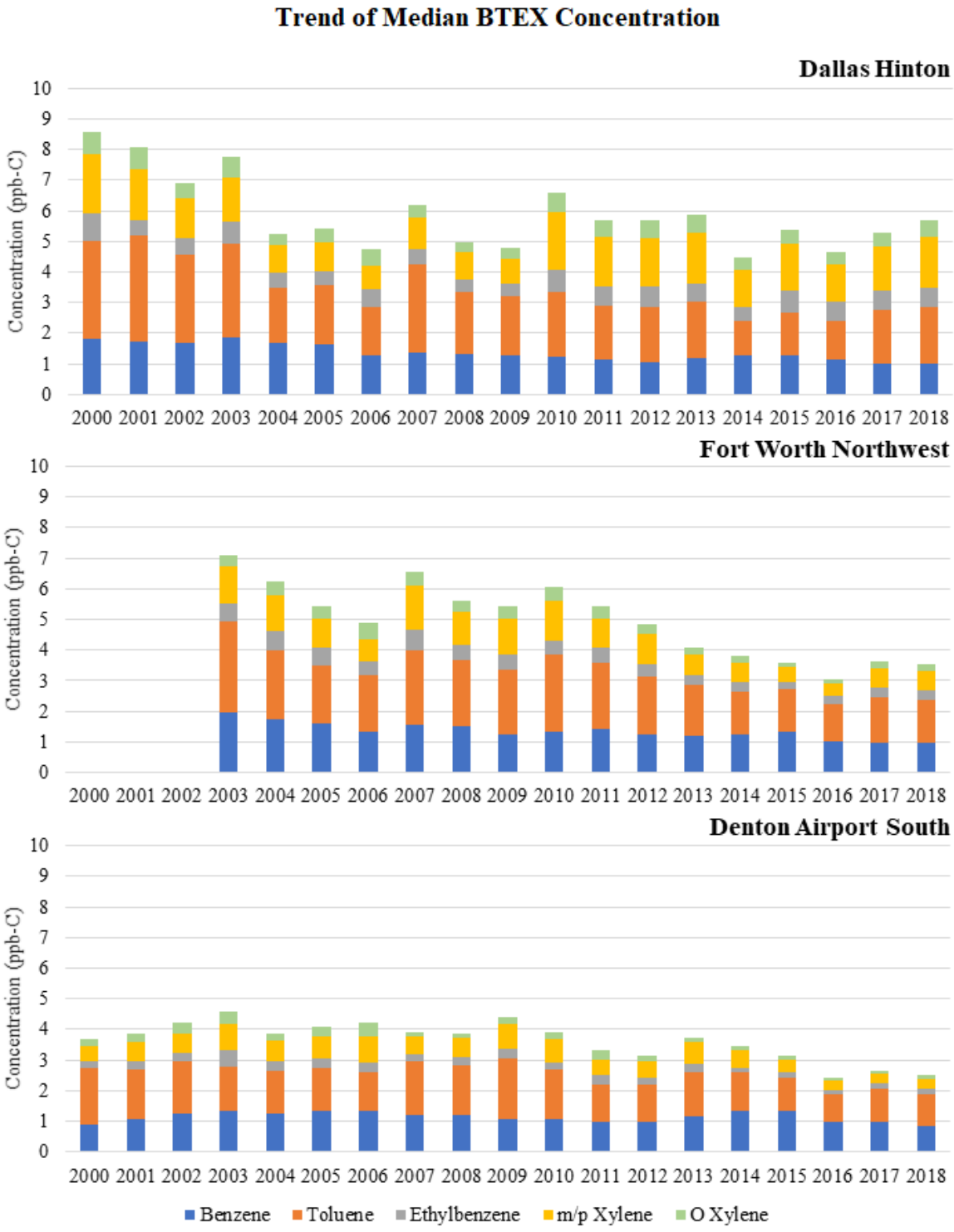

Figure 6.4: Trend of median BTEX concentrations (ppb-C) in Dallas Hinton, Fort Worth Northwest, and Denton Airport South.

The mean concentration of BTEX measured at DAL had decreased during 2000-2006, 2007-2009, and 2013-2018 at the rate of -0.677 ppb-C/year (-6.82%/year), 0.71 ppb-C/year (-9.92%/year), and -0.164 (-0.92%/year), respectively. However, DAL's mean concentration of

BTEX saw in increase of +0.055 ppb-C/year (+1.12%/year) during the 2010-2012 period, which was the effect of increased economic and commercial activities following the rebound from the economic recession. During all four periods, the mean concentration of BTEX measured at FWNW were in decline, at the rate of -0.04 ppb-C/year (-0.55%/year), -1.375 ppb-C/year (-16.17%/year), -0.59 ppb-C/year (-7.93%/year), and -0.202 ppb-C/year (-3.74%/year), respectively. At DEN, the mean concentration of BTEX increased during 2000-2006 and 2007-2009 by +0.158 ppb-C/year (+3.66%/year) and +0.38 ppb-C/year (+7.74%/year), respectively. In 2010-2012, the mean concentration of BTEX measured in DEN dropped at the rate of -0.2 ppb-C/year (-4.1%/year), and it decreased further during 2013-2018 by -0.66 ppb-C/year (-12.56%/year). While BTEX concentrations at DEN was increasing during 2007-2009, the mean concentration in 2007 (4.76 ppb-C) was significantly smaller than 2006 (5.84 ppb-C), which was caused by the impacts from the economic recession starting in 2007.

Between 2008 and 2014, the median concentration of BTEX at DAL, FWNW, and DEN had decreased at the rate of -1.65%/year, -5.25%/year, and -1.82%/year, respectively. While the percent change in the measured concentration of BTEX was different from the NEI for VOC (Table 6.1), we had observed downward trends for both the emission and measured concentrations. BTEX species are commonly found in urban [117, 48, 49]. Since the majority of the 60 EIS emission sectors are conventional urban emission sources [121], the overall trend of the NEI mirrors the measured BTEX concentrations.

Bunch et al. [5] had correlated the mean concentrations of benzene at DAL and FWNW to the natural gas well count in the Barnett Shale. They had stated that conventional urban sources were the primary source of benzene emissions in the region, and the increased Barnett Shale activities do not have a direct correlation with benzene emissions. While decreased in BTEX concentrations were observed at DAL and FWNW, the increase in BTEX concentration at DEN between 2000 and 2010 strongly suggests that the influence of shale gas well

developments. Increased truck traffic in the region during the development phases of wells likely had caused the increase in BTEX concentration at DEN.

6.3.2 Natural Gas Production Impacts on TNMOC Levels

Tarrant and Denton are two major shale gas producing counties within the Barnett Shale. Since DAL is outside of the shale gas region, and there were no gas wells built within 5-km of the monitoring station. Figure 6.5 shows the number of active gas wells within 5-km from FWNW and DEN; and their total annual production. By the end of 2018, there were 157 active gas wells within 5-km of FWNW and 213 active gas wells within 5-km of DEN. From 2000 to 2018, the gas wells within 5-km from FWNW and DEN produced a total of 2.75 × 108 MMBtu and 2.5 × 108 MMBtu in natural gas, respectively. Between 2003 and 2012, FWNW saw an increased in the number of active gas wells surrounding the monitoring station, which correlated well with the increase in measured TNMOC concentrations during this period.

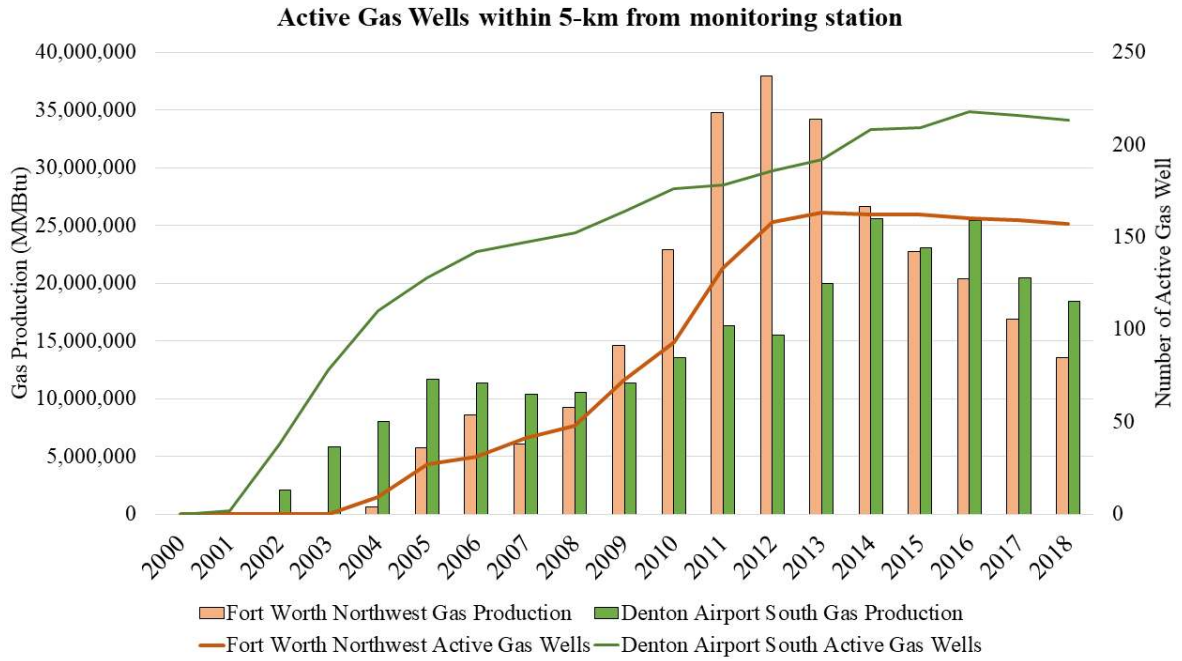

Figure 6.5: Number of active gas wells within 5-km from Fort Worth Northwest and Denton Airport South along with the total natural gas production volume (MMBtu).

The emissions released during the development and production phases of these gas wells contributed significantly to the growth in TNMOC concentrations at FWNW through 2011

(Figure 6.3). While the number of active gas wells surrounding FWNW had stayed relatively constant since 2012, their production volume had dropped significantly. There was a decline in natural gas production across the Barnett Shale gas region due to a drop in natural gas prices [2]. The TNMOC concentrations post-2012 also showed a similar trend to the natural gas production volume from the gas wells that surround FWNW.

The 90^{th}-percentile value of TNMOC measured at DEN had two peaks, one in 2006 and the other in 2013 (Figure 6.3); both peaks were followed by a decrease, as shown during 2007-2009 and 2013-2018. There was a substantial increase in the number of active wells surrounding DEN from 2000 through 2006. The increased gas well development activities had contributed to a rapid increase in the measured TNMOC concentrations, peaking in 2006. Starting in 2007, the growth in the number of active gas wells had significantly dropped due to the economic depression; this had contributed to the decrease in TNMOC concentrations during the 2007-2009 period. The production volume from the gas wells surrounding DEN increased consistently from 2009 through 2014, and this culminated in a peak in mean concentrations of TNMOC during 2013-2014. Since 2014, natural gas production volumes have dropped significantly. As a result, there was a substantial decrease in the measured TNMOC concentrations during 2013-2018.

Acetylene/TNMOC and ethane/TNMOC concentration ratios were used to identify the changes in emissions from vehicle exhaust and natural gas sources, respectively. Ethane is a TNMOC species found abundantly in oil and gas emissions, whereas high concentrations acetylene points to fossil fuel burning and vehicular exhaust emissions [48, 49, 50, 51, 117, 132]. The mean of acetylene/TNMOC concentration ratios calculated for DAL, FWNW, and DEN was 0.028 ± 0.0007, 0.019 ± 0.0004, and 0.01 ± 0.0004, respectively; whereas the mean of ethane/TNMOC concentration ratios was 0.229 ± 0.002 at DAL, 0.296 ± 0.003 at FWNW, and 0.342 ± 0.003 at DEN. Figure 6.6 shows all a decrease in the acetylene/TNMOC

concentration ratio and an increase in the ethane/TNMOC concentration ratio at all three sites.

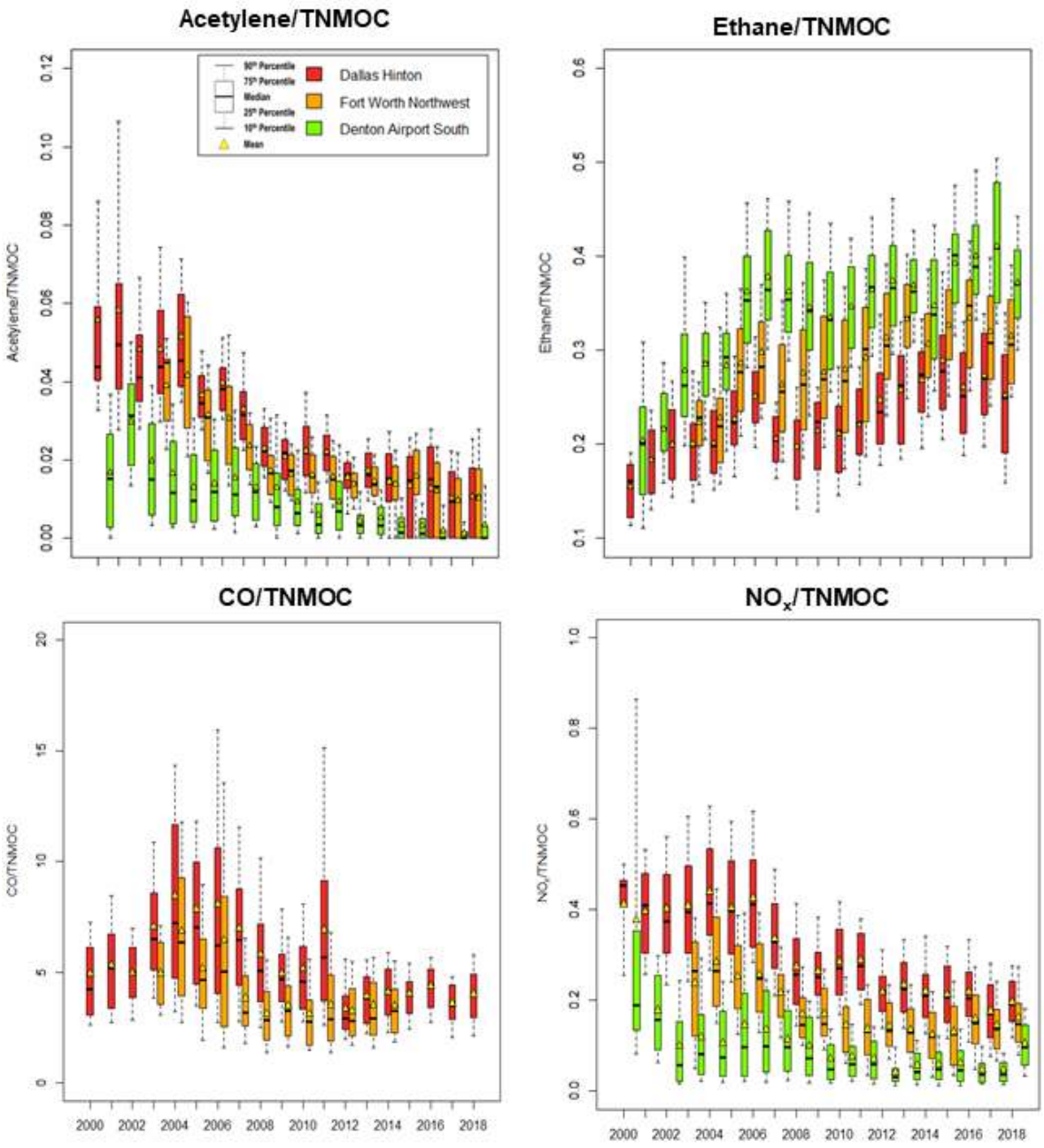

Figure 6.6: Trends of acetylene/TNMOC, ethane/TNMOC, CO/TNMOC, and NO_x/TNMOC concentration ratio.

Like acetylene, CO, and NO_x concentrations in urban regions are also usually emitted from vehicular exhaust sources. The mean of CO/TNMOC concentration ratios was 5.467 ± 0.105 at DAL and 4.184 ± 0.117 at FWNW. In contrast, the mean of NO_x/TNMOC concentration ratios was 0.298 ± 0.004, 0.176 ± 0.003, and 0.0995 ± 0.003 at DAL, FWNW, and DEN, respectively. CO/TNMOC and NO_x/TNMOC concentration ratios increased during 2000-2004

but was followed by a continued decrease throughout 2018 except for a slight increase during 2010-2011. The acetylene/TNMOC, CO/TNMOC, and NO_x/TNMOC concentration ratios all followed a similar downward trend. The decline indicates deceased impacts from the gasoline-powered vehicular exhaust and other combustion-related sources. On the other hand, the increase in ethane/TNMOC concentration ratios suggests the increased impacts of unconventional oil and gas emissions in the region.

According to Baker et al. [133], the typical concentrations of propane in U.S. cities during summertime is between the range of 0.87 ppb-C to 10.53 ppb-C. The mean concentrations of propane measured during summertime at DAL and FWNW were 6.283 ± 0.167 ppb-C and 8.02 ± 0.307 ppb-C, respectively, and were both within the range observed in other major U.S. cities. The mean concentration of propane measured in DEN during summertime was 26.028 ± 2.62 ppb-C, which was much higher than the typical urban propane concentrations. The mean concentration of summertime propane measured at DEN more closely resembled the concentrations measured at other oil and gas regions. The concentration fall between the concentrations measured at Colorado's Northern Front Range metropolitan area (24 ppb-C) [134] and the Marcellus Shale (39 ppb-C) [135].

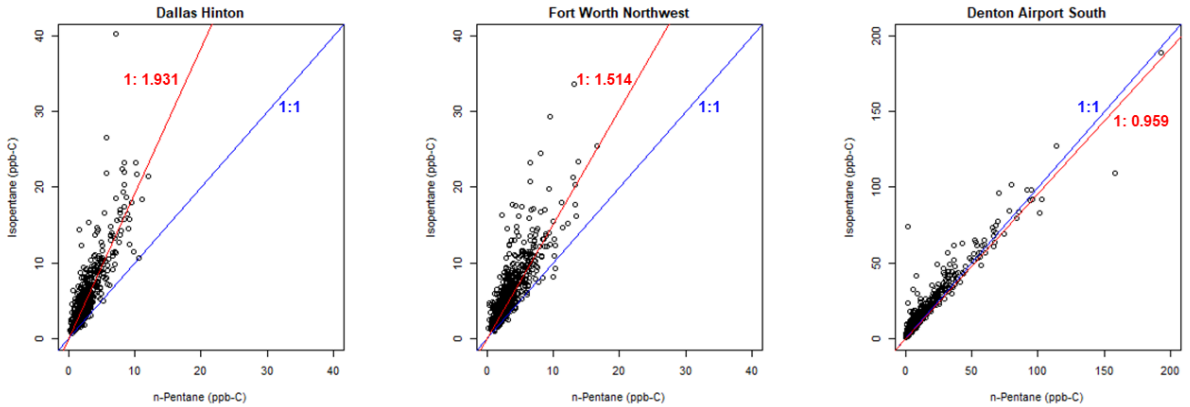

Figure 6.7: Relationship between isopentane and n-pentane at Dallas Hinton, Fort Worth Northwest, and Denton Airport South.

Oil and gas production-related emissions can be differentiated from gasoline-powered

vehicular emissions through isopentane/n-pentane concentration ratios. Regions with higher vehicle emissions have isopentane/n-pentane ratios greater than one. In contrast, regions with higher natural gas emissions have an isopentane/n-pentane ratio under one and closer to 0.9 [135]. As shown in Figure 6.7, DAL and FWNW have isopentane/n-pentane ratios higher than one, at 1.931 and 1.514, respectively. DEN's ratio was lower than one, at 0.959. Thus, there was a stronger impact from gasoline vehicle sources at DAL and FWNW, while DEN had a stronger impact from natural gas sources.

While the gas wells surrounding FWNW had the highest total production volume among the three, FWNW showed a weaker influence from the oil and gas activities compared to DEN. We suspected that local legislatures and regulations on gas well development and production played an important role in lowering the measured TNMOC concentration at FWNW. Lewis et al. [136] stated that setback distance for new wells should be at least a quarter-mile (402.34-m) from human activity. Also, extra distance should be placed when dealing with sensitive groups such as the sick and young children. A setback distance prohibits new wells to be built within a designated distance of residences, hospitals, parks, and religious-use buildings. However, there is no consensus setback distance in the state of Texas. The setback distance in place in the city of Fort Worth is 600-feet (182.88-m). Between 2001 and 2012, the setback distance of new wells in the city of Denton was just 500-ft (152.4-m); the city increased the distance to 1,200-feet (365.8-m) in January 2013 (Fry, et al., 2015). While the difference between the setback distance in the city of Fort Worth and Denton was only 30.48-m throughout most of the study period, it more heavily affects the gas well developments in Fort Worth than Denton. FWNW is in a densely populated urban region in the city of Fort Worth, while DEN is in a sparsely populated exurban region outside of the city of Denton. There are minimal locations where new wells can be built in the city of Fort Worth and comply with the Fort Worth Ordinance's setback distance. In contrast, the wells that surround DEN had

much more building freedom as there are fewer safe use structures that surround the site. Also, regulation of gas well air emissions is maintained by the local government [33]. The gas wells within the city would be regulated more strictly compared to gas wells outside city limits, as the emissions from these gas wells would pose a more severe threat to human health.

6.3.3 Implication on Methane Levels

Emissions from natural gas sources are predominantly composed of methane; however, none of the three monitoring stations have methane monitoring equipment. In a previous study, the ethane-to-methane (C_2/C_1) molar ratios for dry and wet natural gas in the Barnett Shale were 0.03 and 0.15, respectively [137]. A fence line measurement study identified that the mean concentration of methane is significantly higher at regions that produce dry gas compared to regions that produce wet gas [138]. FWNW in Tarrant County is a dry gas site while DEN in Denton County is a wet gas site with productions of both natural gas and liquid condensates [139]. Based on the C_2/C_1 molar ratios, we estimated the mean concentration of methane at FWNW and DEN to be 468.21 ± 14.7 ppb-C and 266.98 ± 13 ppb-C, respectively. Also, there were 84 instances where the estimated methane concentration at FWNW was larger than 1 ppm-C from 2003 to 2018. In contrast, there were only 60 instances at DEN from 2000 to 2018.

6.4 Ozone

Ozone nonattainment is a significant air quality issue in the DFW metroplex region. Nine of the thirteen counties in the DFW metroplex, including Dallas, Tarrant, and Denton, consistently fail to comply with the U.S. EPA's ozone NAAQS [41]. The design value for ozone is the annual fourth-highest daily maximum 8-hour ozone concentration averaged over three years. Since its inception, the U.S. EPA had made several revisions to the ozone compliance thresholds. The ozone design values to obtain ozone attainment status, based on 1997, 2008, and 2015 revisions, are 80-, 75-, and 70-ppb, respectively [140].

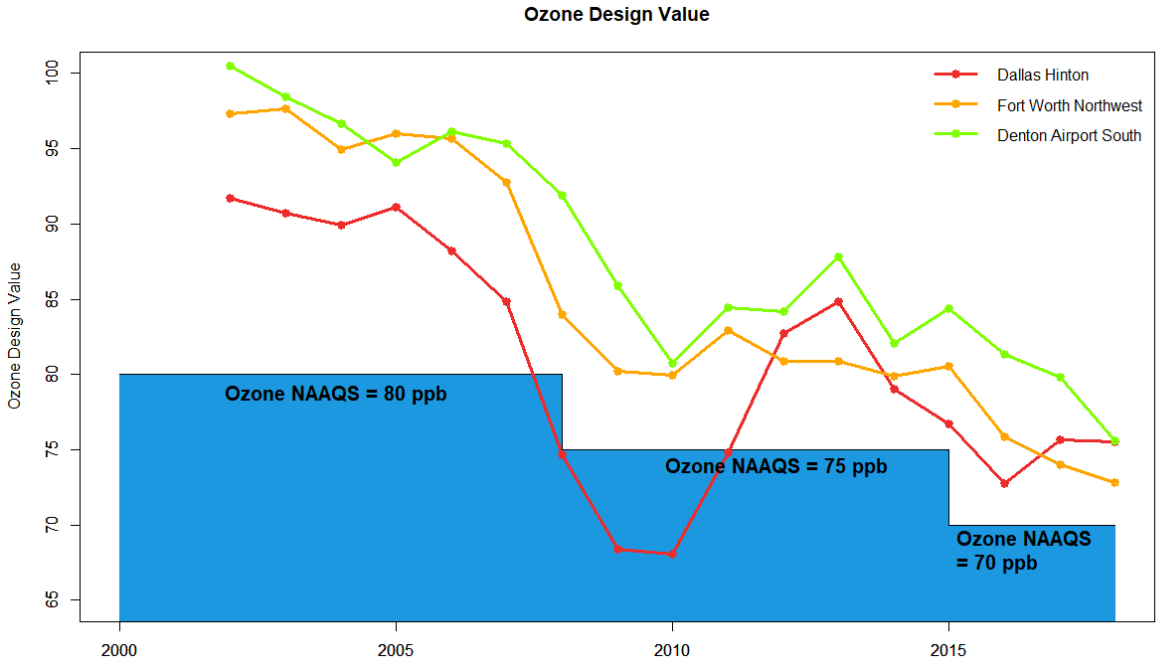

Figure 6.8: Ozone values at for Dallas Hinton, Fort Worth Northwest, and Denton Airport South.

While the three-year averaged annual fourth-highest daily maximum 8-hour ozone concentration (ozone value) in 2018 was lower than in 2002, the most substantial reduction occurred before 2010. Figure 6.8 shows the ozone values for DAL, FWNW, and DEN alongside the U.S. EPA's ozone NAAQS design values. FWNW and DEN were never in attainment throughout the study period. In contrast, DAL was briefly attainment the NAAQS for ozone from 2008 through 2011. Aside from 2005, the ozone value at DEN was consistently higher than the two urbanized sites. DAL's ozone value dropped from 91.7 ppb in 2002 to 75.6 ppb in 2018, a rate of -1 ± 1.17 ppb/year or -1.03%/year. FWNW saw a -1.53 ± 0.69 ppb/year or -1.57%/year decline in the ozone value from 97.3 ppb to 72.8 ppb. DEN's ozone value dropped from 100 ppb to 75.6 ppb, which was a -1.53 ± 0.78 ppb/year or -1.67%/year decrease on average. Ozone values had experienced a decreased at all three sites before 2010. During the 2000-2006 period, the ozone values decreased by -0.88 ± 0.84 ppb/year (-0.96%/year) at DAL, -0.4 ± 0.82 ppb/year (-0.4%/year) at FWNW, and -0.95 ± 1.04 ppb/year (-0.95%/year) at DEN. The ozone values decreased further during 2007-2009, at the rate of -8.25 ± 1.95 ppb/year (-10.22%/year), -6.3 ± 2.5 ppb/year (-7%/year), and -4.7 ± 1.3 ppb/year (-5.05%/year)

at DAL, FWNW, and DEN, respectively. During 2010-2012, the ozone values increased by +7.3 ± 0.6 ppb/year (+10.2%/year) at DAL, +0.45 ± 2.45 ppb/year (+0.61%/year) at FWNW, and +1.7 ± 1.9 ppb/year (+2.11%/year) at DEN. The 2013-2018 period saw a decrease in ozone values at the rate of -1.86 ± 1.54 ppb/year (-2.22%/year) at DAL, -1.62 ± 0.89 ppb/year (-2.06%/year) at FWNW, and -2.44 ± 1.36 ppb/year (-2.89%/year) at DEN.

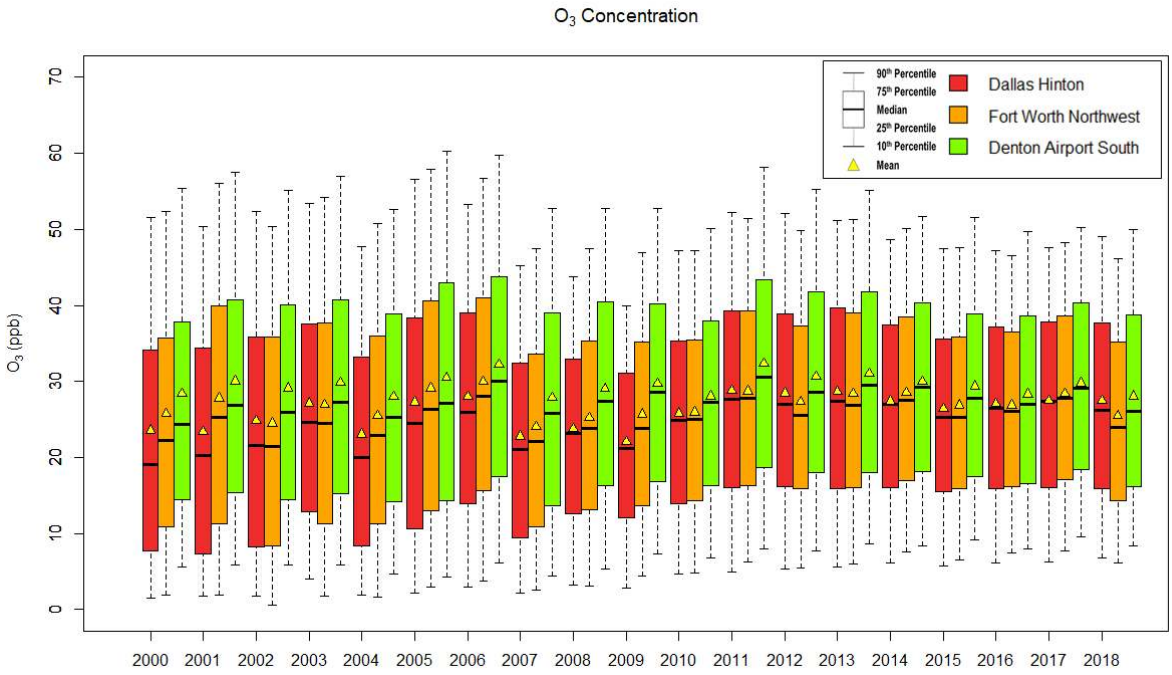

Figure 6.9: Trends of ozone concentration (ppb) at Dallas Hinton, Fort Worth Northwest, and Denton Airport South.

Figure 6.9 shows the mean concentrations of ozone measured at DAL, FWNW, and DEN between 2000 and 2018, which were 25.98 ± 0.044 ppb, 26.91 ± 0.045 ppb, and 29.61 ± 0.046 ppb, respectively. Despite the fact that a uniform decreased in ozone value between 2000 and 2018 across all three sites, the mean concentration of ozone measured at DAL increased by +0.21 ± 0.56 ppb/year (+1.28%/year), from 23.6 ± 0.22 ppb in 2000 to 27.5 ± 0.17 ppb in 2018. FWNW and DEN both saw a slight decrease in the mean concentration of ozone at the rate of -0.02 ± 0.57 ppb/year (-0.3%/year) and -0.02 ± 0.47 ppb/year (-0.15%/year), respectively. During 2000-2006, all three sites saw an increase in the mean concentration of ozone, at the rate of +0.73 ± 1.13 ppb/year (+3.4%/year) at DAL, +0.7 ± 1.07 ppb/year

(+2.96%/year) at FWNW, and +0.633 ± 0.68 ppb/year (+2.25%/year) at DEN. Despite the recession during 2007-2009, DAL was the only site that saw a decreased in the mean concentration of ozone, at the rate of -0.35 ± 1.25 ppb/year (-1.4%/year); at FWNW and DEN, the mean concentration of ozone increased by +0.8 ± 0.3 ppb/year (+3.27%/year) and 0.95 ± 015 ppb/year (+3.35%/year), respectively. All three sites saw a rise in the mean concentration of ozone during 2010-2012. The mean concentration of ozone increased by +1.35 ± 1.65 ppb/year (+5.29%/year) at DAL, +0.7 ± 2.1 ppb/year (+2.97%/year) at FWNW, and +1.3 ± 2.9 ppb/year (+5%/year) at DEN. Finally, the mean concentration of ozone fell by -0.24 ± 0.39 ppb/year (-0.81%/year), -0.58 ± 0.76 ppb/year (-1.98%/year), and -0.6 ± 0.55 ppb/year (-1.94%/year) during 2013-2018 at DAL, FWNW, and DEN, respectively.

Any day with observed eight-hour averaged daily maximum ozone concentration greater than 70 ppb was regarded as a high ozone day. 70 ppb was chosen as the threshold based on the 2015 NAAQS revisions. The total high ozone days during 2000-2018 was 345 at DAL, 416 at FWNW, and 582 at DEN. Despite its location in the least urbanized site of the three, DEN had the highest ozone value, the mean concentration of ozone, and the number of high ozone days. Thus, conventional urban emission sources are not the primary factor that was severely contributing to ozone formation in the region, especially at DEN.

6.4.1 TNMOC-NO_x-Ozone Relationship

TNMOC/NO_x concentration ratios are often integrated into the development of ozone control strategies. These concentration ratios can identify whether a region's ozone generated is limited by either TNMOC or NO_x concentrations [129]. The formation of ozone is highly depended on the reaction of OH radicals between TNMOC and NO_x, where ozone generation peaks when the OH reaction rate from TNMOC and NO_x are equal. The reactions between OH radicals and TNMOC is dominant when the TNMOC/NO_x concentration ratio is high. In contrast, the reactions between OH radicals and NO_x is more dominant when the TNMOC/NO_x

concentration ratio is low. When the OH radical's reaction with TNMOC is more dominant, the ozone generation will be more sensitive to changes in NO_x concentration. The ozone generation will be more susceptible to changes in the TNMOC concentrations if the reaction between OH radicals and NO_x is dominant. In a TNMOC-sensitive ozone regime (TNMOC/NO_x concentration ratio < 4), the percent reduction in TNMOC will result in a higher rate of decrease in ozone relative to percent reduction in NO_x. In a NO_x-sensitive ozone regime (TNMOC/NO_x concentration ratio > 15), the percent reduction in NO_x will be more effective in reducing ozone relative to percent reduction in TNMOC [129].

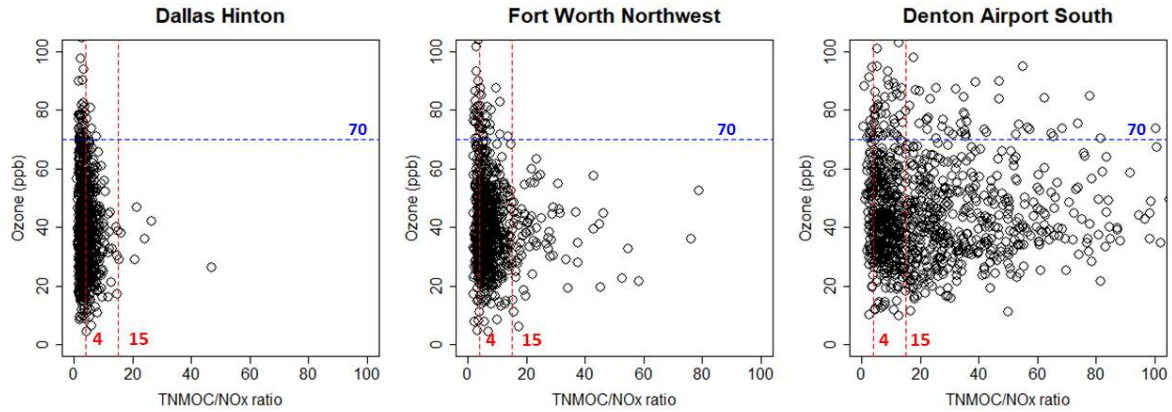

Figure 6.10: Relationship between ozone concentration and the corresponding TNMOC/NO_x ratios.

All the high ozone days in DAL and FWNW between 2000 and 2018 occurred when the TNMOC/NO_x concentration ratio was under 15. In contrast, close to half (48%) of all high ozone days in DEN occurred when the TNMOC/NO_x concentration ratio was over 15, as shown in Figure 6.10. In DAL, 88% of the high ozone days occurred when the TNMOC/NO_x concentration ratios were <4. About 47% of all high ozone days measured in FWNW occurred when the TNMOC/NO_x concentration ratio was between 4 and 15. The average TNMOC/NO_x concentration ratio during high ozone days at DAL was around 2.9. It showed characteristics of a TNMOC-sensitive ozone regime. At FWNW, the average TNMOC/NO_x concentration ratio was 4.76 during high ozone days, which would barely place it in a transitional regime.

Reductions in both TNMOC and NO_x concentrations would help reduce ozone formation [141]. The high ozone days TNMOC/NO_x concentration ratio at DEN had an average ratio of 28.1, which implied a NO_x-sensitive ozone regime.

Figure A3 through Figure A5 shows the TNMOC/NO_x concentration ratios measured at all three sites, had shown a constant increase throughout the four periods. The increase in TNMOC/NO_x concentration ratio at DAL was predominately the result of the decreased in NO_x concentrations (R^2-value for changes in NO_x and TNMOC versus changes in TNMOC/NO_x concentration ratio were 0.88 and 0.1, respectively). In contrast, DEN's TNMOC/NO_x concentration ratio showed stronger influence from increased in TNMOC and decreased in NO_x concentrations (R^2-value for changes in NO_x and TNMOC versus changes in TNMOC/NO_x ratio were 0.38 and 0.56). FWNW's R^2-values for the changes in NO_x and TNMOC versus the changes in TNMOC/NO_x concentration ratio were both <0.001. Thus, there was no linear relationship between changes in NO_x and TNMOC concentration with changes in TNMOC/NO_x concentration ratio at FWNW.

The mean concentrations of TNMOC measured at DAL during high ozone days was 57 ± 2.86 ppb-C and was 15.6% smaller than the concentrations measured during non-high ozone days at 67.52 ± 1.59 ppb-C. The mean concentrations of reactive TNMOC species (species with MIR >2) were 12.8 ± 0.123 ppb-C and 12.4 ± 0.114 ppb-C on high and non-high ozone days, respectively. Reactive TNMOC concentrations were 3.2% larger during high ozone days. The mean concentration of DAL's isoprene was almost three times larger during high ozone days. Isoprene [142]is a highly reactive biogenic species. Isoprene concentrations play a critical role in ozone generation [142] The NO_x concentrations on high ozone days (21.86 ± 1.43 ppb) were 6.3% higher than non-high ozone days (20.57 ± 0.67 ppb). As shown in Figure A3, the TNMOC/NO_x concentration ratios on high ozone days were slightly higher than its non-high

ozone days during 2000-2006 and 2010-2012. In contrast, the non-high ozone days TNMOC/NO_x concentration ratios were significantly higher during 2007-2009 and 2013-2018.

The difference between the mean concentrations of TNMOC measured at FWNW during high (90.87 ± 7.18 ppb-C) and non-high ozone day (89.29 ± 2.23 ppb-C) was minor (1.8%). However, the mean concentration of reactive TNMOC species was 47.6% larger on high ozone days (15.2 ± 0.61 ppb-C) than on non-high ozone days (10.3 ± 0.094 ppb-C). There was also a 50.6% difference in the mean concentrations of NO_x measured during high (22.32 ± 1.82 ppb) and non-high ozone days (14.82 ± 0.46 ppb). As shown in Figure A4, the TNMOC/NO_x concentration ratios measured during high ozone days at FWNW were lower than the concentration ratios measured during non-high ozone days in all four periods. Since the 2007-2009 period, the TNMOC/NO_x concentration ratios at FWNW had consistently exceeded 4, which indicated a transition from TNMOC-sensitive to a transitional ozone regime.

The mean concentration of TNMOC measured at DEN was 33.9% larger during high ozone days (242.66 ± 26.12 ppb-C) compared to non-high ozone days (181.17 ± 8.72 ppb-C). However, the difference in the mean concentration of reactive TNMOC species was only 2.9%. During high ozone days, the reactive TNMOC species had a mean concentration of 7.1 ± 0.08 ppb-C; whereas on non-high ozone days, the mean concentration was 6.9 ± 0.08 ppb-C. While the majority of TNMOC concentrations measured at DEN were slow reactive, elevated concentrations of slow reactive alkanes species can also lead to an increase in ozone concentration (Katzenstein et al., 2003). Thus, the abundant pool of slow reactive TNMOC at DEN has the potential of increasing ozone levels at DEN. The mean concentration of NO_x measured was 24.5% higher (10.83 ± 0.46 ppb versus 8.71 ± 0.23 ppb) during high ozone days. As shown in Figure A5, the TNMOC/NO_x concentration ratios measured at DEN were higher during high ozone days compared to non-high ozone days in all four periods.

High NO_x concentrations were the driving force behind the high ozone days at all three monitoring sites. During high ozone days, an elevated concentration of reactive TNMOC species was measured in DAL and FWNW, while slow reactive TNMOC species were measured in DEN. Thus, in addition to the continuation of NO_x reduction efforts, regulating reactive TNMOC species emissions will be beneficial in reducing ozone generation at DAL and FWNW. Alongside the further continuation of the NOx reduction efforts, the efforts to reduce the number of high ozone days in DEN must include the regulation of slow reactive TNMOC species.

6.4.2 Ozone Formation Potential

Calculating the ozone formation potential (OFP) of each TNMOC species is a crucial step in the development of ozone control strategies [143, 144, 145, 146, 147]. The maximum incremental reactivity (MIR) value used in this study is from Carter's report [148]. The OFP of TNMOC species at DAL, FWNW, and DEN were 35.28 ± 0.87 ppb, 35.98 ± 0.82 ppb, and 50.38 ± 2.04 ppb, respectively. The species that generated the highest OFP of TNMOC at DAL were ethylene (30.64%), propylene (12.19%), ethane (5.66%), 1-butene (5.65%), m/p-xylene (5.62%), and n-butane (5.43%). At FWNW, the species that generated the highest OFP of TNMOC were ethylene (26.93%), ethane (10.17%), propylene (9.79%), propane (7.01%), n-butane (12.88%), and 1-butene (6.21%). At DEN, ethane (20.57%), propane (15.32%), n-butane (16.16%), ethylene (10.38%), isobutane (8.53%), and isopentane (6.2%) contribute to the highest OFP of TNMOC. Figure 6.11 shows the cumulative column chart for measured TNMOC concentration and calculated OFP of TNMOC at the three sites. Alkenes were the dominant group at DAL and FWNW, whereas alkanes were dominant at DEN. OFP of alkene and aromatics TNMOC species increases with the TNMOC concentration at DAL and FWNW but remained relatively constant at DEN. In contrast, the OFP of alkane TNMOC species increases with measured TNMOC concentrations at DEN.

At DAL, the OFP of the alkane, alkene, alkyne, aromatics, and diene TNMOC species were 9.63 ± 0.23 ppb, 18.1 ± 0.53 ppb, 1.03 ± 0.03 ppb, 5.3 ± 0.15 ppb, and 2.15 ± 0.07 ppb, respectively. The OFP of TNMOC at FWNW was 13.8 ± 0.34 ppb from alkanes, 16.8 ± 0.43 ppb from alkenes, 0.82 ± 0.02 ppb from alkynes, 3.99 ± 0.13 ppb from aromatics, and 1.16 ± 0.04 ppb from dienes. Alkanes were the most significant contributors to the OFP of TNMOC in DEN at 38.6 ± 1.89 ppb, followed by alkene (8.43 ± 0.25 ppb), aromatics (2.84 ± 0.23 ppb), diene (1.06 ± 0.05 ppb), and alkyne (0.55 ± 0.01 ppb). Between 2000 and 2018, the OFPs of TNMOC at DAL and FWNW were in constant decrease, but the OFP of TNMOC at DEN mostly followed the TNMOC concentration trend, as shown in Figure A2. DAL and FWNW's OFP of TNMOC decreased by -2.24 ± 0.98 ppb/year (-4.57%/year) and -1.94 ± 1.23 ppb/year (-4.14%/year), respectively; while DEN's saw an increase of 0.02 ± 2.6 ppb/year (+2.7%/year).

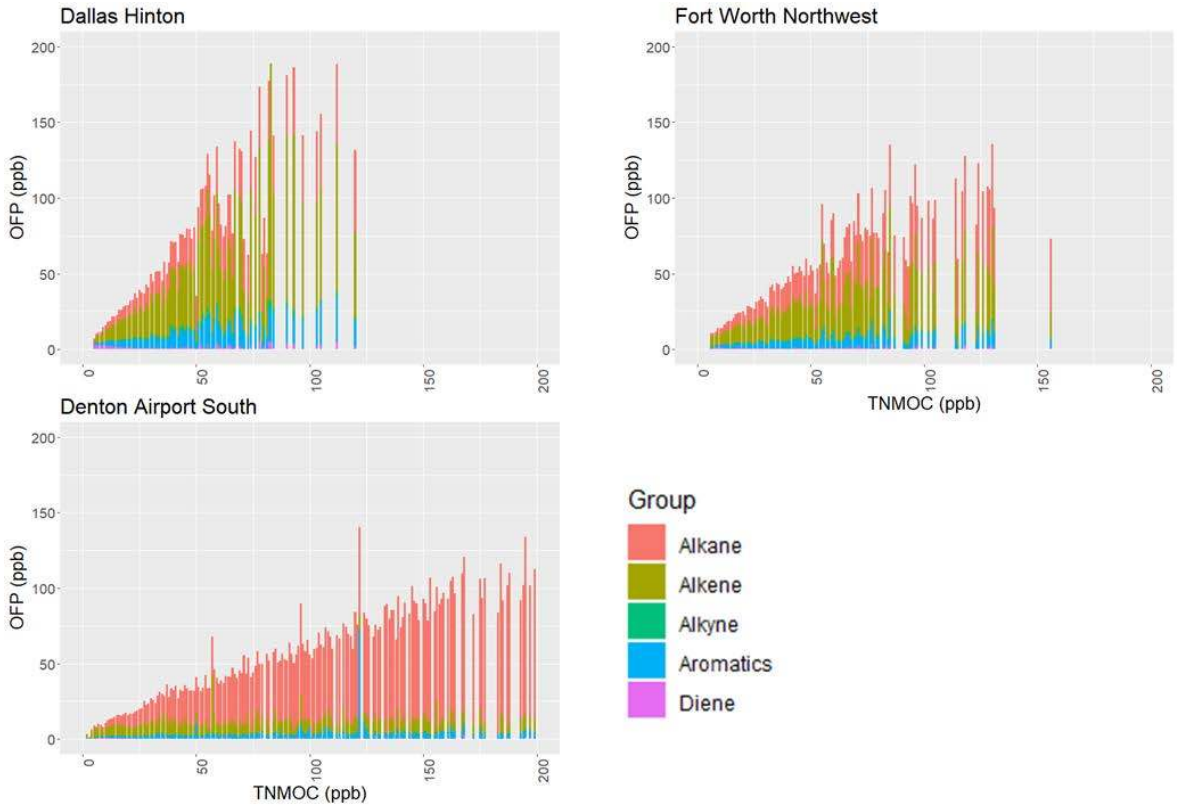

Figure 6.11: Relationship between ozone formation potential (OFP) with the TNMOC concentration by hydrocarbon groups.

Despite a relatively lower reactivity and MIR, alkanes were responsible for 26.59% of total OFP at DAL, 37.74% of total OFP at FWNW, and 74.99% of total OFP at DEN. Alkanes

were the largest group in terms of measured concentrations at all three monitoring stations, which was 79.67% at DAL, 87.79% at FWNW, and 96.95% at DEN. Elevated alkane emissions from natural gas production activities were responsible for the increased in OFP of TNMOC at DEN. Alkane emissions from oil and gas productions were also shown to had contributed to more than half of TNMOC reactivity in other oil and gas regions [149, 150, 134]. At DAL, the correlation between OFP of alkanes and the OFP of non-alkanes reactive groups was high. The Pearson's R-value between OFP of alkanes and the OFP of reactive species at DAL was 0.983, 0.931, 0.998, and 0.898 during 2000-2006, 2007-2009, 2010-2012, and 2013-2018, respectively. The correlation between the OFP of alkanes and the OFP of reactive groups was also high at FWNW except for during 2007-2009. At FWNW, the Pearson's R-value was 0.935 during 2000-2006, -0.608 during 2007-2009, 0.973 during 2010-2012, and 0.974 during 2013-2018. During 2007-2009, the OFP of reactive groups decreased while the OFP of alkanes increased. At DEN, the OFP of alkanes and the OFP of reactive groups had Pearson's R-values of -0.83 during 2000-2006, 0.998 during 2007-2009, -0.996 during 2010-2012, and 0.913 during 2013-2018. During both 2000-2006 and 2010-2012, the OPF of reactive groups at DEN fell during both periods while the OFP of alkanes increased. Both periods saw increased shale gas production from the gas wells surrounding DEN (Figure 6.5).

As shown in Table 6.2, both OFP of reactive group and OFP of alkanes have positive Pearson's R-value with ozone values at DAL. At FWNW, the OFP of alkanes has a negative correlation with ozone values during 2007-2009 and 2010-2012. Also, both the OFP of reactive groups and the OFP of alkanes have a bad correlation with ozone values where Pearson's R-values are 0.167 and -0.066, respectively. At DEN, the OFP of reactive groups has a negative correlation with ozone values during 2010-2012, with Pearson's R-value of -0.614, whereas the OFP of alkanes has a negative correlation with ozone values during 2000-2006, with Pearson's R-value of -0.932. Despite strong growth in OFP of alkanes during 2000-2006, its

correlation with the ozone values measured at DEN was negative. During 2010-2012, there was a rise in ozone values at DEN despite a drop in OFP of reactive species. Therefore, the positive correlation between the OFP of alkanes and the ozone values during this period shows the impacts of elevated slow reactive species on ozone values. Before 2010, ozone values measured at DEN appear to have had a high correlation with the OFP of reactive species. However, there was a shift in the ozone formation regime around 2010, where the OFP of alkanes had a higher correlation with the ozone values.

Table 6.2: The Pearson's R-value between the (i) OFP of reactive groups and (ii) OFP of alkanes with ozone values at Dallas Hinton, Fort Worth Northwest, and Denton Airport South.

	Period	OFP of Reactive Groups versus Ozone Values	OFP of Alkanes versus Ozone Values
Dallas Hinton	2000-2006	0.766	0.760
	2007-2009	0.999	0.946
	2010-2012	0.966	0.950
	2013-2018	0.913	0.700
Fort Worth Northwest	2000-2006	0.574	0.824
	2007-2009	0.997	-0.663
	2010-2012	0.167	-0.066
	2013-2018	0.855	0.939
Denton Airport South	2000-2006	0.809	-0.932
	2007-2009	0.993	0.982
	2010-2012	-0.614	0.682
	2013-2018	0.904	0.768

6.5 Summary Findings

An argument can be made for spatially varying emission control strategy within a single urban airshed based on the predominance of precursor emission. Since 2000, we had observed a decrease in emissions from vehicular exhausts and other combustion-related emissions, as evident from the constant decrease in NO_x and CO concentrations. Despite the decrease in conventional urban source emissions, the ozone values were still consistently failing to achieve

ozone attainment under the NAAQS. However, since 2013, the ozone values at all three sites began to decrease. The decline in ozone values also coincided with the decrease in the measured TNMOC concentrations and overall natural gas production volume in the Barnett Shale. We have strong evidence that the unconventional emissions from the Barnett Shale were a significant influence on the TNMOC concentrations measured in DEN, and to a smaller degree, in FWNW. DEN, the least urbanized of the three sites, had the largest pool of measured TNMOC, which was 3.5 and 2.2 times larger than the concentrations at DAL and FWNW, respectively. DEN was also the only site among the three to see an increase in the mean TNMOC concentration between 2000 and 2018. Ethane was the hydrocarbon species with the highest measured concentrations at all three sites, and it was among the TNMOC species that generated the highest OFP despite a relatively low MIR value. From 2000 to 2018, the OFP of TNMOC species at DAL and FWNW decreased while the OFP of TNMOC at DEN, which was heavily influenced by natural gas-related alkane species, had increased. We believe DAL and FWNW would benefit from a reduction in NO_x and reactive TNMOC species. In contrast, the ozone generation in DEN can be controlled via a reduction in both NO_x concentration and all TNMOC species associated with the shale gas operations.

CHAPTER 7

IMPACTS OF SHALE GAS PRODUCTION ON LONG-TERM AMBIENT HYDROCARBON CONCENTRATION IN DENTON, TEXAS*

The city of Denton is located at the northwest end of the DFW metroplex region and is the 12th most populous city in the region, with 136,268 inhabitants based on the 2017 U.S. Census Bureau data [69]. The city of Denton is also the seat of the Denton County Government. There are two universities in the city of Denton including the University of North Texas and Texas Woman's University. The city had a 17.1% growth in population size between 2010 and 2017. There were 9631 firms and businesses within the city of Denton, and approximately 67.1% of the total population above 16 years old were in the civilian labor force [151]. While several air monitoring studies focused on the greater DFW and the Barnett Shale region, to the best of the authors' knowledge, none focused on the impact of shale gas development on air quality in the city of Denton. However, several energy policy papers used the city of Denton as a testbed to address the socio-political impacts of the 2014 fracking ban and its subsequent nullification [152, 153, 154].

Figure 7.1: Map of the Denton Airport South monitoring station and nearby gas wells.

* This chapter is reproduced from G. Q. Lim and K. John, "Impact of energy production in the Barnett Shale gas region on the measured ambient hydrocarbon concentrations in Denton, Texas," Atmospheric Pollution Research, vol. 11, no. 2, pp. 409-418, 2020, wth permission from Elsevier.

The Denton Airport South (DEN) air quality monitoring station is an exurban region outside of the Denton city limit. It is located west of the city of Denton, is close to the Denton Enterprise Airport, and two major arteries: the U.S. 380 highway and the U.S. Interstate 35W highway. As shown in Figure 7.1, the monitoring station is surrounded by many gas wells, and most of the gas wells in this region are located outside of the city of Denton. This study incorporates 24-hour averaged canister TNMOC concentration samples collected between 2000 and 2017 at the monitoring station. A detailed summary of the 84 measured TNMOC species is available in Table B2.

7.1 Unconventional Gas Development (UGD) in North Texas

UGD in the Barnett Shale experienced tremendous growth over the past two decades, growing from 223,992 MMBtu of natural gas per day in 2000 to 5,955,491 MMBtu per day in 2012, as shown in Figure 7.2. Between 2000 and 2008, there was a +48.7%/year increase in drilling permits issued and a +46.64%/year increase in natural gas production volume. The region was affected by the global downturn in the economy during 2008-2009, followed by a recovery from 2010. The U.S. economy rebounded from the recession since 2010; however, the drilling permits issued, and the natural gas spot price was still in decline, at the rates of -4.78%/year and -6.32%/year, respectively. The recession in the U.S. economy in 2008 severely crippled demand for energy and caused the natural gas spot price to plummet from $8.86/MMBtu to $3.95/MMBtu. Drilling permits issued dropped from 4,065 in 2007 to 1,719 in 2008. While natural gas production continued to grow, the growth was significantly lower than in previous years, at +6.71%/year. From 2014 onwards, the production volumes for natural gas and liquid condensate has declined, likely due to low energy prices and maturing of the gas fields. Natural gas production in the Barnett Shale has been in decline since 2012, primarily due to lower natural gas prices and a maturing play [2]. Based on these observations, four

distinct evaluation periods were established for this study: 2000-2006, 2007-2009, 2010-2013, and 2014-2017.

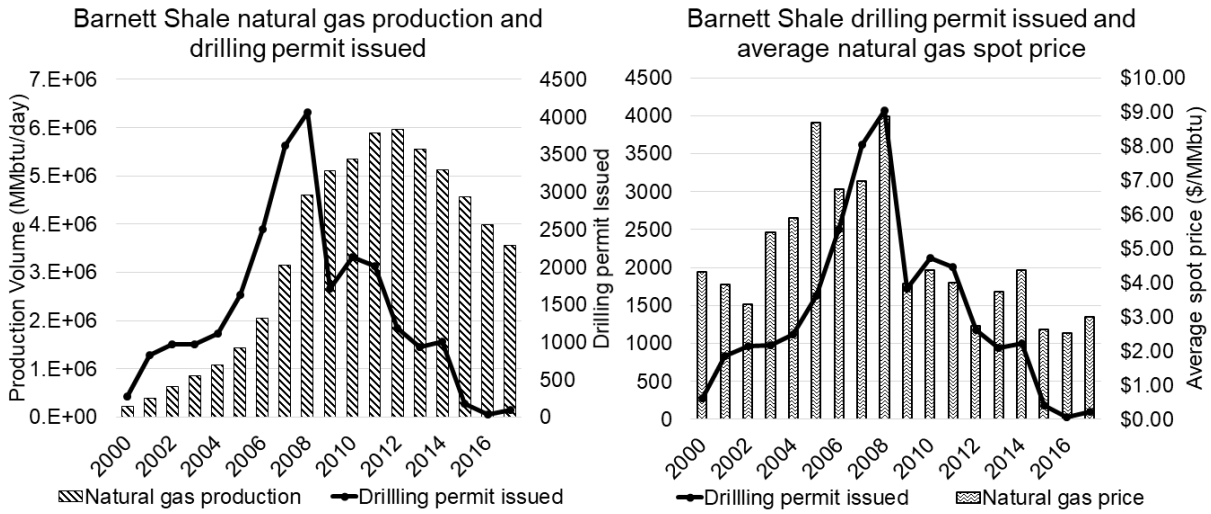

Figure 7.2: Barnett Shale natural gas production (MMBtu/day), new gas well permit issued, and average natural gas spot price ($/MMBtu).

Table 7.1 and Table 7.2 shows that the natural gas and liquid condensate production volume from facilities within 2-km from the monitoring station experienced significant growth between 2002 and 2006, followed by a decline in production volume through 2009. The recession in the U.S. economy caused a decline in production between 2007 and 2009. Since 2010, the economy has rebounded, and the demand for energy has risen once again. The natural gas and liquid condensate productions in the Barnett Shale peaked in 2013. From 2014 onwards, the production volumes for natural gas and liquid condensate has declined, likely due to low energy prices and maturing of the gas fields.

Table 7.1: Number of natural gas wells and their total annual production volume.

Year	Well Count				Production Volume (MMBtu)			
	1-km	2-km	5-km	10-km	1-km	2-km	5-km	10-km
2000	0	0	0	16	0	0	0	728,647
2001	0	0	2	45	0	0	82,887	3,790,163
2002	0	5	38	161	0	388,261	2,064,374	15,106,145
2003	3	16	78	287	238,260	1,448,331	5,847,322	26,145,173

(table continues)

Year	Well Count				Production Volume (MMBtu)			
	1-km	2-km	5-km	10-km	1-km	2-km	5-km	10-km
2004	5	20	110	386	369,144	1,533,774	8,026,249	32,326,549
2005	5	23	128	451	263,073	1,716,966	11,710,660	37,190,709
2006	5	29	142	503	127,782	2,585,061	11,391,068	35,082,785
2007	5	29	147	544	101,228	1,949,661	10,394,317	35,209,822
2008	6	30	152	560	220,045	1,757,127	10,569,948	32,477,684
2009	9	37	164	589	949,838	3,002,149	11,381,193	36,713,021
2010	8	37	176	614	743,463	3,147,381	13,522,651	41,327,564
2011	9	39	178	630	580,236	3,052,748	16,304,777	45,825,426
2012	9	45	186	657	509,964	3,967,714	15,461,203	52,655,317
2013	9	47	192	665	2,129,518	7,138,755	19,964,261	55,673,082
2014	9	47	208	670	1,476,172	5,722,529	25,588,831	59,043,187
2015	9	47	209	667	1,138,068	4,424,722	23,057,589	52,070,084
2016	9	45	218	677	1,107,834	3,998,616	25,425,278	51,959,763
2017	9	44	216	667	953,763	3,546,569	20,426,570	43,751,053

Table 7.2: Number of liquid condensate wells and their total annual production volume.

Year	Well Count				Production Volume (BBL)			
	1-km	2-km	5-km	10-km	1-km	2-km	5-km	10-km
2000	0	0	0	3	0	0	0	235
2001	0	0	0	30	0	0	0	16,157
2002	0	5	36	133	0	2,956	21,938	110,290
2003	3	16	72	230	1,259	6,349	61,727	189,675
2004	5	20	95	264	2,287	6,162	49,937	182,751
2005	5	21	89	260	1,173	8,154	61,207	157,185
2006	4	21	89	275	238	9,044	43,705	146,757
2007	4	23	92	321	442	5,462	30,727	120,761
2008	5	25	99	306	116	2,281	32,464	114,242
2009	6	24	93	293	355	1,945	44,757	104,236
2010	8	23	103	299	503	2,784	40,138	85,196
2011	8	25	107	307	581	3,864	48,786	120,535
2012	9	32	109	294	289	3,970	29,481	69,098
2013	9	32	123	302	3,146	6,904	25,512	79,324
2014	9	29	128	305	2,104	4,072	64,954	143,428

(table continues)

Year	Well Count				Production Volume (BBL)			
	1-km	2-km	5-km	10-km	1-km	2-km	5-km	10-km
2015	9	32	123	306	1,069	2,871	49,765	100,282
2016	9	33	135	313	991	2,347	69,575	113,945
2017	8	31	142	324	413	1,333	30,541	64,004

7.2 Energy Policies in Texas

The United States prohibits fracking activities in some regions of the country because of the environmental backlashes that surround the operations. The state of Texas does not have such prohibitions and had accused the U.S. federal government of overreaching into state affairs [155]. UGD is an unprecedented usage of land for industrial purposes, where it is legal for operators not to disclose the chemical contents used in fracking operations [27]. In 2010, the U.S. EPA found water sources near gas wells had high concentrations of methane and tried to issue an endangerment order against a shale gas company operating within the Barnett Shale. However, due to limited regulations on fracking operations, the U.S. EPA was not able to pursue any further actions against the shale gas operator [27]. In 2014, the citizens deemed fracking activities, close-to or within city limits, to be harmful to human health, the environment, and the quality of life, and voted for a fracking ban. However, House Bill 40 in the Texas legislature nullified the fracking ban in mid-2015. House Bill 40 was written to ensure control of oil and gas activity regulations lies with the state and not by the local governing body. It also explicitly prevents any oil and gas bans within Texas [152, 153, 154].

While UGD has helped improve the local economy by indirectly generating more jobs, however, Fry et al. [152] argued that the burdens placed on the city of Denton and its citizens, especially non-mineral owners, by UGD outweigh the potential economic benefits. In Denton County, the setback distance between new wells and existing infrastructure varies between 300-ft (or 91.4 m) to 1,500-ft (or 457.2 m). The city of Denton adopted an ordinance to increase the setback distance from 500-feet (or 152.4 m) to 1,200 feet (or 365.8 m) in 2013 [156].

Unfortunately, setback distances were not determined based on scientific consensus, but rather, a compromise reached between citizens and policymakers [152].

7.3 Air Quality in Denton, Texas

Since the 2000s, there have been numerous air quality measurement studies in DFW that had shown the heightened environmental impact from UGD in the Barnett Shale. Methane concentrations were above detection limits in 98% of the samples collected in the SGR and were higher than the urban background concentration range of 1.8 to 2 ppm [7]. A mobile measurement around natural gas production facilities showed that 9.7% of fence-line air quality samples collected in Denton County had methane concentrations exceeding 3 ppm [138].

7.3.1 Total Non-Methane Organic Carbons (TNMOC)

The mean measured TNMOC concentration during 2000 – 2017 in Denton was 226.17 ± 10.84 ppb-C, and it increased by +8.03 ± 12.92 ppb-C/year (+12.75 %/year) from 57.27 ppb-C in 2000 to 193.75 ppb-C in 2017. As shown in Figure 7.3, two peaks were noted in the mean and 95th-percentile TNMOC concentration trends. The mean concentration peaked in 2005 and 2014 while the 95th-percentile peaked in 2006 and 2013. A significant increase in drilling permits was issued in the Barnett Shale during the early 2000s that mirrored the growth shown in the measured TNMOC concentrations, and this peaked in 2005. Activities tied to the gas well development stage of UGD, which includes drilling and increased truck traffic, resulted in elevated measured TNMOC concentrations during the pre-2007 period. The economic recession that started in 2007 caused the drilling permits issued to drop, resulting in a decrease in the measured TNMOC concentrations from 2007 through 2009. Post-2010, the Barnett Shale gas region had largely matured, and the number of new permits issued dropped significantly. Post-recession, the natural gas production volume continued to increase through 2012, despite a relatively stagnant number of producing wells, and this explained the growth in the measured

TNMOC concentrations as it peaked in 2013. Natural gas production and subsequently, the measured TNMOC concentrations have declined since 2013.

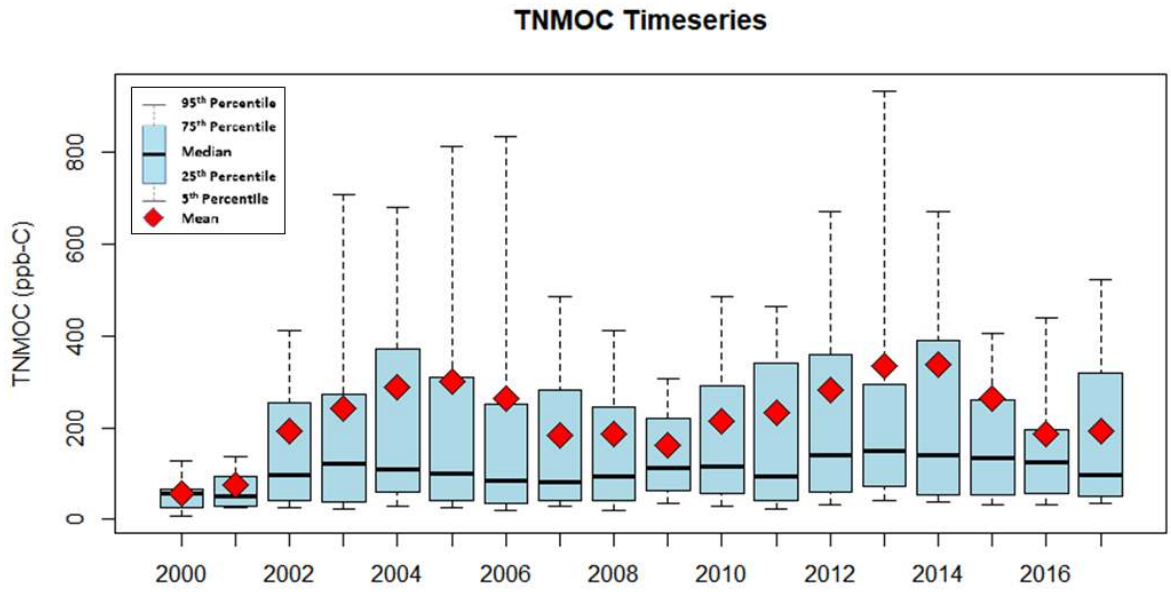

Figure 7.3: TNMOC concentration (ppb-C) timeseries plot for 2000 – 2017.

Table 7.3: Mean TNMOC concentration measured and the average change in annual TNMOC during the 2000-2006, 2007-2009, 2010-2013, and 2014-2017 periods.

Period	Mean TNMOC Concentration (ppb-C)	Average change in annual TNMOC
2000 – 2006	211.34 ± 17.57	+37.58%/year
2007 - 2009	178 ± 16.31	-5.88%/year
2010 - 2013	265.8 ± 23.51	+16.1%/year
2014 - 2017	246.27 ± 26.95	-15.74%/year

The TNMOC concentrations measured in Denton increased by +37.58%/year during 2000-2006 and had a mean concentration of 211.34 ± 17.57 ppb-C during this period, as shown in Table 7.3. This dropped significantly during the economic downturn during the recession period in 2007-2009. The TNMOC concentrations decreased by -5.88%/year, and the mean TNMOC concentration of 178 ± 16.31 ppb-C was lower than the earlier period. Since the economy rebounded in 2010, TNMOC concentration saw an increase at the rate of +16.1%/year, and the mean concentration grew to 265.8 ± 23.51 ppb-C during the 2010-2013 period. Finally, during the 2014-2017 period, a -15.74%/year decrease was noted in the

TNMOC concentrations, and the mean TNMOC concentration was observed to be 246.27 ± 26.95 ppb-C.

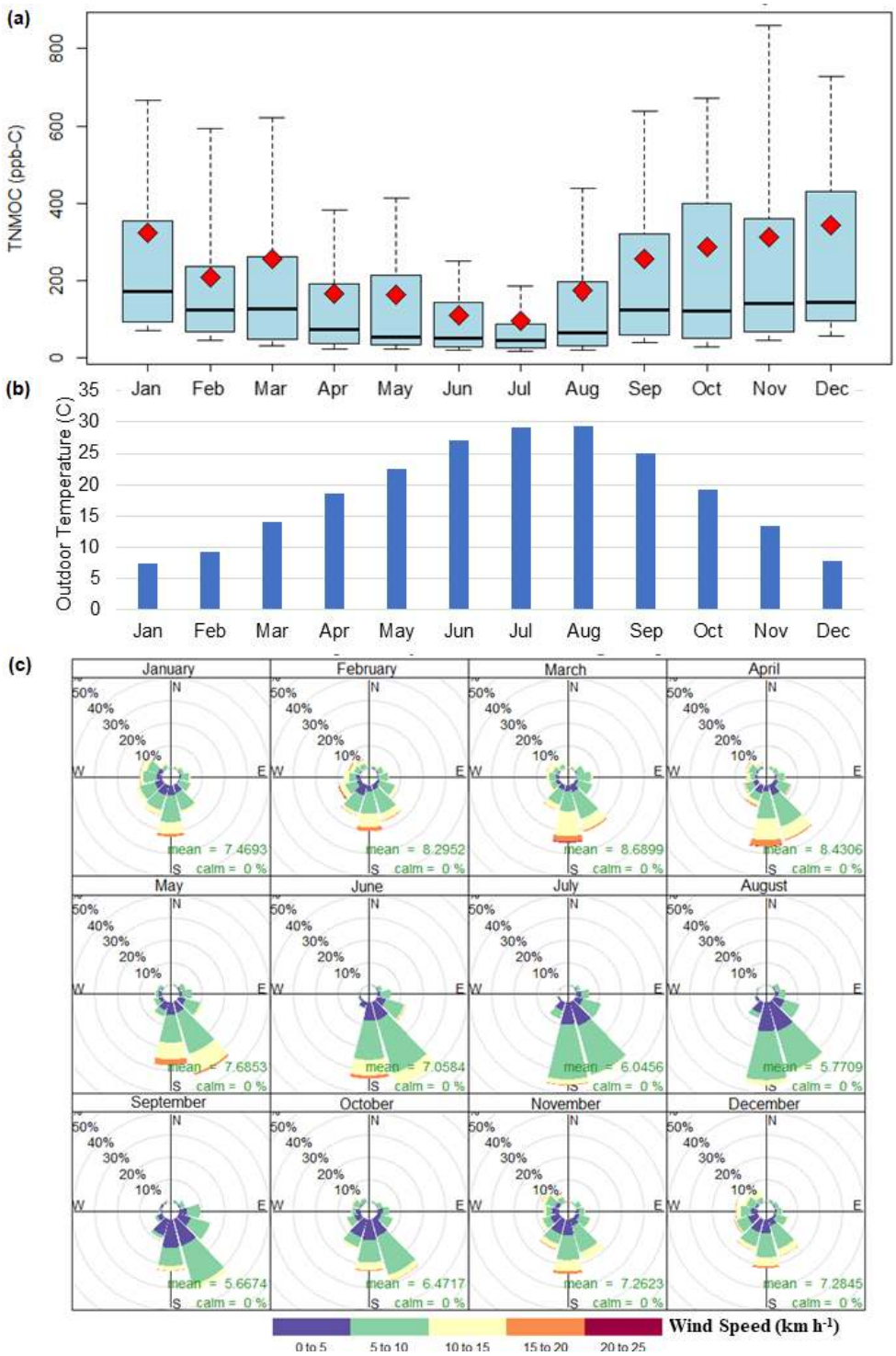

Figure 7.4: TNMOC concentration [ppb-C] box-whiskers plot, (b) ambient temperature [°C], and (c) windrose diagrams [km h^{-1}].

The observed TNMOC concentrations were higher during the winter months than in the summer in Denton. Figure 7.4 shows the monthly TNMOC concentration along with the

monthly outdoor temperatures, and the corresponding wind rose plots. Mean TNMOC concentration was the highest in November and was lowest in July, which was inverse of the temperature profile. Although TNMOCs are more volatile with warmer temperatures, TNMOC reactivity lowers during winter months due to smaller concentrations of free OH radicals, leading to a higher TNMOC concentration during winter months [157, 158, 159, 123]. The wind was blowing predominantly from the southeast of the monitoring site year-round, and westerly winds were the least uncommon during summer months. Faster winds usually result in lower measured TNMOC concentrations, and November's average wind speed was 1.7 km/hour greater than July. However, the influence of the lowered OH radicals was more significant than that of the increased wind speed, resulting in higher TNMOC concentrations.

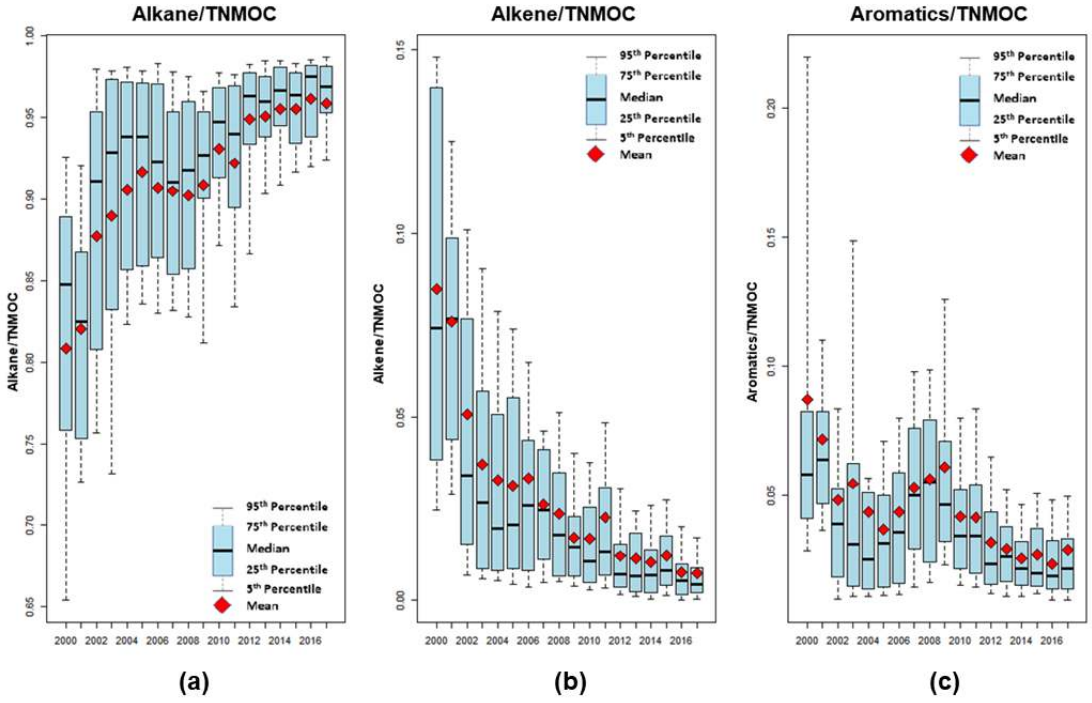

Figure 7.5: (a) Alkane/TNMOC, (b) alkene/TNMOC, and (c) aromatics/TNMOC concentration ratios box-whiskers plots.

Alkanes were the largest TNMOC group at Denton, and their compositions (alkane/TNMOC ratio) had increased significantly since 2000, whereas the alkene/TNMOC and aromatics/TNMOC ratios were consistently in decline, as shown in Figure 7.5. Alkanes are the predominant TNMOC group emitted during UGD production activities, and the

increased alkane composition in the measured TNMOC concentrations suggest an increasing influence from UGD emission sources between 2000 and 2017. The alkene and aromatic species' decline in the TNMOC composition suggests a lowered influence of urban emission sources, which indicated an improvement because of conventional emission source controls.

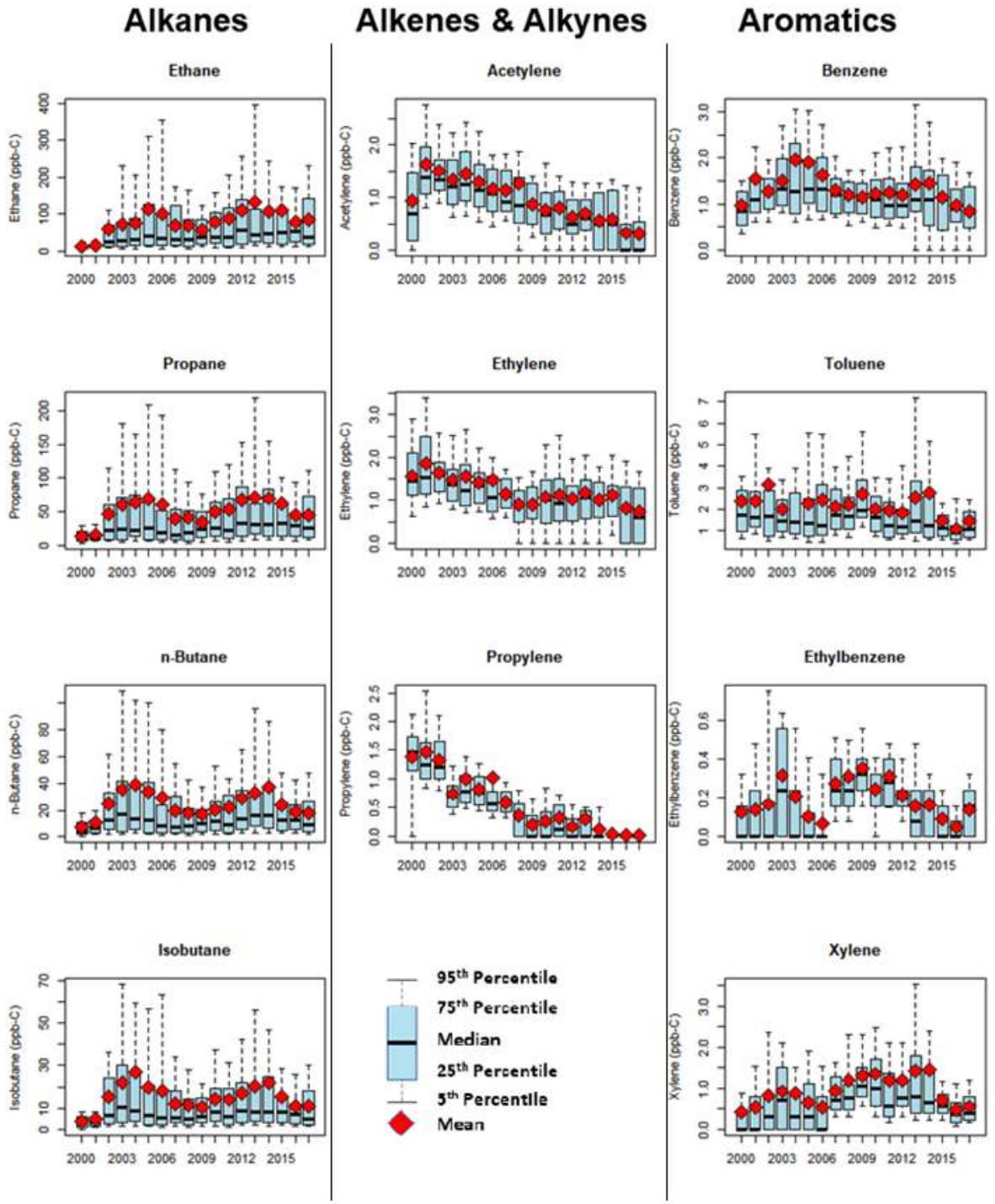

Figure 7.6: Alkanes (ethane, propane, and n-butane), alkenes, and alkynes (acetylene, ethylene, and propylene), and aromatics (benzene, toluene, ethylbenzene, and xylene) concentrations from 2000 to 2017.

Figure 7.6 shows box-whiskers plots for select alkane (ethane, propane, n-butane, and isobutane), alkene (ethylene, and propylene), alkyne (acetylene), and aromatics (benzene, toluene, ethylbenzene, and (O + M/P) xylenes) species. All four alkane species experienced trends similar to the measured TNMOC concentration and the UGD production, which strengthens the correlation between both variables. Since 2000, the alkene and alkyne species had seen a decline in measured concentration. Acetylene, an alkyne species, along with ethylene and propylene, which are alkene hydrocarbon species, are commonly associated with the combustion of gasoline-powered engines [116]. Thus, the decrease in the observed concentration of these species strongly suggests the influence of decreasing exhaust emissions from vehicles. Unlike other TNMOC groups, each of the aromatic species had different trends that were independent of all the other members of the group.

The trend showed by benzene was similar to that shown by the alkane species and TNMOC, which would indicate some correlation between benzene and natural gas production. Benzene is a hazardous air pollutant (HAP) species known to be carcinogenic and can cause serious health issues [160]. While the primary source of benzene in an urban region is vehicle exhaust emissions, benzene is also found in natural gas emissions. Benzene concentrations in the other parts of DFW were shown to be decreasing and were stated to be mostly released from sources other than natural gas production [5]. However, the benzene concentrations measured at the Denton site had a higher correlation with ethane than acetylene with R^2-values of 0.212 and 0.09, respectively. Ethane is a dominant natural gas species, whereas acetylene is commonly emitted from vehicle exhausts [116]. The higher correlation between benzene and ethane indicated that the benzene concentrations observed in Denton were more likely to be emitted from natural gas sources. Nevertheless, the benzene concentrations measured at the Denton site, with a mean and median value of 1.39 ppb-C and 1.14 ppb-C, respectively, were

lower than the median background concentration of benzene in the United States cities (2.05 ppb-C) [132] and were not likely to be a significant hazard to human health.

Toluene can be emitted from internal combustion engines of on-road vehicles, where its decrease coincided with the decline in alkene and alkyne concentrations. Ethylbenzene concentrations showed a fluctuating upward trend from 2000 through 2008, followed by a consistent decrease in post-2009. Truck traffic increased during the development phase of the UGD wells prior to 2008 was likely the primary contributor to the ethylbenzene concentration; the truck traffic volume dropped with the decrease in UGD. Xylene concentrations saw rapid growth from 2000 through 2014, which was followed by a significant drop from 1.46 ppb-C to 0.723 ppb-C from 2015 onwards. Xylenes are commonly found in industrial solvents and fracturing fluids; the decline in xylene concentrations post-2015 may be the result of reduced fracking activities after the initiation of the fracking ban.

7.4 Impacts of UGD on TNMOC Concentrations

Between 2001 and 2002, the mean TNMOC concentrations showed a significant increase of +156.32% from 75.16 ppb-C to 192.64 ppb-C (Figure 7.3). During the same timeframe, the natural gas production volumes from wells within 2-km from the Denton site had also increased from zero to 388,261 MMBtu (Figure 7.2). The increase in liquid condensate production during the early 2000s also correlated with the peak in the mean TNMOC concentration in 2005. Mean concentrations of ethane (79.77 ppb-C), propane (50.37 ppb-C), n-butane (24.12 ppb), and isobutane (14.79 ppb) observed in Denton, suggested the influence of natural gas sources. These four are considered to be natural gas emission species [116] and can be found in high concentrations throughout the Barnett Shale gas region [161]. While the reactivity of alkane species is low towards the formation of ozone, alkanes were crucial contributors to the bulk of TNMOC reactivity observed in other oil and gas regions [134, 149].

Thus, we believe that the elevated concentrations of alkanes at the Denton site potentially could impact the local ozone formation despite lower reactivity.

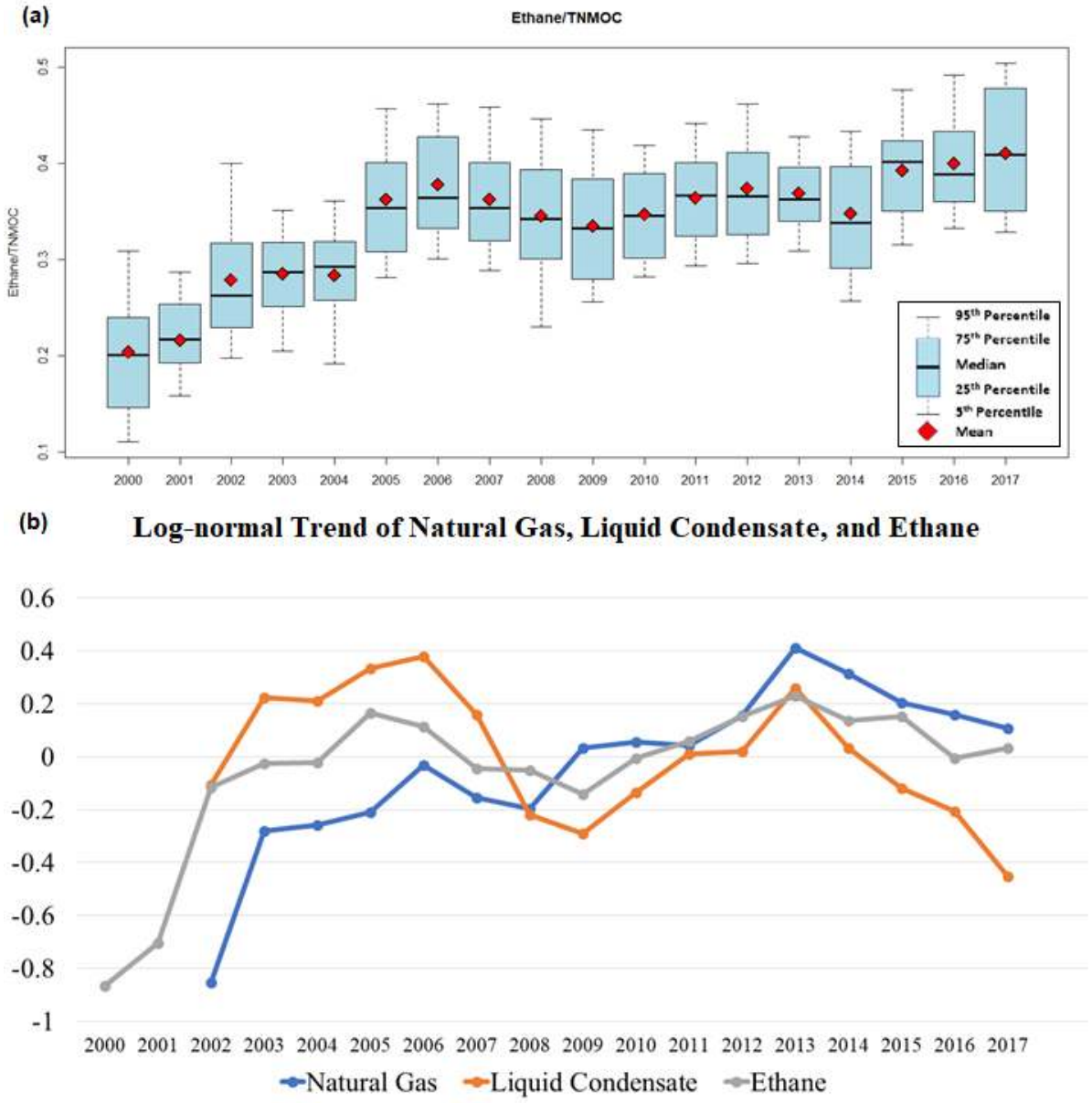

Figure 7.7: (a) Ethane/TNMOC concentration ratio; (b) log-normal trend of natural gas and liquid condensate production volume and mean ethane concentration.

Ethane/TNMOC concentration ratios, as shown in Figure 7.7(a), saw significant growth (p-value = 0.0009) during 2000-2006, but remained relatively constant post-2007. The growth in the pre-2007 ethane/TNMOC ratio was the product of rapid growth in UGD and an increase in the issuance of drilling permits. The normalized log trends (Figure 7.7(b)) for natural gas and liquid condensate production within 2-km from the Denton air monitoring site and the

observed ethane concentrations showed a high correlation, and there was no significant difference between the three variables (p-value = 0.828). The lack of significant difference between the ethane concentration and UGD production strongly suggests UGD activities were the predominant source of ethane and in-extension the major contributor to TNMOC concentration in the region. Thus, the decreased in TNMOC concentration post-2013 (Figure 7.3) was likely caused by the decrease in natural gas production in the region (Figure 7.2). On the contrary, an increase in natural gas production will likely increase the TNMOC emissions in the region if emission regulation and emission control technology remains the same.

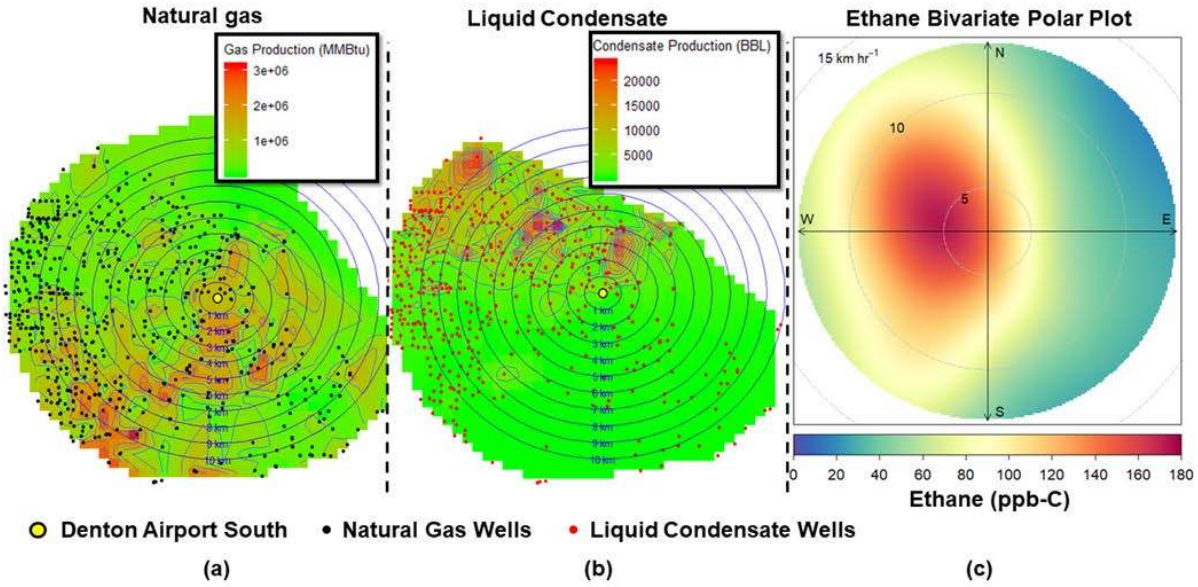

Figure 7.8: (a) Location of natural gas wells overlaid with total production volume contour [MMBtu]; (b) location of liquid condensate facilities overlaid with total production volume contour [BBL]; and (c) bivariate polar plot for measured ethane concentrations [ppb-C].

Figure 7.8 shows the cumulative sum of natural gas and liquid condensate production volume and the ethane bivariate polar plot for the entire study period (2000 to 2017), while the annual natural gas production, liquid condensate production, and ethane bivariate polar plots are available in Figure A6 through Figure A8. The production volume plots scale from green to red, where green represents the lowest production volume, and red represents the highest production volume. The rings on the bivariate polar plots represent wind speed, where a high concentration region near the origin, or 0 km/hour, shows that the measured air pollutant

concentration was not carried in by high-speed winds and is an indication of a local emission source. Natural gas wells with higher production volumes were located south-southwest of the Denton site, whereas liquid condensate facilities with higher production volumes were located north-northwest of the monitoring station. The largest concentration of ethane was found on the west side of the monitoring station. This high concentration region was close to the 5km/hour radius, which would strongly suggest the influence of a localized source.

The ethane bivariate polar plots (Figure A8) follows the high production regions of the liquid condensate production volume (Figure A8) very closely between 2002 and 2008; the regions with high liquid condensate production volume were in the west-northwest side of the monitoring station between 2002 and 2008, which coincided with the high concentration regions on the ethane bivariate polar plot. Between 2011 and 2014, the region with high ethane concentrations (Figure A8) appeared to have a higher correlation with natural gas production volume (Figure A6) more closely than liquid condensate (Figure A8). Also, high ethane concentrations observed after 2008 were predominately linked to regions in the west of the monitoring site with a high density of both natural gas and liquid condensate facilities. The ethane concentrations observed were very likely to be from fugitive emissions from natural gas compressor stations and liquid condensate storage tanks. Compressor stations, storage tanks, and gas processing plants were likely sources of elevated TNMOC levels as opposed to the operation of single gas wells. More importantly, the number of existing facilities and production volume do not always translate directly to the measured emissions. In an earlier study, it was found that just 10% of the facilities were mainly responsible for 90% of the emissions within the Barnett Shale [162].

7.5 Summary Findings

Over the past two decades, shale gas activities have had a significant influence on the TNMOC concentration measured in Denton, Texas. The annual mean TNMOC concentrations

grew from 57.3 ppb-C to 194 ppb-C from 2000 through 2017, and it followed the trend set by natural gas and liquid condensate production from wells located within 2-km from the monitoring site. Ethane was the most abundant component in the measured TNMOC concentration, and it originated from regions with a high density of active natural gas and liquid condensate facilities. Furthermore, while the concentration of alkane hydrocarbon species increased, the alkene, alkyne, and aromatic species decreased during the study period. The TNMOC concentrations measured has declined since 2014, which coincided with a decrease in shale gas production due to lower gas prices. This study showed that shale gas activities in Denton had a strong influence on the measured TNMOC concentrations in the ambient atmosphere. While lower reactivity alkane species dominated the observed TNMOC concentrations, the large concentration of alkanes was sufficient to offset their lower reactivity and potentially contributed to elevated ozone levels in the region. For now, the shale gas play in this region has matured, and a declining trend in both production and corresponding ambient concentrations of TNMOC was noted. However, in the future, if shale gas production were to rise again within this mature play, it would likely cause a potential increase in the ambient TNMOC concentrations. Further studies are required using hourly measured TNMOC concentration data along with the photochemical modeling of these UGD emission sources to understand the complex air quality challenges faced by exurban areas with significant oil and gas development and production activities.

CHAPTER 8

SOURCE APPORTIONMENT ANALYSIS OF AMBEINT TNMOC CONCENTRATIONS USING POSITIVE MATRIX FACTORIZATION TECHNIQUE

The previous chapters had established that the ambient TNMOC concentrations measured at the exurban Denton Airport South (DEN) monitoring station were more severely affected by oil and gas emissions compared to those measured at the highly urbanized Dallas Hinton (DAL) and Fort Worth Northwest (FWNW) monitoring stations. In this chapter, a source apportionment analysis was performed to identify and quantify the various emission source factors impacting TNMOC concentrations at all three sites using the long-term canister dataset. Source apportionment is a useful tool that can aid in the decision making of urban planners and policymakers [163]. The positive matrix factorization (PMF), a statistical analysis tool has been used to quantify sources of TNMOC emissions [116, 117, 164, 165]. In this study, we employ PMF to apportion potential emission sources affecting the measured ambient hydrocarbon concentrations at three air quality monitoring stations within the study region.

8.1 Breakdown of the Measured Hydrocarbon Groups

Between 2000 and 2018, the mean concentration of TNMOC was estimated to be highest in DEN (217.18 ppb-C), followed by FWNW (89.65 ppb-C), and finally in DAL (68.28 ppb-C). Figure 8.1 shows that the n-alkane hydrocarbon group had the predominant share of the TNMOC concentrations measured at all three sites. Alkanes are most commonly found in oil and gas emissions [45, 46, 47, 116, 166]. Alkanes made up pf 96.11% of the TNMOC concentration measured in DEN, in comparison, the alkane group was 76.31% and 84.61% of the measured TNMOC concentration at DAL and FWNW, respectively. The aromatic group was the second-largest hydrocarbon group, which was followed by alkenes, alkynes, and dienes. All four of these hydrocarbon groups can be found abundantly in conventional urban source emissions, such as vehicle exhaust, power plant, and solvent emissions [116, 166, 167].

Since DAL and FWNW are in highly urbanized regions within the DFW metroplex, unsurprisingly, these two sites had larger amounts of measured alkenes, alkynes, aromatics, and dienes than compared to DEN.

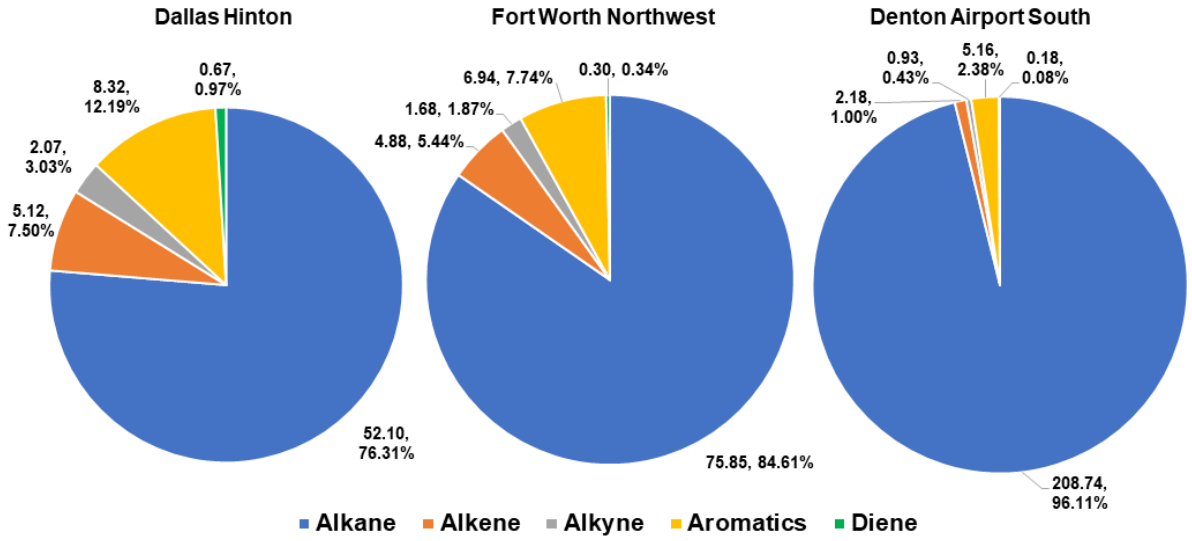

Figure 8.1: Hydrocarbon group profile breakdown (ppb-C, %).

8.2 PMF Source Apportionment Analysis

The PMF requires two input datasets: a concentration file and an uncertainty file. Based on the uncertainty, some subsets of the input files will be removed to decrease the error of the model run. Based on S/N ratios (Table B3), 38, 40, and 35 species were considered for the PMF run of the DAL, FWNW, and DEN dataset, respectively. The optimal number of factors depends on the $Q_{true}/Q_{expected}$ value generated by the PMF, where the decrease in $Q_{true}/Q_{expected}$ value is insignificant after the optimal number of factors were met. After repeatedly running the PMF with an increasing number of factors, it was identified that the optimal number of factors for DAL, FWNW, and DEN were five, six, and five, respectively. A factor profile consists of the concentration and percentage of each TNMOC species within the factor. Table 8.1 shows the factor profiles of the resolved models for DAL, FWNW, and DEN alongside the key signature species used to classify them. The key signature species of each

factor are the most common TNMOC species associated with the factor, found from cross-validating results published in various studies on TNMOC source apportionment.

Table 8.1: Resolved PMF sources factor profile (ppb-C, %) and their respective key species.

Sources	DAL	FWNW	DEN	Key Species
Diesel		7.13, 9%		1-Butene, n-Undecane, 1,2,3-Trimethylbenzene, 1,2,4-Trimethylbenzene, n-Nonane
Fuel Evaporative	11.02, 18%	10.03, 13%	10.07, 6%	n-Pentane, isopentane, n-Butane, 2-Methylpentane
Natural Gas	19.66, 32%	32.03, 40%	115.04, 69%	Propane, ethane, n-Butane, isobutane
Refrigerant	5.1, 8%	6.65, 8%	16.35, 10%	Chloromethane, Dichlorodifluoromethane, Trichlorofluoromethane, p-Ethyltoluene
Solvent	16.35, 27%	14.12, 18%	10.99, 7%	2-Methylhexane, 1,2,4-Trimethylbenzene, 2,3,4-Trimethylpentane, 3-Methylhexane
Vehicle Exhaust	9.25, 15%	10.05, 13%	14.23, 9%	Acetylene, Ethylene, Propylene, Benzene

8.2.1 Dallas Hinton (DAL)

DAL is in a highly urbanized region with a large population density within the city of Dallas. Dallas is currently the third-largest city in the state of Texas by population [151] and is a major economic hub in the southern United States. DAL is the only one of the three sites in this study that is not located within a shale gas region (SGR) within the Barnett Shale. As shown in Figure 8.2, the PMF had resolved fuel evaporative, natural gas, refrigerant, solvent, and vehicle exhaust as the five dominant factors contributing to the measured TNMOC concentration in DAL. The spatial extent analysis for each factor was performed using a conditional probability function (CPF) bivariate polar plots. These CPF plots consider the impact of wind speed and wind direction to identify major hotspots where the source of each factor was likely originating from. The CPF plot corresponding to the five factors resolved for DAL is shown in Figure 8.3.

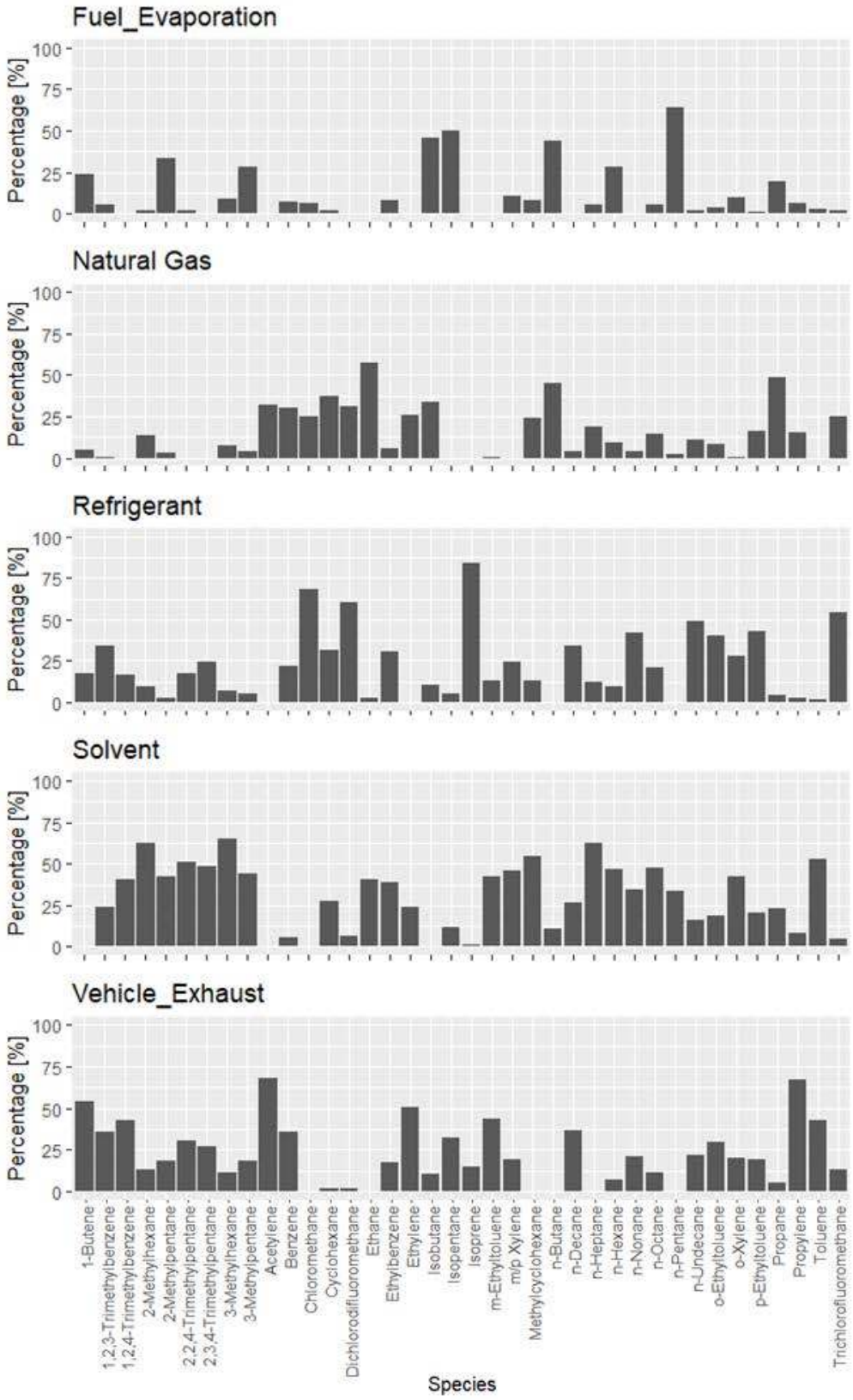

Figure 8.2: Summary of the 5-factor profile at DAL: (a.) Fuel evaporation; (b.) natural gas; (c.) refrigerants; (d.) solvent; and (e.) vehicle exhausts.

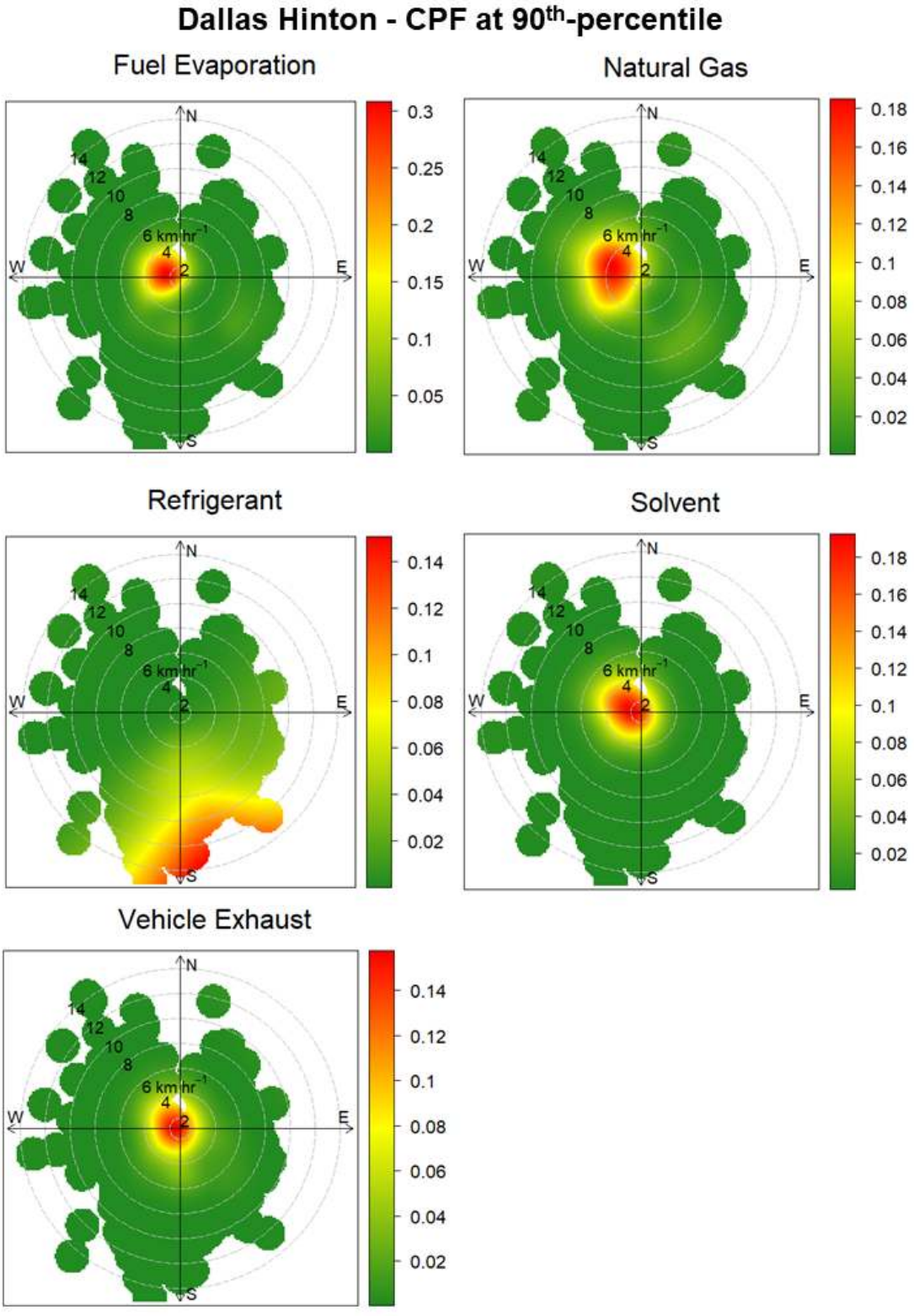

Figure 8.3: 90th-percentile CPF plots (%) for the 5-factors at DAL: (a.) Fuel evaporation; (b.) natural gas; (c.) refrigerants; (d.) solvent; and (e.) vehicle exhausts.

Fuel evaporative was 18% of the TNMOC composition and had a concentration of 11.024 ppb-C. The key species of the fuel evaporative factor were n-pentane, isopentane, n-butane, and 2-methylpentane [45, 166, 167]. According to the CPF plot, the fuel evaporative factor was mainly from a nearby source west of the monitoring station. The natural gas factor has high concentrations of ethane, propane, n-butane, and isobutane [45, 46, 47, 116, 166]. Natural gas emissions had a concentration of 19.66 ppb-C and were the most substantial factor contributing to measured TNMOC concentration at 32%. Natural gas was predominantly carried in from the west side of the monitoring station during low wind speeds, which could indicate the influence of a higher localized source in close proximity. The CPF plot for natural gas was very similar to fuel evaporative, which would indicate a correlation between the two factors. There were natural gas and refined liquid petroleum pipelines less than 5-km west of the monitoring station. The fuel evaporative and natural gas factors were subsequently influence by the fugitive emissions from these pipelines. The refrigerant factor was 5.1 ppb-C and contributed to 8% of the measured TNMOC at DAL. The key signature species found in refrigerant emissions are chloromethane, dichlorodifluoromethane, trichlorofluoromethane, and p-ethyltoluene [168, 169]. Refrigerant emissions were carried in by southerly winds, indicating that the source was not local and the monitoring station was influenced by long-range transport of the refrigerant chemicals. The solvent factor has high concentrations of 2-methylhexane, 1,2,4-trimethylbenzene, 2,3,4-trimethylpentane, and 3-methylhexane. While the exact chemical compositions of the solvent differ depending on the type of solvent used, they generally are composed of aromatics, n-alkanes, pentanes, and butanes [116, 170, 46, 167]. The solvent factor at DAL was 16.35 ppb-C and was the second most significant factor contributing to the measured TNMOC concentration at 27%. The CPF plot shows the highest probability surrounding the origin, which indicates an extremely localized source. The CPF plot also showed solvent factors carried in by low-speed winds from the northwest side of the

monitoring station, which suggests commercial solvent use by local businesses near the monitoring station. There were more commercial buildings towards the northwest of the monitoring station compared to the southeast, which primarily consists of residential housing. The final factor was vehicle exhausts, which was characterized by acetylene, ethylene, propylene, and benzene [116, 166, 167]. Vehicle exhaust contributed to 15% of the TNMOC measured at DAL and was 9.25 ppb-C. Like solvent, the vehicle exhaust factor was an extremely localized source with a more significant frequency from the northwest side of the site, indicating the influence of nearby highways and major roadway arteries.

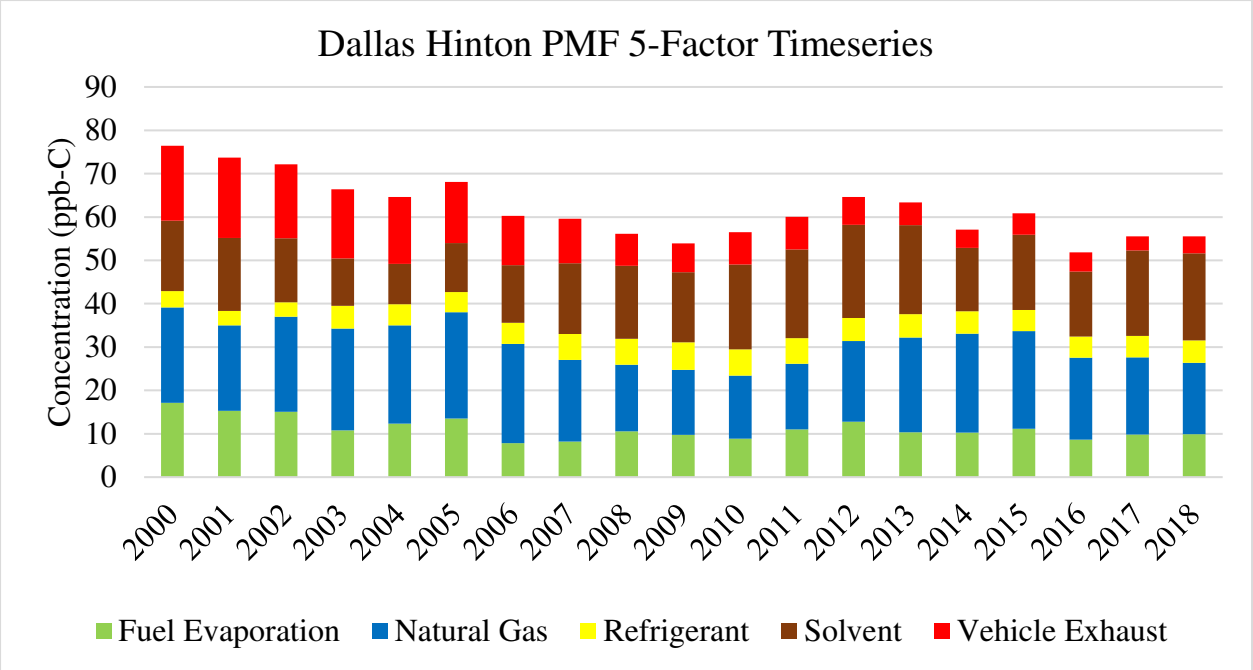

Figure 8.4: Annual variation in the mean concentration of the 5-factors at DAL.

The mean concentration of TNMOC measured in DAL was lower in 2018 than it was in 2000, as shown in Figure 8.4. TNMOC concentrations were in decline from 2000 through 2009, which marked the end of the U.S. economic recession in 2008. From 2010 to 2012, TNMOC concentration saw a brief period of increase, which corresponded to the increased activity of the post-recession economic rebound in the DFW metroplex. Since 2013, the measured TNMOC concentrations have shown a declining trend. From 2000 to 2018, the fuel evaporative, natural gas, and vehicle exhaust factors were in decline at the rate of -0.4 ppb-

C/year (-3.58%/year), -0.31 ppb-C/year (-1.55%/year), and -0.75 ppb-C/year (-7.8%/year), respectively. On the other hand, the solvent and refrigerant factors experienced an increased by +0.22 ppb-C/year (+1.33%/year) and +0.07 ppb-C/year (+1.48%/year), respectively. The massive decrease in fuel evaporative and vehicle exhausts was successful in mitigating the slight increase in solvents and refrigerants; thus, the overall influence of urban emissions at DAL showed a decrease between 2000 and 2018.

8.2.2 Fort Worth Northwest (FWNW)

The mean concentrations of alkene, alkyne, aromatics, and diene hydrocarbon species measured in FWNW were lower than those measured in DAL. However, the concentrations of alkanes measured at FWNW were higher than DAL, which indicated a more substantial influence from oil and gas-related emissions in FWNW. The chemical profile of the six factors contributing to the measured TNMOC concentrations in FWNW as well as their corresponding CPF bivariate polar plots are shown in Figure 8.5 and Figure 8.6, respectively. The six emission source factors resolved by the PMF were diesel, fuel evaporation, natural gas, refrigerants, solvent, and vehicle exhausts.

The key TNMOC species used to identify the diesel source factor were 1-butene, n-undecane, 1,2,3-trimethylbenzene, 1,2,4-trimethylbenzene, and n-nonane [167, 171]. Diesel contributed to 7.13 ppb-C or 9% of the measured TNMOC concentration at FWNW. The diesel emissions were carried in during low wind speeds from downtown Fort Worth (southeast of the monitoring station). Gasoline-powered vehicle exhaust emissions had a concentration of 10.05 ppb-C and was 13% of the measured TNMOC at FWNW. Similar to the diesel factor, vehicle exhaust emissions had extremely localized sources. Solvents were responsible for 14.12 ppb-C or 18% of the measured TNMOC concentration in FWNW. The CPF plot shows that solvents were emitted from extremely localized sources surrounding the monitoring station, likely from commercial and industrial uses from residents and local businesses.

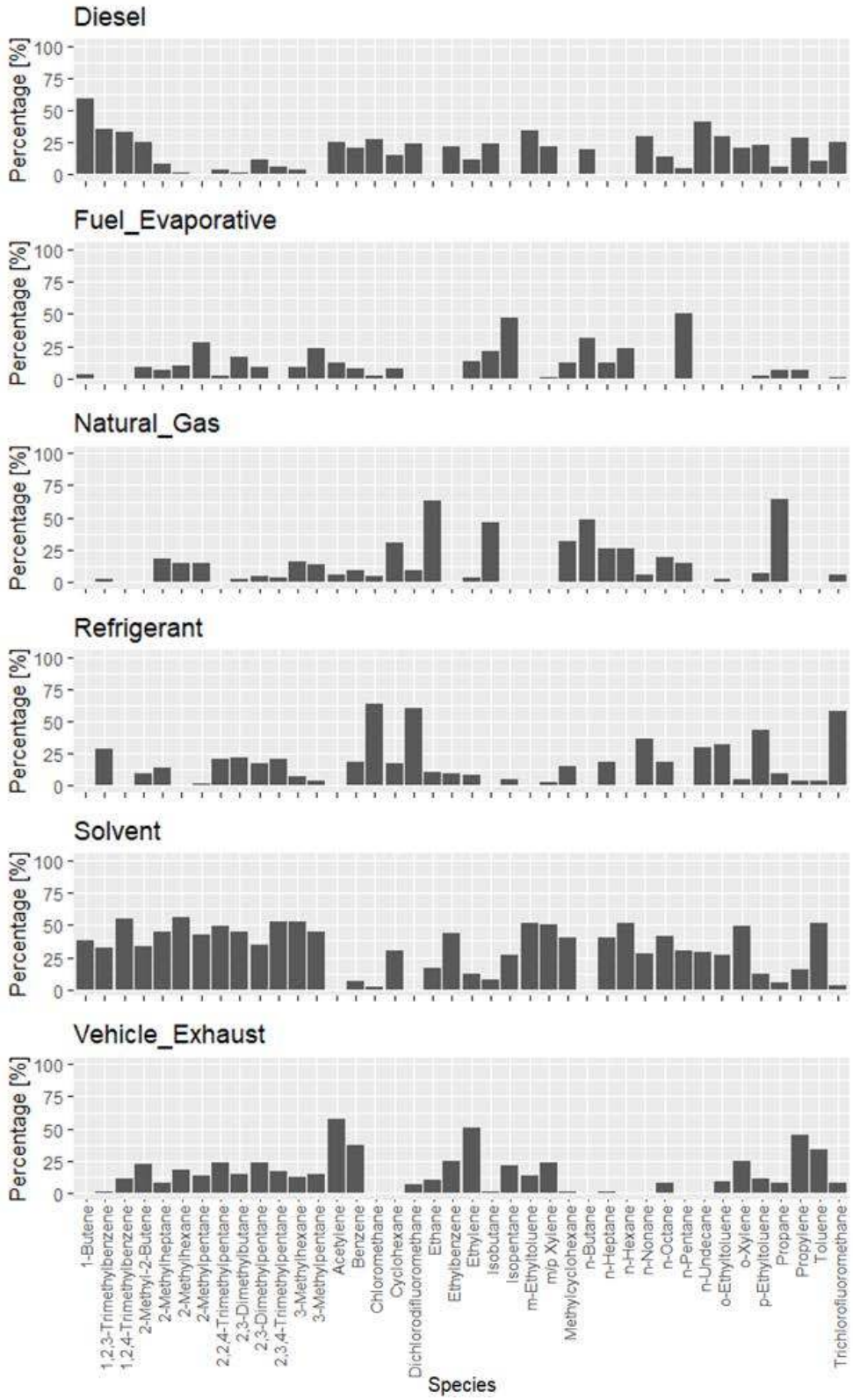

Figure 8.5: Summary of the 6-factor profile at FWNW: (a.) Diesel, (b.) fuel evaporation, (c.) natural gas, (d.) refrigerants, (e.) solvent, and (f.) vehicle exhausts.

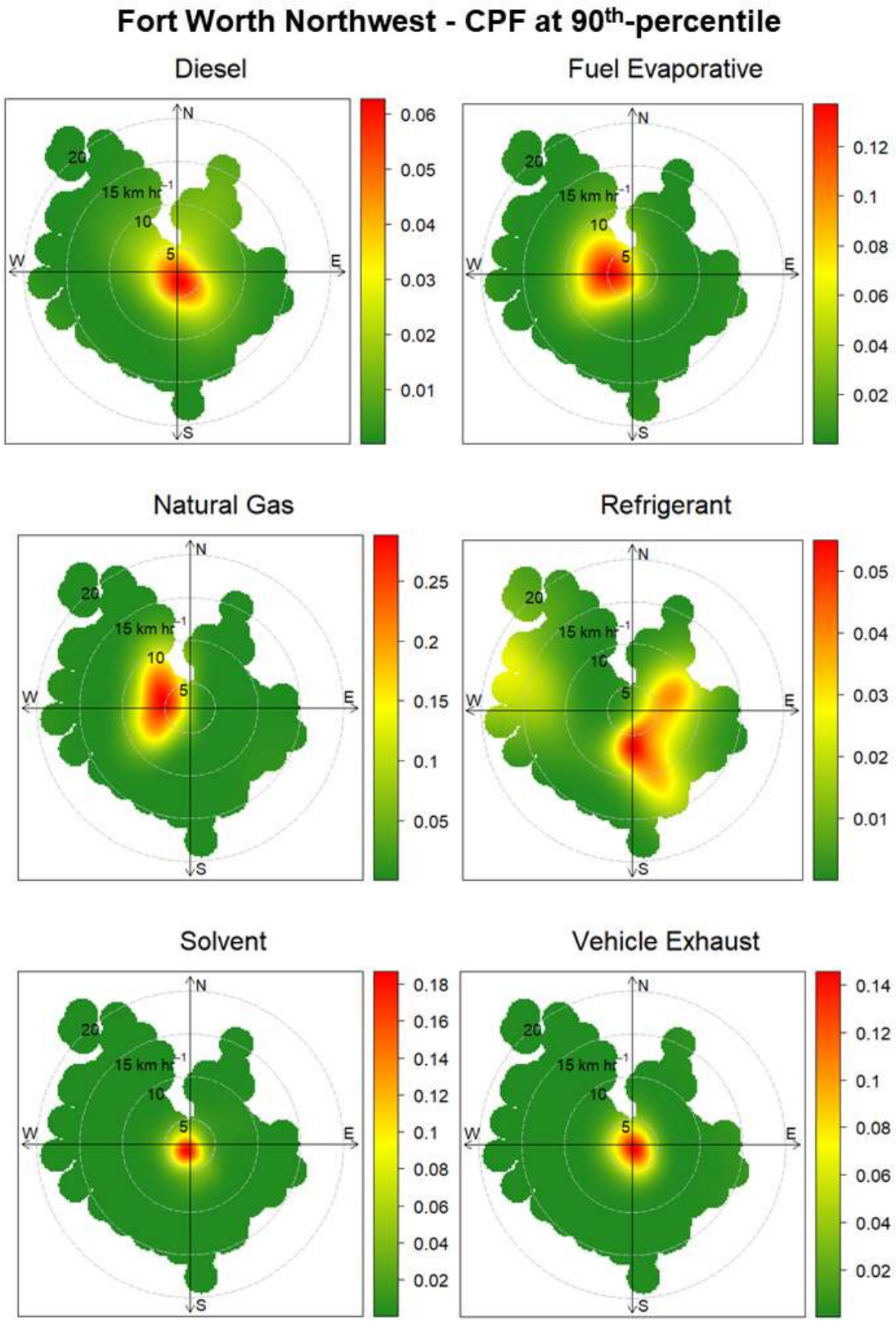

Figure 8.6: 90th-percentile CPF plots (%) for the 6-factors at FWNW: (a.) Diesel, (b.) fuel evaporation, (c.) natural gas, (d.) refrigerants, (e.) solvent, and (f.) vehicle exhausts.

Emissions from refrigerant sources had a concentration of 6.65 ppb-C and was 8% of the measured TNMOC concentration at FWNW. Since the refrigerant factor was carried in by high-speed easterly-, southeasterly-, and southerly winds, the factor was likely influenced by long-range transport of refrigerant chemicals.

Fuel evaporative emissions were responsible for 10.03 ppb-C or 13% of the measured TNMOC concentration at FWNW. Emissions from fuel evaporative were carried-in to the monitoring station by low-speed westerly winds; fuel evaporative had a non-local source within a close proximity to the west of the FWNW monitoring station. Lastly, natural gas was the most significant source of TNMOC at FWNW; the natural gas factor had a concentration of 32.03 ppb-C and was 40% of the measured TNMOC concentration at FWNW. Despite being surrounded by active natural gas wells in all direction, the largest concentrations of natural gas emissions were carried in to the monitoring station during low-speed westerly winds. Since the Fort Worth city limit stops around 8-km west of the monitoring station, the gas wells located outside of the city limit operated on less stringent requirements and were more prone to leakages when compared to the gas wells located within city limits. Since the FWNW monitoring station is located on the eastern edges of the Barnett Shale play SGR, the natural gas factor was also likely influenced by the long-distance transport of oil and gas emissions through westerly winds.

The mean concentration of TNMOC measured at FWNW had decreased considerably between 2003 and 2018, as shown in Figure 8.7. From 2004 to 2007, the mean concentration of TNMOC concentration experienced an increasing trend, which corresponded to an increased production in the Barnett Shale SGR. A decline in the mean concentration of TNMOC was measured between 2007 and 2009 due to the effects of the U.S. economic recession. Corresponding to the rebound experienced shortly after the 2008 recession, the mean concentration of TNMOC measured during 2010 to 2012 experienced an increase. Since 2013,

the mean concentration of TNMOC measured at FWNW had declined mainly due to the overall decreased in natural gas production activities in the Barnett Shale [172]. Similar to DAL, the refrigerant and solvents factors had experienced growth between 2003 and 2018, at the rates of +0.24 ppb-C/year (+3.64%/year) and +0.18 ppb-C/year (+1.33%/year), respectively. Diesel, fuel evaporative, natural gas, and vehicle exhaust declined by -0.61 ppb-C/year (-8.19%/year), -0.22 ppb-C/year (-2.13%/year), -0.45 ppb-C (-0.47%/year), and -0.78 ppb-C (-7.38%/year), respectively. Diesel, fuel evaporative, and vehicle exhaust saw consistent decrease throughout the monitoring period whereas the natural gas factor saw a significant increase prior to 2013 but was followed by a massive decrease since 2013. Thus, it was shown that the increased in impact from natural gas sources had significantly mitigated the efforts in regulating urban emission sources prior to 2013.

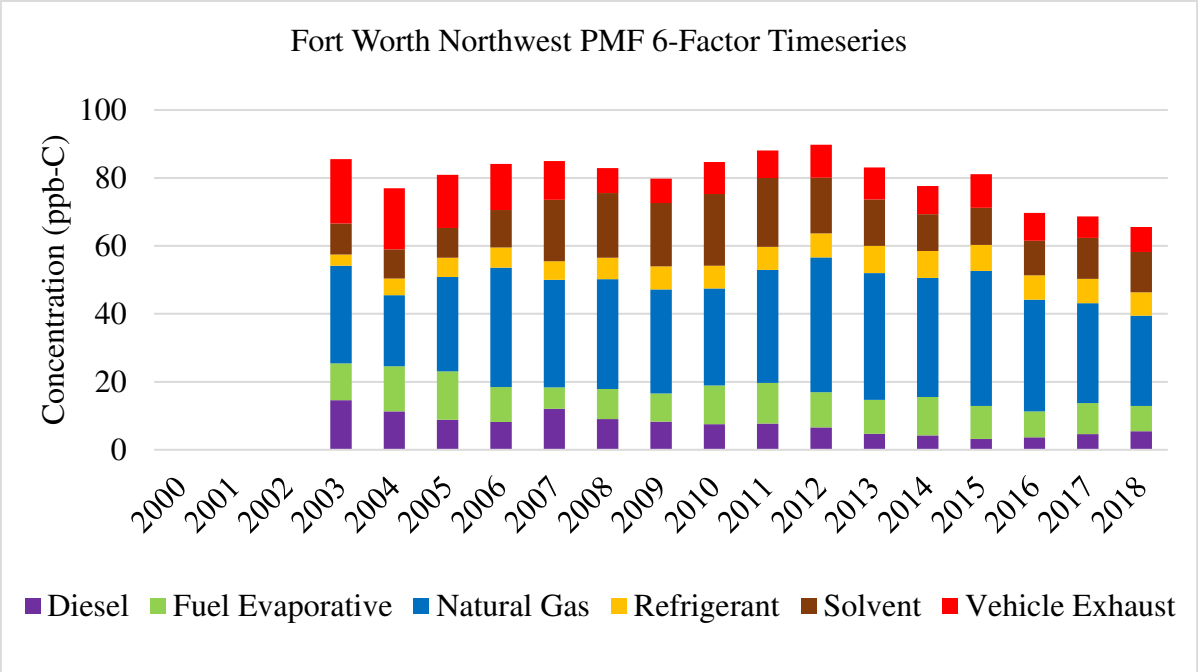

Figure 8.7: Annual variation in the mean concentration of the 6-factors at FWNW.

8.2.3 Denton Airport South (DEN)

The DEN monitoring station is located in an exurban SGR site just outside of the jurisdiction of the Denton City Council. The monitoring station in the Industrial Center District

of Denton County, where the minimum setback distance was 76.2 m [173], which was much lower than the city of Fort Worth's 182.9 m [174]. The mean concentration of TNMOC and alkanes measured at DEN were significantly higher compared to those measured at DAL and FWNW, which suggests larger influence from unconventional oil and gas emissions. The mean concentration of alkene, alkyne, aromatics, and diene measured at DEN were also substantially lower than those measured at DAL and FWNW, suggesting much smaller influence from conventional urban emission sources. Figure 8.8 and Figure 8.9 shows the chemical profiles of the five source factors resolved for DEN and their corresponding CPF bivariate polar plots. The five factors resolved for DEN were fuel evaporation, natural gas, refrigerants, solvent, and vehicle exhausts.

Natural gas was the most dominant factor in DEN, it had a concentration of 115.04 ppb-C and was responsible for 69% of the TNMOC concentration measured at DEN. While natural gas were significant sources of TNMOC at all three sites, the concentration of the natural gas factor at DEN was 5.9 and 3.6 times larger compared to those resolved for DAL and FWNW, respectively. The CPF plot for DEN's natural gas factor showed to had extremely localized sources within close proximity to the monitoring station, the highest concentrations were carried in to the monitoring station by low-speed southwesterly winds from a region with a high number of active natural gas wells. Solvent had a concentration of 10.99 ppb-C and was 7% of the TNMOC concentration measured at DEN. The CPF plot for solvent was almost identical to natural gas, suggesting a high degree of overlap between the both sources. Fuel evaporative contributed to 10.07 ppb-C or 6% of the TNMOC concentration measured at DEN. The primary source of fuel evaporative was from the southwest side of the monitoring station, likely from the storage facilities of nearby oil and gas operations. Traces of solvent were also carried in from city of Denton by northeasterly winds, mainly from commercial and industrial solvent usage in the city of Denton.

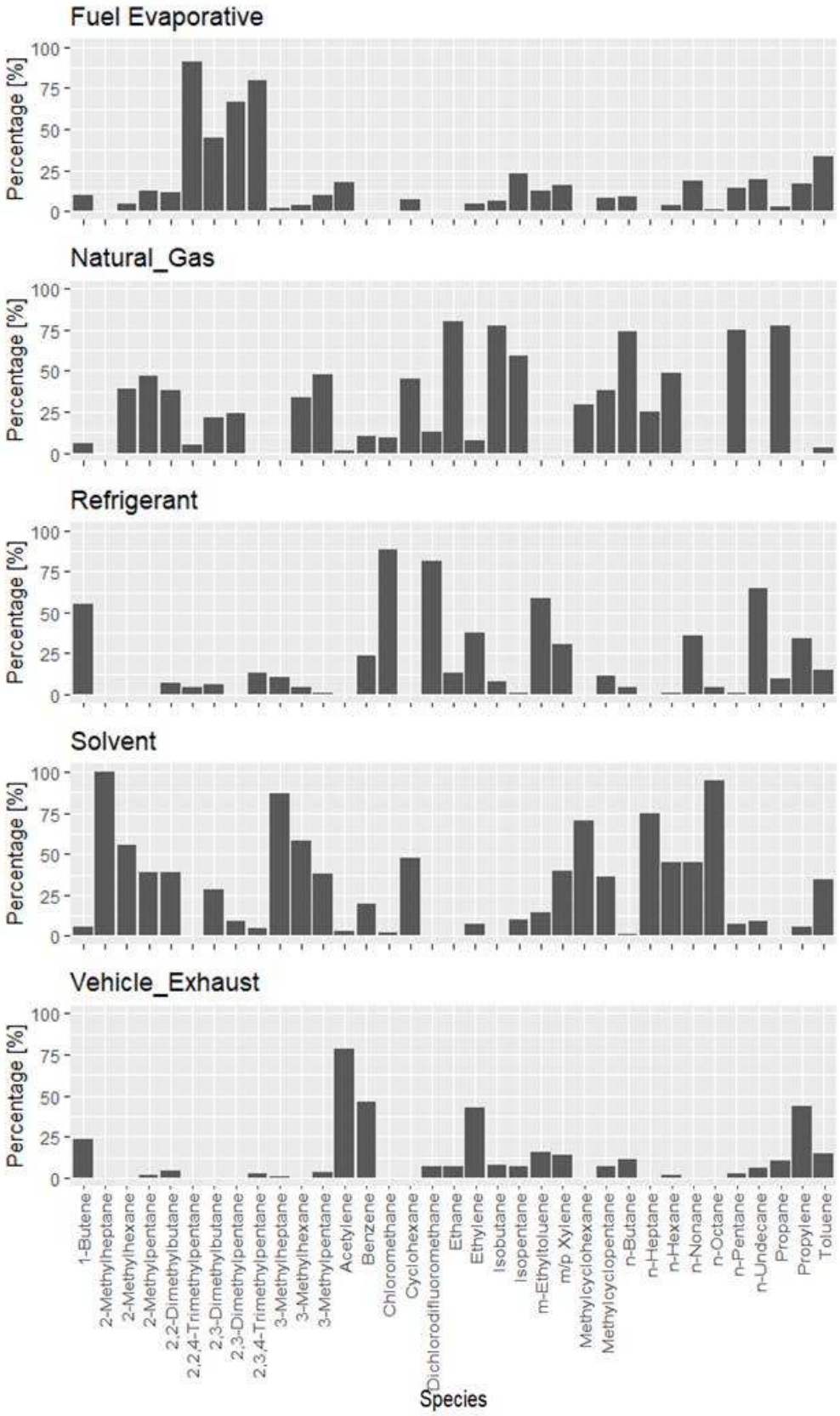

Figure 8.8: Summary of the 5-factor profile at DEN: (a.) Fuel evaporation, (b.) natural gas, (c.) refrigerants, (d.) solvent, and (e.) vehicle exhausts.

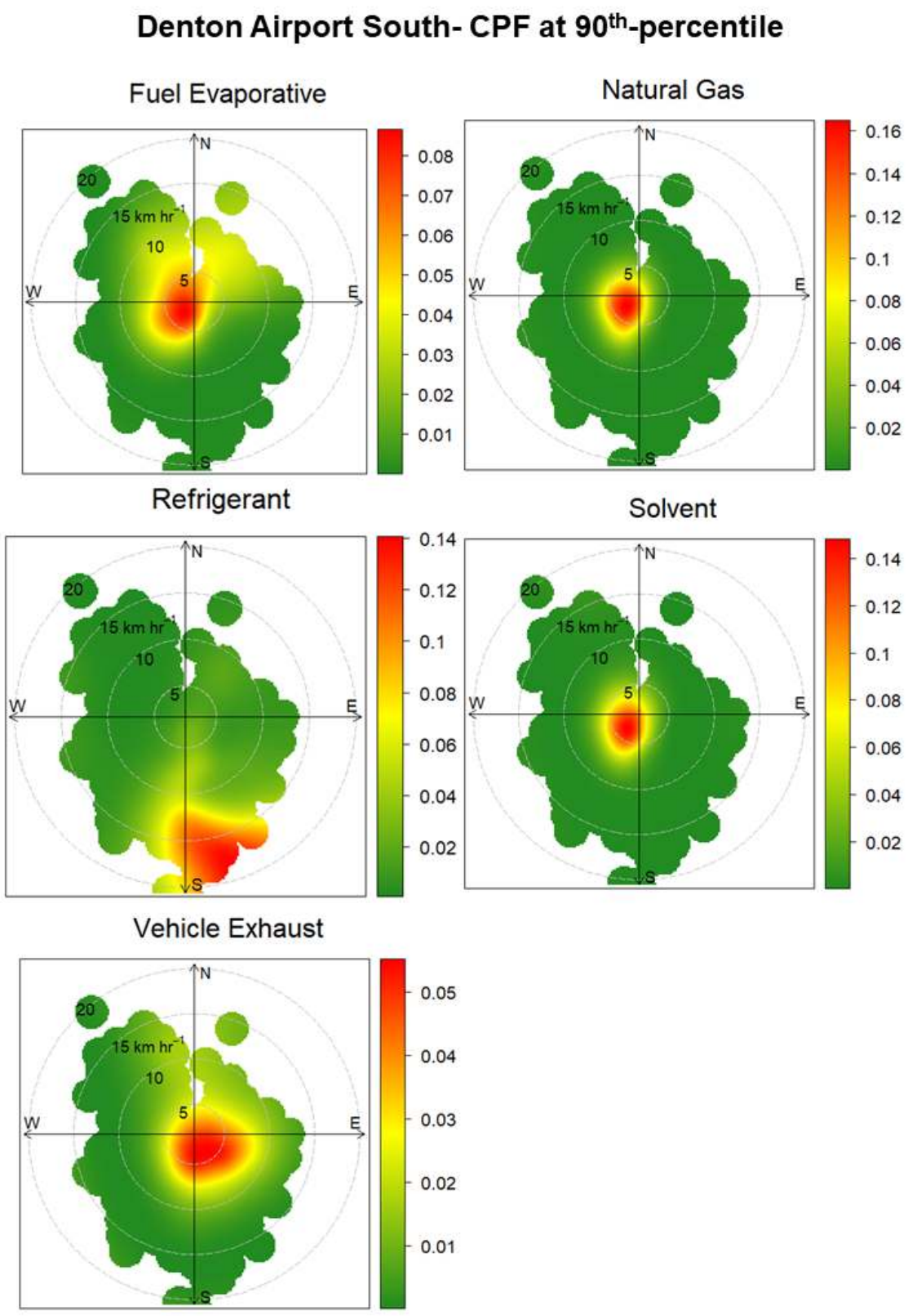

Figure 8.9: 90th-percentile CPF plots (%) for the 5-factors at DEN: (a.) Fuel evaporation, (b.) natural gas, (c.) refrigerants, (d.) solvent, and (e.) vehicle exhausts.

Vehicle exhaust had a concentration of 14.23 ppb-C and had contributed to 9% of the TNMOC concentration. It is important to point out that the vehicle exhaust factor resolve for DEN was larger compared to those resolved for DAL and FWNW, despite a comparatively smaller population and traffic volume surrounding the DEN monitoring station. DEN's vehicle exhaust was a highly localized source that had originated from the Industrial Center District on the northwest side of the monitoring station instead of the city of Denton. The notable commercial structures in the Industrial Center District includes the Peterbilt Motors manufacturing plant and distributing centers for Fastenal, Target, and WinCo Foods. The vehicle exhaust factor at DEN also had a significantly larger composition of ethane and propane compared to the two urban sites, which may be influenced by the manufacturing plants of Peterbilt Motors, a leading manufacturer in natural gas-powered commercial vehicles. Lastly, refrigerants had a concentration of 16.35 ppb-C and was 10% of the TNMOC concentration measured at DEN. The CPF plot for refrigerant shows a significant influence from long-distance deposition of refrigerant chemicals during high-speed southerly winds. Since the DEN monitoring station is downwind from the DFW metroplex, the refrigerant chemicals were likely carried in from the major urban regions in the metroplex, which explains why the refrigerant factor in DEN was 3.2 and 2.5 times larger than those at DAL and FWNW, respectively.

As shown in Figure 8.10, the mean TNMOC concentration measured at DEN was heavily influenced by its natural gas factor. From 2000 to 2018, the natural gas factor grew at the rate of +3.03 ppb-C/year (+2.69%/year). There was significant growth in the natural gas factor in between 2000 and 2006, where the concentration increased from 6.66 ppb-C to 130.81 ppb-C, which corresponded to the enhanced shale gas production across the Barnett Shale region. The natural gas factor dropped to 83.04 ppb-C at the beginning of the economic recession in 2007, but had climbed back to 89.11 ppb-C by the end of the recession period in 2009. Following the economic rebound in 2010, natural gas emissions saw a continued

increased until it peaked in 2012. Since 2013, natural gas emissions dropped significantly corresponding to the decreased in shale gas production throughout the Barnett Shale [172]. Solvent was the only other factor that had experienced a growth since 2000, at the rate of +0.15 ppb-C/year (+1.35%/year). Since the CPF plots for natural gas and solvent were nearly identical, solvent use during oil and gas operations surrounding the DEN monitoring station were significant and the amount of solvent used likely depended heavily on oil and gas operations. Fuel evaporative, refrigerant, and vehicle exhaust all experienced a decrease between 2000 and 2018, at the rates of -0.68 ppb-C/year (-6.66%/year), -0.08 ppb-C/year (-0.47%/year), and -0.3 ppb-C/year (-2.1%/year), respectively.

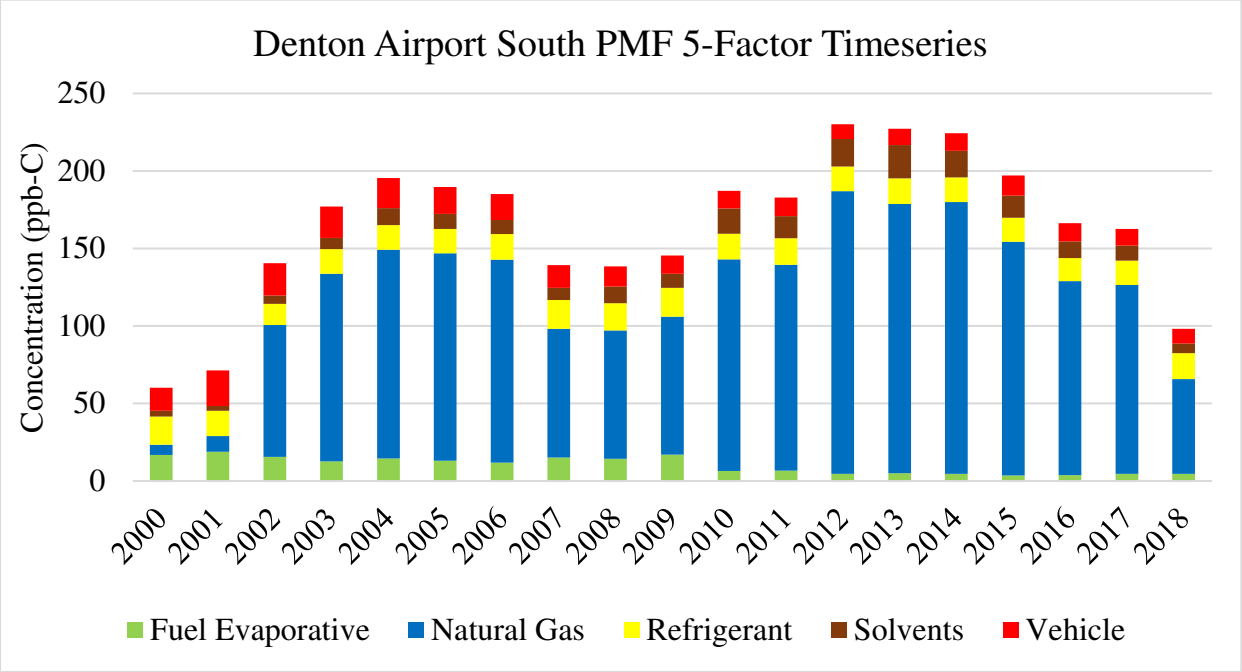

Figure 8.10: Annual variation in the mean concentration of the 5-factors at DEN.

8.3 Summary Findings

Despite being the least urbanized site among the three, the highest mean concentration of TNMOC from 2000 to 2018 was measured in DEN. DEN also had the highest concentration of alkanes, whereas DAL had the highest concentrations of alkene, alkyne, aromatics, and diene. Since 2000, the mean concentrations of TNMOC measured at DAL and FWNW had

showed significant decline; however, the mean concentration of TNMOC measured at DEN was more abundant in 2018 when compared to 2000 despite a considerable decline since 2012. Using the PMF method, the TNMOC concentrations measured at DAL, FWNW, and DEN were resolved into five, six, and five-factor models, respectively. The TNMOC concentration measured at DAL was influenced by natural gas (32%), solvent (27%), fuel evaporative (18%), vehicle exhaust (15%), and refrigerant (8%). At FWNW, the TNMOC concentration was mainly influenced by natural gas (40%), solvent (18%), fuel evaporative (13%), vehicle exhaust (13%), diesel (9%), and refrigerant (8%). The factors that were influencing the TNMOC concentration measured at DEN includes natural gas (69%), refrigerant (10%), vehicle exhaust (9%), solvent (7%), and fuel evaporative (6%). Across all three monitoring stations, localized emission sources had a higher influence local TNMOC concentrations compared to those from long-range transport. Natural gas was a significantly larger factor at DEN compared to the other two sites and it had a direct impact on the measured TNMOC concentration at DEN since 2002. While the impact of the natural gas factor in FWNW was smaller than DEN, there was also strong evidence of its impact on measured TNMOC concentrations in FWNW. Before 2013, the TNMOC concentrations in FWNW had remained high despite a decline in conventional urban emission factors due to enhance influence from the natural gas factor. The natural gas factor was also the largest component of the measured TNMOC in DAL, despite not being located within an active SGR, which implied fugitive emissions from oil and gas storage and transport facilities. Thus, it can be concluded that the decrease in the measured TNMOC concentrations since 2013 was a direct result of the decrease in shale gas production volume across the Barnett Shale.

CHAPTER 9

ADOPTING MACHINE LEARNING TECHNIQUES FOR AIR QUALITY DATA ANALYSIS

In recent years, the increase in computing power in everyday computers has provided the data-driven machine learning (ML) approach as an alternative to traditional deterministic or physics-based air pollutant predicting and forecasting strategies [58, 59, 60, 61, 62, 63]. Unlike more conventional methods, mechanical and chemical models that dictate air pollution concentration are not required in ML approaches; instead, the variables are fed to the black box, and it will try to produce a model with the least error between measured and predicted values [63]. Five ML algorithms were trained with Fort Worth Northwest (FWNW) dataset to predict ozone concentration. The five ML algorithms are artificial neural network (ANN), classification and regression tree (CaRT), k-nearest neighbor (kNN), random forest (RF), and support vector machine (SVM). Ultimately, the models will be tested using data collected from a different location, with different terrain, emission characteristics, and data quality, to determine whether the ML approach can mitigate the lack of good quality air pollution data in majority of the country including rural locations. The goal was not to build a model to predict future air pollution episodes, but to generate data samples that would fill in non-available data.

9.1 Training and Validating Dataset Variables

To successfully predict air pollutant concentrations, the training dataset of the ML model frequently includes both meteorological and pollutant emissions variables [63]. Temperature, relative humidity, and wind speeds are meteorological variables that play an essential role in ozone generation. Ozone generation is high when the temperature is high, and the wind condition is calm; and it decreases with the increase in relative humidity [175]. Table 9.1 shows the summary of the training (2000 -2016) and validating (2017 – 2018) dataset, which consists of hourly concentrations of air pollutants (previous-day-ozone, NO_x, and

TNMOC categorized by hydrocarbon groups) and meteorological data (outdoor temperature, relative humidity, and wind speed) measured at the FWNW monitoring station. The training dataset has 91,815 individual samples, and the validating dataset has 7,014 individual samples.

Table 9.1: Summary of the training (2000 – 2016) and validating (2017 – 2018) datasets.

	Variables	Mean	Median	Min-Max	IQR
Training dataset (2000 – 2016)	Ozone (ppb)	28.216 ± 0.059	26.614	-3.596 - 144.565	15.178 - 38.734
	Alkane (ppb-C)	72.971 ± 0.298	44.108	0.388 - 3996.47	26.108 – 82.578
	Alkene (ppb-C)	3.879 ± 0.016	2.356	0 - 155.708	1.491 - 4.153
	Alkyne (ppb-C)	0.7867 ± 0.004	0.5298	0 - 42.417	0.2581 - 0.9111
	Aromatics (ppb-C)	6.917 ± 0.034	3.97	0 - 1271.373	2.382 – 7.375
	Diene (ppb-C)	0.4643 ± 0.002	0.2747	0 - 10.5535	0.1169 - 0.6161
	NO_x (ppb)	15.421 ± 0.072	8.202	-3.889 - 438.969	4.142 - 17.498
	Relative humidity (%)	58.793 ± 0.069	58.793	7.492 - 100	41.827 - 75.849
	Wind speed (Mph)	7.499 ± 0.014	6.969	0.044 - 32.297	4.431 - 9.802
	Outdoor temperature (^oF)	68.15 ± 0.056	70.34	11.45 - 108.07	55.58 - 81.33
Validating dataset (2017 – 2018)	Ozone (ppb)	29.657 ± 0.187	29.232	-4.564 – 93.061	18.465 – 40.008
	Alkane (ppb-C)	54.41 ± 0.645	36.528	0.978 – 715.381	23.301 – 64.381
	Alkene (ppb-C)	2.883 ± 0.033	2.064	0 – 43.572	1.495 – 3.195
	Alkyne (ppb-C)	0.475 ± 0.007	0.35	0 – 7.615	0.186 – 0.573
	Aromatics (ppb-C)	4.872 ± 0.066	3.21	0 – 103.118	2.131 – 5.2
	Diene (ppb-C)	0.48 ± 0.007	0.288	0 – 9.816	0.139 - 0.618
	NO_x (ppb)	10.516 ± 0.177	5.832	-2.09 – 189.556	2.678 – 12.005
	Relative humidity (%)	57.88 ± 0.233	57.776	9.727 – 97.302	43.56 – 73.506
	Wind speed (Mph)	7.653 ± 0.051	7.069	0.239 – 30.426	4.563 – 9.968
	Outdoor temperature (^oF)	68.77 ± 0.185	71.35	14.12 – 100.46	558.26 – 80.33

9.2 Simple vs Ensemble ML Model

The training dataset can be divided into two groups, the mechanical meteorological data, and the chemical air pollutant concentration data. An ensemble ML model where the mechanical and chemical ML models were trained separately and then combined at the end was built to ensure these datasets do not get lumped together. According to Graczy et al. [176], there are three popular methods of creating ensemble ML models: bagging, boosting, and

stacking. The bagging process builds multiple models of the same type using different subsets of the same training dataset; the predictions made are then averaged. Boosting builds several models of the same type in a chain. Each subsequent model fixes the errors in the prediction made by the model before it on the chain. Lastly, stacking builds multiple different models and a supervisor model at the end to identify the best way to combine the predictions made by the various models [176]. Since the ensemble model divides the training dataset into subsections and separately trains them using the same algorithm, the bagging ensemble method is ideal.

A simple, all-encompassing ANN model was trained alongside the ensemble ANN model that split the mechanical and chemical datasets, using 80% of the training dataset and validated using validating datasets. The prediction made by both side of the ensemble ANN model were averaged into a single prediction. However, the mean error of the ensemble ANN model was -0.583 ±8.767 ppb, which was more than twice as high as the mean error of the simple ANN model at -0.219 ± 7.633 ppb. Attempting the ensemble method once more with the RF algorithm again showed higher mean errors produced by the ensemble model compared to the simple RF model, at -0.681 ± 8.641 ppb and -0.583 ± 8.767 ppb, respectively. Errors were introduced during the partitioning of the training dataset and averaging of the predicted values. The training dataset was not partitioned for the rest of this study to avoid these errors.

9.3 Identifying the Ideal Training Dataset Sample Size

Over- and underfitting an ML model decreases its prediction accuracy [177]. Overfitting happens when the model is trained with too much data, and it picks up knowledge from noise and inaccurate data. On the other hand, when a model is under fitted, it cannot capture the entirety of the trend due to a lack of data [177]. To overcome over- and underfitting, an RF model was trained repeatedly with increasing training size and validated using a randomly generated subset of validating dataset. Table 9.2 shows the performance statistics of the ML model with the training dataset size of 100 through 20,000. The performance of the

ML increases with the size of the training dataset; however, the improvement in the model's performance past 3,000 training dataset samples were not as significant. The percentage changes in performance improvement from the size of 3,000 onward were under the standard error. Thus, a training dataset size of 3,000 was the most ideal for training the ML models.

Table 9.2: The performance of the ML model using different training dataset sizes.

Size	RMSE	MAE	R^2	FB	FE	MNB	MNE
100	9.64	7.52	0.63	10.72%	32.72%	28.19%	69.91%
500	7.86	6.08	0.76	12%	30.48%	22.66%	52.91%
1,000	7.41	5.69	0.79	9.32%	26.54%	18.18%	47.54%
2,000	7.24	5.54	0.80	8.89%	25.81%	17.44%	46.75%
3,000	7.18	5.49	0.80	8.74%	26.09%	16.54%	45.17%
4,000	7.18	5.48	0.80	9.73%	27.09%	15.82%	44.08%
5,000	7.18	5.49	0.80	6.8%	24.36%	14.54%	43.43%
6,000	7.17	5.48	0.80	6.48%	23.71%	14.47%	42.94%
7,000	7.08	5.39	0.80	6.51%	23.37%	14.28%	42.69%
8,000	7.07	5.39	0.80	6.9%	24.08%	13.69%	41.54%
9,000	7.06	5.38	0.80	5.9%	23.15%	13.04%	41.83%
10,000	7.04	5.37	0.80	6.98%	24.02%	13.35%	42.3%
15,000	7.01	5.34	0.80	6.97%	24.33%	12.7%	41.97%
20,000	6.98	5.32	0.81	8.04%	25.22%	13.07%	42.18%

1.1. Performance of ML models

The multivariate linear regression (MLR) is very commonly used in statistical applications and assumes that the relationship between the target and associated variables can be modeled using linear predictor functions [178]. The MLR correlates each variable and associates a coefficient number according to the relationship. A higher coefficient is given to the variables with a higher importance in predicting the target variable. However, the MLR model is limited to linear relationships and can be severely affected by an outlier [179]. Since most air pollutant concentration datasets are full of outliers, it would be challenging to produce

an accurate prediction using the MLR model. The performance statistics of the MLR serves as a benchmark for the ML models. Figure 9.1(a) ozone concentration predicted by the MLR versus the measured concentrations in the validation data. The MR predicted significantly more negative values than the ones in the validation data, at 109 versus 29.

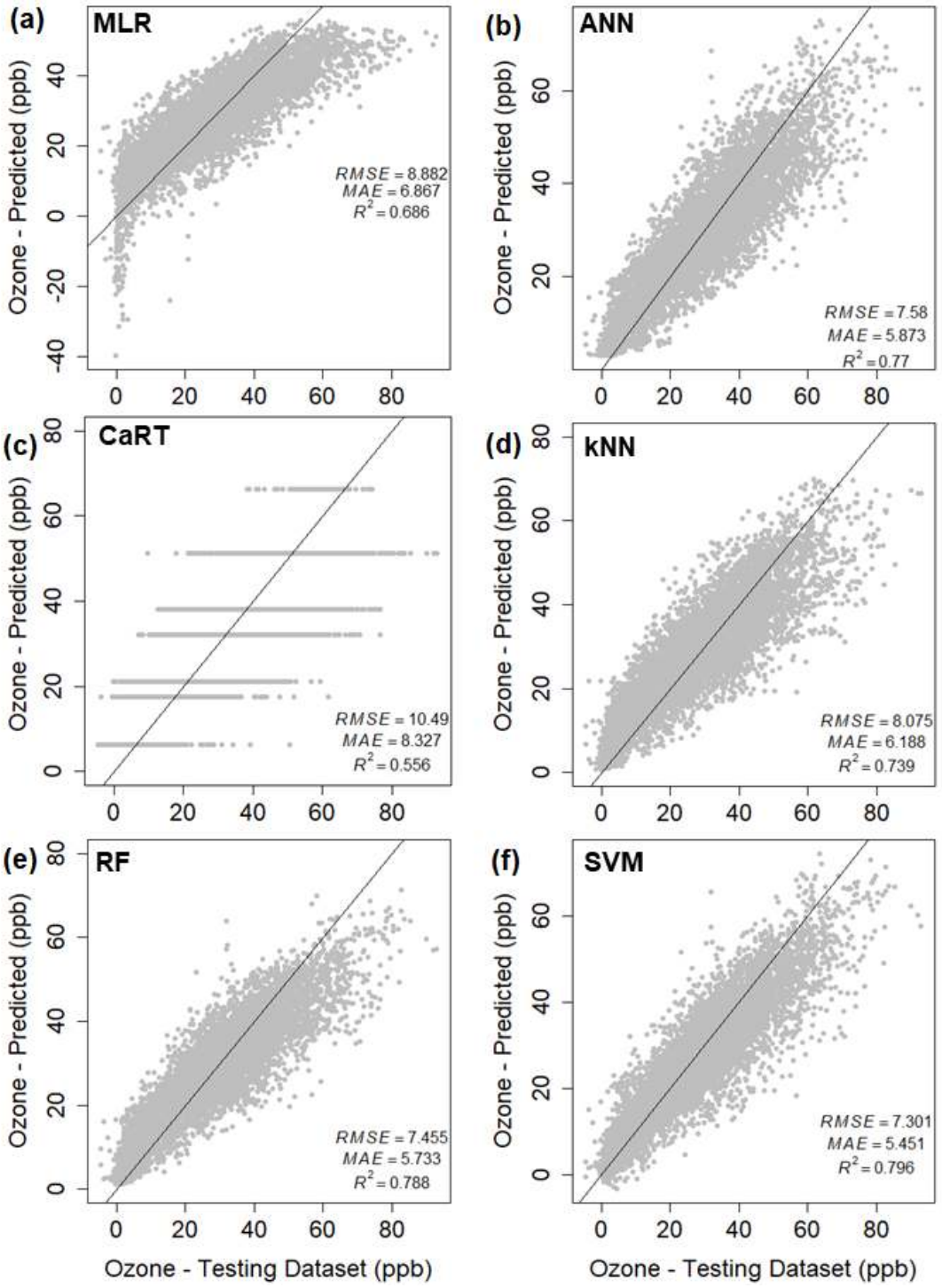

Figure 9.1: Predicted versus measured ozone concentration (ppb) for (a) MLR, (b) ANN, (c) CaRT, (d) kNN, (e) RF, and (f) SVM with their respective RMSE, MAE, and R^2-values.

9.3.1 Artificial Neural Network (ANN)

The performance of an ANN model can be manipulated by adjusting the weight decay and the size of the model. Weight decay prevents the weight assign to each link from growing too large [89]. A grid with different combinations of weight decay (0.1 to 0.5) and size (1 to 10) was constructed. ANN models with different combinations were built, and the optimal model would be the model with the smallest RMSE, smallest MAE, and largest R^2-value. It was identified that the best performing model had a size of 9 and a weight decay of 0.2. As shown in Figure 9.1(b), the ANN model's predicted ozone concentration had an RMSE of 7.58, MAE of 5.873, and an R^2-value of 0.77. Compared to the MLR, the ANN's predicted values had a 14.66% lower RMSE, 14.48% lower MAE, and a 12.14% higher R^2-value.

9.3.2 Classification and Regression Tree (CaRT)

When building a regression tree model, a large tree is first grown and then pruned to balance fitting versus over-fitting [180]. Figure 9.2 depicts the relationship between tree size, complexity parameter (cp), and the relative error. Cp controls the decision tree size and is used to select the optimal size for the decision tree. If adding a variable to the decision tree from the current node will cost more than the cp value, then the additional variable will not be added to the decision tree [93]. The tree was pruned to 7 terminal nodes or cp of 0.015 because the decrease in relative error after 7 terminal nodes was insignificant, and represents the best regression tree model based on the training data (Figure 9.3). As shown in Figure 9.1(c), the RMSE, MAE, and R^2-value of the predicted values were 10.49, 8.327, and 0.556, respectively, and these were -18.12%, -21.27%, and -18.93% worse than the MLR. As discussed by Mitchell [80], decision trees have problems making an out-of-sample prediction since the predicted values were strictly limited to the values on the terminal nodes. Also, the predictions are sensitive to minor changes as a slight difference can lead to an entirely different terminal node.

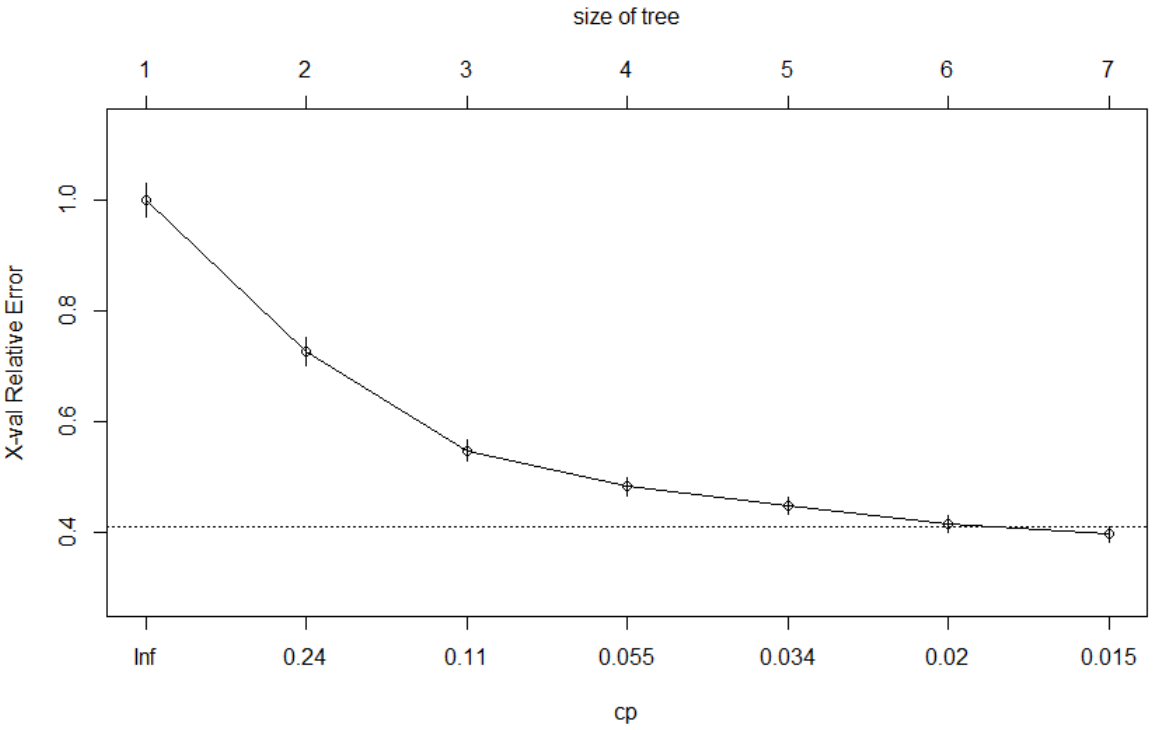

Figure 9.2: Relative error versus cp and tree size.

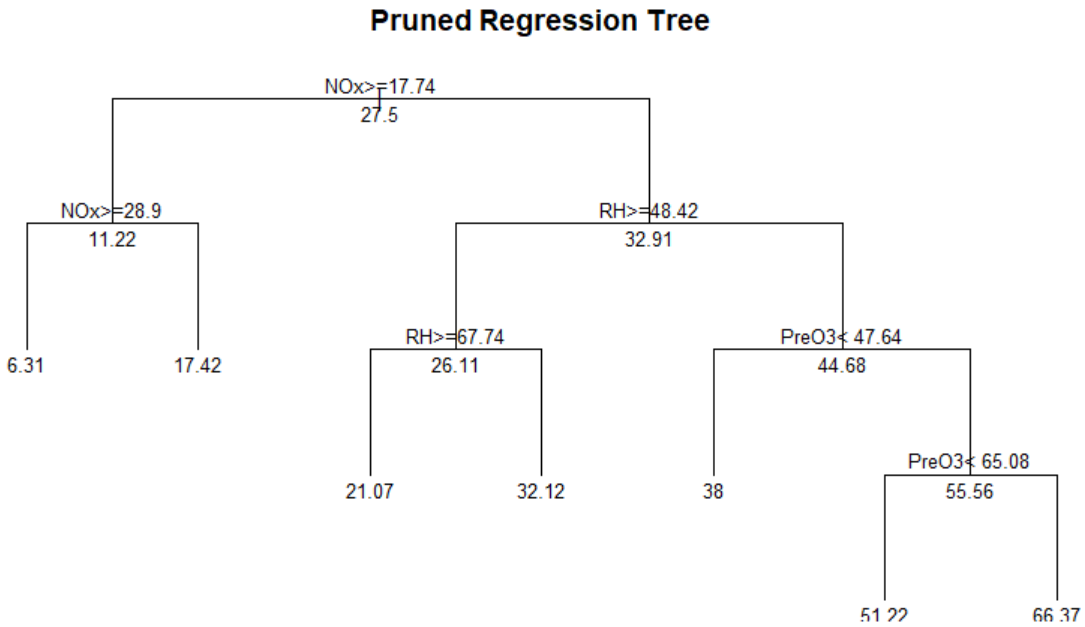

Figure 9.3: Pruned regression decision tree.

9.3.3 k-Nearest Neighbor (kNN)

The kNN model does not learn anything from the training data; instead, it memorizes the training data and uses it to populate the validating dataset. Thus, the kNN is often used in

applications where the dataset is continuously updated [94, 95, 96]. The kNN model was trained to predict based on the Euclidean distance. To maximize its performance, the most critical step in training a kNN model is choosing the optimal number of neighbors, *k* [94, 95, 96]. The kNN model was trained repeatedly with increasing *k*-value until there was no significant decrease in the RMSE. As shown in Figure 9.4, the decrease in RMSE significantly drop after the *k*-value of 10; thus, 10 was the optimal *k*-value for this training dataset. In Figure 9.1(d), the optimized kNN model had predicted ozone concentration with an RMSE of 8.075, an MAE of 6.188, and an R^2-value of 0.739 with the measured values. These predicted values were 9.09%, 9.89%, and 7.68% better than the MLR, respectively.

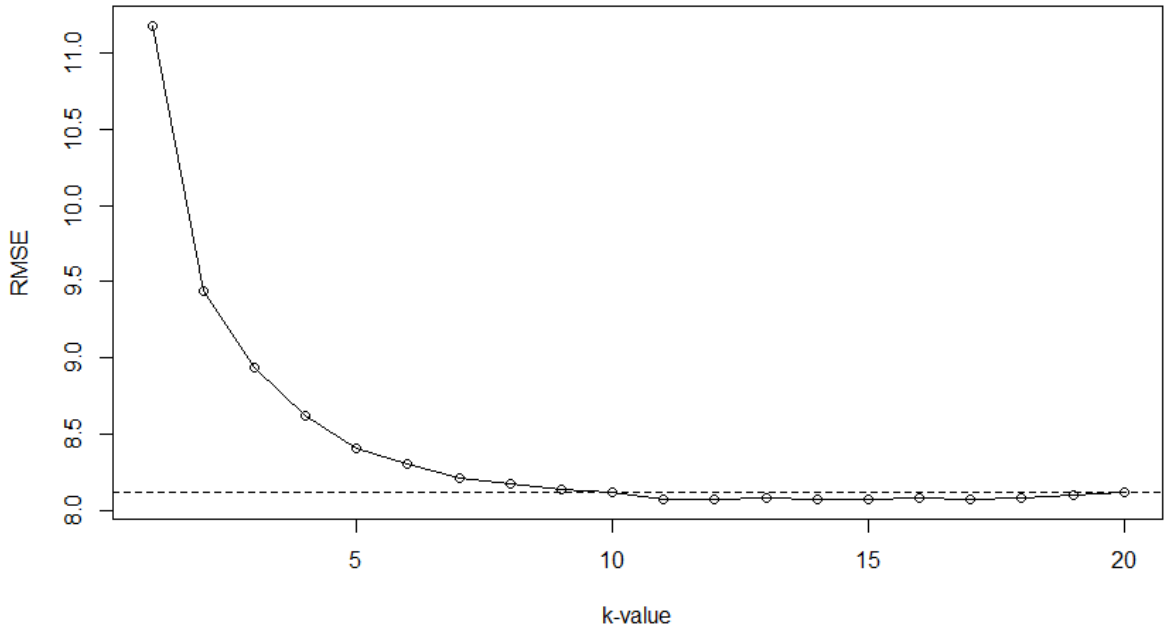

Figure 9.4: Number of k-values versus RMSE for the kNN regression.

9.3.4 Random Forest (RF)

While the RF is composed of multiple individual decision trees, it overcomes the lack of smoothness in predicted values through aggregating the predicted values of the individual trees [100]. As shown in Figure 9.1(e), the ozone concentrations predicted by the RF model had an RMSE of 7.455, an MAE of 5.733, and an R^2-value of 0.788. The performance of the RF model was 16.07%, 16.52%, and 14.79% better than the MLR model in terms of RMSE,

MAE, and R^2-value, respectively. The importance of each variable to an RF model can be found using the "Boruta" and "caret" packages. The "Boruta" use mean-decrease-in-accuracy as an estimate of importance [181]. Mean-decrease-in-accuracy is a measure of the increase in error when the variable is removed from the training dataset. The "varImp" function in "caret" tracks the changes in the generalized cross-validation (GCV) estimate of error when a variable is added to the model. The lower the overall GCV estimate of error, the less valuable a variable is to the model [89]. As shown in Table 9.3, relative humidity and previous day ozone were the two most important variables to the RF function. The "Boruta" function shows the outdoor temperature to be the third most crucial feature, whereas the "caret" function showed had NO_x as its third most important variable.

Table 9.3: Training dataset variable importance to the RF model.

Variable	"Boruta" - MeanImp	"caret" - Overall
Alkane	30.9950	33.1972
Alkene	23.3755	18.5858
Alkyne	20.4013	28.5692
Aromatics	23.9412	24.8781
Diene	34.3227	56.5070
NO_x	36.4179	*63.7649*
Relative Humidity	*69.9235*	*124.9604*
Wind Speed	29.2461	47.2515
Temperature	37.0579	42.5721
Previous-day-O_3	*50.1916*	*81.1483*

9.3.5 Support Vector Machine (SVM)

The SVM model was constructed using the polynomial kernel. The epsilon (ϵ) -value defines the tolerance margin of the SVM model where no penalty is given to errors within the specified range; the default ϵ-value in the "e1071" package is 0.1 [107]. The SVM model also has an adjustable cost parameter, which avoids overfitting by balancing margin maximization and loss [107]. The process of tuning the SVM model involves identifying the best possible

combination of the ϵ-value and the cost parameter. Numerous SVM models were trained with different ϵ-values (0 to 1 with intervals of 0.1) and cost parameters (2^2 to 2^4 with intervals of 2) to find a combination with the best performance using the "tune" function in "e1071".

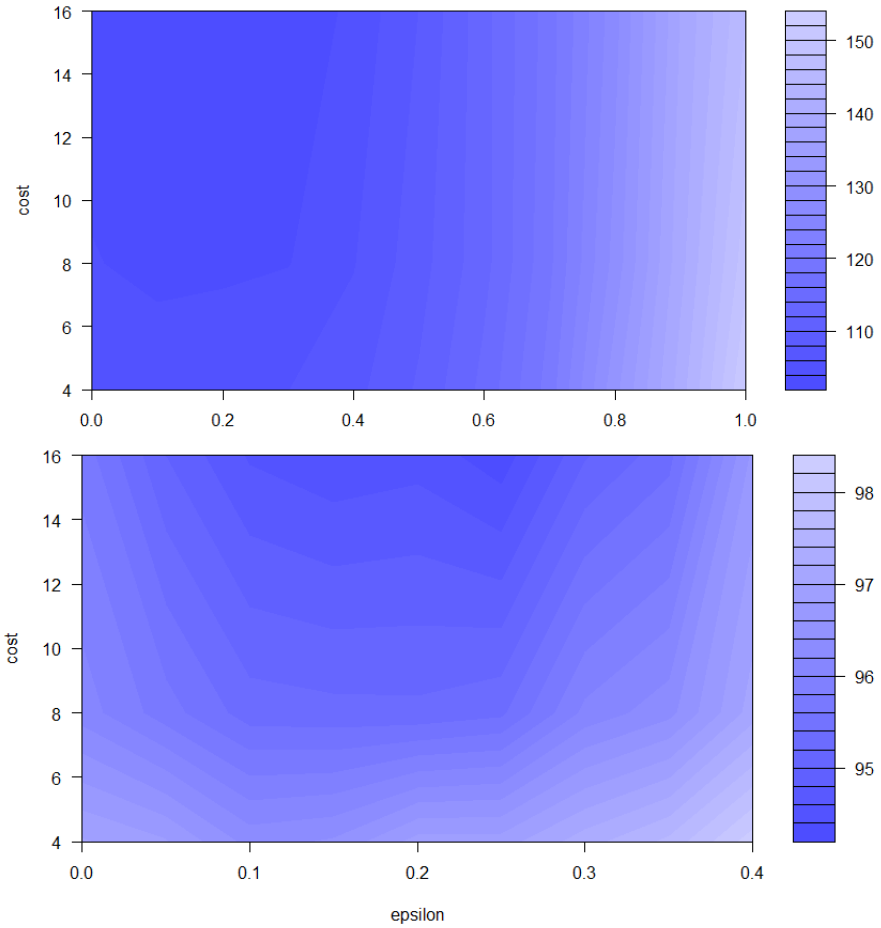

Figure 9.5: Tuning graph of the SVM model: (a) ϵ = 0 – 1, and (b) ϵ = 0 – 0.4.

Figure 9.5 shows the tuning graphs for the SVM regression model with ϵ-value ranging from (a) 0-to-1 and (b) 0-to-0.4, respectively, where the darker shaded regions represent combinations of cost and ϵ-value with lower errors as shown in the sidebar [107]. In Figure 9.5 (a), the model combination with the least error was found in ϵ-values between 0 and 0.4, and cost between 7 and 16. According to the model summary, the best model can be trained using ϵ-value at 0.3 and cost parameter at 16; and the error of the best performing model was 102.337. The performance of the SVM regression model can be further turned by narrowing the ϵ-values range to 0-to-0.4, as shown in Figure 9.5(b). The intervals between ϵ-values were narrowed

from 0.1 to 0.01. The model with the least error was found in the region between the cost of 13 to 16 and ϵ-values between 0.2 and 0.3. The best performing model had an error of 94.279, and its best parameters were ϵ-value of 0.25 and the cost parameter of 16. As shown in Figure 9.1(f), the predicted values of the tuned SVM model have RMSE, MAE, and R^2-value of 7.301, 5.451, and 0.796, respectively. The performance of the tuned SVM model is better than the MLR by 17.81%, 20.62%, and 15.9% in terms of RMSE, MAE, and R^2-value, respectively.

9.3.6 ML Model Performance Comparison

Table 9.4 shows the performance of each ML algorithm compared to the MLR model. The SVM is the best performing algorithm, followed by RF, ANN, and kNN. Of the five ML models, the CaRT was the only one with a worse performance compared to the MLR. The CaRT algorithm's weakness is the inability to produce predictions outside of the terminal nodes [80], which had resulted in a weaker performance than the other ML models and the MLR. The terminal node value produced by the CaRT represents the mean value of variables with similar characteristics in training data [80]. However, air pollution concentrations do not follow a linear pattern; thus, the CaRT is likely unsuitable for air pollution concentration predictions. While the performance of the kNN model was better than the MLR, it was significantly worse than SVM, RF, and ANN. The kNN model does not learn from the training dataset; instead, it memorizes the training dataset and uses it in tandem with the validation set to make a prediction. The performance of the kNN drops when faced with imbalanced data, missing data, and outliers [94, 95, 96]; thus, it leads to a weaker performance when used in tandem with air pollution concentration data that is imbalance and has plenty of missing or outlier data. The ANN is weaker than the RF and SVM because it tends to be unstable when the training dataset is large due to generalization [88]. The SVM is exceptionally robust when solving large datasets with many variables, which makes the algorithm a good fit for predicting air pollution concentration [182].

Table 9.4: The performance of the MLR and each ML models on the validating dataset.

Model	RMSE	MAE	R^2	FB	FE	NMB	NME
MLR	8.882	6.867	0.686	10.281%	26.784%	6.077%	97.991%
ANN	7.580	5.873	0.770	8.652%	27.698%	16.368%	52.587%
CaRT	10.491	8.327	0.556	8.977%	36.430%	32.480%	83.968%
kNN	8.075	6.188	0.739	10.188%	27.757%	19.116%	57.298%
RF	7.455	5.733	0.788	7.65%	25.981%	15.964%	48.131%
SVM	7.301	5.451	0.796	5.319%	18.773%	10.282%	39.087%

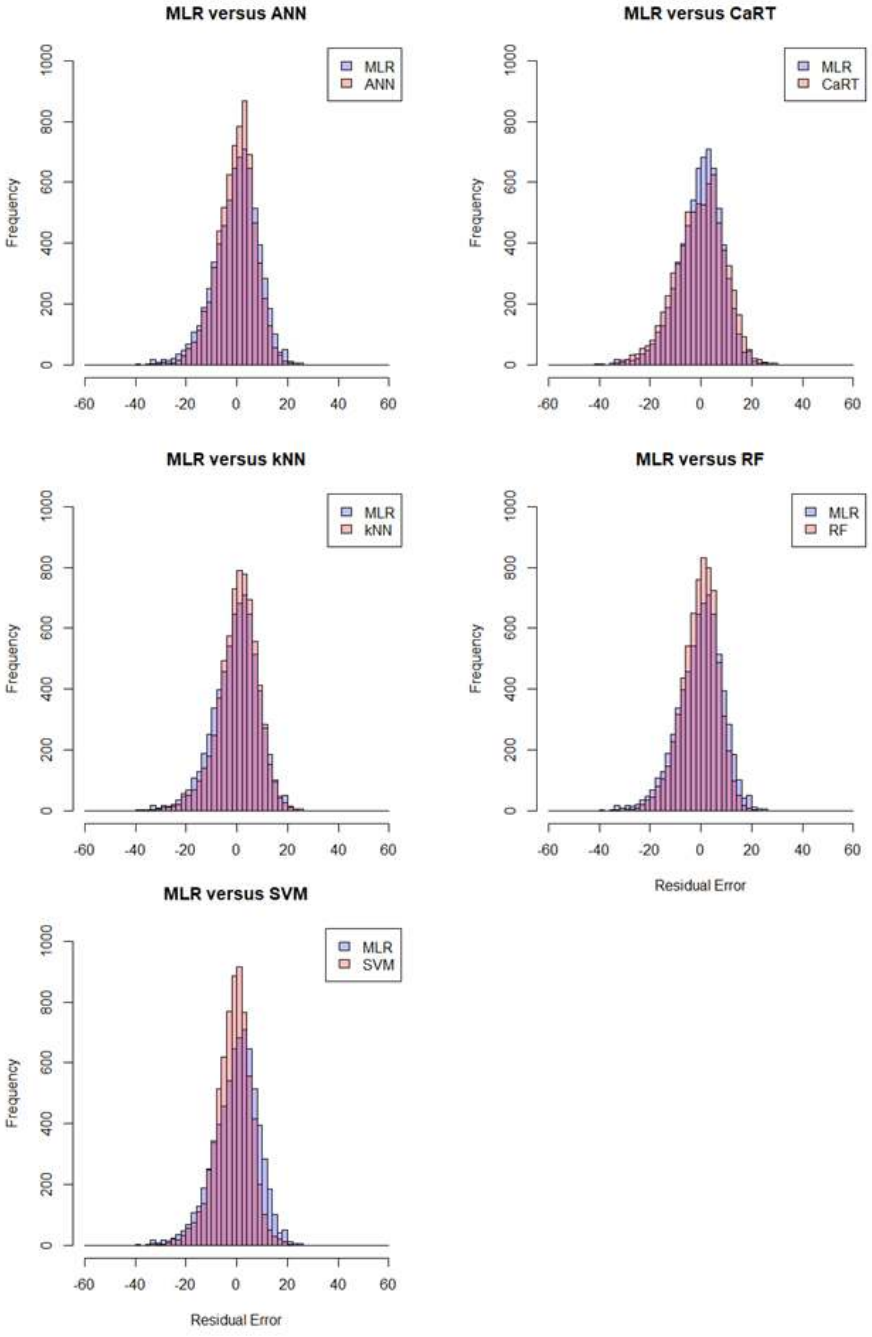

Figure 9.6: Error residuals of the predicted values using ML models versus MLR.

Error residuals are the difference between predicted and measured values, and they were used as a measure to assess the quality of an ML model. Figure 9.6 shows the detailed comparisons between the residual distributions of MLR and each ML models. Four of the five ML models, excluding the CaRT, have higher frequencies at the zero compared to the MLR. A higher frequency of zero residuals indicates higher prediction accuracy and lower errors. The SVM has the highest frequency at the zero, followed by the ANN, RF, and kNN. Again, the CaRT model was the only one that produced a lower frequency at the zero than the MLR.

9.4 Testing the ML Models against Photochemical Models

Photochemical models are often used to predict air pollutant concentration and deposition with numeric algorithms, which take into consideration the effects of mechanical transport, particle physics, emission sources, deposition, and atmospheric chemistry [8]. The TCEQ's 4-km domain 2012 ozone base case scenario is the most up to date model for simulating 8-hour ozone currently available for the DFW and the Houston-Galveston-Brazoria (HGB) regions [82]. The base case is to be used in tandem with the Comprehensive Air-Quality Model with Extensions (CAMx) photochemical model. TCEQ stated that their base case model could generate prediction at equal or better quality than the 69 photochemical models documented by Simon et al. [8, 82].

The operations of the CAMx photochemical model is described in detail in CAMx Version 6.50 user guide [183]. The CAMx is commonly used to stimulate concentration and deposition of ozone, particulate matter, and other toxics. It can be applied from neighborhood to continental geographical scales. CAMx has a two-way nested grid structure, where the user can specify grid spacing in the model. The user can define a coarse grid when high spatial resolution is not required and still run a finer grid in areas of interest in the same model run. CAMx simulations consider physical governing models. Vertical diffusion is simulated using a hybrid of the local K-theory diffusion [184] and non-local convective surface-and-upper-

layer transport. CAMx accounts for and simulates the effects of lateral and top boundary conditions using chemical models such as GEOS-Chem or MOZART. The CAMx also considers the pollutant mass sorption and deposition, the degradation and transformation of chemicals, and the re-emission of pollutants back into the air. In terms of chemistry governing equations, the CAMx has several photochemical chemistry mechanisms models, including several carbon-bond-chemistry-models and the 2007 Statewide Air Pollution Research Center chemistry (SAPRC07TC) model. In terms of chemistry models, the CAMx has several algorithms for particulate matters and mercury, including inorganic aqueous chemistry (RADM-AQ), inorganic gas-aerosol partitioning (ISORROPIA or EQSAM), and organic gas-aerosol partitioning and oxidation (SOAP or VBS). The user can also use their chemistry model to the CAMx.

Table 9.5: The performance of each ML model in comparison to TCEQ's 2012 base case ozone on CAMx.

Model	RMSE	MAE	R^2	FB	FE	MNB	MNE
TCEQ 2012 base case + CAMx [82]	11.87	9.513	0.626	8.32%	33.15%	44%	63.99%
ANN	9.803	7.672	0.734	14.43%	26.62%	34.87%	45.60%
kNN	9.641	7.364	0.722	7.32%	25.21%	23.64%	38.93%
RF	8.38	6.200	0.801	11.06%	21.94%	23.81%	33.39%
SVM	8.882	6.867	0.686	10.281%	26.784%	6.077%	97.991%

The CAMx simulation run, performed by the TCEQ, using their 4-km grid 2012 ozone scenario base case on a testing period from May 1, 2012, to September 31, 2012 [82], was treated as a benchmark for the ML models. The four ML models were trained using 3,000 randomized samples from the training dataset, with the sample from the testing period removed. The ML model's performance in comparison to the CAMx is available in Table 9.5. The ozone concentration predicted by all four ML models has smaller errors and higher R^2-values than the CAMx. The CAMx predictions have a mean error of 2.277 ± 11.652 ppb, which

was more significant in magnitude than all four ML models. The mean error for ANN, kNN, RF, and SVM were -0.389 ± 8.874 ppb, -2.04 ± 10.942 ppb, -0.065 ± 9.573 ppb, and -0.894 ± 9.542 ppb, respectively. The CAMx model over-predicted the ozone concentrations, whereas all four ML models had under-predicted. RF was the ML model with the best performance in terms of RMSE, MAE, and R^2-value, followed by SVM, kNN, and finally, ANN. However, the FB, MNB, and NME of the RF's predicted ozone concentrations were higher than the SVM's. Since the SVM had a lower bias, this meant the SVM had a lower tendency to under- or over-estimate predicted values compared to the RF. The ANN model had the worst performance among the four ML models. The ANN algorithm tends to overfit and considers noises as part of the pattern. It also tends to converge on the local minima rather than the global minima, which leads to higher bias and errors [80].

Figure 9.7 shows the measured ozone concentration versus the values predicted by the CAMx and the four ML models. The daily averaged values of the measured and predicted ozone concentrations are available in Figure 9.8. The values predicted by all four ML models were closer to the measured values than the values predicted by the CAMx. However, the CAMx model had a lower error during the period between August 28 and September 3. The error residuals of the ML models for the entire May 1 – September 31 run and the error residuals from during August 28 – September 3 are shown in Figure 9.9. The ANN and kNN models tend to slightly over-predict the May 1 – September 31 training dataset, whereas the RF and SVM models tend to slightly under-predicts. However, all four models severely overpredict the ozone concentration on the August 28 – September 3 testing dataset. The mean concentration of NO_x and the mean relative humidity measured during the August 28 – September 3 period were about 19% lower than the August 28 – September 3 period. Ozone generation should be higher when the relative humidity is lowered [175], but a decrease in NO_x would lead to a decrease in the ozone concentration [42]. Since relative humidity was a more

critical variable than NO_x concentration (Table 9.3), the ML models may have had a bias on the drop in relative humidity and over-predict the ozone concentration.

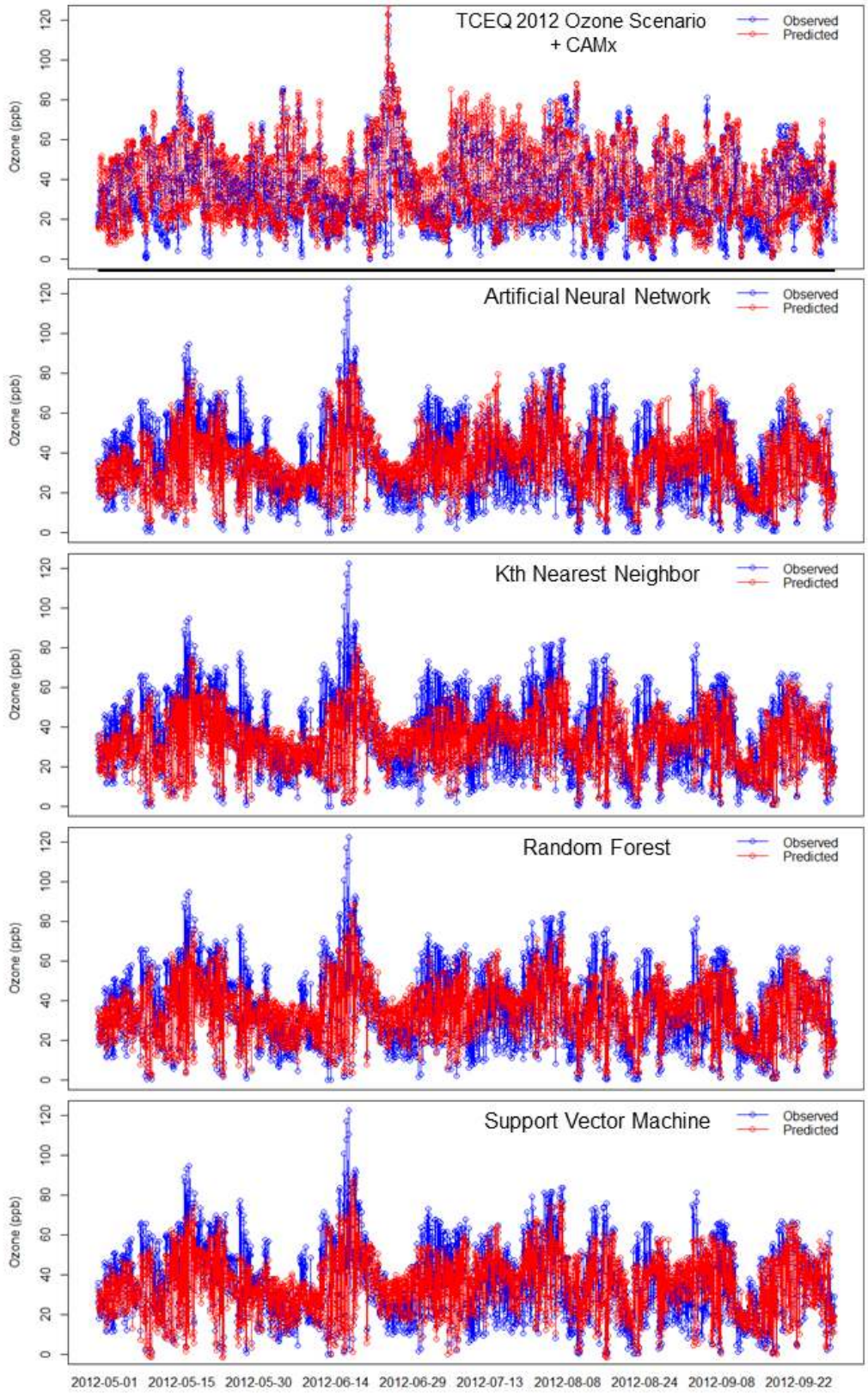

Figure 9.7: Observed versus predicted ozone concentration (ppb) using the TCEQ photochemical model and ML models.

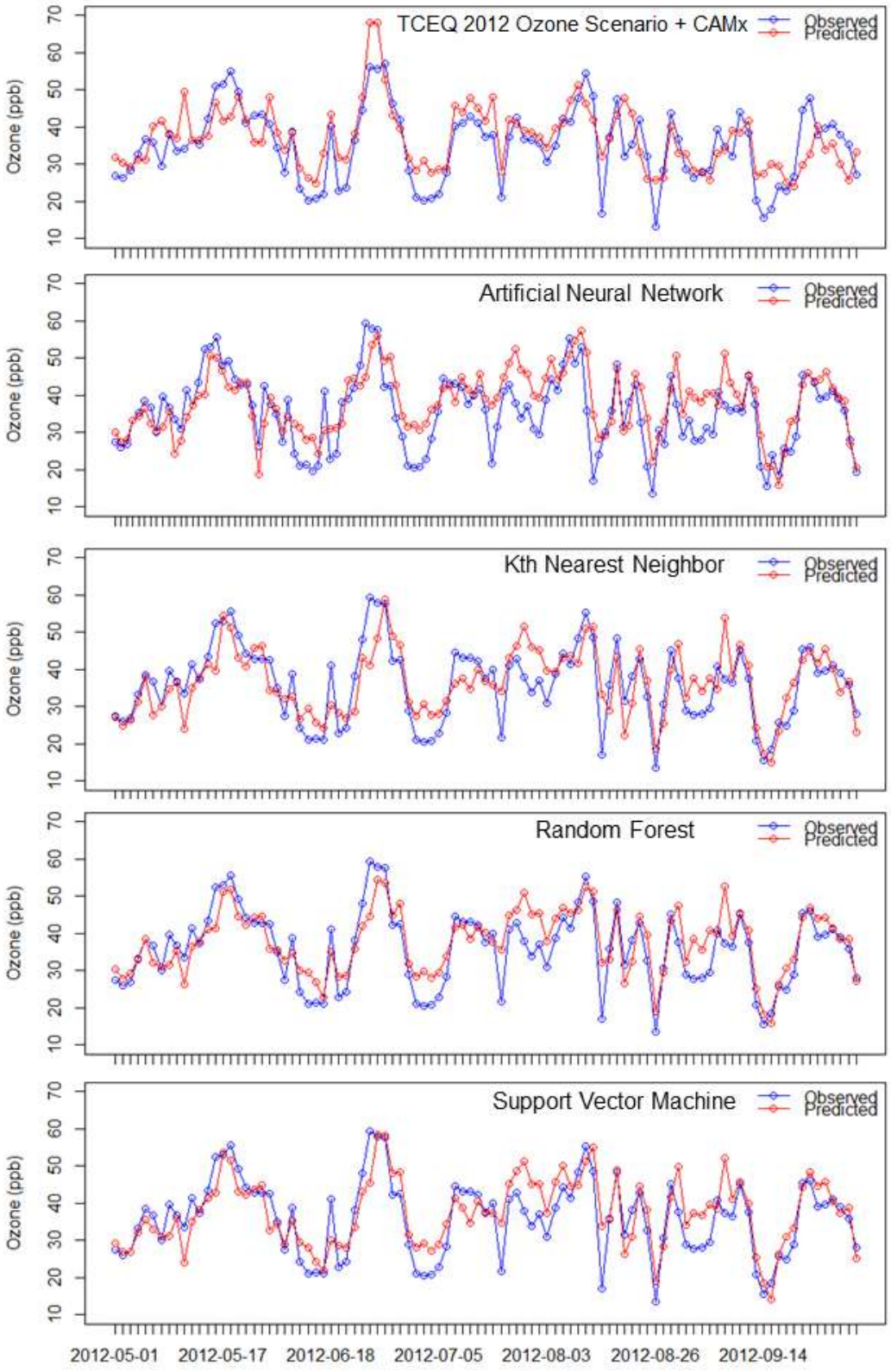

Figure 9.8: Daily averaged observed versus predicted ozone concentration (ppb) using the TCEQ photochemical model and ML models.

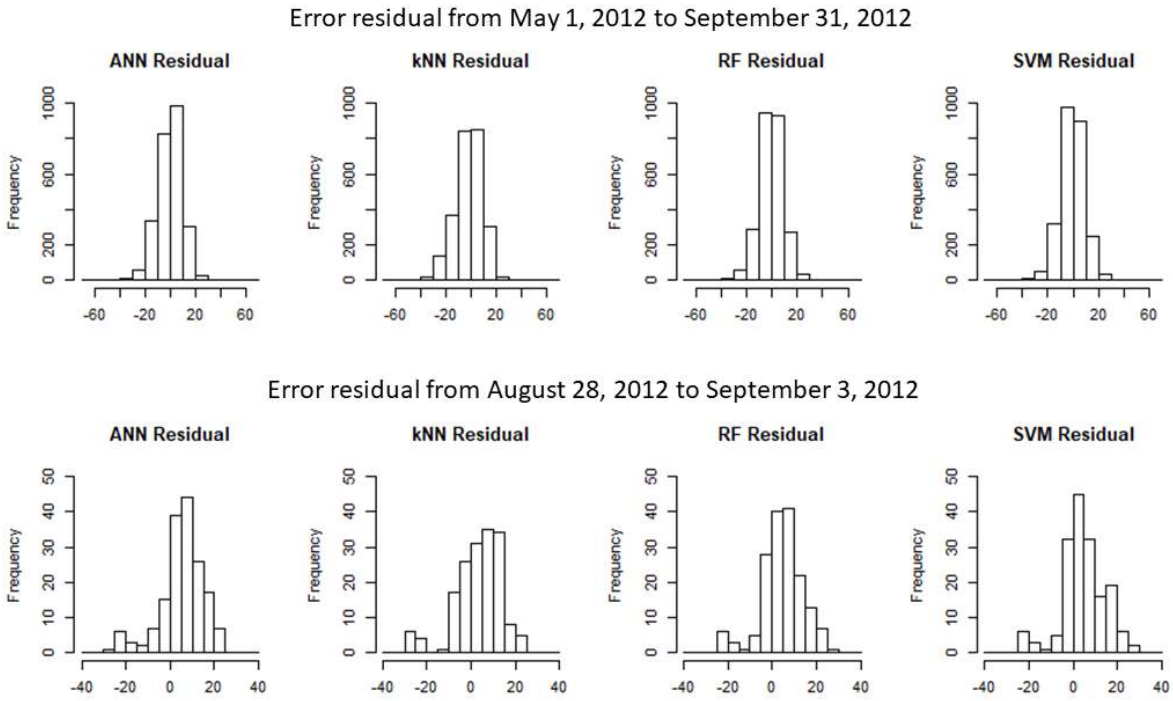

Figure 9.9: Error residuals for ANN, kNN, RF, and SVM of the May 1 to September 31, 2012, and the August 28 and September 3, 2012, testing dataset.

9.5 Testing the ML Models for Various Locations

The ANN, kNN, RF, and SVM models were used to predict the ozone concentrations using an hourly-updated dataset collected from Eagle Mountain Lake (EML) and Dallas Hinton (DAL) and sixth-day daily average data collected from FWNW (FWNW-CAN) and Denton Airport South (DEN). Table 9.6 shows a summary of the four testing datasets, which were collected during 2018 at EML, DAL, FWNW-CAN, and DEN, respectively. Among the four testing datasets, EML was the most similar to the training dataset (Table 9.1) in terms of ozone, alkane, diene, and meteorological conditions. The training dataset had a significantly higher concentration of the anthropogenic species (alkene, alkyne, aromatics, and NO_x) compared to all four testing datasets as a result of the reduction in anthropogenic emissions throughout the United States. While FWNW-CAN was collected at the same location as the training dataset, it is significantly augmented. FWNW-CAN and DEN served as a test to identify whether the ML models can retain their accuracy when faced with extremely aggregated data.

Table 9.6: Summary of the EML, DAL, FWNW-CAN, and DEN datasets collected.

	Variables	Mean	Median	Min-Max	IQR
Eagle Mountain Lake	Ozone (ppb)	28.661 ± 0.213	26.95	-0.43 - 100.27	18.22 - 37.9
	Alkane (ppb-C)	71.493 ± 1.239	43.72	4.34 - 1274.28	23.2 - 82.4
	Alkene (ppb-C)	1.456 ± 0.0168	1.08	0.14 - 13.38	0.74 - 1.73
	Alkyne (ppb-C)	0.359 ± 0.004	0.29	0 - 2.86	0.14 - 0.48
	Aromatics (ppb-C)	2.628 ± 0.026	1.63	0.2 - 16.46	1 - 2.59
	Diene (ppb-C)	0.486 ± 0.011	0.21	0 - 9.02	0.01 - 0.71
	NO_x (ppb)	5.843 ± 0.098	3.52	0.13 - 80.94	1.95 - 6.43
	Relative humidity (%)	61.47 ± 0.290	62.21	14.78 - 96.57	45.06 - 78.33
	Wind speed (Mph)	8.568 ± 0.060	8.04	0.08 - 26.22	5.67 - 11.3
	Outdoor temperature (°F)	69.35 ± 0.266	73.71	17.12 - 108.57	55.63 - 83.79
Dallas Hinton	Ozone (ppb)	30.318 ± 0.176	29.835	-0.473 - 95.759	18.665 - 40.622
	Alkane (ppb-C)	38.98 ± 0.441	28.15	5.63 - 945.35	18.46 - 44.78
	Alkene (ppb-C)	2.531 ± 0.0263	1.919	0.376 - 56.099	1.397 - 2.826
	Alkyne (ppb-C)	0.622 ± 0.005	0.517	0.036 - 12.123	0.335 - 0.744
	Aromatics (ppb-C)	7.379 ± 0.091	4.893	0.394 - 189.625	2.818 - 8.678
	Diene (ppb-C)	0.899 ± 0.015	0.277	0 - 13.808	0.107 - 1.003
	NO_x (ppb)	9.364 ± 0.133	5.734	-2.069 - 201.336	3.559 - 10.31
	Relative humidity (%)	58.86 ± 0.202	58.77	11.92 - 95.94	44.75 - 73.75
	Wind speed (Mph)	5.408 ± 0.027	5.193	0.035 - 17.482	3.536 - 6.979
	Outdoor temperature (°F)	75.63 ± 0.149	77.78	16.95 - 103.35	67.31 - 85.67
FWNW - Canister	Ozone (ppb)	37.34 ± 1.267	37.82	16.87 - 53.01	30.8 - 44.32
	Alkane (ppb-C)	65.9 ± 6.657	50.59	18.73 - 259.95	33.91 - 80.32
	Alkene (ppb-C)	2.72 ± 0.296	2.2	0.1 - 9.3	1.27 - 3.37
	Alkyne (ppb-C)	1.323 ± 0.116	1.2	0 - 3.12	1.04 - 1.76
	Aromatics (ppb-C)	4.22 ± 0.36	3.54	1.29 - 13.66	2.29 - 5.07
	Diene (ppb-C)	0.415 ± 0.046	0.31	0 – 1.5	0.15 – 0.55
	NO_x (ppb)	11.43 ± 1.451	7.66	1.02 - 51.26	4.6 - 14.54
	Relative humidity (%)	55.71 ± 0.381	54.89	24.53 - 80.84	47.72 - 64.74
	Wind speed (Mph)	7.44 ± 1.734	6.75	3.03 - 14.7	5.51 - 9.37
	Outdoor temperature (°F)	68.77 ± 2.059	69.54	25.61 - 90.03	60.58 - 80.41
	Ozone (ppb)	39.11 ± 1.91	40.83	18.41 - 86.65	29.29 - 49.37
	Alkane (ppb-C)	55.84 ± 21.42	117.88	12.16 - 889.23	33.04 - 113.67
	Alkene (ppb-C)	1.08 ± 0.124	0.9409	0 - 3.28	0.02 - 1.61
	Alkyne (ppb-C)	1.16 ± 0.078	1.04	0 - 2.02	1.02 - 1.32

(table continues)

	Variables	Mean	Median	Min-Max	IQR
Denton Airport South	Aromatics (ppb-C)	2.15 ± 0.238	2.462	0.08 - 9.89	1.29 - 2.87
	Diene (ppb-C)	0.39 ± .036	0.35	0 - 1.1	0.195 - 0.45
	NO_x (ppb)	6.4 ± 0.516	7.125	1.01 - 17.81	4.511 - 8.854
	Relative humidity (%)	61.95 ± 1.837	61.85	33.81 - 94.28	50.4 - 71.12
	Wind speed (Mph)	6.71 ± 0.486	7.602	2.966 - 17.923	4.86 - 9.819
	Outdoor temperature (^oF)	62.19 ± 2.303	64.32	21.45 - 95.64	51.87 - 80.01

Table 9.7 shows the performance statistic of the four ML models on the EML, DAL, FWNW-CAN, and DEN testing dataset. The ML models retained significant performance predicting ozone concentrations using the EML and FWNW-CAN dataset. The RF was the best performing model on the EML and DEN dataset, whereas kNN had the highest accuracy on the DAL and FWNW-CAN dataset. The SVM was consistently one of the worst-performing models. The support vector and hyperplane constructed by the SVM may have only fit FWNW's characteristics and are inflexible. Compared to the average performance of the four ML models on validating data, the RMSE and R^2-value of the RF model on the EML dataset was only weaker by 1.36% and 5.05%, respectively. The MAE of the RF model using the EML dataset was 0.12% smaller than the average MAE of the four ML models on the validating data. The RMSE and MAE of the RF model on FWNW-CAN data was 18.52% and 13.54% smaller than the validating dataset's average. However, the R^2-value between predicted and measured FWNW-CAN ozone concentrations was 12.39% weaker than the validating dataset. The smaller sample size of the FWNW-CAN dataset likely contributed to smaller RMSE and MAE. When used on the DAL dataset, there was at least a 20.48% increase in RMSE, a 21.05% increase in MAE, and a 10.98% decrease in R^2-value. TNMOC concentrations at DAL was about half of that at FWNW, despite only a 7-ppb difference in ozone concentration; the slight difference in ozone generation regime at both sites, as discussed in Chapter 6.4, had likely caused the errors. The performance of the ML models was significantly weaker when tested on the DEN dataset, where RMSE, MAE, and R^2-values were 98.34%, 109.54%, and 27.45%,

respectively. There was also a heavy negative bias when predicting ozone concentrations at DEN, which indicates significant under-prediction.

Table 9.7: Performance of the ANN, kNN, RF, and SVM models on the EML, DAL, FWNW-CAN, and DEN testing datasets.

		RMSE	MAE	R^2	FB	FE	MNB	MNE
EML	ANN	8.164	6.245	0.698	7.948%	27.394%	31.668%	51.872%
	kNN	8.501	6.462	0.674	5.252%	28.012%	24.642%	45.724%
	RF	7.706	5.804	0.734	8.056%	25.363%	27.351%	45.324%
	SVM	8.733	6.544	0.676	-2.202%	28.04%	13.284%	41.159%
DAL	ANN	11.484	8.658	0.512	6.45%	36.298%	37.468%	91.029%
	kNN	9.160	7.035	0.688	14.209%	30.874%	44.29%	82.073%
	RF	9.451	7.295	0.668	14.515%	31.294%	44.641%	76.146%
	SVM	11.599	8.563	0.502	7.357%	34.255%	26.611%	73.279%
FWNW-CAN	ANN	6.647	5.143	0.658	-2.572%	19.046%	0.742%	17.892%
	kNN	6.195	5.024	0.677	-3.411%	19.051%	-0.486%	18.152%
	RF	6.701	5.283	0.624	-2.171%	19.495%	1.086%	18.602%
	SVM	6.822	5.438	0.571	-0.086%	19.388%	2.861%	18.993%
DEN	ANN	15.856	12.821	0.538	-37.13%	37.685%	-29.36%	29.935%
	kNN	20.178	15.848	0.239	-49.42%	50.332%	-35.36%	36.348%
	RF	15.079	12.178	0.561	-33.30%	34.506%	-26.59%	27.837%
	SVM	18.235	15.038	0.445	-44.77%	45.115%	-34.21%	34.571%

Figure 9.10 shows the error residual of each ML model for each of the four testing datasets. The EML, DAL, and FWNW-CAN error residuals have the highest frequency at zero. However, there were higher frequencies of negative error residuals compared to positive ones, which indicate all four ML models have a higher tendency to under-predict ozone concentrations. NO_x is one of the most critical variables (Table 9.3); the lower NO_x concentration in 2018 may have caused the models to underpredict ozone concentrations. All four ML models appeared to have significantly underpredicted ozone concentration at DEN as the error residuals produced were almost entirely negative. All four ML models severely under-predicted the measured ozone concentration at DEN. This was likely due to FWNW and DEN not being in a similar ozone production regime. At FWNW, ozone production is highly

dependent on the photochemical reactions between NO_x and fast-reactive TNMOC species. However, the slow-reactive TNMOC species plays a significant role in the ozone productions at DEN (Chapter 6.4.1). Since the production of ozone is dependent upon different variables under different ozone production regimes, the FWNW training dataset was unable to produce an accurate model for predicting ozone concentrations at DEN.

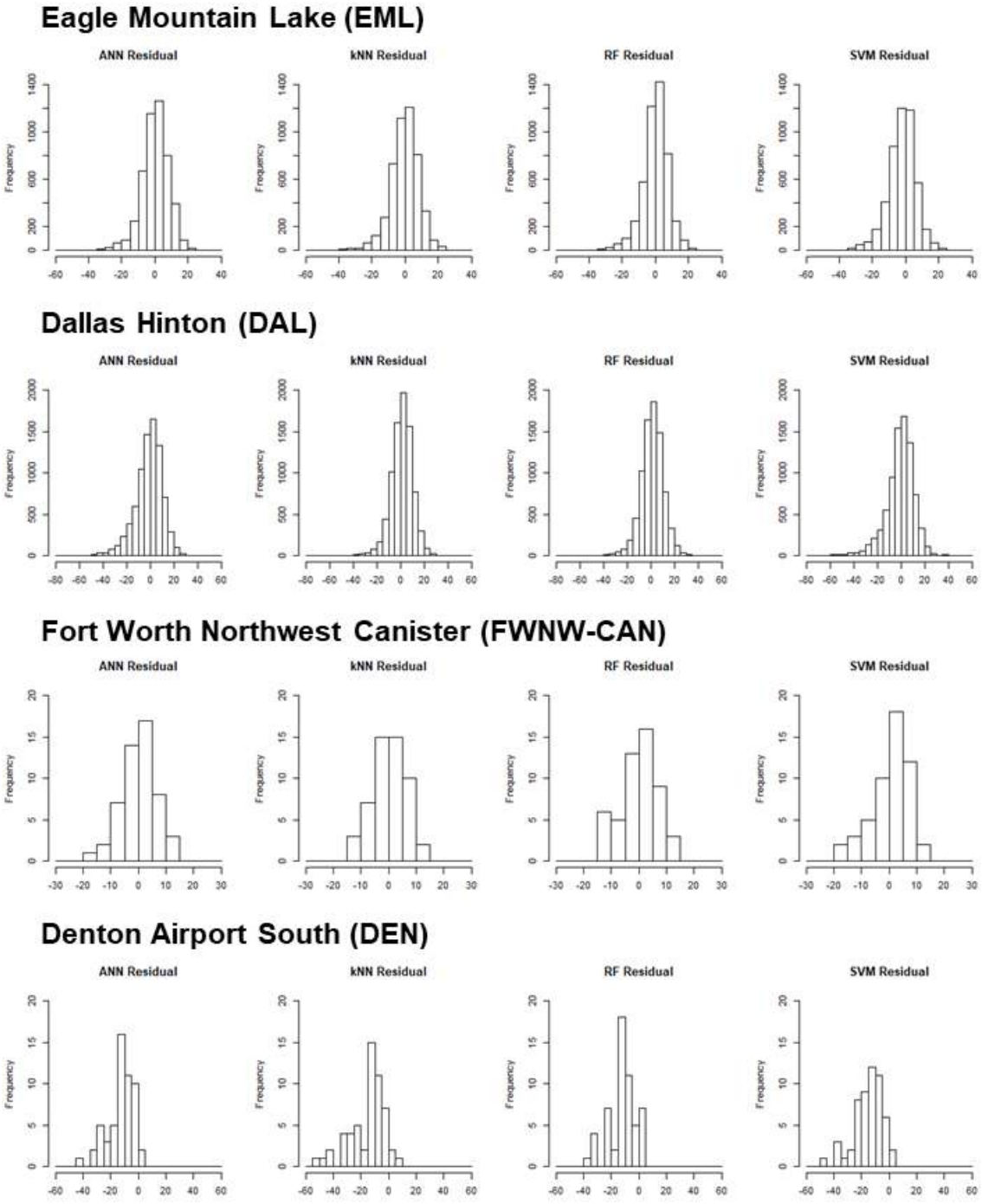

Figure 9.10: Error residual of the ozone concentration prediction using the ANN, kNN, RF, and SVM models using EML, DAL, FWNW-CAN, and DEN testing dataset.

9.6 Summary Findings

Ozone formation in the atmosphere is a heavily non-linear process and is influenced by multiple factors including physical and chemical conditions of the atmosphere. In this chapter, we attempt to develop predictive tools for ozone using statistical and heuristic techniques. Compared to an MLR approach, the ANN, kNN, RF, and SVM algorithms were able to produce better models that could make predictions with an R^2-value of up to 79.6% when compared to the measured values. The CaRT was not a suitable algorithm for ozone concentration prediction due to a lack of data smoothness and high variance. The SVM was the best performing model when used to predict future ozone concentration. The SVM is significantly more robust compared to the ANN when the training dataset is large and has many variables, which makes the SVM much more suitable for air pollution concentration prediction than ANN. However, the performance of the SVM significantly drops when used to predict ozone concentration at different locations, whereas the RF was the best performing location-dependent model. The RF aggregates the prediction made by numerous individual decision trees, which makes it less sensitive to outliers and the size of the dataset. The error and bias of the ML models were lower than that of the discrete gridded photochemical model (CAMx) using TCEQ's base case of high ozone season simulation. However, the ML models were not able to simulate the effects of long-range transport in contrast to the CAMx model simulations. When tested using datasets collected from the EML monitoring station, the decreased in performance was insignificant. In the case of the FWNW-CAN dataset, the ML models were also able to retain most of its predictive accuracies even when the testing data were significantly aggregated. The difference in the ozone generation regime had a significant impact on the ML model's predictive accuracies. Training a separate ML model with data from each of the ozone production regime may be a potential fix to this weakness. In the future, more variables with domain knowledge,

such as mixing-level height, terrain data, and land cover, should be included in the dataset, as these factors should significantly improve the predictive accuracies of the ML model.

CHAPTER 10

CONCLUSION AND RECOMMENDATIONS

10.1 Conclusion

The unconventional shale gas emissions from the Barnett Shale in North Texas has directly affected the measured ambient air quality in the Dallas-Fort Worth (DFW) metroplex region. Despite a significant decrease in conventional urban emissions, as observed in the decline in oxides of nitrogen (NO_x) and carbon monoxide (CO) concentrations, the region still consistently failed to attain the National Ambient Air Quality Standards (NAAQS) for ozone. Denton Airport South (DEN) is an exurban monitoring site in Denton county located in North Texas. The ozone and total non-methane organic carbon (TNMOC) concentrations measured at DEN were higher than at the Dallas Hinton (DAL) and Fort Worth Northwest (FWNW) sites, located within highly urbanized regions of Dallas and Tarrant counties, respectively. TNMOC concentrations at DEN (220.69 ± 10.36 ppb-C) was at least twice as large as those measured at DAL (67.4 ± 1.51 ppb-C) and FWNW (89.31 ± 2.12 ppb-C). The large pool of TNMOC concentration found in the ambient was a major contributor to local and regional ozone levels. The disproportionately larger concentration of TNMOC measured in DEN in comparison to the urban sites, as well as the continued decline in NO_x and CO concentrations across all sites, leads to the conclusion that unconventional emission sources were mainly responsible for the region's inability to comply with the ozone NAAQS.

Using positive matrix factorization (PMF), a factor-based source apportionment analysis tool, natural gas was identified as the dominant contributor to the measured TNMOC concentration across all three sites. The TNMOC concentration at DAL was made up of natural gas (32%), solvent (27%), fuel evaporative (18%), vehicle exhaust (15%), and refrigerant (8%). At FWNW, the source factors included natural gas (40%), solvent (18%), fuel evaporative (13%), vehicle exhaust (13%), diesel (9%), and refrigerant (8%). Emissions from natural gas

(69%) were significantly more at DEN than compared to the other emission sources, including refrigerant (10%), vehicle exhaust (9%), solvent (7%), and fuel evaporative (6%). Furthermore, the sources of natural gas emissions were from highly localized shale gas wells in close proximity to the monitoring sites. The current emissions inventory (EI) showed a consistent decline in countywide emissions of volatile organic compounds (VOC) across the study region, however, this was not reflected in the measured TNMOC concentrations. We suggest that the current EI severely underestimates the impact of localized unconventional emission sources, such as shale gas emissions. The unconventional TNMOC emissions from the Barnett Shale also affected the measured ozone concentration across the DFW region. While the majority of measured TNMOC at DEN were slow-reacting n-alkane species, the ozone formation potential (OFP) of TNMOC at DEN was estimated to be higher than DAL and FWNW. Unlike DEN, the OFP of the measured TNMOC at DAL and FWNW were from reactive species such as alkenes and aromatics typically associated with traffic and other combustion-related sources. While the alkane species observed in the study region were predominantly from unconventional shale gas sources. These typically have lower reactivity in the formation of ozone than the hydrocarbon species from conventional sources, however their abundance in the ambient has led to higher ozone formation across the region.

While the air pollutant trends and characteristics of an urban airshed can be determined using long-term ambient air quality measurements, however this was difficult in regions with sparse air quality monitoring. An air pollutant predicting model was built using machine learning (ML) algorithms and historic air quality data to overcome the lack of air quality data in remote regions. Using long-term air quality data collected from the FWNW monitoring station, various ML regression algorithms were used to train a computer cluster to predict ozone concentration. Based on the results, the Classification and Regression Tree (CaRT) algorithm was not good at predicting air pollution concentrations due to its binary nature and higher

variance. The Random Forest (RF) algorithm produced the best performing model whereas the models implementing the Artificial Neural Network (ANN), k-th Nearest Neighbor (kNN), and Support Vector Machine (SVM) algorithms have comparable performance that were able to generate predictions with an average R^2-value of 0.771 to the measured values. These four ML models were also able to generate a prediction with smaller margins of error when compared with the model-predicted results from a discrete photochemical modeling system (CAMx) running TCEQ's 4-km 2012 base case ozone scenario. The models were tested against measurements from several monitoring stations and their performance were satisfactory when the emissions characteristics of the tested sites were similar to FWNW. However, when tested against severely aggregated datasets or sites with massively different emission characteristics, the accuracy of the model dropped significantly. In its current iteration, the ozone production regime of the tested dataset plays an important role in the model's prediction performance. Further analysis is required to develop a robust ozone prediction tool for the region.

10.2 Recommendations

Based on the findings of this dissertation, we recommend additional analysis and studies needed for the study region. Some initial recommendations include the following –

- Increase the number of air quality monitoring stations with hourly updated Auto-GC monitors throughout the region to improve the spatial and temporal texture of ambient air quality data. The deployment of a system of robust low-cost sensors across the DFW region can also aid in mitigating the spatial disparity in air quality data.

- A comprehensive local and regional scale EI should be developed to account for unconventional sources of air emission including those from shale gas activities. These unconventional emission sources had a severe impact on local and regional air pollutant concentrations. By not accounting for these unconventional sources may have harmed the region's ability to achieve ozone attainment designation.

- Since ozone production regimes were a significant factor in the ML model's prediction, building separate models for each regime may overcome this weakness. Future studies should incorporate more variables with domain-specific knowledge, such as mixing-level heights, terrain data, and land cover, to improve the accuracy of the ML model.
- Exploring new artificial intelligence or deep learning approach may be an improvement over the application of ML algorithms. ML algorithms that incorporate physics, instead of just a black box, are considered state-of-the-art. The implications of these ML models incorporating physical and chemical governing equations should also be studied in the future.

APPENDIX A

SUPPLEMENTAL FIGURES

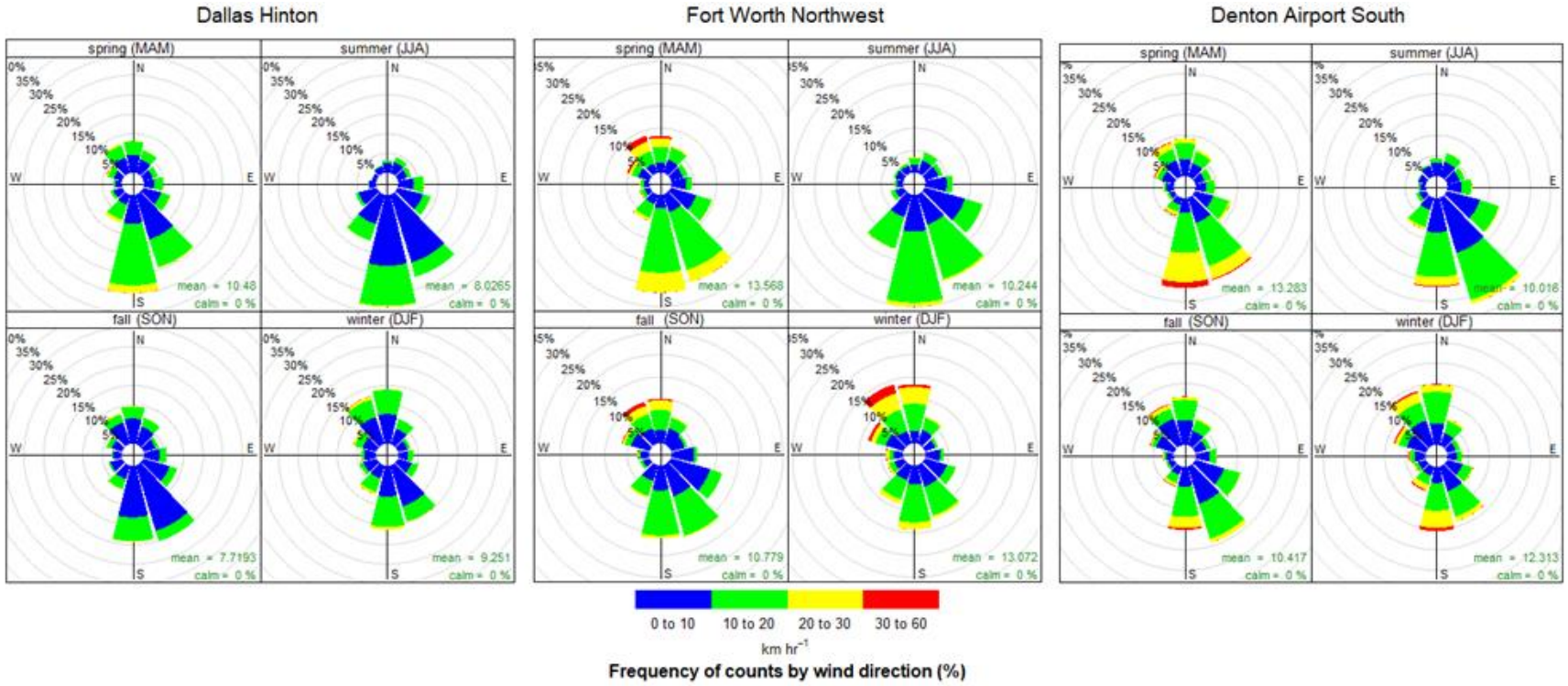

Figure A1 - The wind rose diagrams for Dallas Hinton, Fort Worth Northwest, and Denton Airport South.

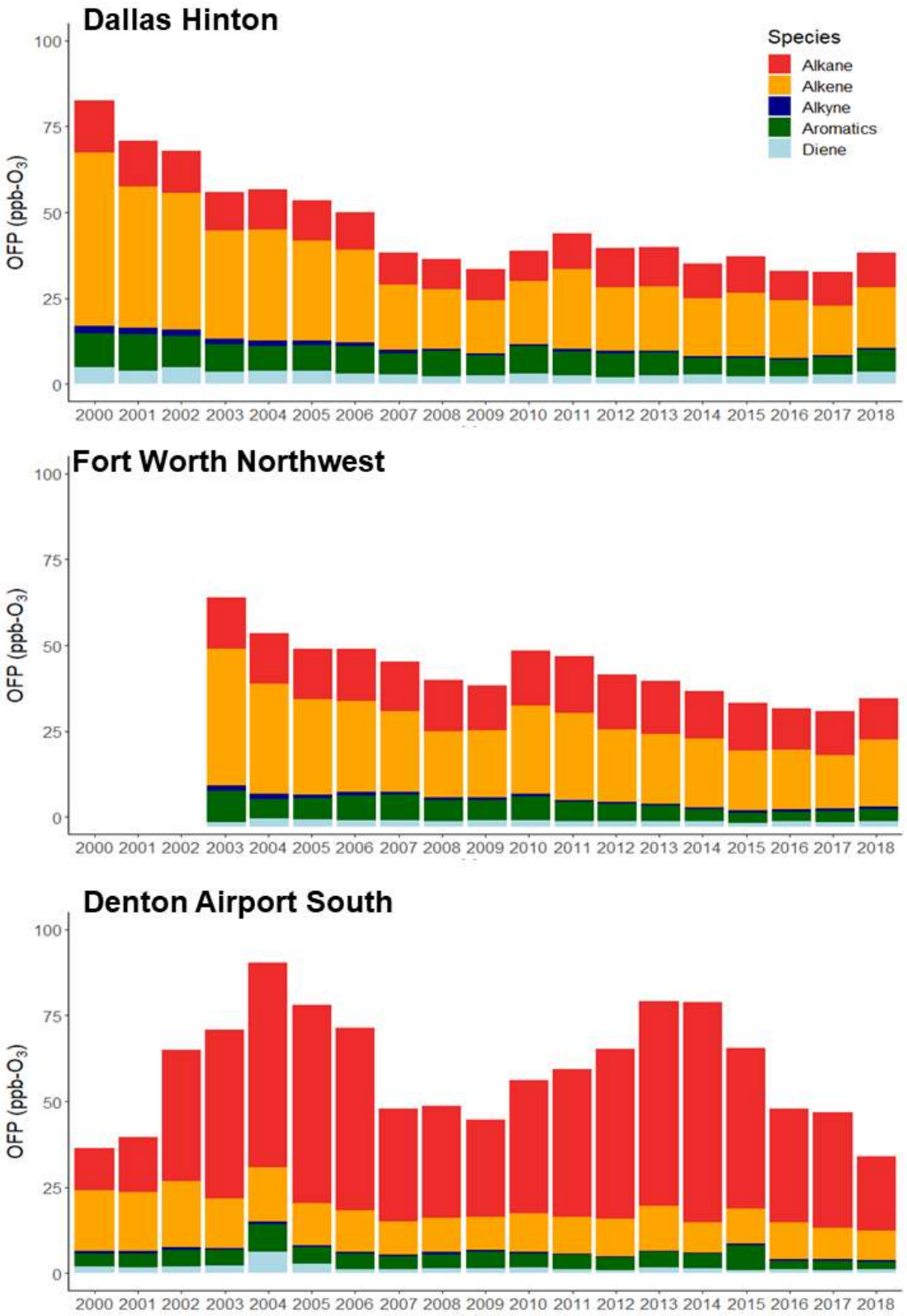

Figure A2 - Annual trend of ozone formation potential (OFP) by hydrocarbon groups.

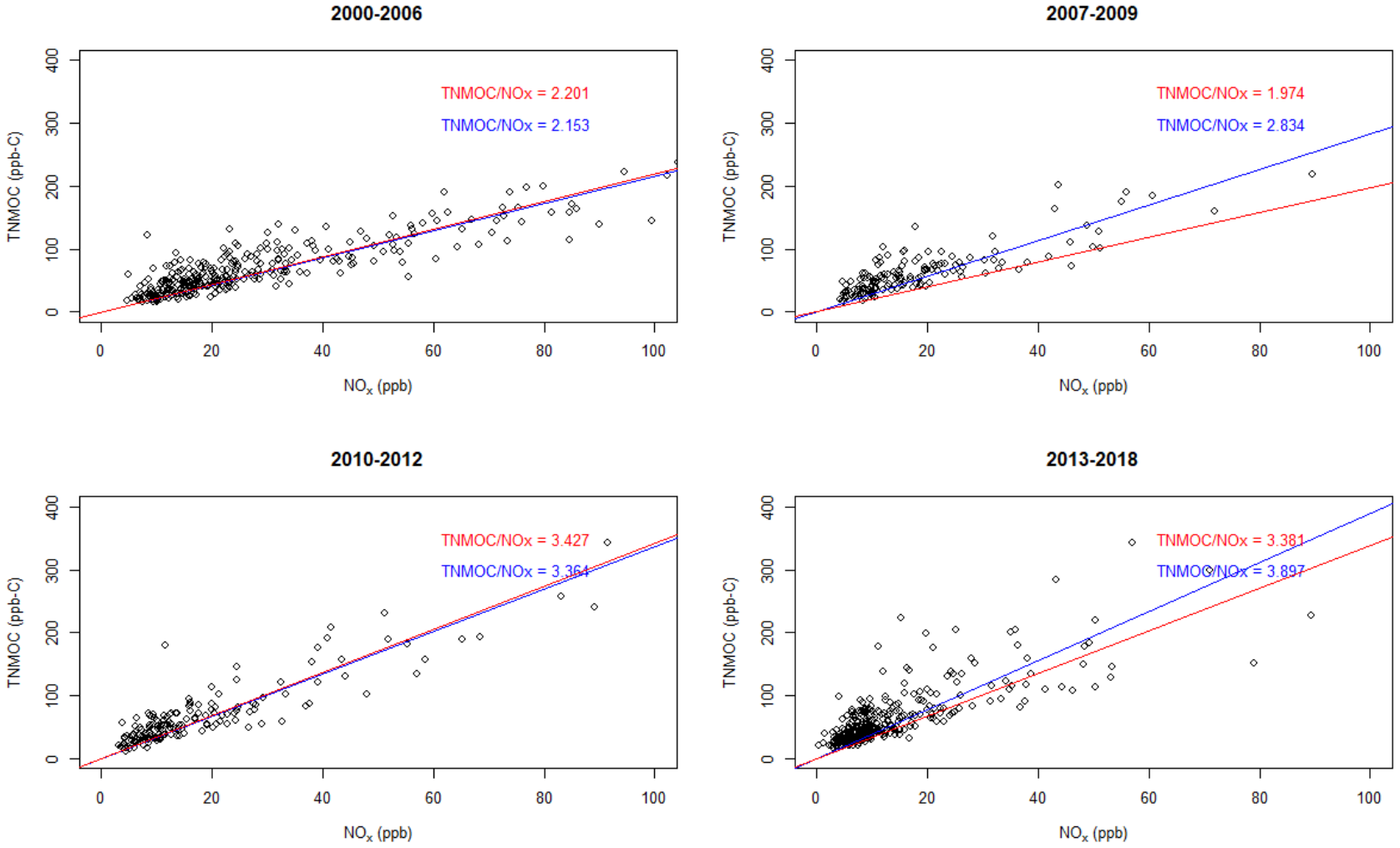

Figure A3 - Correlation between TNMOC and NO_x concentration at Dallas Hinton.

**Red slope line: High ozone days (daily max 8-hour O3 > 70 ppb.); Blue slope line: Daily max 8-hour O3 < 70 ppb.*

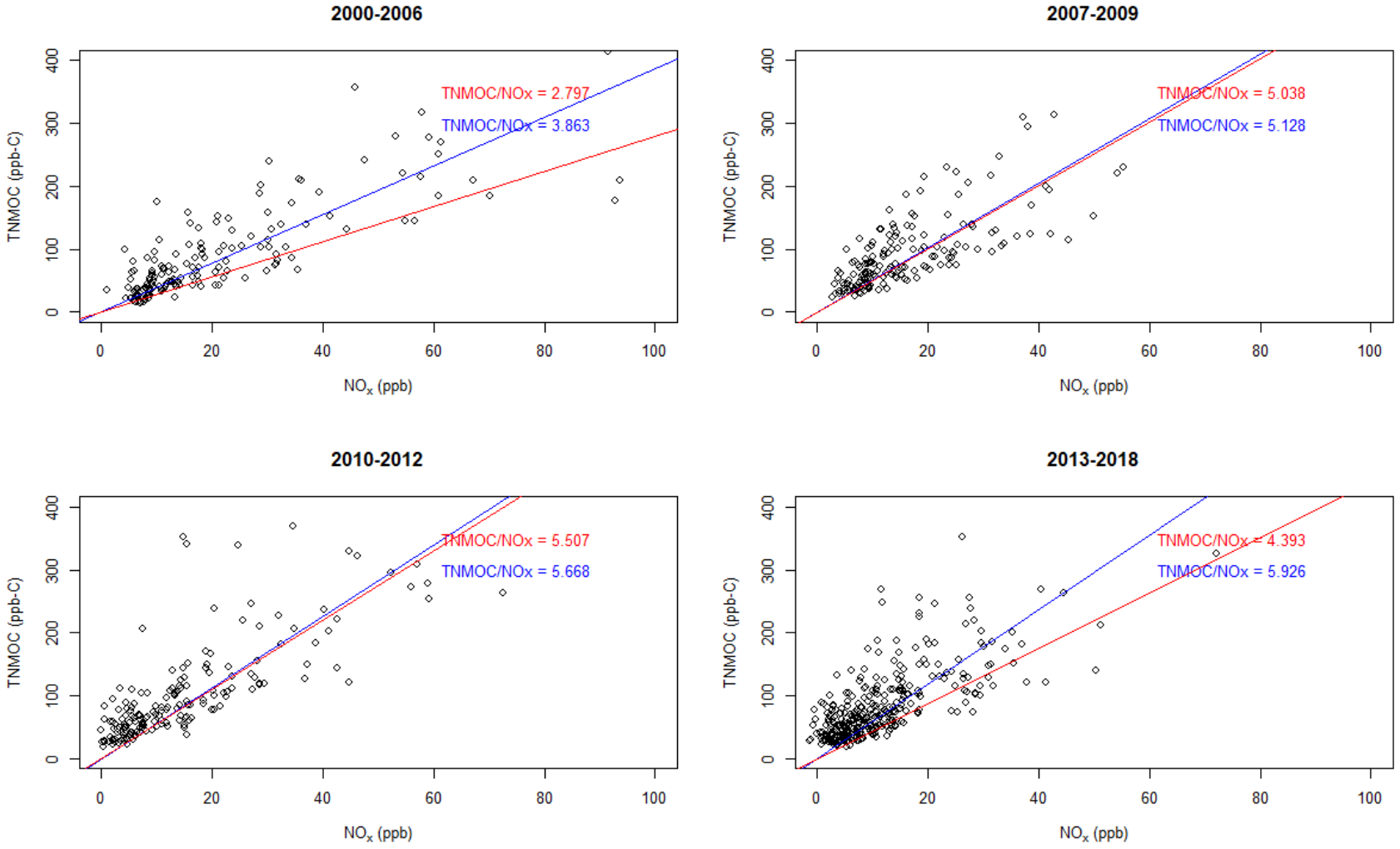

Figure A4 - Correlation between TNMOC and NO_x concentration at Fort Worth Northwest.

**Red slope line: High ozone days (daily max 8-hour O3 > 70 ppb.); Blue slope line: Daily max 8-hour O3 < 70 ppb.*

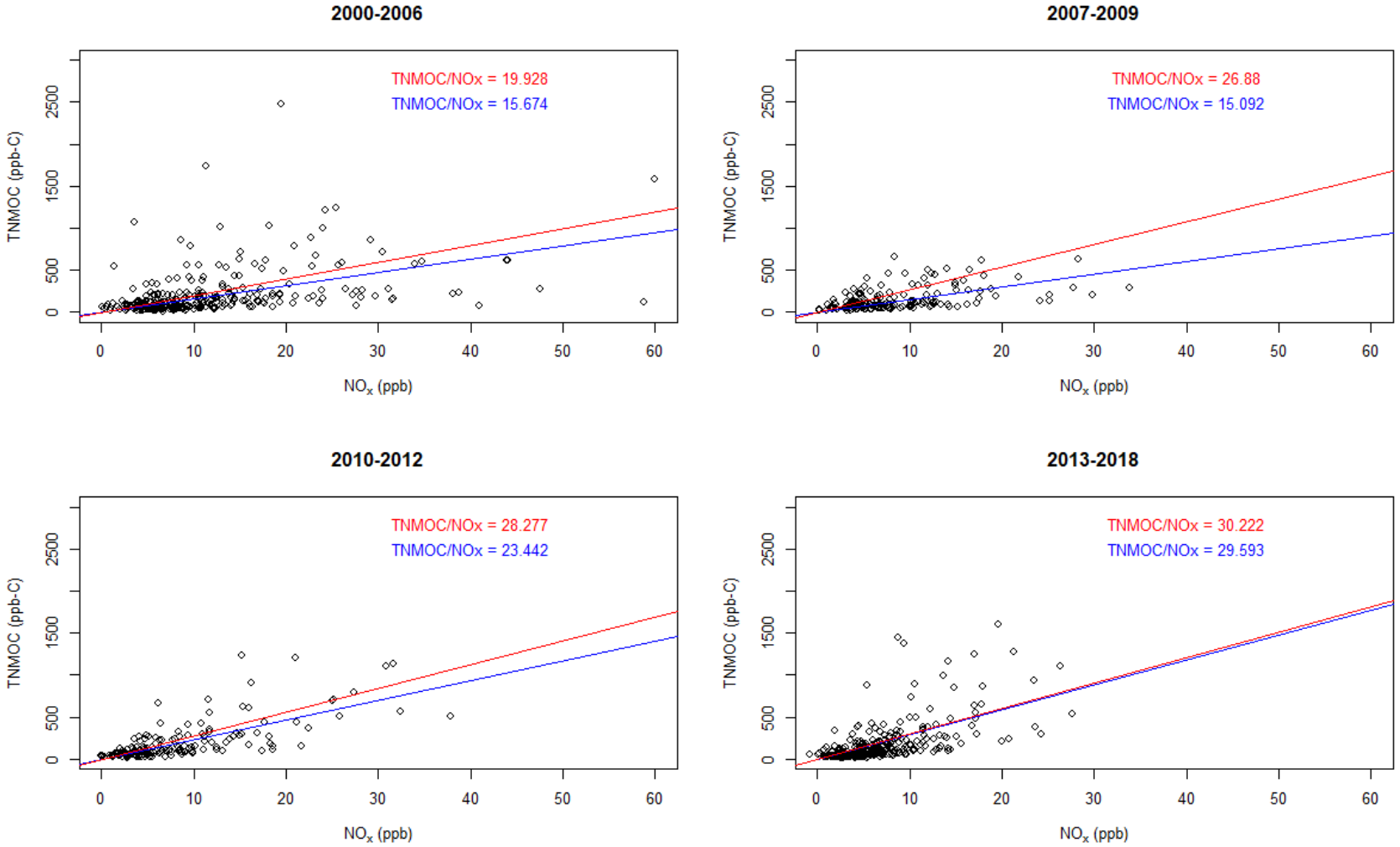

Figure A5 - Correlation between TNMOC and NO_x concentration at Denton Airport South.

**Red slope line: High ozone days (daily max 8-hour O3 > 70 ppb.); Blue slope line: Daily max 8-hour O3 < 70 ppb.*

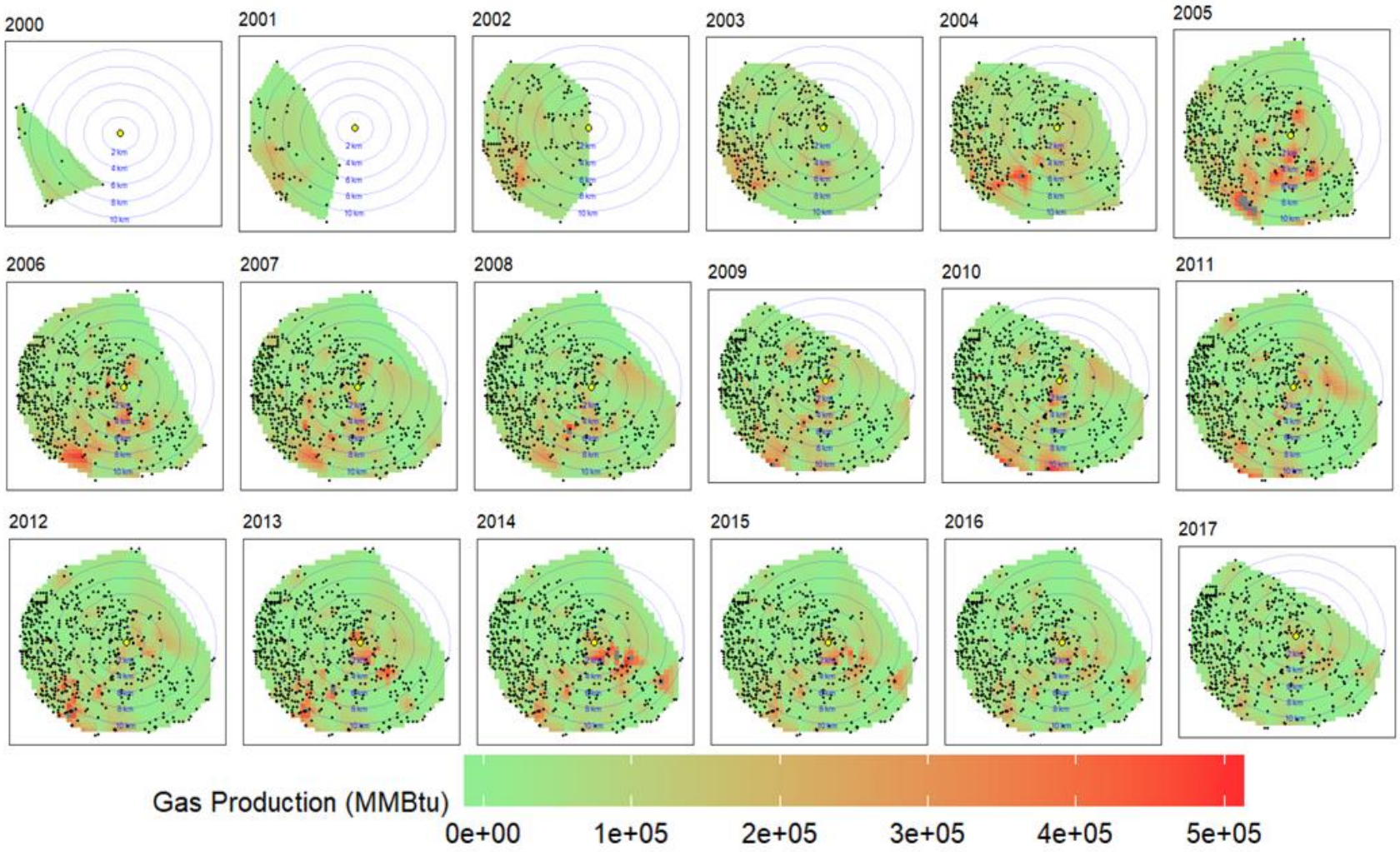

Figure A6 - Annual location of natural gas wells overlaid with total production volume contour at Denton Airport South.

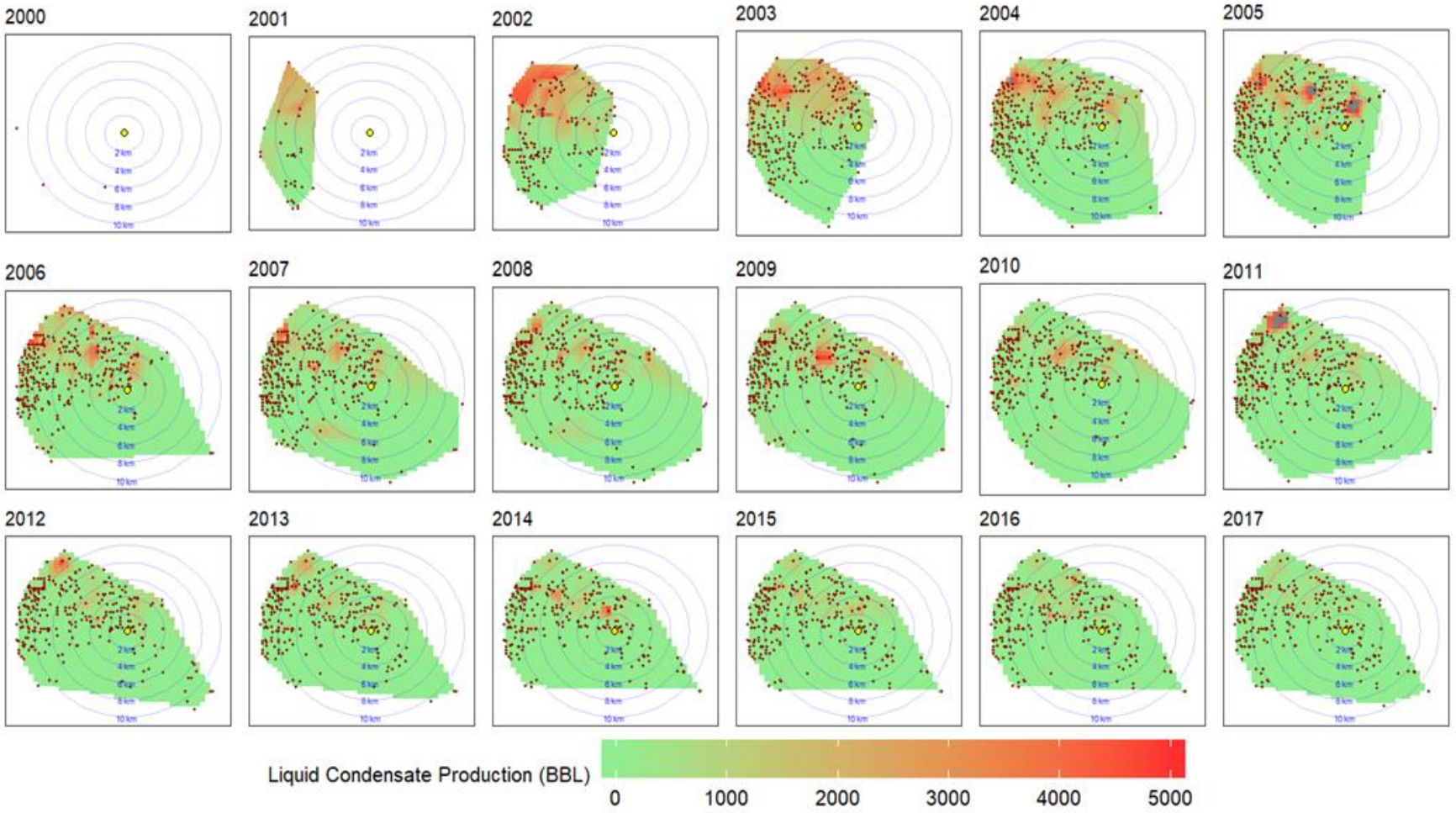

Figure A7 - Annual location of liquid condensate facilities overlaid with total production volume contour at Denton Airport South.

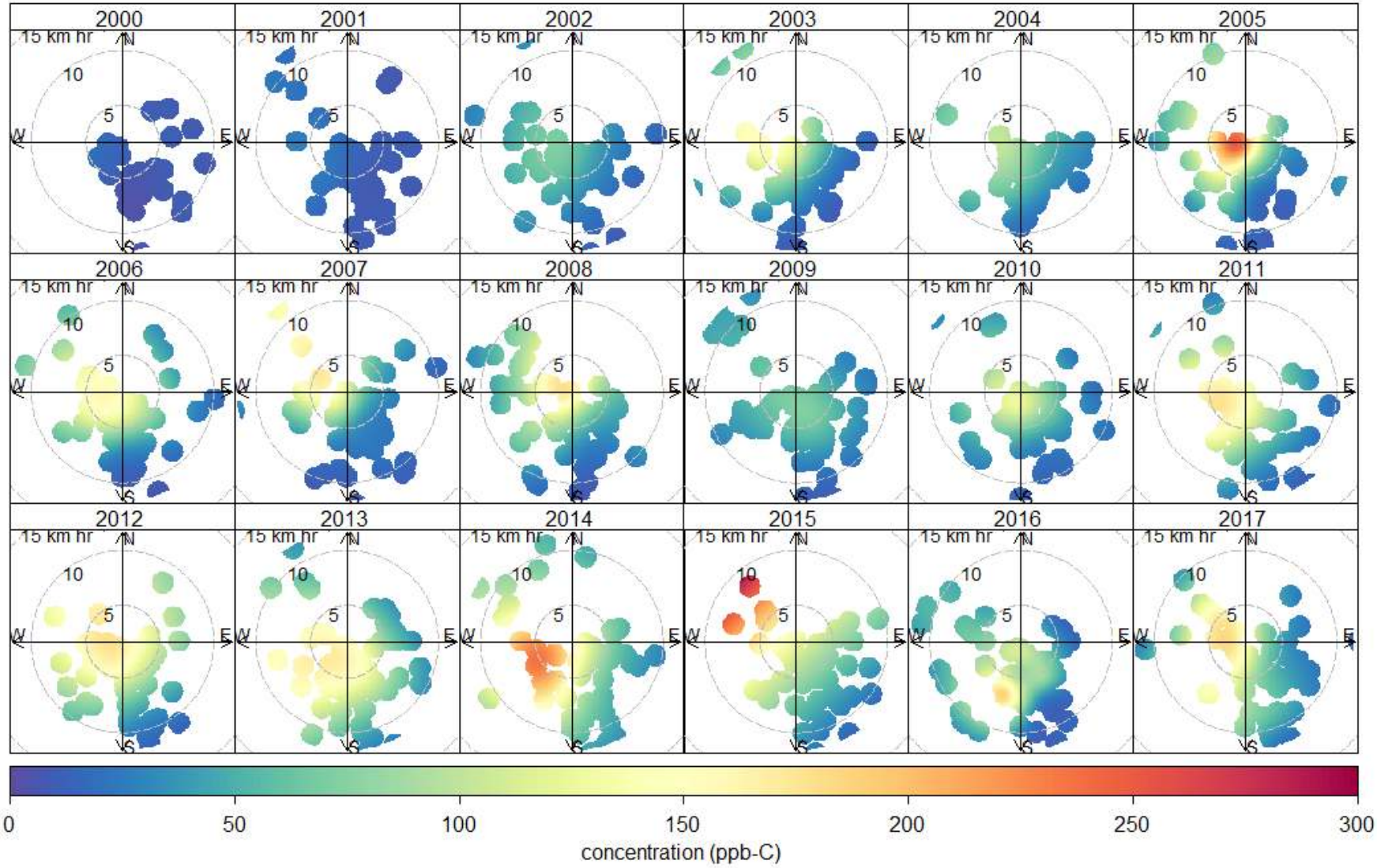

Figure A8 - Annual bivariate polar plot for measured ethane concentration [ppb-C] at Denton Airport South.

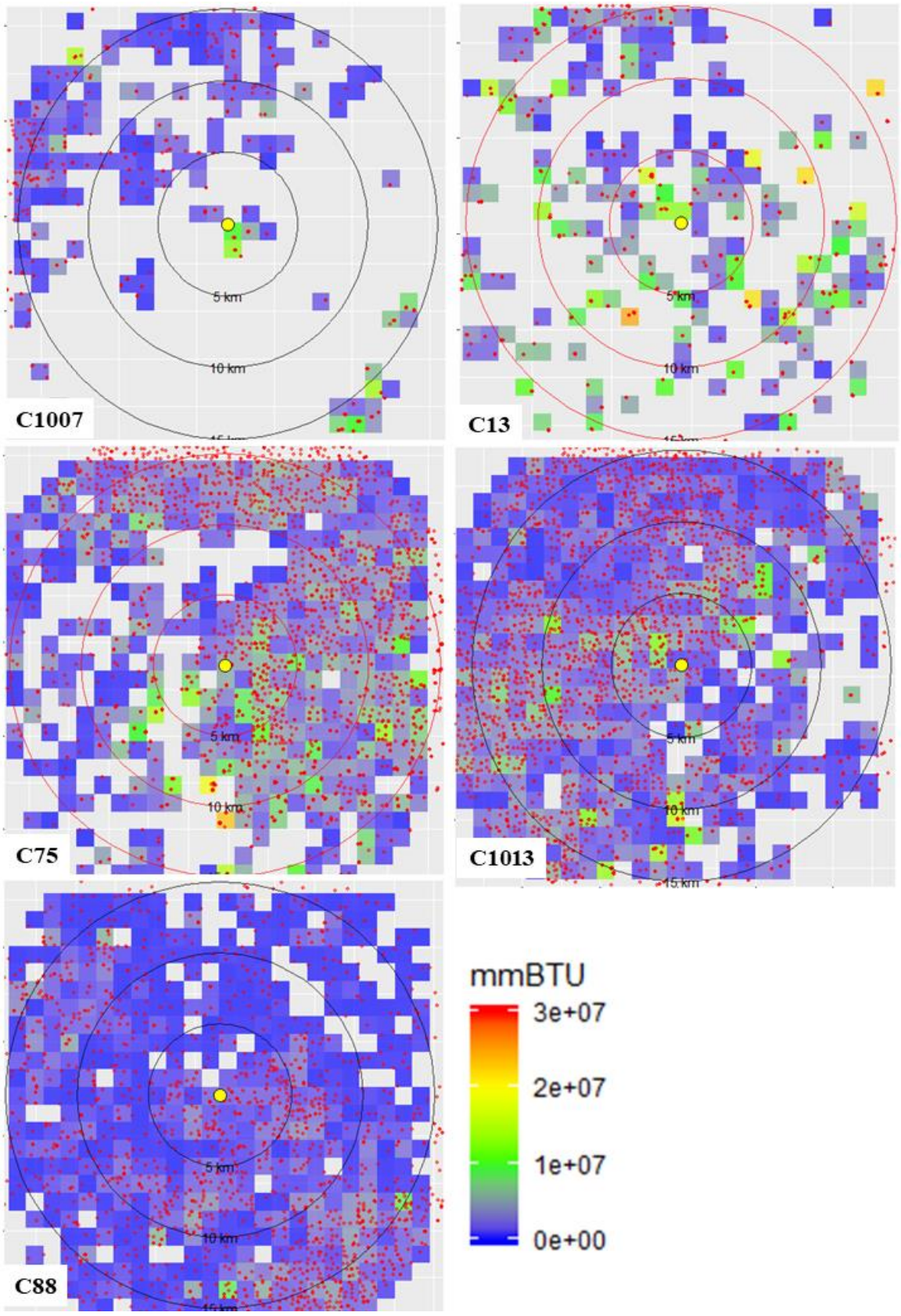

Figure A9 - Production volume of natural gas (MMBtu) within 15 km of the monitoring station.

APPENDIX B

SUPPLEMENTAL TABLES

Table B1 - Mean, median (Med), standard error (SE), and total available data points (N) for canister TNMOC species (ppb-C) at Dallas Hinton, Fort Worth Northwest, and Denton Airport South.

	Dallas Hinton				Fort Worth Northwest				Denton Airport South			
TNMOC Species	**Mean**	**Med**	**SE**	**N**	**Mean**	**Med**	**SE**	**N**	**Mean**	**Med**	**SE**	**N**
1-Butene	1.024	0.720	0.033	886 (83%)	1.093	0.960	0.025	778 (87%)	0.519	0.400	0.015	700 (65%)
1-Hexene & 2-Methyl-1-Pentene	0.150	0.120	0.012	83 (8%)	0.173	0.120	0.011	126 (14%)	0.109	0.060	0.016	51 (5%)
1-Pentene	0.287	0.200	0.021	160 (15%)	0.255	0.200	0.018	120 (13%)	0.198	0.100	0.027	94 (9%)
1,1-Dichloroethane	0.022	0.020	0.002	11 (1%)	0.020	0.020	0.000	9 (1%)	0.026	0.020	0.006	7 (1%)
1,1-Dichloroethylene	0.045	0.020	0.004	113 (11%)	0.043	0.020	0.003	120 (13%)	0.046	0.020	0.003	105 (10%)
1,1,2-Trichloroethane	0.040	0.020	0.020	8 (1%)	0.025	0.020	0.005	4 (0%)	0.024	0.020	0.004	10 (1%)
1,1,2,2-Tetrachloroethane	0.023	0.020	0.003	23 (2%)	0.022	0.020	0.001	19 (2%)	0.025	0.020	0.003	30 (3%)
1,2-Dichloropropane	0.184	0.120	0.033	41 (4%)	0.238	0.150	0.042	42 (5%)	0.376	0.150	0.096	46 (4%)
1,2,3-Trimethylbenzene	0.301	0.180	0.022	267 (25%)	0.204	0.180	0.010	277 (31%)	0.172	0.090	0.036	113 (10%)
1,2,4-Trimethylbenzene	0.574	0.360	0.025	640 (60%)	0.492	0.360	0.019	571 (64%)	0.278	0.180	0.029	382 (35%)
1,3-Butadiene	0.273	0.200	0.015	250 (23%)	0.244	0.200	0.012	208 (23%)	0.160	0.080	0.043	53 (5%)
1,3,5-Trimethylbenzene	0.254	0.180	0.013	329 (31%)	0.172	0.090	0.007	327 (36%)	0.163	0.090	0.026	162 (15%)
2-Chloropentane	0.083	0.050	0.021	12 (1%)	0.080	0.100	0.012	5 (1%)	0.080	0.075	0.011	10 (1%)
2-Methyl-2-Butene	0.323	0.150	0.021	371 (35%)	0.337	0.250	0.017	438 (49%)	0.093	0.050	0.006	147 (14%)
2-Methylheptane	0.174	0.160	0.006	457 (43%)	0.208	0.160	0.006	513 (57%)	0.939	0.400	0.131	576 (53%)
2-Methylhexane	0.739	0.560	0.047	565 (53%)	0.724	0.630	0.021	532 (59%)	2.245	1.120	0.182	657 (61%)
2-Methylpentane	1.041	0.780	0.029	932 (87%)	1.254	1.020	0.031	825 (92%)	3.631	1.530	0.239	926 (85%)
2,2-Dimethylbutane	0.179	0.120	0.007	372 (35%)	0.217	0.180	0.007	411 (46%)	0.593	0.360	0.033	514 (47%)
2,2,4-Trimethylpentane	0.823	0.640	0.023	945 (88%)	1.085	0.880	0.026	833 (93%)	1.573	0.720	0.074	889 (82%)
2,3-Dimethylbutane	0.285	0.240	0.011	450 (42%)	0.370	0.300	0.011	497 (55%)	0.748	0.420	0.043	556 (51%)
2,3-Dimethylpentane	0.332	0.210	0.025	378 (35%)	0.331	0.280	0.010	423 (47%)	0.975	0.630	0.057	474 (44%)
2,3,4-Trimethylpentane	0.325	0.240	0.012	682 (64%)	0.410	0.320	0.011	693 (77%)	0.653	0.320	0.032	707 (65%)
2,4-Dimethylpentane	0.169	0.140	0.007	446 (42%)	0.206	0.140	0.006	492 (55%)	0.500	0.280	0.031	590 (54%)
3-Methyl-1-Butene	0.088	0.050	0.005	155 (14%)	0.100	0.050	0.006	200 (22%)	0.069	0.050	0.005	51 (5%)
3-Methylheptane	0.184	0.160	0.008	415 (39%)	0.213	0.160	0.008	475 (53%)	0.690	0.320	0.080	541 (50%)

Table B1 - Continued.

	Dallas Hinton				Fort Worth Northwest				Denton Airport South			
TNMOC Species	**Mean**	**Med**	**SE**	**N**	**Mean**	**Med**	**SE**	**N**	**Mean**	**Med**	**SE**	**N**
3-Methylhexane	0.717	0.490	0.040	787 (73%)	0.663	0.560	0.016	731 (82%)	1.656	0.770	0.128	785 (72%)
3-Methylpentane	0.706	0.540	0.018	981 (92%)	0.862	0.660	0.021	853 (95%)	2.019	0.840	0.132	958 (88%)
4-Methyl-1-Pentene	0.083	0.060	0.016	8 (1%)	0.073	0.060	0.009	9 (1%)	0.100	0.090	0.020	6 (1%)
Acetylene	2.223	1.580	0.070	946 (88%)	1.762	1.440	0.043	803 (90%)	1.173	1.060	0.027	852 (79%)
Benzene	1.534	1.320	0.028	1004 (94%)	1.475	1.320	0.025	842 (94%)	1.389	1.140	0.041	1014 (93%)
Bromomethane	0.017	0.010	0.001	286 (27%)	0.021	0.010	0.003	305 (34%)	0.017	0.010	0.001	313 (29%)
Carbon Tetrachloride	0.094	0.100	0.001	1016 (95%)	0.097	0.100	0.001	863 (96%)	0.095	0.100	0.001	1010 (93%)
Chlorobenzene	0.078	0.060	0.006	48 (4%)	0.074	0.060	0.004	55 (6%)	0.085	0.060	0.007	68 (6%)
Chloroform	0.024	0.020	0.000	693 (65%)	0.018	0.020	0.000	605 (68%)	0.020	0.020	0.001	512 (47%)
Chloromethane	0.596	0.580	0.004	900 (84%)	0.598	0.590	0.003	896 (100%)	0.595	0.580	0.004	901 (83%)
cis-1,3-Dichloropropene	0.083	0.030	0.023	16 (1%)	0.077	0.030	0.018	20 (2%)	0.252	0.030	0.119	15 (1%)
cis-2-Butene	0.148	0.080	0.011	247 (23%)	0.164	0.120	0.009	308 (34%)	0.076	0.040	0.011	66 (6%)
cis-2-Hexene	0.074	0.060	0.005	29 (3%)	0.075	0.060	0.007	40 (4%)	0.080	0.060	0.009	12 (1%)
cis-2-Pentene	0.160	0.100	0.013	186 (17%)	0.167	0.100	0.010	268 (30%)	0.069	0.050	0.006	52 (5%)
Cyclohexane	0.430	0.360	0.017	350 (33%)	0.557	0.480	0.018	412 (46%)	2.011	1.080	0.143	590 (54%)
Cyclopentane	0.179	0.150	0.006	405 (38%)	0.224	0.200	0.006	457 (51%)	0.349	0.250	0.019	460 (42%)
Cyclopentene	0.085	0.050	0.010	44 (4%)	0.078	0.050	0.007	72 (8%)	0.056	0.050	0.004	18 (2%)
Dichlorodifluoromethane	0.512	0.510	0.002	900 (84%)	0.518	0.520	0.002	896 (100%)	0.514	0.520	0.002	901 (83%)
Dichloromethane	0.124	0.100	0.005	874 (82%)	0.083	0.070	0.003	725 (81%)	0.094	0.060	0.008	755 (70%)
Ethane	15.35	12.01	0.391	1072 (100%)	28.145	20.610	0.881	896 (100%)	79.767	31.230	3.896	1084 (100%)
Ethylbenzene	0.699	0.560	0.018	867 (81%)	0.516	0.400	0.014	676 (75%)	0.305	0.240	0.010	669 (62%)
Ethylene	2.541	1.900	0.063	1041 (97%)	2.297	1.910	0.050	862 (96%)	1.376	1.210	0.031	942 (87%)
Ethylene Dibromide	0.050	0.020	0.015	21 (2%)	0.037	0.020	0.008	19 (2%)	0.040	0.020	0.009	34 (3%)
Ethylene Dichloride	0.031	0.020	0.001	294 (27%)	0.034	0.040	0.001	277 (31%)	0.034	0.040	0.001	271 (25%)
Isobutane	3.305	2.480	0.087	1067 (100%)	4.357	3.240	0.201	895 (100%)	14.787	6.280	0.738	1079 (99%)
Isopentane	4.302	3.200	0.112	1055 (98%)	5.328	4.250	0.129	895 (100%)	11.798	5.200	0.580	1057 (97%)

Table B1 - Continued.

	Dallas Hinton				Fort Worth Northwest				Denton Airport South			
TNMOC Species	**Mean**	**Med**	**SE**	**N**	**Mean**	**Med**	**SE**	**N**	**Mean**	**Med**	**SE**	**N**
Isoprene	1.013	0.750	0.036	629 (59%)	0.476	0.350	0.019	472 (53%)	0.523	0.400	0.026	351 (32%)
Isopropylbenzene	0.140	0.090	0.005	270 (25%)	0.121	0.090	0.004	224 (25%)	0.119	0.090	0.007	142 (13%)
m-Diethylbenzene	0.290	0.100	0.062	51 (5%)	0.275	0.100	0.055	32 (4%)	0.232	0.150	0.035	22 (2%)
m-Ethyltoluene	0.464	0.270	0.020	654 (61%)	0.354	0.270	0.014	534 (60%)	0.221	0.090	0.032	271 (25%)
m/p Xylene	1.738	1.360	0.047	1027 (96%)	1.112	0.880	0.030	857 (96%)	0.891	0.560	0.047	897 (83%)
Methyl Chloroform	0.028	0.020	0.001	313 (29%)	0.027	0.020	0.001	307 (34%)	0.029	0.020	0.001	307 (28%)
Methylcyclohexane	0.370	0.280	0.016	562 (52%)	0.440	0.350	0.014	571 (64%)	2.035	0.910	0.182	728 (67%)
Methylcyclopentane	0.443	0.360	0.013	725 (68%)	0.539	0.420	0.014	708 (79%)	1.115	0.480	0.174	748 (69%)
n-Butane	7.110	4.680	0.204	1069 (100%)	9.107	6.460	0.256	896 (100%)	24.117	10.520	1.185	1082 (100%)
n-Decane	0.529	0.300	0.037	423 (39%)	0.301	0.200	0.015	340 (38%)	0.410	0.200	0.052	307 (28%)
n-Heptane	0.513	0.420	0.020	756 (71%)	0.597	0.490	0.015	741 (83%)	2.324	0.910	0.236	812 (75%)
n-Hexane	0.985	0.780	0.025	909 (85%)	1.251	1.020	0.031	808 (90%)	5.068	1.680	0.651	915 (84%)
n-Nonane	0.555	0.360	0.046	318 (30%)	0.490	0.360	0.027	241 (27%)	0.739	0.360	0.081	332 (31%)
n-Octane	0.281	0.240	0.010	536 (50%)	0.304	0.240	0.010	566 (63%)	1.175	0.480	0.159	633 (58%)
n-Pentane	2.294	1.750	0.059	871 (81%)	3.053	2.450	0.076	838 (94%)	10.455	3.800	0.654	931 (86%)
n-Propylbenzene	0.222	0.180	0.010	511 (48%)	0.164	0.090	0.006	402 (45%)	0.159	0.090	0.018	211 (19%)
n-Undecane	0.381	0.220	0.026	302 (28%)	0.338	0.220	0.026	322 (36%)	0.312	0.220	0.026	279 (26%)
o-Ethyltoluene	0.254	0.180	0.013	355 (33%)	0.181	0.180	0.007	299 (33%)	0.161	0.090	0.030	119 (11%)
o-Xylene	0.618	0.480	0.017	889 (83%)	0.411	0.320	0.012	735 (82%)	0.274	0.160	0.013	703 (65%)
p-Diethylbenzene	0.237	0.100	0.026	163 (15%)	0.229	0.100	0.026	103 (11%)	0.236	0.100	0.030	67 (6%)
p-Ethyltoluene	0.269	0.180	0.012	498 (46%)	0.186	0.180	0.006	441 (49%)	0.171	0.090	0.019	205 (19%)
Propane	12.05	9.090	0.286	1071 (100%)	16.437	12.420	0.452	896 (100%)	50.366	21.780	2.342	1085 (100%)
Propylene	1.590	1.200	0.047	765 (71%)	1.366	1.080	0.036	610 (68%)	0.926	0.720	0.048	599 (55%)
Styrene	0.187	0.080	0.011	305 (28%)	0.158	0.080	0.008	347 (39%)	0.125	0.080	0.012	139 (13%)
Tetrachloroethylene	0.052	0.040	0.002	635 (59%)	0.035	0.020	0.001	491 (55%)	0.035	0.020	0.005	449 (41%)
Toluene	2.782	1.960	0.081	1067 (100%)	2.443	1.820	0.108	891 (99%)	2.452	1.400	0.343	1070 (99%)

Table B1 - Continued.

	Dallas Hinton				Fort Worth Northwest				Denton Airport South			
TNMOC Species	**Mean**	**Med**	**SE**	**N**	**Mean**	**Med**	**SE**	**N**	**Mean**	**Med**	**SE**	**N**
trans-1,3-Dichloropropene	0.057	0.030	0.021	10 (1%)	0.041	0.030	0.007	17 (2%)	0.049	0.030	0.013	14 (1%)
trans-2-Butene	0.243	0.120	0.021	171 (16%)	0.230	0.160	0.015	224 (25%)	0.131	0.080	0.018	63 (6%)
trans-2-Hexene	0.100	0.060	0.009	43 (4%)	0.095	0.060	0.007	67 (7%)	0.083	0.060	0.008	21 (2%)
trans-2-Pentene	0.267	0.150	0.016	356 (33%)	0.284	0.200	0.015	381 (43%)	0.092	0.050	0.007	97 (9%)
Trichloroethylene	0.041	0.020	0.003	238 (22%)	0.024	0.020	0.001	105 (12%)	0.073	0.020	0.046	67 (6%)
Trichlorofluoromethane	0.259	0.250	0.001	1071 (100%)	0.260	0.260	0.001	896 (100%)	0.252	0.250	0.001	1083 (100%)
Vinyl Chloride	0.024	0.020	0.003	14 (1%)	0.024	0.020	0.002	20 (2%)	0.025	0.020	0.003	19 (2%)

Table B2 - Denton Airport South TNMOC concentrations (ppb-C) mean, standard deviation (SD), minimum, maximum, the number of non-zero data (N), and percentage of non-zero data (%).

Species	Mean	SD	Min	Max	N	%
Ethane	79.77	128.26	0.50	1292.30	1084	99.91%
Propane	50.37	77.15	0.96	714.27	1085	100%
n-Butane	24.12	38.99	0.40	508.32	1082	99.72%
Isobutane	14.79	24.24	0.16	285.24	1079	99.45%
Isopentane	11.80	18.87	0.25	275.20	1057	97.42%
n-Pentane	10.45	19.96	0.15	316.80	931	85.81%
n-Hexane	5.07	19.70	0.06	514.56	915	84.33%
2-Methylpentane	3.63	7.27	0.06	145.98	926	85.35%
Toluene	2.45	11.22	0.21	353.92	1070	98.62%
n-Heptane	2.32	6.73	0.07	162.96	812	74.84%
2-Methylhexane	2.25	4.68	0.07	97.16	657	60.55%
Methylcyclohexane	2.03	4.90	0.07	108.15	728	67.10%
3-Methylpentane	2.02	4.09	0.06	85.02	958	88.29%
Cyclohexane	2.01	3.46	0.06	66.00	590	54.38%
3-Methylhexane	1.66	3.59	0.07	80.29	785	72.35%
2,2,4-Trimethylpentane	1.57	2.20	0.08	20.96	889	81.94%
Benzene	1.39	1.30	0.12	19.86	1014	93.46%
Ethylene	1.38	0.94	0.06	18.54	942	86.82%
n-Octane	1.17	4.00	0.08	89.20	633	58.34%
Acetylene	1.17	0.80	0.24	12.90	852	78.53%
Methylcyclopentane	1.11	4.76	0.06	122.34	748	68.94%
2,3-Dimethylpentane	0.97	1.24	0.07	19.04	474	43.69%
2-Methylheptane	0.94	3.14	0.08	68.00	576	53.09%
Propylene	0.93	1.17	0.18	25.08	599	55.21%
m/p Xylene	0.89	1.41	0.08	29.36	897	82.67%
2,3-Dimethylbutane	0.75	1.03	0.06	15.42	556	51.24%
n-Nonane	0.74	1.47	0.09	16.47	332	30.60%
3-Methylheptane	0.69	1.87	0.08	37.36	541	49.86%
2,3,4-Trimethylpentane	0.65	0.86	0.08	6.40	707	65.16%
Chloromethane	0.59	0.11	0.29	1.20	901	83.04%
2,2-Dimethylbutane	0.59	0.76	0.06	10.50	514	47.37%
Isoprene	0.52	0.48	0.05	5.10	351	32.35%
1-Butene	0.52	0.39	0.04	2.96	700	64.52%
Dichlorodifluoromethane	0.51	0.06	0.20	0.77	901	83.04%
2,4-Dimethylpentane	0.50	0.76	0.07	13.16	590	54.38%
n-Decane	0.41	0.91	0.10	11.90	307	28.29%
1,2-Dichloropropane	0.38	0.65	0.03	3.66	46	4.24%
Cyclopentane	0.35	0.42	0.05	4.80	460	42.40%
n-Undecane	0.31	0.44	0.11	3.96	279	25.71%
Ethylbenzene	0.30	0.26	0.08	3.44	669	61.66%
1,2,4-Trimethylbenzene	0.28	0.57	0.09	9.81	382	35.21%
o-Xylene	0.27	0.34	0.08	4.00	703	64.79%
cis-1,3-Dichloropropene	0.25	0.46	0.03	1.71	15	1.38%

Table B2 - Continued.

Species	Mean	SD	Min	Max	N	%
Trichlorofluoromethane	0.25	0.03	0.14	0.48	1083	99.82%
p-Diethylbenzene	0.24	0.24	0.10	1.40	67	6.18%
m-Diethylbenzene	0.23	0.16	0.10	0.70	22	2.03%
m-Ethyltoluene	0.22	0.52	0.09	8.19	271	24.98%
1-Pentene	0.20	0.26	0.05	1.65	94	8.66%
1,2,3-Trimethylbenzene	0.17	0.38	0.09	4.05	113	10.41%
p-Ethyltoluene	0.17	0.27	0.09	3.78	205	18.89%
1,3,5-Trimethylbenzene	0.16	0.34	0.09	3.96	162	14.93%
o-Ethyltoluene	0.16	0.33	0.09	3.60	119	10.97%
1,3-Butadiene	0.16	0.31	0.04	2.28	53	4.88%
n-Propylbenzene	0.16	0.26	0.09	3.51	211	19.45%
trans-2-Butene	0.13	0.14	0.04	0.56	63	5.81%
Styrene	0.13	0.14	0.08	1.36	139	12.81%
Isopropylbenzene	0.12	0.09	0.09	0.99	142	13.09%
1-Hexene & 2-Methyl-1-Pentene	0.11	0.11	0.06	0.66	51	4.70%
4-Methyl-1-Pentene	0.10	0.05	0.06	0.18	6	0.55%
Carbon Tetrachloride	0.09	0.02	0.01	0.42	1010	93.09%
Dichloromethane	0.09	0.22	0.01	4.87	755	69.59%
2-Methyl-2-Butene	0.09	0.08	0.05	0.55	147	13.55%
trans-2-Pentene	0.09	0.07	0.05	0.40	97	8.94%
Chlorobenzene	0.08	0.06	0.06	0.36	68	6.27%
trans-2-Hexene	0.08	0.04	0.06	0.18	21	1.94%
2-Chloropentane	0.08	0.03	0.05	0.15	10	0.92%
cis-2-Hexene	0.08	0.03	0.06	0.12	12	1.11%
cis-2-Butene	0.08	0.09	0.04	0.72	66	6.08%
Trichloroethylene	0.07	0.38	0.02	3.12	67	6.18%
cis-2-Pentene	0.07	0.04	0.05	0.25	52	4.79%
3-Methyl-1-Butene	0.07	0.04	0.05	0.25	51	4.70%
Cyclopentene	0.06	0.02	0.05	0.10	18	1.66%
trans-1,3-Dichloropropene	0.05	0.05	0.03	0.21	14	1.29%
1,1-Dichloroethylene	0.05	0.04	0.02	0.12	105	9.68%
Ethylene Dibromide	0.04	0.05	0.02	0.24	34	3.13%
Tetrachloroethylene	0.04	0.10	0.02	1.84	449	41.38%
Ethylene Dichloride	0.03	0.02	0.02	0.34	271	24.98%
Methyl Chloroform	0.03	0.02	0.02	0.12	307	28.29%
1,1-Dichloroethane	0.03	0.02	0.02	0.06	7	0.65%
1,1,2,2-Tetrachloroethane	0.03	0.02	0.02	0.10	30	2.76%
Vinyl Chloride	0.03	0.01	0.02	0.08	19	1.75%
1,1,2-Trichloroethane	0.02	0.01	0.02	0.06	10	0.92%
Chloroform	0.02	0.02	0.01	0.41	512	47.19%
Bromomethane	0.02	0.01	0.01	0.11	313	28.85%

Table B3 - The mean (± standard deviation), minimum to maximum, and signal-to-noise (S/N) ratio of TNMOC [ppb-C].

	Dallas Hinton			**Fort Worth Northwest**			**Denton Airport South**		
Species	Mean (± SD)	Min - Max	S/N	Mean (± SD)	Min - Max	S/N	Mean (± SD)	Min - Max	S/N
(1.) 1-Butene	1.024 (± 0.985)	0.08 - 8.56	1.546	1.093 (± 0.695)	0.08 - 5.2	2.361	0.519 (± 0.389)	0.04 - 2.96	0.933
(2.) 1-Hexene & 2-Methyl-1-Pentene	0.15 (± 0.109)	0.06 - 0.48	0.003	0.173 (± 0.123)	0.06 - 0.96	0.018	0.109 (± 0.112)	0.06 - 0.66	0.000
(3.) 1-Pentene	0.287 (± 0.264)	0.05 - 1.4	0.001	0.255 (± 0.202)	0.05 - 1.35	0.001	0.198 (± 0.264)	0.05 - 1.65	0.000
(4.) 1,1-Dichloroethane	0.022 (± 0.006)	0.02 - 0.04	0.000	0.02 (± 0)	0.02 - 0.02	0.000	0.026 (± 0.015)	0.02 - 0.06	0.000
(5.) 1,1-Dichloroethylene	0.045 (± 0.037)	0.02 - 0.16	0.000	0.043 (± 0.037)	0.02 - 0.16	0.000	0.046 (± 0.035)	0.02 - 0.12	0.000
(6.) 1,1,2-Trichloroethane	0.04 (± 0.057)	0.02 - 0.18	0.000	0.025 (± 0.01)	0.02 - 0.04	0.000	0.024 (± 0.013)	0.02 - 0.06	0.000
(7.) 1,1,2,2-Tetrachloroethane	0.023 (± 0.013)	0.02 - 0.08	0.000	0.022 (± 0.006)	0.02 - 0.04	0.000	0.025 (± 0.018)	0.02 - 0.1	0.000
(8.) 1,2-Dichloropropane	0.184 (± 0.208)	0.03 - 0.87	0.009	0.238 (± 0.271)	0.03 - 1.29	0.015	0.376 (± 0.649)	0.03 - 3.66	0.022
(9.) 1,2,3-Trimethylbenzene	0.301 (± 0.364)	0.09 - 4.23	0.226	0.204 (± 0.161)	0.09 - 1.08	0.207	0.172 (± 0.382)	0.09 - 4.05	0.028
(10.) 1,2,4-Trimethylbenzene	0.574 (± 0.624)	0.09 - 5.67	0.383	0.492 (± 0.45)	0.09 - 4.32	0.388	0.278 (± 0.566)	0.09 - 9.81	0.032
(11.) 1,3-Butadiene	0.273 (± 0.24)	0.04 - 1.32	0.045	0.244 (± 0.168)	0.04 - 1.04	0.046	0.16 (± 0.315)	0.04 - 2.28	0.000
(12.) 1,3,5-Trimethylbenzene	0.254 (± 0.236)	0.09 - 1.44	0.064	0.172 (± 0.12)	0.09 - 0.9	0.018	0.163 (± 0.336)	0.09 - 3.96	0.000
(13.) 2-Chloropentane	0.083 (± 0.072)	0.05 - 0.3	0.000	0.08 (± 0.027)	0.05 - 0.1	0.000	0.08 (± 0.035)	0.05 - 0.15	0.000
(14.) 2-Methyl-2-Butene	0.323 (± 0.399)	0.05 - 2.15	0.090	0.337 (± 0.351)	0.05 - 3.75	0.259	0.093 (± 0.078)	0.05 - 0.55	0.000
(15.) 2-Methylheptane	0.174 (± 0.134)	0.08 - 0.88	0.053	0.208 (± 0.144)	0.08 - 1.04	0.175	0.939 (± 3.143)	0.08 - 68	0.559
(16.) 2-Methylhexane	0.739 (± 1.118)	0.07 - 22.96	0.666	0.724 (± 0.484)	0.07 - 3.64	0.848	2.245 (± 4.677)	0.07 - 97.16	0.868
(17.) 2-Methylpentane	1.041 (± 0.893)	0.06 - 6.96	1.216	1.254 (± 0.894)	0.06 - 8.34	1.587	3.631 (± 7.275)	0.06 - 145.98	1.025
(18.) 2,2-Dimethylbutane	0.179 (± 0.131)	0.06 - 0.84	0.035	0.217 (± 0.138)	0.06 - 1.02	0.134	0.593 (± 0.758)	0.06 - 10.5	0.448
(19.) 2,2,4-Trimethylpentane	0.823 (± 0.708)	0.08 - 6.08	1.407	1.085 (± 0.75)	0.08 - 6.24	1.894	1.573 (± 2.196)	0.08 - 20.96	1.020
(20.) 2,3-Dimethylbutane	0.285 (± 0.229)	0.06 - 1.86	0.106	0.37 (± 0.248)	0.06 - 2.22	0.322	0.748 (± 1.025)	0.06 - 15.42	0.482
(21.) 2,3-Dimethylpentane	0.332 (± 0.477)	0.07 - 7.98	0.138	0.331 (± 0.204)	0.07 - 1.33	0.270	0.975 (± 1.239)	0.07 - 19.04	0.544
(22.) 2,3,4-Trimethylpentane	0.325 (± 0.302)	0.08 - 2.24	0.266	0.41 (± 0.297)	0.08 - 2.16	0.614	0.653 (± 0.855)	0.08 - 6.4	0.499
(23.) 2,4-Dimethylpentane	0.169 (± 0.155)	0.07 - 1.82	0.000	0.206 (± 0.132)	0.07 - 0.91	0.002	0.5 (± 0.756)	0.07 - 13.16	0.149
(24.) 3-Methyl-1-Butene	0.088 (± 0.064)	0.05 - 0.4	0.000	0.1 (± 0.081)	0.05 - 0.6	0.001	0.069 (± 0.039)	0.05 - 0.25	0.000
(25.) 3-Methylheptane	0.184 (± 0.172)	0.08 - 1.52	0.037	0.213 (± 0.175)	0.08 - 1.28	0.112	0.69 (± 1.866)	0.08 - 37.36	0.448
(26.) 3-Methylhexane	0.717 (± 1.109)	0.07 - 26.67	1.125	0.663 (± 0.442)	0.07 - 3.85	1.373	1.656 (± 3.589)	0.07 - 80.29	0.929

Table B3 - Continued.

	Dallas Hinton			Fort Worth Northwest			Denton Airport South		
(27.) 3-Methylpentane	0.706 (± 0.575)	0.06 - 4.62	1.427	0.862 (± 0.611)	0.06 - 5.4	1.739	2.019 (± 4.087)	0.06 - 85.02	1.083
(28.) 4-Methyl-1-Pentene	0.083 (± 0.045)	0.06 - 0.18	0.000	0.073 (± 0.026)	0.06 - 0.12	0.000	0.1 (± 0.049)	0.06 - 0.18	0.000
(29.) Acetylene	2.223 (± 2.148)	0.26 - 20.52	1.989	1.762 (± 1.223)	0.12 - 10.64	2.393	1.173 (± 0.8)	0.24 - 12.9	2.024
(30.) Benzene	1.534 (± 0.886)	0.3 - 7.44	2.637	1.475 (± 0.721)	0.42 - 4.92	2.649	1.389 (± 1.305)	0.12 - 19.86	2.237
(31.) Bromomethane	0.017 (± 0.015)	0.01 - 0.09	0.000	0.021 (± 0.052)	0.01 - 0.72	0.000	0.017 (± 0.015)	0.01 - 0.11	0.000
(32.) Carbon Tetrachloride	0.094 (± 0.018)	0.01 - 0.16	0.000	0.097 (± 0.015)	0.03 - 0.16	0.000	0.095 (± 0.022)	0.01 - 0.42	0.000
(33.) Chlorobenzene	0.078 (± 0.041)	0.06 - 0.24	0.000	0.074 (± 0.028)	0.06 - 0.18	0.000	0.085 (± 0.058)	0.06 - 0.36	0.000
(34.) Chloroform	0.024 (± 0.011)	0.01 - 0.08	0.000	0.018 (± 0.006)	0.01 - 0.04	0.000	0.02 (± 0.02)	0.01 - 0.41	0.000
(35.) Chloromethane	0.596 (± 0.106)	0.31 - 1.36	3.074	0.598 (± 0.102)	0.3 - 1.12	3.706	0.595 (± 0.106)	0.29 - 1.2	3.031
(36.) cis-1,3-Dichloropropene	0.083 (± 0.093)	0.03 - 0.3	0.000	0.077 (± 0.079)	0.03 - 0.33	0.000	0.252 (± 0.461)	0.03 - 1.71	0.001
(37.) cis-2-Butene	0.148 (± 0.165)	0.04 - 1.24	0.001	0.164 (± 0.156)	0.04 - 1.04	0.001	0.076 (± 0.09)	0.04 - 0.72	0.000
(38.) cis-2-Hexene	0.074 (± 0.026)	0.06 - 0.12	0.000	0.075 (± 0.042)	0.06 - 0.3	0.000	0.08 (± 0.03)	0.06 - 0.12	0.000
(39.) cis-2-Pentene	0.16 (± 0.171)	0.05 - 1.1	0.002	0.167 (± 0.169)	0.05 - 1.45	0.005	0.069 (± 0.041)	0.05 - 0.25	0.000
(40.) Cyclohexane	0.43 (± 0.324)	0.06 - 2.4	0.296	0.557 (± 0.374)	0.06 - 2.64	0.587	2.011 (± 3.465)	0.06 - 66	0.780
(41.) Cyclopentane	0.179 (± 0.128)	0.05 - 0.95	0.001	0.224 (± 0.136)	0.05 - 1.05	0.002	0.349 (± 0.415)	0.05 - 4.8	0.048
(42.) Cyclopentene	0.085 (± 0.064)	0.05 - 0.3	0.000	0.078 (± 0.057)	0.05 - 0.4	0.001	0.056 (± 0.016)	0.05 - 0.1	0.000
(43.) Dichlorodifluoromethane	0.512 (± 0.065)	0.2 - 0.87	2.971	0.518 (± 0.064)	0.23 - 1.09	3.611	0.514 (± 0.06)	0.2 - 0.77	3.003
(44.) Dichloromethane	0.124 (± 0.142)	0.02 - 3.44	0.099	0.083 (± 0.071)	0.01 - 1.19	0.005	0.094 (± 0.221)	0.01 - 4.87	0.002
(45.) Ethane	15.349 (± 12.796)	2.34 - 121.4	2.760	28.14 (± 26.36)	2.9 - 256.02	2.304	79.767 (± 128.26)	0.5 - 1292.3	1.224
(46.) Ethylbenzene	0.699 (± 0.523)	0.08 - 5.76	0.887	0.516 (± 0.367)	0.08 - 3.36	0.568	0.305 (± 0.26)	0.08 - 3.44	0.110
(47.) Ethylene	2.541 (± 2.028)	0.3 - 16.92	2.157	2.297 (± 1.467)	0.1 - 10.1	2.211	1.376 (± 0.943)	0.06 - 18.54	1.641
(48.) Ethylene Dibromide	0.05 (± 0.067)	0.02 - 0.24	0.000	0.037 (± 0.034)	0.02 - 0.14	0.000	0.04 (± 0.05)	0.02 - 0.24	0.000
(49.) Ethylene Dichloride	0.031 (± 0.021)	0.02 - 0.32	0.000	0.034 (± 0.014)	0.02 - 0.1	0.000	0.034 (± 0.023)	0.02 - 0.34	0.000
(50.) Isobutane	3.305 (± 2.856)	0.2 - 31.88	2.407	4.357 (± 6.02)	0.12 - 156.16	2.459	14.787 (± 24.24)	0.16 - 285.24	1.230
(51.) Isopentane	4.302 (± 3.653)	0.35 - 40.35	2.584	5.328 (± 3.857)	0.25 - 33.65	2.752	11.798 (± 18.871)	0.25 - 275.2	1.244
(52.) Isoprene	1.013 (± 0.899)	0.05 - 5.2	0.452	0.476 (± 0.41)	0.05 - 2.55	0.102	0.523 (± 0.482)	0.05 - 5.1	0.095
(53.) Isopropylbenzene	0.14 (± 0.084)	0.09 - 0.54	0.000	0.121 (± 0.059)	0.09 - 0.45	0.000	0.119 (± 0.089)	0.09 - 0.99	0.000

Table B3 - Continued.

	Dallas Hinton			Fort Worth Northwest			Denton Airport South		
(54.) m-Diethylbenzene	0.29 (± 0.442)	0.1 - 3	0.030	0.275 (± 0.312)	0.1 - 1.3	0.007	0.232 (± 0.164)	0.1 - 0.7	0.009
(55.) m-Ethyltoluene	0.464 (± 0.513)	0.09 - 5.49	0.876	0.354 (± 0.325)	0.09 - 2.97	0.777	0.221 (± 0.52)	0.09 - 8.19	0.175
(56.) m/p Xylene	1.738 (± 1.499)	0.16 - 15.84	1.081	1.112 (± 0.881)	0.08 - 7.2	0.694	0.891 (± 1.412)	0.08 - 29.36	0.371
(57.) Methyl Chloroform	0.028 (± 0.015)	0.02 - 0.1	0.000	0.027 (± 0.014)	0.02 - 0.16	0.000	0.029 (± 0.015)	0.02 - 0.12	0.000
(58.) Methylcyclohexane	0.37 (± 0.368)	0.07 - 5.6	0.297	0.44 (± 0.344)	0.07 - 2.52	0.506	2.035 (± 4.904)	0.07 - 108.15	0.871
(59.) Methylcyclopentane	0.443 (± 0.353)	0.06 - 3	0.002	0.539 (± 0.372)	0.06 - 3.3	0.012	1.115 (± 4.764)	0.06 - 122.34	0.183
(60.) n-Butane	7.11 (± 6.662)	0.68 - 45.72	2.007	9.107 (± 7.662)	0.84 - 54	2.003	24.117 (± 38.986)	0.4 - 508.32	1.298
(61.) n-Decane	0.529 (± 0.752)	0.1 - 9.7	0.273	0.301 (± 0.284)	0.1 - 2.9	0.136	0.41 (± 0.909)	0.1 - 11.9	0.133
(62.) n-Heptane	0.513 (± 0.545)	0.07 - 11.34	0.778	0.597 (± 0.407)	0.07 - 3.5	1.142	2.324 (± 6.726)	0.07 - 162.96	0.942
(63.) n-Hexane	0.985 (± 0.742)	0.06 - 6.24	1.872	1.251 (± 0.869)	0.06 - 6.78	2.274	5.068 (± 19.7)	0.06 - 514.56	0.936
(64.) n-Nonane	0.555 (± 0.822)	0.09 - 12.24	0.292	0.49 (± 0.423)	0.09 - 2.88	0.234	0.739 (± 1.467)	0.09 - 16.47	0.346
(65.) n-Octane	0.281 (± 0.24)	0.08 - 1.92	0.294	0.304 (± 0.23)	0.08 - 1.84	0.471	1.175 (± 3.995)	0.08 - 89.2	0.670
(66.) n-Pentane	2.294 (± 1.742)	0.2 - 12	2.140	3.053 (± 2.201)	0.1 - 16.6	2.579	10.455 (± 19.956)	0.15 - 316.8	0.995
(67.) n-Propylbenzene	0.222 (± 0.227)	0.09 - 3.24	0.001	0.164 (± 0.117)	0.09 - 1.08	0.001	0.159 (± 0.261)	0.09 - 3.51	0.000
(68.) n-Undecane	0.381 (± 0.453)	0.11 - 3.96	0.250	0.338 (± 0.475)	0.11 - 5.83	0.249	0.312 (± 0.436)	0.11 - 3.96	0.153
(69.) o-Ethyltoluene	0.254 (± 0.249)	0.09 - 2.34	0.235	0.181 (± 0.127)	0.09 - 1.08	0.199	0.161 (± 0.328)	0.09 - 3.6	0.021
(70.) o-Xylene	0.618 (± 0.503)	0.08 - 4	0.660	0.411 (± 0.316)	0.08 - 2.4	0.298	0.274 (± 0.342)	0.08 - 4	0.053
(71.) p-Diethylbenzene	0.237 (± 0.329)	0.1 - 3.4	0.090	0.229 (± 0.259)	0.1 - 1.6	0.062	0.236 (± 0.242)	0.1 - 1.4	0.023
(72.) p-Ethyltoluene	0.269 (± 0.27)	0.09 - 2.25	0.318	0.186 (± 0.132)	0.09 - 0.99	0.224	0.171 (± 0.271)	0.09 - 3.78	0.034
(73.) Propane	12.05 (± 9.348)	1.77 - 64.89	2.362	16.437 (± 13.52)	1.86 - 91.74	2.142	50.366 (± 77.145)	0.96 - 714.27	1.320
(74.) Propylene	1.59 (± 1.307)	0.15 - 10.14	0.720	1.366 (± 0.898)	0.09 - 6.24	0.683	0.926 (± 1.173)	0.18 - 25.08	0.273
(75.) Styrene	0.187 (± 0.196)	0.08 - 1.28	0.000	0.158 (± 0.14)	0.08 - 1.44	0.000	0.125 (± 0.144)	0.08 - 1.36	0.000
(76.) Tetrachloroethylene	0.052 (± 0.058)	0.02 - 0.8	0.001	0.035 (± 0.03)	0.02 - 0.3	0.000	0.035 (± 0.096)	0.02 - 1.84	0.000
(77.) Toluene	2.782 (± 2.644)	0.35 - 25.62	2.162	2.443 (± 3.224)	0.21 - 76.44	2.563	2.452 (± 11.222)	0.21 - 353.92	1.693
(78.) trans-1,3-Dichloropropene	0.057 (± 0.067)	0.03 - 0.24	0.000	0.041 (± 0.03)	0.03 - 0.15	0.000	0.049 (± 0.048)	0.03 - 0.21	0.000
(79.) trans-2-Butene	0.243 (± 0.271)	0.04 - 1.56	0.040	0.23 (± 0.222)	0.04 - 1.32	0.093	0.131 (± 0.143)	0.04 - 0.56	0.001
(80.) trans-2-Hexene	0.1 (± 0.057)	0.06 - 0.24	0.000	0.095 (± 0.061)	0.06 - 0.36	0.000	0.083 (± 0.035)	0.06 - 0.18	0.000

Table B3 - Continued.

	Dallas Hinton			Fort Worth Northwest			Denton Airport South		
(81.) trans-2-Pentene	0.267 (± 0.307)	0.05 - 1.75	0.001	0.284 (± 0.285)	0.05 - 2.6	0.001	0.092 (± 0.069)	0.05 - 0.4	0.000
(82.) Trichloroethylene	0.041 (± 0.051)	0.02 - 0.48	0.000	0.024 (± 0.01)	0.02 - 0.08	0.000	0.073 (± 0.378)	0.02 - 3.12	0.000
(83.) Trichlorofluoromethane	0.259 (± 0.035)	0.16 - 0.48	0.168	0.26 (± 0.034)	0.19 - 0.49	0.167	0.252 (± 0.03)	0.14 - 0.48	0.113
(84.) Vinyl Chloride	0.024 (± 0.012)	0.02 - 0.06	0.000	0.024 (± 0.008)	0.02 - 0.04	0.000	0.025 (± 0.015)	0.02 - 0.08	0.000

REFERENCES

[1] U.S. Census Bureau, "Newsroom," 22 March 2018. [Online]. Available: https://www.census.gov/newsroom/press-releases/2018/popest-metro-county.html. [Accessed 23 August 2018].

[2] Railroad Commissions of Texas, "Barnett Shale Information," 6 September 2018. [Online]. Available: http://www.rrc.state.tx.us/oil-gas/major-oil-and-gas-formations/barnett-shale-information/. [Accessed 24 September 2018].

[3] U.S. EPA, "Ozone Pollution," 18 May 2016. [Online]. Available: https://www.epa.gov/ozone-pollution. [Accessed 28 October 2016].

[4] TCEQ, "Dallas-Fort Worth: Current Attainment Status: Compliance of Dallas-Fort Worth (DFW) area counties with the National Ambient Air Quality Standards (NAAQS).," 15 June 2016. [Online]. Available: https://www.tceq.texas.gov/airquality/sip/dfw/dfw-status. [Accessed 15 September 2016].

[5] A. Bunch, C. Perry, L. Abraham, D. Wikoff, J. Tachovsky, J. Hixon, J. Urban, M. Harris and L. Haws, "Evaluation of impact of shale gas operations in the Barnett Shale region on volatile organic compounds in air and potential human health risks," *Science of The Total Environment*, vol. 15, pp. 832-842, 2014.

[6] M. Ahmadi and K. John, "Statistical evaluation of the impact of shale gas activities on ozone pollution in North Texas," *Science of the Total Environment*, vol. 536, pp. 457-467, 2015.

[7] A. Rich, J. P. Grover and M. L. Sattler, "An exploratory study of air emissions associated with shale gas development and production in the Barnett Shale," *Journal of the Air & Waste Management Association*, vol. 64, no. 1, pp. 61-72, 2014.

[8] H. Simon, K. R. Baker and S. Phillips, "Compilation and interpretation of photochemical model performance statistics published between 2006 and 2012," *Atmospheric Environment*, vol. 61, pp. 124-139, 2012.

[9] G. Q. Lim, M. Matin and K. John, "Spatial and temporal characteristics of ambient atmospheric hydrocarbons in an active shale gas region in North Texas," *Science of the Total Environment*, vol. 656, pp. 347-363, 2019.

[10] G. Q. Lim and K. John, "Impact of energy production in the Barnett Shale gas region on the measured ambient hydrocarbon concentrations in Denton, Texas," *Atmospheric Pollution Research*, vol. 11, no. 2, pp. 409-418, 2020.

[11] R. W. Howarth, R. Santoro and A. Ingraffea, "Methane and the greenhouse-gas footprint of natural gas from shale formations A letter," *Climatic Change*, vol. 106, p. 679–690, 2011.

[12] S. Henner and A. Lamadrid, "Shale gas vs. coal: Policy implications from environmental impact comparisons of shale gas, conventional gas, and coal on air, water, and land in the United States," *Energy Policy*, vol. 53, pp. 442-453, 2013.

[13] J. deGouw, D. Parrish, G. Frost and M. Trainer, "Reduced emissions of CO2, NOx, and SO2 from U.S. power plants owing to switch from coal to natural gas with combined cycle technology," *Earth's Future*, vol. 2, pp. 75-82, 2014.

[14] T. Vinciguerra, S. Yao, J. Dadzie, A. Chittams, T. Deskins, S. Ehrman and R. Russell, "Regional air quality impacts of hydraulic fracturing and shale natural gas activity: evidence from ambient VOC observations," *Atmospheric Environment*, vol. 110, pp. 144-150, 2015.

[15] ExxonMobil, "Natural Gas," ExxonMobil, 14 May 2019. [Online]. Available: https://corporate.exxonmobil.com/en/Energy-and-environment/Energy-resources/Natural-gas. [Accessed 15 May 2019].

[16] EIA, "Annual Energy Outlook 2019 with projections to 2050," U.S. Energy Information Administration, 2019.

[17] U.S. EPA, "Unconventional Oil and Natural Gas Development," 9 April 2019. [Online]. Available: https://www.epa.gov/uog. [Accessed 15 May 2019].

[18] IEA, World Energy Outlook 2018, Paris: International Energy Agency, 2018.

[19] EIA, "How much shale gas is produced in the United States?," 3 October 2018. [Online]. Available: https://www.eia.gov/tools/faqs/faq.php?id=907&t=8. [Accessed 17 May 2019].

[20] A. K. Manda, J. L. Heath, W. A. Klein, M. T. Griffin and B. E. Montz, "Evolution of multi-well pad development and influence of well pads on environmental violations and wastewater volumes in the Marcellus shale (USA)," *Journal of Environmental Management*, vol. 142, pp. 36-45, 2014.

[21] T. J. Centner and L. Petetin, "Permitting program with best management practices for shale gas wells to safeguard public health," *Journal of Environmental Management*, vol. 163, pp. 174-183, 2015.

[22] J.-P. Nicot and B. R. Scanlon, "Water use for shale-gas production in Texas, U.S.," *Environmental Science and Technology*, vol. 46, pp. 3580-3586, 2012.

[23] M.-T. Le, "An assessment of the potential for the development of the shale gas industry in countries outside of North America," *Heliyon*, vol. 4, no. 2, 2018.

[24] Q. Wang, X. Chen, A. N. Jha and H. Rogers, "Natural gas from shale formation – The evolution, evidences and challenges of shale gas revolution in United States," *Renewable and Sustainable Energy Reviews*, vol. 30, pp. 1-28, 2014.

[25] R. Vidic, S. Brantley, J. Vandenbossche, D. Yoxtheimer and J. Abad, "Impact of shale gas development on regional water quality," *Science*, vol. 340, no. 6134, p. DOI: 10.1126/science.1235009, 2013.

[26] M. Zoback, S. Kitasei and B. Copithorne, "Addressing the environmental risks from shale gas developments," Worldwatch Institute , Washington, D.C., 2010.

[27] M. Fry, A. Briggle and J. Kincaid, "Fracking and environmental (in)justice in a Texas city," *Ecological Economics*, vol. 117, p. 97–107, 2015.

[28] K. Brasier, M. Filteau, D. McLaughlin, J. Jacquet, R. Stedman, T. Kelsey and S. Goetz, "Residents' persceptions of community and environmental impacts from development of natural gas in the Marcellus Shale: A comparison of Pennsylvania and New York cases'," *Journal of Rural Sciences*, vol. 26, no. 1, pp. 32-31, 2011.

[29] L. McKenzie, R. Witter, L. Newman and J. Adgate, "Human health risk assessment of air emissions from development of unconventional natural gas resources," *Science of the Total Environment* , vol. 424, pp. 79-87, 2012.

[30] A. Burnham, J. Han, C. E. Clark, M. Wang, J. B. Dunn and I. Palou-Rivera, "Life-cycle greenhouse gas emissions of shale gas, natural gas, coal, and petroleum," *Environmental Science and Technology*, vol. 46, pp. 619-627, 2012.

[31] D. T. Allen, "Atmospheric emissions and air quality impacts from natural gas production and Use," *The Annual Review of Chemical and Biomolecular Engineering*, vol. 5, pp. 55-75, 2014.

[32] D. R. Lyon, D. Zavala-Araiza, R. A. Alvarez, R. Harriss, V. Palacios, X. Lan, R. Talbot, T. Lavoie, P. Shepson, T. I. Yacovitch, S. C. Herndon, A. J. Marchese, D. Zimmerle and A. L. Robinson, "Constructing a Spatially Resolved Methane Emission Inventory for the Barnett Shale Region," *Environmental Science and Technology*, vol. 19, no. 13, p. 8147–8157, 2015.

[33] S. Ethridge, T. Bredfeldt, K. Sheedy, S. Shirley, G. Lopez and M. Honeycutt, "The Barnett Shale: From problem formulation to risk management," *Journal of Unconventional Oil and Gas Resources*, vol. 11, pp. 95-110, 2015.

[34] IPCC, "Climate change 2014: synthesis report," IPCC, Geneva, Switzerland, 2014.

[35] A. L. Robinson, "Air pollutant emissions from shale gas development and production," in Institute of Medicine workshop on the Health Impact Assessment of New Energy Sources: Shale Gas Extraction, Washington, D.C., 2012.

[36] A. Litovitz, A. Curtright, S. Abramzon, N. Burger and C. Samaras, "Estimation of regional air-quality damages from Marcellus Shale natural gas extraction in Pennsylvania," *Environmental Research Letters*, pp. 14-17, 2013.

[37] U.S. EPA, "What is the definition of VOC?," 15 March 2019. [Online]. Available: https://www.epa.gov/air-emissions-inventories/what-definition-voc. [Accessed 8 June 2019].

[38] U.S. EPA, "Volatile Organic Compounds' Impact on Indoor Air Quality," 6 November 2017. [Online]. Available: https://www.epa.gov/indoor-air-quality-iaq/volatile-organic-compounds-impact-indoor-air-quality. [Accessed 24 June 2019].

[39] G. Schade and G. Roest, "Source apportionment of non-methane hydrocarbons, NOx and H2S data from a central monitoring station in the Eagle Ford shale, Texas," *Elementa: Science of the Anthropocene*, vol. 49, pp. 3175-3184, 2015.

[40] G. Roest and G. Schade, "Quantifying alkane emissions in the Eagle Ford Shale using boundary layer enhancement," *Atmos. Chem. Phys*, vol. 17, p. 11163–11176, 2017.

[41] TCEQ, "Dallas-Fort Worth: Current attainment status," 4 June 2018. [Online]. Available: https://www.tceq.texas.gov/airquality/sip/dfw/dfw-status.

[42] U.S. EPA, "Nitrogen Oxides (NOx) Control Regulations," 11 October 2019. [Online]. Available: https://www3.epa.gov/region1/airquality/nox.html. [Accessed 26 November 2019].

[43] J. G. Watson, J. C. Chow and E. M. Fujita, "Review of volatile organic compounds source apportionment by chemical mass balance," *Atmospheric Environment*, vol. 35, pp. 1567-1584, 2001.

[44] B. Barletta, S. Meinardi, I. J. Simpson, H. A. Khwaja, D. R. Blake and F. S. Rowland, "Mixing ratios of volatile organic compounds (VOCs) in the atmosphere of Karachi, Pakistan," *Atmospheric Environment*, vol. 36, pp. 3429-3443, 2002.

[45] B. Buzcu and M. P. Fraser, "Source identification and apportionment of volatile organic compound in Houston, TX," *Atmospheric Environment*, vol. 40, pp. 2385-2400, 2006.

[46] A. P. Rutter, R. J. Griffin, B. K. Cevik, K. M. Shakya, L. Gong, S. Kim, J. H. Flynn and B. L. Lefer, "Sources of air pollution in a region of oil and gas exploration downwind of a large city," *Atmospheric Environment*, vol. 120, pp. 89-99, 2015.

[47] B. Zielinska, D. Campbell and V. Samburova, "Impact of emissions from natural gas production facilities on ambient air quality in the Barnett Shale area: A pilot study," *Journal of the Air & Waste Management Association*, vol. 64, no. 12, pp. 1369-1383, 2014.

[48] M. A. Bari, W. B. Kindzierski, A. J. Wheeler, M.-E. Heroux and L. A. Wallace, "Source apportionment of indoor and outdoor volatile organic compounds at homes in Edmonton, Canada.," *Building and Environment*, vol. 90, pp. 114-124, 2015.

[49] H. Cheng, M. J. Small and N. J. Pekney, "Application of nonparametric regression and statistical testing to identify the impact of oil and natural gas development on local air quality.," *Atmospheric Environment*, vol. 119, pp. 381-392, 2015.

[50] J. Liao, T. Wang, Z. Jiang, B. Zhuang, M. Xie, C. Yin, X. Wang, J. Zhu, Y. Fu and Y. Zhang, "WRF/Chem modeling of the impacts of urban expansion on regional climate and air pollutants in Yangtze River Delta, China..," *Atmospheric Environment*, vol. 106, pp. 204-214, 2015.

[51] Y. Liu, M. Shao, L. Fu, S. Lu, L. Zeng and D. Tang, "Source profiles of volatile organic compounds (VOCs) measured in China: Part I.," *Atmospheric Environment*, vol. 42(25), pp. 6247-6260, 2008.

[52] M. C. McCarthy, Y.-A. Aklilu, S. G. Brown and D. A. Lyder, "Source apportionment of volatile organic compounds measured in Edmonton, Alberta.," *Atmospheric Environment,* vol. 81, pp. 504-516, 2013.

[53] Y. Pang, M. Fuentes and P. Rieger, "Trends in selected ambient volatile organic compound (VOC) concentrations and a comparison to mobile source emission trends in California's South Coast Air Basin.," *Atmospheric Environment*, vol. 122, pp. 686-695, 2015.

[54] T. Vinciguerra, S. Yao, J. Dadzie, A. Chittams, T. Deskins, S. Ehrman and R. R. Dickerson, "Regional air quality impacts of hydraulic fracturing and shale natural gas activity: Evidence from ambient VOC observations.," *Atmospheric Environment*, vol. 110, pp. 144-150, 2015.

[55] J. Ma, J. C. Cheng, C. Lin, Y. Tan and J. Zhang, "Improving air quality prediction accuracy at larger temporal resolutions using deep learning and transfer learning techniques," *Atmospheric Environment,* vol. 214, p. 116885, 2019.

[56] M. Catalano and F. Galatioto, "Enhanced transport-related air pollution prediction through a novel metamodel approach," *Transportation Research Part D: Transport and Environment*, vol. 55, pp. 262-276, 2017.

[57] A. Suleiman, M. Tight and A. Quinn, "Applying machine learning methods in managing urban concentrations of traffic-related particulate matter (PM 10 and PM 2.5)," *Atmospheric Pollution Research*, vol. 10, no. 1, pp. 134-144, 2018.

[58] K. P. Singh, S. Gupta and P. Rai, "Identifying pollution sources and predicting urban air quality using ensemble learning methods," *Atmospheric Environment*, vol. 80, pp. 426-437, 2013.

[59] G. D. Betrie, R. Sadiq, K. A. Morin and S. Tesfamariama, "Uncertainty quantification and integration of machine learning techniques for predicting acid rock drainage chemistry: A probability bounds approach," *Science of Total Environment*, vol. 490, pp. 182-190, 2014.

[60] D. J. Lary, A. H. Alavi, A. H. Gandomi and A. L. Walker, "Machine learning in geoscience and remote sensing," *Geoscience Frontiers*, vol. 7, pp. 3-10, 2016.

[61] C. Brokamp, R. Jandorov, M. Rao, G. LeMasters and P. Ryan, "Exposure assessment models for elemental components of particulate matter in an urban environment: A comparison of regression and random forest approaches," *Atmospheric Environment*, vol. 151, pp. 1-11, 2017.

[62] K. M. Ransom, B. T. Nolan, J. A. Traum, C. C. Faunt, A. M. Bell, J. A. M. Gronberg, D. C. Wheeler, C. Z. Rosecrans, B. Jurgens, G. E. Schwarz, K. Belitz, S. M. Eberts, G. Kourakos and T. Harter, "A hybrid machine learning model to predict and visualize nitrate concentration throughout the Central Valley aquifer, California, USA," *Science of the Total Environment*, Vols. 601-602, p. 1160–1172, 2017.

[63] S. M. Cabaneros, J. K. Calautit and B. R. Hughes, "A review of artificial neural network models for ambient air pollution prediction," *Environmental Modelling & Software*, vol. 119, pp. 285-304, 2019.

[64] Data USA, "Dallas-Fort Worth-Arlington, TX Metro Area," 2017. [Online]. Available: https://datausa.io/profile/geo/dallas-fort-worth-arlington-tx-metro-area/. [Accessed 26 March 2019].

[65] U.S. BLS, "Dallas-Fort Worth Area Economic Summary," 1 August 2018. [Online]. Available: https://www.bls.gov/regions/southwest/summary/blssummary_dallasfortworth.pdf. [Accessed 23 August 2018].

[66] S. Ethridge, T. Bredfeldt, K. Sheedy, S. Shirley, G. Lopez and M. Honeycutt, "The Barnett Shale: From problem formulation to risk management.," *Journal of Unconventional Oil and Gas Resources* (11), pp. 95-110, 2015.

[67] Railroad Commission of Texas, "Barnett Shale Information," 30 November 2017. [Online]. Available: http://www.rrc.state.tx.us/oil-gas/major-oil-and-gas-formations/barnett-shale-information/.

[68] C. J. Meyer, "PAMS Continuous VOC Monitoring Overview of Chromatographic Applications," in National Ambient Air Monitoring Conference - PAMS Workshop, Portland, 2016.

[69] U.S. Census Bureau, "Quickfacts - Denton city, Texas; Fort Worth city, Texas; Dallas city, Texas," 31 January 2019. [Online]. Available: https://www.census.gov/quickfacts/fact/table/dentoncitytexas,fortworthcitytexas,dallascitytexas/PST045217.

[70] TxDOT, "Roadway Inventory Annual Reports 2017," Texas Department of Transport, Austin, 2018.

[71] U.S. Census Bureau, "Community Facts," 2010. [Online]. Available: https://factfinder.census.gov/faces/nav/jsf/pages/community_facts.xhtml. [Accessed 8 October 2018].

[72] R Core Team, "R: A language and environment for statistical," R Foundation for Statistical Computing, Vienna, Austria, 2018.

[73] H. Wickham, J. Hester and W. Chang, "devtools: Tools to Make Developing R Packages Easier," R package version 2.2.1, 2019.

[74] I. Uria-Tellaetxe and D. C. Carslaw, "Conditional bivariate probability function for source identification," *Environmental Modelling & Software*, vol. 59, pp. 1-9, 2014.

[75] M.-H. Shu, D.-C. Dang, T.-L. Nguyen, B.-M. Hsu and K.-Q. Pham, "The application of bivariate polar plots and k-means clustering to analysis air pollution in Taoyuan, Taiwan," *International Journal of Advance Engineering and Research Development*, vol. 4, no. 4, pp. 553-557, 2017.

[76] E. Pebesma and R. Bivand, "Classes and methods for spatial data in R.," *R News*, vol. 5, no. 2, 2005.

[77] T. Pohlert, "Trend: Non-parametric trend tests and change-point detection," 30 July 2018. [Online]. Available: https://CRAN.R-project.org/package=trend.

[78] E. McBean and F. Rover, *Statistical Procedures for Analysis of Environmental Monitoring Data and Risk Assessment*, Prentice Hall, New Jersey, 1998.

[79] A. Dinno, "Package ‘dunn.test’," 27 October 2017. [Online]. Available: https://cran.r-project.org/web/packages/dunn.test/dunn.test.pdf.

[80] T. Mitchell, *Machine Learning*, New York: McGraw Hill, 1997.

[81] T. Chai and R. R. Draxler, "Root mean square error (RMSE) or mean absolute error (MAE)? – Arguments against avoiding RMSE in the literature," *Geoscientific Model Development*, vol. 7, pp. 1247-1250, 2014.

[82] TCEQ, "Texas Photochemical Modeling Results—Model Performance Statistics by Area and Day," 11 October 2019. [Online]. Available: https://www.tceq.texas.gov/airquality/airmod/data/stats_area?eps=20120501-20120531. [Accessed 23 November 2019].

[83] A. K. Gautam, A. Chelani, V. K. Jain and S. Devotta, "A new scheme to predict chaotic time series of air pollutant concentrations using artificial neural network and nearest neighbor searching," *Atmospheric Environment*, vol. 42, no. 18, pp. 4409-4417, 2008.

[84] M. Pandey, A. K. Pandey, A. Mishra and B. Tripathi, "Application of chemometric analysis and self Organizing Map-Artificial Neural Network as source receptor modeling for metal speciation in river sediment," *Environmental Pollution*, vol. 204, pp. 64-73, 2015.

[85] M. D. Adams and P. S. Kanaroglou, "Mapping real-time air pollution health risk for environmental management: Combining mobile and stationary air pollution monitoring with neural network models," *Journal of Environmental Management*, vol. 168, pp. 133-141, 2016.

[86] M. G. Bonelli, M. Ferrini and A. Manni, "Artificial neural networks to evaluate organic and inorganic contamination in agricultural soils," *Chemosphere*, vol. 186, pp. 124-131, 2017.

[87] G. Ciaburro and B. Venkateswaran, *Neural Networks with R*, Birmingham, United Kingdom: Packt Publishing, 2017.

[88] S. Urolagin, P. K.V. and N. S. Reddy, "Generalization Capability of Artificial Neural Network Incorporated with Pruning Method," in International Conference on Advanced Computing, Networking and Security, Surathkal, India, 2011.

[89] M. Kuhn, "caret: Classification and Regression Training.," R package version 6.0-84., 2019.

[90] B. Choubin, H. Darabi, O. Rahmati, F. Sajedi-Hosseini and B. Kløve, "River suspended sediment modelling using the CART model: A comparative study of machine learning techniques," *Science of the Total Environment* 615, p. 272–281, 2018.

[91] W.-Y. Loh, "Classification and regression trees," *WIREs Data Mining and Knowledge Discovery*, vol. 1, pp. 14-23, 2011.

[92] L. Breiman, J. Friedman, C. Stone and R. Olshen, *Classification and Regression Trees*, Boca Raton: CRC Press, 1984.

[93] T. Therneau and B. Atkinson, "rpart: Recursive Partitioning and Regression Trees.," *R package*, 2019.

[94] Q. Liu, S. Deng, C. Lu, B. Wang and Y. Zhou, "Relative density based k-nearest neighbors clustering algorithm," *IEEE International Conference on Machine Learning and Cybernetics*, pp. 133-217, 2003.

[95] C. Wan, L. Lee, R. Rajkumar and D. Isa, "A hybrid text classification approach with low dependency on parameter by integrating K-nearest neighbor and support vector machine," *Expert Syst. Appl*. 39, pp. 11880-11888, 2012.

[96] Ö. F. Ertuğrul and M. E. Tağluk, "A novel version of k nearest neighbor: Dependent nearest neighbor," *Applied Soft Computing* 55, pp. 480-490, 2017.

[97] M. Goldstein and S. Uchida, "A Comparative Evaluation of Unsupervised Anomaly Detection Algorithms for Multivariate Data," *PLoS One*, vol. 11, no. 4, p. e0152173, 2016.

[98] M. A. Schuh, T. Wylie and R. A. Angryk, "Mitigating the Curse of Dimensionality for Exact kNN Retrieval," in *Proceedings of the Twenty-Seventh International Florida Artificial Intelligence Research Society Conference*, Marco Island , 2014.

[99] W. N. Venables and B. D. Ripley, *Modern Applied Statistics with S*., vol. 40, New York: Springer, 2002, pp. 1-29.

[100] L. Breiman, "Random forests," *Machine Learning*, p. 5–32, 2001.

[101] A. Liaw and M. Wiener, "Classification and Regression by random Forest," *R News*, vol. 2, no. 3, pp. 18-22, 2002.

[102] V. Vapnik, S. Golowich and A. Smola, "Support vector method for function approximation, regression estimation and signal processing," Advances in Beural Information Processing Systems, pp. 281-287, 1997.

[104] I. Steinwart and A. Christmann, *Support Vector Machines*, New York: Springer-Verlag, 2008.

[105] W. Lu and W. Wang, "Potential assessment of the "support vector machine" method in forecasting ambient air pollution trends," *Chemosphere*, pp. 693-701, 2005.

[106] A. J. Torija, D. P. Ruiz and Á. F. Ramos-Ridao, "A tool for urban soundscape evaluation applying Support Vector Machines for developing a soundscape classification model," *Science of the Total Environment* 482-483, p. 440–451, 2014.

[107] D. Meyer, E. Dimitriadou, K. Hornik, A. Weingessel and F. Leisch, "e1071: Misc Functions of the Department of Statistics, Probability Theory Group (Formerly: E1071), TU Wien," R package version 1.7-2, 2019.

[108] C. Sagar, "Building Regression Models in R using Support Vector Regression," March 2017. [Online]. Available: https://www.kdnuggets.com/2017/03/building-regression-models-support-vector-regression.html. [Accessed 28 August 2019].

[109] P. Paatero, "The multilinear engine table-driven least square program for solving multilinear problems, including the n-way parallel factor analysis model," *Journal of Computational and Graphical Statistics*, vol. 8, no. 4, pp. 854-888, 1999.

[110] U.S. EPA, "EPA Positive Matrix Factorization (PMF) 5.0 fundamentals and user guide," U.S. Environmental Protection Agency, Washington, 2014.

[111] G. Norris, R. Duvall, S. Brown and S. Bai, "PA Positive Matrix Factorization (PMF) 5.0 Fundamentals and User Guide," U.S. Environmental Protection Agency, Washington, DC, 2014.

[112] P. Paatero and P. Hopke, "Discarding or downweighting high-noise variables in factor analytic models," *Analytica Chemica Acta*, vol. 490, no. 1-2, p. 277–289, 2003.

[113] K. H. Kim, S.-B. Lee, D. Woo and G.-N. Bae, "Influence of wind direction and speed on the transport of particle-bound PAHs in a roadway environment," *Atmospheric Pollution Research*, vol. 6, no. 6, pp. 1024-1034, 2015.

[114] C. Park, G. Schade and I. Boedeker, "Characteristics of the flux of isoprene and its oxidation products in an urban area," *Journal of Geophysical Research*, vol. 116, p. D21303, 2011.

[115] C. Wiedinmyer, S. Friedfeld, W. Baugh, J. Greenberg, A. Guenther, M. Fraser and D. Allen, "Measurement and analysis of atmospheric concentrations of isoprene and its reaction products in central Texas," *Atmospheric Environment*, vol. 35, no. 6, pp. 1001-1013, 2001.

[116] Y. Xie and C. M. Berkowitz, "The use of positive matrix factorization with conditional probability functions in air quality studies: An application to hydrocarbon emissions in Houston, Texas," *Atmospheric Environment*, vol. 40, pp. 3070-3091, 2006.

[117] M. Leuchner and B. Rappengluck, "VOC source-receptor relationships in Houston during TexAQS-II," *Atmospheric Environment*, vol. 44, pp. 4056-4067, 2010.

[118] R. Seco, J. Penuelas, I. Filella, J. Llusia`, R. Molowny-Horas, S. Schallhart, A. Metzger, M. Muller and A. Hansel, "Contrasting winter and summer VOC mixing ratios at a forest site in the Western Mediterranean Basin: the effect of local biogenic emissions," *Atmospheric Chemistry and Physics*, p. 13161–13179, 2011.

[119] R. Seco, J. Penuelas, I. Filella, J. Llusia, S. Schallhart, A. Metzger, M. Muller and A. Hansel, "Volatile Organic Compounds in the Western Mediterranean Basin:Urban and Rural Winter Measurements during the DAURE Campaign," *Atmospheric Chemistry and Physics*, p. 4291–4306, 2013.

[120] Z. Mo, M. Shao, W. Wang, Y. Liu, M. Wang and S. Lu, "Evaluation of biogenic isoprene emissions and their contribution to ozone formation by ground-based measurements in Beijing, China," *Science of The Total Environment*, vol. 627, pp. 1485-1494, 2018.

[121] U.S. EPA, "Air Pollutant Emissions Trends Data," 31 May 2019. [Online]. Available: https://www.epa.gov/air-emissions-inventories/air-pollutant-emissions-trends-data.

[122] H.-d. He, Z.-x. Qiao, W. Pan and W.-Z. Lu, "Multiscale multifractal properties between ground-level ozone and its precursors in rural area in Hong Kong," *Journal of Environmental Management*, vol. 196, pp. 270-277, 2017.

[123] H. S. Kenagy, T. L. Sparks, C. J. Ebben, P. J. Wooldrige, F. D. Lopez-Hilfiker, B. H. Lee, J. A. Thornton, E. E. McDuffie, D. L. Fibiger, S. S. Brown, D. D. Montzka, A. J. Weinheimer, J. C. Schroder and P. Campu, "NOx Lifetime and NOy Partitioning During WINTER," *Journal of Geophysical Research: Atmospheres*, vol. 123, p. 9813–9827, 2018.

[124] A. L. Kalleberg and T. M. Von Wachter, "The U.S. labor market during and after the great recession: continuities and transformations," *RSF*, vol. 3, no. 3, p. 1–19, 2017.

[125] A. A. Roy, P. J. Adams and A. L. Robinson, " Air pollutant emissions from the development, production, and processing of Marcellus Shale natural gas," *Journal of the Air & Waste Management Association*, vol. 64, no. 1, pp. 19-37, 2014.

[126] Y. Wang, X. Ren, D. Ji, J. Zhang, J. Sun and F. Wu, "Characterization of volatile organic compounds in the urban area of Beijing from 2000 to 2007," *Journal of Environmental Sciences*, vol. 24, no. 1, pp. 95-101, 2012.

[127] Q. Zhang, B. Yuan, M. Shao, X. Wang, S. Lu, K. Lu, M. Wang, L. Chen, C. Chang and S. Liu, "Variations of ground-level O3 and its precursors in Beijing in summertime between 2005 and 2011," *Atmospheric Chemistry and Physics*, vol. 14, pp. 6089-6101, 2014.

[128] S. H. Kota, H. Zhang, G. Chen, G. W. Schade and Q. Ying, "Evaluation of on-road vehicle CO and NOx National Emission Inventories using an urban-scale source-oriented air quality model," *Atmospheric Environment*, vol. 85, pp. 99-108, 2014.

[129] S. Sillman, "The relation between ozone, NOx and hydrocarbons in urban and polluted rural environments," *Atmospheric Environment*, vol. 33, no. 12, pp. 1821-1845, 1999.

[130] U.S. EPA, "Hazardous Air Pollutants," 27 September 2018. [Online]. Available: https://www.epa.gov/haps. [Accessed 20 November 2018].

[131] L. Miller, X. Xu, A. Wheeler, T. Zhang, M. Hamadani and U. Ejaz, "Evaluation of missing value methods for predicting ambient BTEX concentrations in two neighbouring cities in Southwestern Ontario Canada," *Atmospheric Environment*, pp. 126-134, 2018.

[132] M. C. McCarthy, H. R. Hafner and S. A. Montzka, "Background concentrations of 18 air toxics for North America," *Journal of Air & Waste Management Association*, vol. 56, pp. 3-11, 2006.

[133] A. K. Baker, A. J. Beyersdorf, L. A. Doezema, A. Katzenstein, S. Meinardi, I. J. Simpson, D. R. Blake and F. S. Rowland, "Measurements of nonmethane hydrocarbons in 28 United States cities," *Atmospheric Environment*, vol. 42, no. 1, pp. 170-182, 2008.

[134] A. Abeleira, I. B. Pollack, B. Sive, Y. Zhou, E. V. Fischer and D. F. Farmer, "Source characterization of volatile organic compounds in the Colorado Northern Front Range

Metropolitan Area during spring and summer 2015," *Journal of Geophysical Research: Atmosphere*, vol. 122, pp. 3595-3613, 2017.

[135] R. F. Swarthout, R. S. Russo, Y. Zhou, B. M. Miller, B. Mitchell, E. Horsman, E. Lipsky, D. C. McCabe, E. Baum and B. C. Sive, "Impact of Marcellus Shale natural gas development in southwest Pennsylvania on volatile organic compound emissions and regional air quality," *Environmental Science and Technology*, vol. 49, pp. 3175-3184, 2015.

[136] C. Lewis, L. Greiner and D. Brown, "Setback distances for unconventional oil and gas development: Delphi study results," *PLoS ONE*, vol. 13, no. 8, p. e0202462, 2018.

[137] E. A. Kort, M. L. Smith, L. T. Murray, A. Gvakharia, A. R. Brandt, J. Peischl, T. B. Ryerson, C. Sweeney and K. Travis, "Fugitive emissions from the Bakken shale illustrate role of shale production in global ethane shift," *Geophysical Research Letters*, vol. 43, p. 4617–4623, 2016.

[138] G. R. Eapi, M. S. Sabnis and M. L. Sattler, "Mobile measurement of methane and hydrogen sulfide at natural gas production site fence lines in the Texas Barnett Shale," *Journal of the Air & Waste Management Association*, vol. 64, no. 8, pp. 927-944, 2014.

[139] A. L. Rich, "Air emissions from natural gas exploration and mining in the Barnett Shale geologic reservoir," The University of Texas at Arlington, Arlington, 2011.

[140] U.S. EPA, "NAAQS Table," 20 December 2016. [Online]. Available: https://www.epa.gov/criteria-air-pollutants/naaqs-table. [Accessed 20 August 2018].

[141] S. Sillman, "The relation between ozone, NOx and hydrocarbons in urban and polluted rural environments," *Atmospheric Environment*, vol. 33, pp. 1821-1845, 1999.

[142] W. Chameides, R. Lindsay, J. Richardson and C. Kiang, "The role of biogenic hydrocarbons in urban photochemical smog: Atlanta as a case study," *Science*, vol. 241, no. 4872, p. 1473–1475, 1988.

[143] M. Li, Q. Zhang, D. G. Streets, K. B. He, Y. F. Cheng, L. K. Emmons, H. Huo, S. C. Kang, Z. Lu, M. Shao, H. Su, X. Yu and Y. Zhang, "Mapping Asian anthropogenic emissions of non-methane volatile organic compounds to multiple chemical mechanisms," *Atmospheric Chemistry and Physics*, vol. 14, p. 5617–5638, 2014.

[144] J. P. Garzon, J. I. Huertas, M. Magana, M. E. Huertas, B. Cardenas, T. Watanabe, T. Maeda, S. Wakamatsu and S. Blanco, "Volatile organic compounds in the atmosphere of Mexico City," *Atmospheric Environment*, vol. 119, pp. 415-429, 2015.

[145] B. Liu, D. Liang, J. Yang, Q. Dai, X. Bi, Y. Feng, J. Yuan, Z. Xiao, Y. Zhang and H. Xu, "Characterization and source apportionment of volatile organic compounds based on 1-year of observational data in Tianjin, China," *Environmental Pollution*, vol. 218, pp. 757-769, 2016.

[146] B. Li, S. S. H. Ho, Y. Xue, Y. Huang, L. Wang, Y. Cheng, W. Dai, H. Zhong, J. Cao and S. Lee, "Characterizations of volatile organic compounds (VOCs) from vehicular emissions at roadside environment: The first comprehensive study in Northwestern China," *Atmospheric Environment*, vol. 161, pp. 1-12, 2017.

[147] H. Zhu, H. Wang, S. Jing, Y. Wang, T. Cheng, S. Tao, S. Lou, L. Qiao, L. Li and J. Chen, "Characteristics and sources of atmospheric volatile organic compounds (VOCs) along the mid-lower Yangtze River in China," *Atmospheric Environment*, vol. 190, pp. 232-240, 2018.

[148] W. P. L. Carter, "Updated maximum increment reactivity scale and hydrocarbon bin reactivities for regulatory applications," College of Engineering Center for Environmental Research and Technology, University of California, Riverside, CA, 2009.

[149] J. B. Gilman, B. M. Lerner, W. C. Kuster and J. A. deGouw, "Source signature of volatile organic compounds from oil and natural gas operations in northeastern Colorado," *Environmental Science and Technology*, vol. 47, no. 3, pp. 1297-1305, 2013.

[150] R. F. Swarthout, R. S. Russo, Y. Zhou, A. H. Hart and B. C. Sive, "Volatile organic compound distributions during NACHTT campaign at the Boulder Atmospheric Observatory: Influence of urban and natural gas sources," *Journal of Geophysical Research: Atmosphere*, vol. 118, pp. 10614-10637, 2013.

[151] U.S. Census Bureau, "Annual Estimates of the Resident Population: April 1, 2010 to July 1, 2017," 2018. [Online]. Available: https://factfinder.census.gov/faces/tableservices/jsf/pages/productview.xhtml?src=bkmk. [Accessed 20 August 2018].

[152] M. Fry, C. Brannstrom and T. Murphy, "How Dallas became frack free: hydrocarbon governance under neoliberalism," *Environment and Planning A,* vol. 47, p. 2591–2608, 2015.

[153] J. M. Fisk, Y. Park and Z. Mahafza, "“Fractivism” in the city: Assessing defiance at the neighborhood level," *State and Local Government Review*, vol. 49, no. 2, pp. 105-116, DOI: 10.1177/0160323X17720712, 2017.

[154] J. Whitton, K. Brasier, I. Charnley-Parry and M. Cotton, "Shale gas governance in the United Kingdom and the United States: Opportunities for public participation and the implications for social justice," *Energy Research & Social Science*, vol. 26, pp. 11-22, 2017.

[155] D. Rahm, "Regulating hydraulic fracturing in shale gas play. The case of Texas.," *Energy Policies*, vol. 39, pp. 2974-2981, 2011.

[156] M. Fry, "Urban gas drilling and distance ordinances in the Texas Barnett Shale," *Energy Policy*, vol. 62, pp. 79-89, 2013.

[157] I. Filella and J. Penuelas, "Daily, weekly and seasonal relationships among VOCs, NOx and O3 in a semi-urban area near Barcelona," *Journal of Atmospheirc Chemistry*, vol. 54, p. 189–201, 2006.

[158] S. Vaughan, T. Ingham, L. K. Whalley, D. Stone, M. J. Evans, K. A. Read, J. D. Lee, S. J. Moller, L. J. Carpenter, A. C. Lewis, Z. L. Fleming and D. E. Heard, "Seasonal observations of OH and HO2 in the remote tropical marine boundary layer," *Atmospheric Chemistry and Physics*, vol. 12, p. 2149–2172, 2012.

[159] J. Lelieveld, S. Gromov, A. Pozzer and D. Taraborrelli, "Global tropospheric hydroxyl distribution, budget and reactivity," *Atmospheric Chemistry and Physics*, vol. 16, p. 12477–12493, 2016.

[160] U.S. EPA, "Hazardous Air Pollutants," 27 September 2018. [Online]. Available: https://www.epa.gov/haps. [Accessed 27 June 2019].

[161] B. Zielinska, E. Fujita and D. Campbell, "Monitoring of emissions from Barnett Shale natural gas production facilities for population exposure assessment," Desert Research Institute, Reno, NV, 2010.

[162] D. Zavala-Araiza, D. R. Lyon, R. A. Alvarez, K. J. Davis, R. Harriss, S. C. Herndon, A. Karion, E. A. Kort, B. K. Lamb, X. Lan, A. J. Marchese, S. W. Pacala, A. L. Robinson, P. B. Shepson and C. Sweeney, "Reconciling divergent estimates of oil and gas," *PNAS*, vol. 112, no. 51, p. 15597–15602, 2015.

[163] S. Almeida, C. Pio, M. Freitas, M. Reis and M. Trancoso, "Source apportionment of atmospheric urban aerosol based on weekdays/weekend variability: evaluation of road re-suspended dust contribution," *Atmospheric Environment*, vol. 40, no. 11, pp. 2058-2067, 2006.

[164] S. Karnae and K. John, "Source apportionment of PM2.5 measured in South Texas near U.S.A - Mexico border," *Atmospheric Pollution Research*, 2019.

[165] E. Kim, S. G. Brown, H. R. Hafner and P. K. Hopke, "Characterization of non-methane volatile organic compounds sources in Houston during 2001 using positive matrix factorization," *Atmospheric Environment*, vol. 39, pp. 5934-5946, 2005.

[166] M. Sanchez, S. Karnae and K. John, "Source characterization of volatile organic compounds affecting the air quality in a coastal urban area of South Texas," *International Journal of Environmental Research and Public Health*, 5 (3), pp. 130-138, 2008.

[167] C.-H. Chen, Y.-C. Chuang, C.-C. Hsieh and C.-S. Lee, "VOC characteristics and source apportionment at a PAMS site near an industrial complex in central Taiwan," *Atmospheric Pollution Research*, 2019.

[168] B. Xiang, P. K. Patra, S. A. Montzka, S. M. Miller, J. W. Elkins, F. L. Moore, E. L. Atlas, B. R. Miller, R. F. Weiss, R. G. Prinn and S. C. Wofsy, "Global emissions of refrigerants HCFC-22 and HFC-134a: Unforeseen seasonal contributions," *PNAS,* vol. 111, no. 49, p. 17379–17384, 2014.

[169] P. Purohit and L. Höglund-Isaksson, "Global emissions of fluorinated greenhouse gases 2005–2050 with abatement potentials and costs," *Atmospheric Chemistry and Physics*, vol. 17, p. 2795–2816, 2017.

[170] S. G. Brown, A. Frankel and H. R. Hafner, "Source apportionment of VOCs in the Los Angeles area using positive matrix factorization," *Atmospheric Environment*, vol. 41, pp. 227-237, 2007.

[171] Z. Yuan, A. K. H. Lau, M. Shao, P. K. K. Louie, S. C. Liu and T. Zhu, "Source analysis of volatile organic compounds by positive matrix factorization in urban and rural environments in Beijing," *Journal of Geographical Research*, vol. 114, 2009.

[172] RRC, "Barnett Shale Information," 26 March 2019. [Online]. Available: https://www.rrc.state.tx.us/oil-gas/major-oil-and-gas-formations/barnett-shale-information/. [Accessed 26 March 2019].

[173] Denton City Council, "An ordinance of the city of Denton, Texas, amending subchapters 5, 16 and 22 of the Denton Development Code," Denton, 2015.

[174] American Legal Publishing Corporations, City of Fort Worth Texas Ordianances, Fort Worth, Texas, 2014.

[175] S. C. Kavassalis and J. G. Murphy, "Understanding ozone-meteorology correlations: A role for dry deposition," *Geophysical Research Letters*, vol. 44, no. 6, pp. 2922-2931, 2017.

[176] M. Graczyk, T. Lasota, B. Trawiński and K. Trawiński, "omparison of Bagging, Boosting and Stacking Ensembles Applied to Real Estate Appraisal," *Asian Conference on Intelligent Information and Database Systems*, pp. 340-350, 2010.

[177] G. E. A. P. A. Batista, R. C. Prati and M. C. Monard, "A Study of the Behavior of Several Methods for Balancing Machine Learning Training Data," *Sigkdd Explorations* 6 (1), pp. 20-29, 2004.

[178] D. Dominick, H. Juahir, M. T. Latif, S. M. Zain and A. Z. Aris, "Spatial assessment of air quality patterns in Malaysia using multivariate analysis," *Atmospheric Environment*, vol. 60, pp. 172-181, 2012.

[179] J. Jeon, "The Strengths and Limitations of the Statistical Modeling of Complex Social Phenomenon: Focusing on SEM, Path Analysis, or Multiple Regression Models," *International Journal of Social, Behavioral, Educational, Economic, Business and Industrial Engineering*, vol. 9, no. 5, pp. 1634-1642, 2015.

[180] E. Frank, "Pruning Decision Trees and Lists," University of Waikato, Hamilton, 2000.

[181] M. B. Kursa and W. R. Rudnicki, "Feature Selection with the {Boruta} Package," *Journal of Statistical Software*, vol. 36, no. 11, pp. 1-13, 2010.

[182] J.-L. Chiang and Y.-S. Tsai, "Suspended sediment load estimate using support vector machines in Kaoping river basin," in *Consumer Electronics, Communications and Networks (CECNet)*, XianNing, China, 2011.

[183] Ramboll Environment and Health, "CAMx Version 6.50 User's Guide," Ramboll US Corporation, Novato, 2018.

[184] R. G. Lamb, "Note on the application of K-Theory to diffusion problems involving nonlinear chemical reactions," *Atmospheric Environment*, vol. 7, no. 3, pp. 257-263, 1973.